THE MIDDLE PLEISTOCENE EXTINCTION OF BATHYAL BENTHIC FORAMINIFERA IN THE SOUTH ATLANTIC (ODP SITES 1082 AND 1088)

A thesis presented in partial fulfilment of the
requirements for the degree of
Master of Science
in
Earth Science

at Massey University,
Palmerston North,
New Zealand

Massey University

Tanya Ann O'Neill

2005

Abstract

The youngest major turnover in deep-sea benthic foraminifera (termed the *Stilostomella* extinction) is documented in two ODP sites in the South Atlantic Ocean. This study is the first detailed investigation of its kind in this region, and reveals the pulsed decline and eventual extinction of 33 species of elongate, cylindrical benthic foraminifera belonging to the families Stilostomellidae, Pleurostomellidae, and part of the Nodosariidae during the mid-Pleistocene climatic transition (MPT, ~1200 – 600 ka). Furthermore, the *Stilostomella* extinction is limited to elongate species with highly specific apertural characteristics (e.g. cribrate, slit lunate, and hooded with secondary teeth), such as *Chrysalogonium*, *Ellipsoglandulina*, and *Pleurostomella* species, respectively.

Micropaleontological and sedimentological data from lower bathyal Sites 1082 and 1088 (1290 m and 2082 m water depth, respectively) provide a proxy record of oceanographic changes in the South Atlantic Ocean through the MPT. This study compares the timing and causes of the *Stilostomella* extinction between two highly contrasting environmental settings in relation to paleoceanographic history, sediment regime and paleoproductivity.

In the South Atlantic, the abundance and accumulation rate of Extinction Group (EG) taxa began to decline between ~1070 and 1000 ka at both core sites. The rate of decline was pulsed, with major declines usually associated with cool periods, and partial recoveries during intervening warm periods. The timing of highest occurrences (HOs) was diachronous between sites, and the final *Stilostomella* extinction datum is marked by the uppermost occurrence of *Myllostomella matanzana* and *Siphonodosaria sagrinensis* at ~705 ka in Site 1082, and *Myllostomella matanzana* and *Pleurostomella alternans* at ~600 ka in Site 1088. This corresponds with the previously documented global *Stilostomella* extinction datum within the period of 700 and 570 ka. Detailed comparisons with North Atlantic and Southwest Pacific studies confirm the highly diachronous nature of HOs of EG species, and furthermore, reveal that there is a lead time of ~100 kyr between HOs of the same species in the North Atlantic, compared with the South Atlantic.

This study suggests that declines and extinctions at Site 1082 were primarily driven by highly fluctuating food supply associated with increased productivity caused by intensified upwelling during MPT glacial periods. In contrast, extinctions at Site 1088 appear to have been a result of the MPT reorganisation of the global deep-water 'conveyor belt', with $\delta^{13}C$ gradients revealing that high dissolved oxygen Glacial North Atlantic Intermediate Water (GNAIW) bathed the region during cool periods. Far from a simple response to change in a single parameter, numerous factors have interacted and appear to have caused the demise of the *Stilostomella* extinction taxa. These factors include encroachment by well-ventilated (high dissolved oxygen) GNAIW, fluctuations in food supply, and possibly winnowing (of the phytodetritus layer) by vigorous bottom currents during MPT glacial periods.

Acknowledgements

I am very grateful to Bruce Hayward for the opportunity to embark on this project, for his enthusiasm, supervision and financial support over the course of this study. I thank the Ocean Drilling Program for providing the samples, isotopic and age model data. A special thanks to the team at Geomarine Research, Hugh Grenfell, Ashwaq Sabaa and Shungo Kawagata, for their hospitality, support and time, which they always so generously bestowed. I would also like to thank those mentioned above for providing data sets from previous *Stilostomella* Extinction studies for very useful comparative purposes, and their suggestions for improving this thesis. Kindest regards to the Hayward household for making me feel so at home!

Thanks to Doug Hopcroft of Hort Research, Palmerston North, for his time and use of the SEM. The supervision of Vince Neall and Julie Palmer was greatly appreciated, as is their unwavering support during my university career. Thank you Vince for your time, encouragement, enthusiasm, our travels, and all the amazing opportunities you have directed my way during the course of my studies. Thanks to all the staff of the Massey University Soil and Earth Sciences Group and postgraduate students. I am especially grateful to Moira Hubbard and Michael Turner for their support and friendship.

Lastly, but most importantly, to my family, I love you and know that without your on-going love and support none of this would have been possible. To my Heavenly Father, for His blessings and grace. Thank you.

Table of Contents

CHAPTER 2 ~ ODP METHODS

CHAPTER 3 ~ METHODS

CHAPTER 4 ~ TAXONOMY

CHAPTER 5 ~ RESULTS

CHAPTER 6 ~ DISCUSSION

List of Figures

List of Tables

List of Plates

Abbreviations and Acronyms

AAIW	Antarctic Intermediate Water
APC	Advanced piston corer
AR	Accumulation rate
B/M	Brunhes/Matuyama paleomagnetic boundary
CC	Core catcher
CCD	Carbonate compensation depth
cos	cosmopolitan
CPDW	Circum Polar Deep Water
DIC	Carbon isotope gradient between intermediate and deep watermasses
DO	Dissolved oxygen
DSDP	Deep Sea Drilling Program
EG	Extinction Group
FI	Fragmentation index
GNAIW	Glacial North Atlantic Intermediate Water
GRA	Gamma-ray attenuation
HO	Highest occurrence
IRD	Ice-rafted debris
lCPDW	lower-Circum Polar Deep Water
LGM	Last Glacial Maximum
lNADW	lower-North Atlantic Deep Water
LOTG	Low-oxygen tolerant Group
LPTM	Late Paleocene Thermal Maximum
MAR	Mass accumulation rate
mbsf	metres below seafloor
mcd	metres composite depth
MIS	Marine Oxygen Isotope Stage
MPT	Middle Pleistocene Climatic Transition
MST	Mulit-sensor track
na	North Atlantic
NADW	North Atlantic Deep Water
NCW	Northern Component Water

NRM	Natural remnant magnetism
ODP	Ocean Drilling Program
%PF	Percent planktic foraminifera
PETM	Paleocene-Eocene Thermal Maximum
PDB	PeeDee Belemnite
psu	Practical Salinity Unit
sa	South Atlantic
SAF	Subantarctic Front
SAMW	Subantarctic Mode Water
SASW	Subantarctic Surface Water
SCW	Southern Component Water
SEM	Scanning electron microscope
SG	Survivor Group
SR	Sedimentation rate
SSSTs	Summer sea-surface temperates
STF	Subtropical Front
swp	South-west Pacific
TOC	Total organic carbon
XCB	Extended core barrel
XRD	X-ray diffraction
uCPDW	upper-Circum Polar Deep Water
uNADW	upper-North Atlantic Deep Water

1. INTRODUCTION

1.1 Objectives

This study is the first high resolution investigation into the *Stilostomella* extinction event in the South Atlantic Ocean. The primary aim of the research was to document the progressive decline, the timing of local disappearances, and the eventual extinction of deep-sea benthic foraminifera in two cores from the South Atlantic Ocean during the mid-Pleistocene Climatic Transition (MPT). This youngest period of benthic foraminiferal extinctions has been attributed to global climate cooling during the MPT between ~ 1200 – 600 ka (Hayward, 2001, 2002; Kawagata *et al.* in press).

Previous studies have revealed that the pulsed decline and extinctions were limited to a specific group of foraminifera, namely, elongate deep-sea foraminifera belonging to the families Stilostomellidae, Pleurostomellidae, and part of the Nodosariidae. Furthermore, the *Stilostomella* extinction selectively affected foraminifera with certain shell morphologies and highly specific apertural characteristics.

South Atlantic ODP Sites 1082 and 1088 have been purposefully chosen to allow for comparisons between two highly contrasting environmental settings, in relation to paleoceanographic history, sediment regime and paleoproductivity. Regional intersite comparisons will be undertaken to investigate whether the timings and causes of the *Stilostomella* extinction were similar at both sites.

Timings of declines and extinctions in the South Atlantic will be compared with proxy data for various environmental factors to provide clues to the cause of these mid-Pleistocene extinctions. Additionally, results will be compared with similar detailed *Stilostomella* extinction studies in the North Atlantic and Southwest Pacific Oceans, in an effort to understand the different timings of highest occurrences in different watermasses (depth) and in different parts of the oceans.

Another aspect to be investigated is the possible link between the morphologic characteristics of the Stilostomella Extinction Group taxa (particularly apertural modifications) and the ordering of highest occurrences both in the South Atlantic and the global scene.

1.2 Southeastern Atlantic Site 1082

1.2.1 Regional Geology

Thirteen sites (1075-1087) were drilled during ODP Leg 175, spanning the western coast of Africa from 5° to 32° S (Fig. 1.1). Site 1082 is located on the Abutment Plateau of the Frio Ridge segment of the Walvis Ridge where it adjoins the continental slope of Namibia. The Walvis Ridge is an aseismic basaltic ridge formed from hotspot activity during the early Cretaceous period (Dean and Gardner, 1985). It extends south-westwards from the continental margin for >2500 km towards the Mid-Atlantic Ridge (Shannon and Nelson, 1996), and may have served as a dam to paleocirculation and current-transported sediment (Bolli *et al.*, 1978), above which thick, mainly biogenic sediment has accumulated.

1.2.2 Location and Modern Oceanographic Setting

ODP Site 1082 (21.5°S, 11.5°E) was drilled during Leg 175 in 1290 m water depth on the Walvis Ridge, c. 250 km offshore from the coast of Namibia. Positioned at the outer edge of the modern Benguela Current Upwelling System (Namibian upwelling cell), the core site is overlain by well-oxygenated, low-salinity Antarctic Intermediate Water (AAIW) (Fig. 1.2), which flows equatorward along the slope off Namibia above which is the Benguela Current (Wefer *et al.*, 1998).

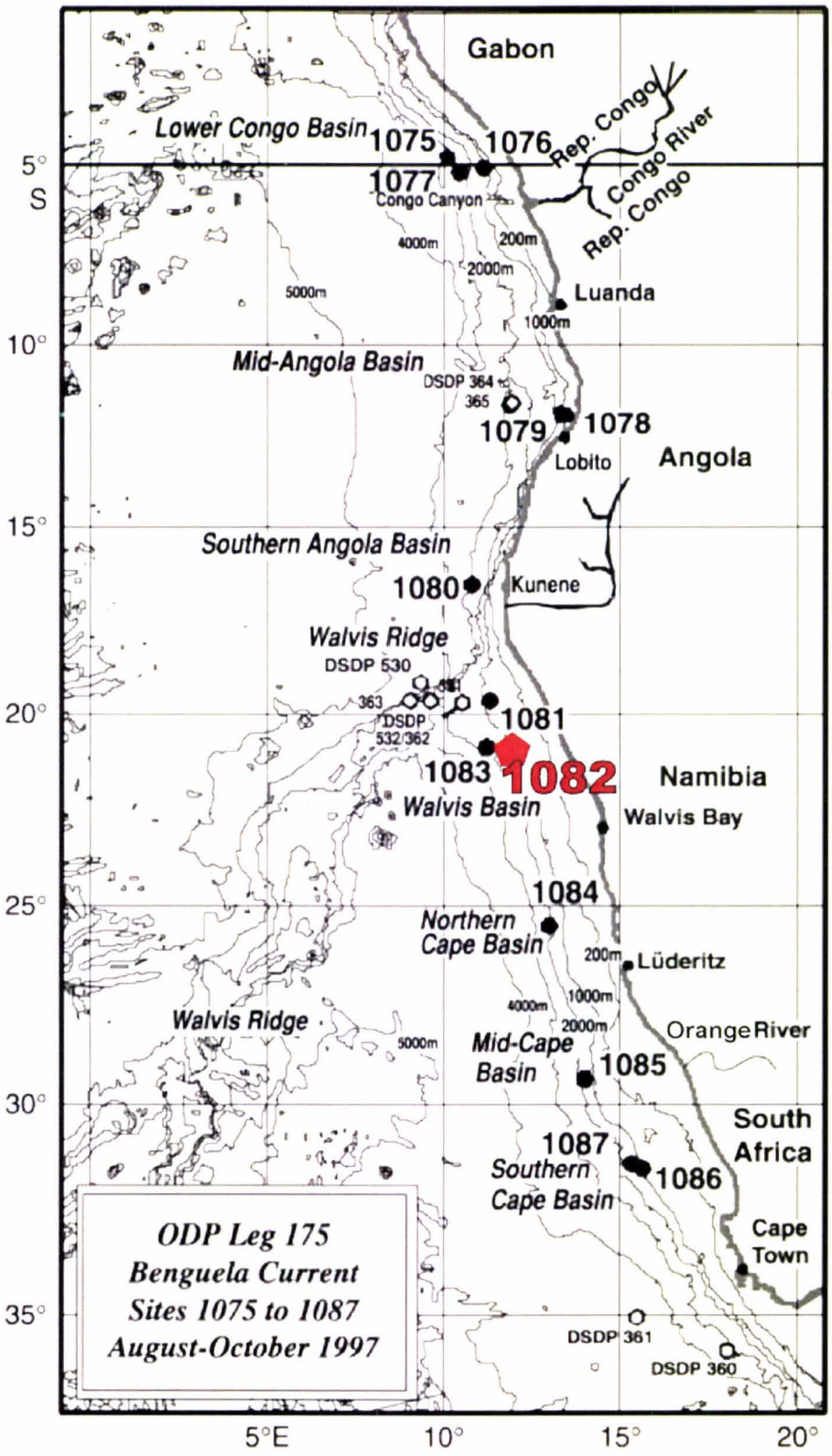

Figure 1.1: Location of Site 1082 in relation to other ODP Leg 175 sites, major bathymetric features and previously drilled ODP and DSDP sites in the South Atlantic study region (modified from Wefer *et al.*, 2001).

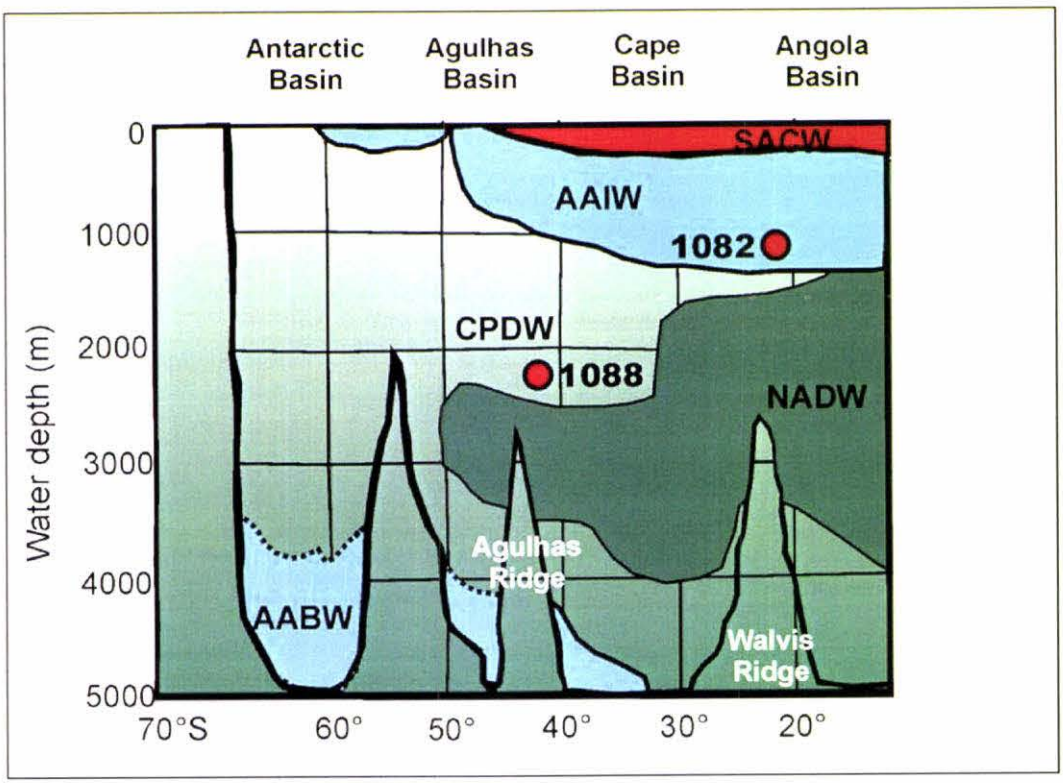

Figure 1.2: A cross-section through the major intermediate- and deep-water masses in the region of Site 1082, South Atlantic Ocean (modified from Gersonde *et al.*, 1999).. AABW = Antarctic Bottom Water; CPDW = Circum-polar Deep Water; NADW = North Atlantic Deep Water; AAIW = Antarctic Intermediate Water; SACW = South Atlantic Central Water.

Modern oceanographic conditions off Southwest Africa have been documented by Moroshkin *et al.* (1970), Bang (1971), Nelson and Hutchings (1983), Shannon (1985a, 1985b), and more recently by Hay and Brock (1992) and Dowsett and Willard (1996). A major component of the heat transfer system from the southeastern Atlantic is the Angola-Benguela Current (ABC) system, comprising the Angola Current and the Benguela Current (Fig. 1.3). The Benguela Current is a shallow (<80 m) equatorward-flowing cool surface current, flowing parallel to and within ~ 320 km off the southwest margin of the African continent (Durham *et al.*, 2001). At ~ 16° S latitude, these northward flowing waters meet the warm and saline southward-flowing Angola Current and develop the Angola-Benguela Front (ABF) (Summerhayes *et al.*, 1995). At this front, the Benguela Current is deflected west and merges with the South Equatorial Current, making up the eastern limb of the South Atlantic Subtropical Gyre. Upwelling of cold, nutrient-rich South Atlantic Central Water (SACW) (from depths between 200-500 m) occurs over the shelf break in response to offshore divergence and along the southwestern African coast in response to offshore Ekman transport (Fig. 1.2). Beneath the SACW lies cold nutrient-rich Antarctic Intermediate Water (AAIW). AAIW is

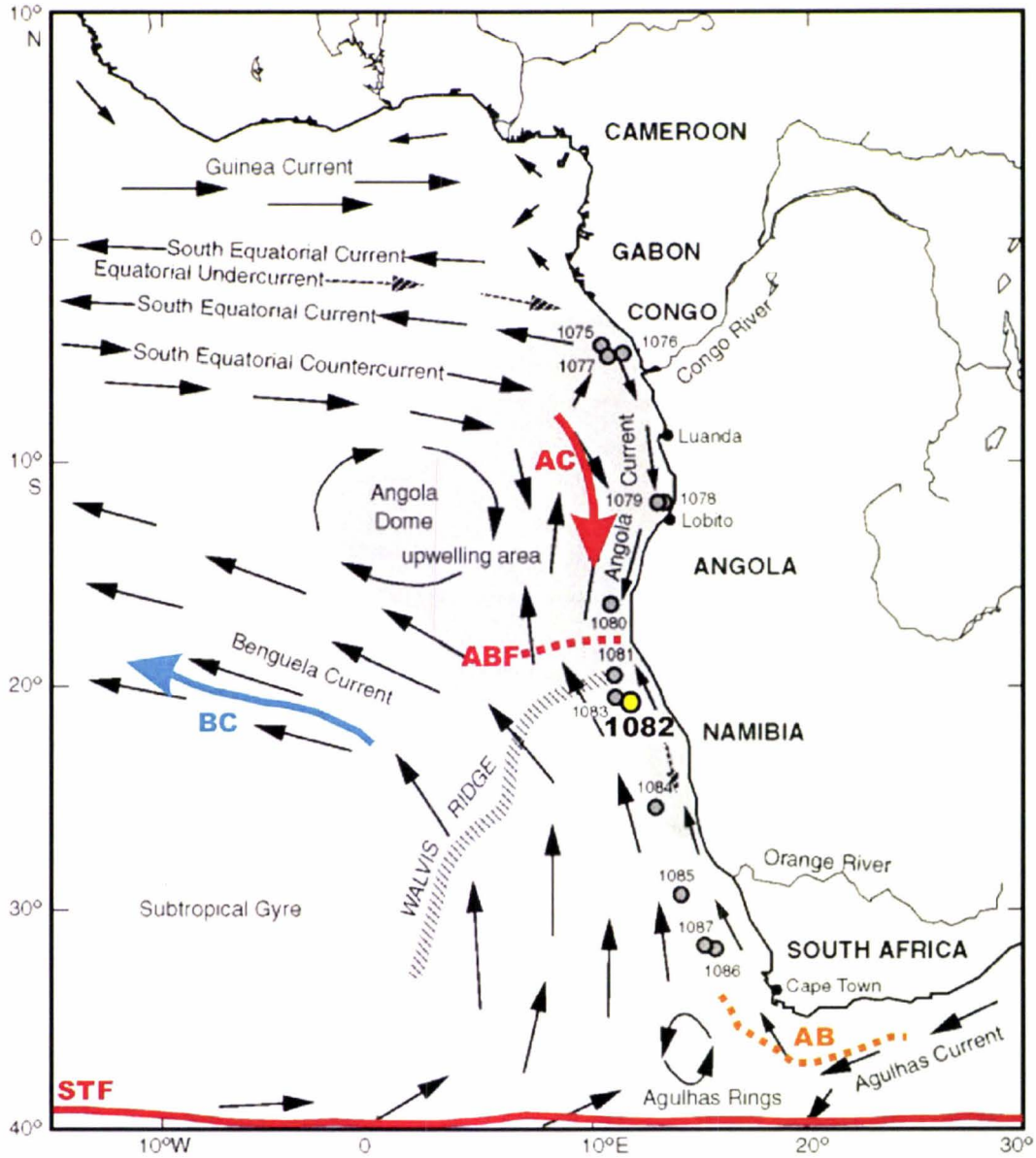

Figure 1.3: Location of ODP Site 1082 and the major surface currents influencing the region today. Arrows represent present day surface currents in the Southeast Atlantic Ocean (modified from Motoyama, 2001). AB = Agulhas Bank; ABF = Angola-Benguela Front; STF = Subtropical Front; AC = Angola Current; BC = Benguela Current.

found in all sectors of the Southern Hemisphere oceans to the north of the Antarctic polar front. Throughout the tropical South Atlantic, AAIW occupies the depth range from 650 to 1050 m (Reid, 1994), with typical temperature and salinity values of 3° C and 34.3 psu, respectively. AAIW spreads across the equator where traces can be found as far north as 30° N in the North Atlantic (Talley, 1996).

The Benguela Current is unusually productive because it delivers an admixture of nutrient-rich AAIW and SACW to the surface through a two-step process (Fig. 1.4)

(Hay and Brock, 1992). Below the surface Benguela Current, a poleward flowing cyclonic subsurface gyre wells up nutrient-rich AAIW (A in Fig. 1.4) to just below the pycnocline, which shoals to less than 250 m off Walvis Bay (Dowsett and Willard, 1996). Here it mixes with the nutrient-rich SACW, and surface upwelling processes, in turn, bring this water up from between 200 m and 330 m to the surface (B in Fig. 1.4), creating a region of cold, nutrient-rich water where primary productivity is very high.

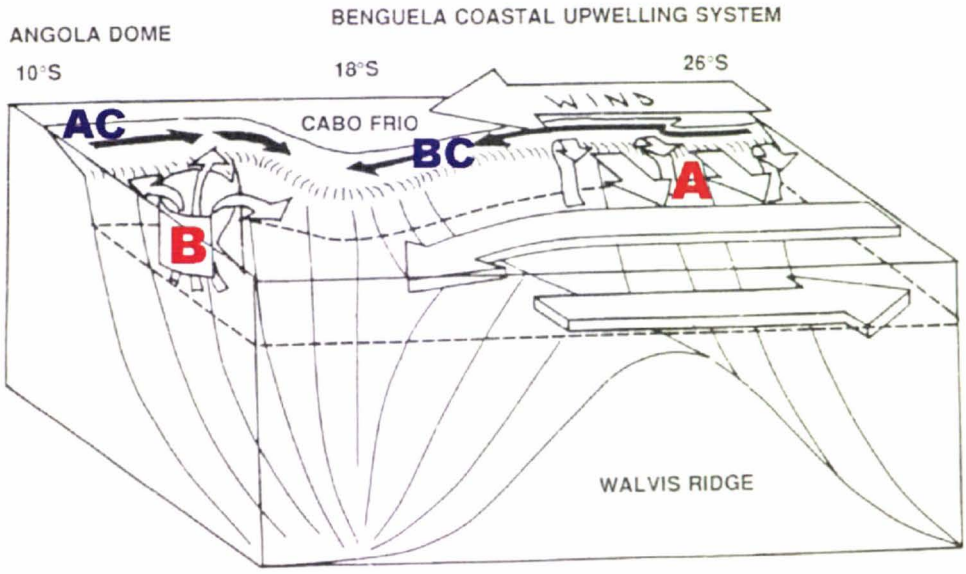

Figure 1.4: Schematic view of the southwest African margin and Walvis Ridge, showing the Angola Current (AC), Benguela Current (BC), coastal upwelling system, and the Angola Dome. Note: A and B refer to upwelling of Antarctic Intermediate Water (AAIW) and South Atlantic Central Water (SACW) (refer to text) (Modified from Hay and Brock, 1992).

Wind conditions along the coast, responsible for the upwelling, are extremely stable because winds circulating around the South Atlantic subtropical high pressure cell are constrained by the steep Kalahari escarpment. The wind stress that intensifies during the Southern Hemisphere summer results in maximum upwelling between December and April each year (Dowsett and Willard, 1996).

To the north, the Benguela Current Upwelling System (BCUS) is bounded, at about 16° S, by the Angola-Benguela Front (ABF) (Fig. 1.3). The ABF migrates seasonally between about 14° S and 16.5° S (Summerhayes *et al.*, 1995). In the late austral summer the front weakens and warm, saline, Angolan water penetrates south along the coast, occasionally reaching 20° S in 'Benguela El Nino' events.

To the south, the BCUS is bounded by the Agulhas Bank (AB in Fig. 1.3), south of which lies the Subtropical Front (STF). This front is known to induce the northward flow of cold filaments of Subantarctic Surface Water (SASW). South of the African coastline and north of the STF warm waters of the Agulhas Current flow in from the Indian Ocean and return east, generating eddies of warm water that spin off to the northwest in the Benguela Current (Summerhayes *et al.*, 1995).

The western margin of the upwelling region is not well defined in terms of sea-surface-temperature anomalies. Satellite imagery has shown large-scale frontal features, resembling 'giant rip-currents', extending up to 500 km offshore (Hay and Brook, 1992).

Present day coastal upwelling varies seasonally, with the seasonal signal more pronounced off Namibia (north of the Orange River) than further south. During the austral winter and spring, water cooler than 16° C extends along the entire coast, but in the summer and autumn its northward extent is reduced. Lutjeharms and Meeuwis (1987) have subdivided the present day Namibian coastal upwelling into four zones or cells, based on the relative strength of the upwelling cell (Fig. 1.5). Their investigations showed upwelling to be particularly strong at ~25° S (centre of the Luderitz upwelling cell), somewhat less so at ~22° S (Walvis cell, ODP Site 1082) and at ~19° S (Namibia cell), and weakest ~17° S (Cunene cell). The Luderitz cell is the coldest, the most persistent, and extends the farthest offshore. Lutjeharms and Meeuwis (1987) also found a strong correlation between intensity of upwelling and the direction and strength of coastal winds. Further, there is also a loose association between the location of upwelling cells and the shape of the seabed, upwelling being more intense where the deep water is closest to the coast (Shannon, 1985). The highest productivity is currently reached off Namibia between 20°S and 25°S. At this latitude optimumal productivity prevails because of the rate of upwelling and the nutrient content of the upwelled waters. Trade winds are strong, offshore transport is vigorous, and cold upwelled water is high in both phosphate and silicate (Wefer *et al.*, 2001).

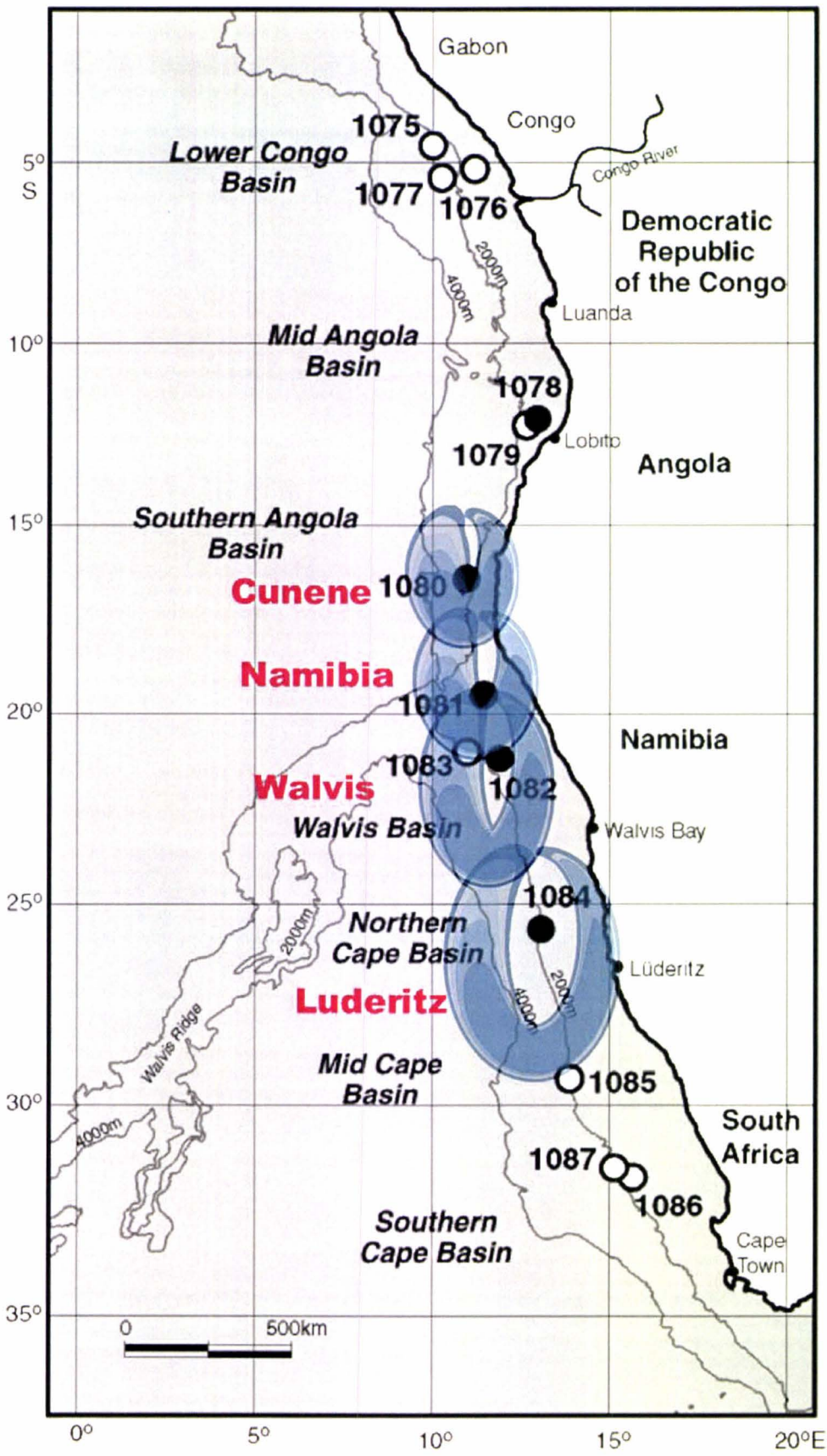

Figure 1.5: Locations of Benguela Current Upwelling System Cells (Modified from Wefer *et al.*, 2001). Note: The size of the upwelling cell is based on its relative upwelling strength.

1.2.3 Past changes in Benguela Current Upwelling System

Previous evidence from the region of the Walvis Ridge has proved to be contentious over the issue of glacial-interglacial upwelling intensity changes, and has been debated by several authors. Studies by Oberhansli (1991), Summerhayes *et al.* (1995) and Little *et al.* (1997) concluded that upwelling at the latitude of the Walvis Ridge generally increased during glacial periods, conversely, other studies suggest that intensity increased during interglacial periods (Diester-Haass, 1985). It has since been suggested, however, that the discrepancy between these studies may in fact be due to the complexity of the site, resulting from past changes in thermohaline circulation, and poor preservation of upwelling indicators (Durham *et al.*, 2001).

Productivity records from nearby Site 1081 (also on the Walvis Ridge) generally provide evidence for increased productivity during glacial intervals, particularly prior to ~1000 ka (Durham *et al.*, 2001). The Mid-Pleistocene Transition (MPT) and associated increased cooling and aridity on the adjacent landmass, brought about changes in the chemical and physical properties of the upwelling water masses and their nutrient content. Durham *et al.*'s 2001 study revealed a significant and rapid drop in overall productivity at ~800 ka. Between 800 and 500 ka productivity began to increase again, however, this was followed by another rapid decrease in productivity at ~500 ka. Post-500 ka fluctuations in productivity were common, with short-lived peaks in response to (1) nutrient-enriched bottom waters being closer to the surface due to sea-level drop and (2) less volume of water in which nutrients were distributed (Hay and Brock, 1992). These peaks were short-lived as enhanced productivity removed nutrients faster than they could be replaced, and consequently, the system stabilized, and productivity decreased once again.

During the Last Glacial Maximum (LGM) the 7° of latitude northward displacement of the Polar Front (PF), the 2° northward displacement of the STF, and the 2-5° C cooling of the Subantarctic Surface Waters, all suggest that the thermal gradient south of Africa steepened in glacial intervals, displacing the South Atlantic mid-latitude high pressure cell north by 2-5° of latitude (Tyson, 1986). The equatorward movement of the pressure system forced a similar shift in the upwelling-favourable Trade Winds, with the steeper thermal gradient also strengthening them. This strengthening of the coastal and shelf-

edge wind field is thereby thought to have enhanced upwelling (intensity and increased productivity) along the Namibian margin during glacial and cooler interstadial periods.

Productivity records from past studies in the region of Site 1082 show that there may not necessarily be a simple response to apparently linear changes, and that in fact, numerous factors may interact together and influence the records of deep-sea sediments in these complex regions of high productivity.

1.2.4 Sediment Regime

Site 1082 has a continuous sedimentary record based on density, magnetic susceptibility and colour reflectance data, spliced in small intervals from Holes 1082B and 1082C, where sediment column was disturbed or missed during the coring process. The 600 m long sediment sequence of Hole 1082A has well-developed cyclic sedimentation, with glacial and interglacial cycles represented as cycles of carbonate dissolution, productivity, and terrigenous sediment supply. Sediment is composed of continuous hemipelagic mud spanning the latest Miocene to Holocene (5.8 – 0 Ma), with the early-mid to late-Pleistocene, investigated in this study, composed of alternating intervals of bioturbated olive and black nannofossil- and foraminifer-rich clay (Jahn *et al.*, 2003). Varying abundances of diatoms, nannofossils, foraminifers, and radiolarians, and minor authigenic minerals, such as glauconite and gypsum, are found throughout the study interval (Wefer *et al.*, 2001).

Sedimentation rates are comparatively high within Leg 175 sites, varying between 70 to 150 m/myr (Durham *et al.*, 2001), Glacial-interglacial cyclicity of the late Quaternary is represented by cycles of carbonate dissolution, productivity, and terrigenous sediment supply, and is recorded as dark and light colour variations in the sediment retrieved from Site 1082. These colour cycles (total reflectance) reflect sharp changes in concentrations of calcium carbonate, organic carbon, and total sulphur. Generally, the darker layers have higher concentrations of organic carbon and total sulphur, and lower concentrations of calcium carbonate and biogenic opal (Wefer *et al.*, 1998). Changes in magnetic susceptibility down the core can also be utilized and reflect changes in terrestrial sediment input and calcium carbonate deposition across climatic cycles. At Site 1082, these well-developed cycles, in which concentrations of calcium carbonate

and organic carbon vary between 1 and 85% and <0.1 and 16.1 wt%, respectively, reflect fluctuations in the elevated marine production associated with the Benguela Current Upwelling System; higher concentrations of organic carbon recording higher productivities over the past 2 Ma (Wefer *et al.*, 1998). This high supply of organic matter drove intense diagenetic activity and periods of elevated carbonate dissolution. Studies by Berger (1970), Berger *et al.* (1982), and Emerson and Bender (1982), suggest that carbonate dissolution on continental margins in water depths above the oceanic lysocline or carbonate compensation depth (i.e. Site 1082) can only be attributed to decomposition of organic matter and resultant production of pore water CO_2. This dissolution is controlled by two processes: (a) surface water productivity (Berger, 1970) and (b) lateral supply of organic matter from the shelf and/or upper continental slope (Diester-Haass *et al.*, 1986). The equatorward movement of the South Atlantic high pressure system produced a similar shift in the upwelling-favourable Trade Winds (Tyson, 1986), strengthening of the coastal and shelf-edge wind field, and is thereby thought to have enhanced upwelling (intensity and increased productivity) along the Namibian margin during glacial and cooler interstadial periods.

The terrigenous input signal inferred from nearby Site 1081 reveals an increase in the supply of aeolian material during glacial periods (Durham *et al.*, 2001). In addition to increased supply of terrestrial material in response to the lowering of sea-level (global cooling and increased ice volume) and erosion of the now exposed continental shelf and slope areas, the strengthening of the coastal wind field during glacial intervals (and continental aridity) is inferred to have enhanced aeolian transport of sediment (including Fe and Si, recognized as having key roles in increasing primary productivity during glacial periods (Boyd *et al.*, 2004)) from the Namib desert into the region of the Walvis Ridge (Diester-Haass *et al.*, 1988). These two processes, an increase in surface water productivity and increase in the lateral supply of organic matter from continental shelf/upper slope areas, resulted in an increase in net organic matter accumulation and thus an enhanced carbonate dissolution during glacial times (Diester-Haass *et al.*, 1992). Ice-rafted debris (IRD) has not been encountered in previous studies as far north as Site 1082 (Siesser, 1980; Diester-Haass *et al.*, 1986, 1992).

1.3 *Southern Ocean sector of Southeastern Atlantic - Site 1088*

1.3.1 Regional Geology

Sites drilled during Leg 177 are associated with the Agulhas Basin and are arranged along a north-south transect extending from the Agulhas Fracture Zone Ridge in the north, to Bouvet Island in the south (Fig. 1.6). The Agulhas Basin lies on the African Plate and is bounded by the Agulhas Fracture Zone to the north, the Southwest Indian Ridge to the south, the Meteor Rise to the west, and the Agulhas Plateau to the east (Gersonde *et al.*, 1999).

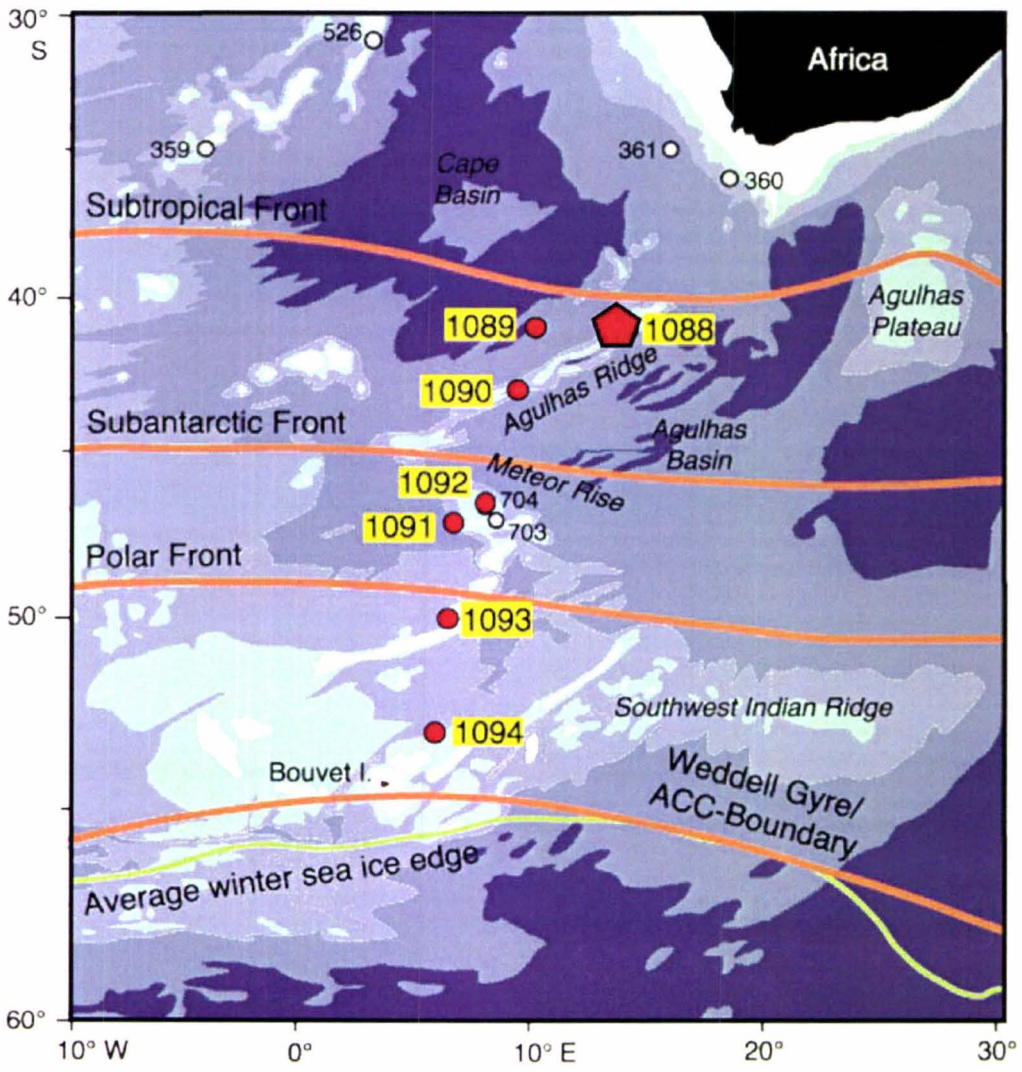

Figure 1.6: Location of Site 1088 in relation to other ODP Leg 177 sites (1088 - 1094), major bathymetric features and oceanic frontal boundaries (after Gersonde *et al.*, 1999) Note: The position of previous ODP sites in the Southern Ocean sector of the South Atlantic Ocean are also given.

The Agulhas Ridge is an elongate topographic feature that parallels the Agulhas Fracture Zone and extends from the northern tip of the Meteor Rise to terminate abruptly at 40°S, 15°E, where it intersects the northern end of an abandoned spreading-ridge axis in the Agulhas Basin (Gersonde *et al.*, 1999). Formation of the Agulhas Ridge is hotly debated; theories include formation from extension at the fracture zone resulting in serpentinite diapirism (Bonatti, 1978), and volcanic construction resulting from extension and/or a mantle plume, such as the Shona Hotspot (Kastens, 1987; Hartnady and le Roex, 1985). A thick sequence of pelagic mud covers the basement rocks of the Agulhas Ridge.

1.3.2 Location and Modern Oceanographic Setting

ODP Site 1088 (41.8°S, 13.3°E) was drilled during Leg 177 in 2082 m water depth on the broad northeastern end of the Agulhas Ridge, in the Southern Ocean sector of the South Atlantic Ocean, c. 700 km southwest of the tip of South Africa (Fig. 1.6).

The southeastern South Atlantic is an important component of the global conveyor circulation, representing the junction point of major ocean currents and the initial entry point of North Atlantic Deep Water (NADW) into the Southern Ocean. Site 1088 is located in the northern Subantarctic Zone between the Subtropical Front (STF) and the Subantarctic Front (SAF) (Fig. 1.6). This site is influenced by distal eddies and filaments of the Agulhas Current retroflection (Diekmann and Kuhn, 2002). Site 1088 is one of the shallowest of sites in ODP Leg 177 (well above the regional CCD) and is located at the boundary between upper Circum Polar Deep Water (CPDW) and North Atlantic Deep Water (NADW) (Fig. 1.7).

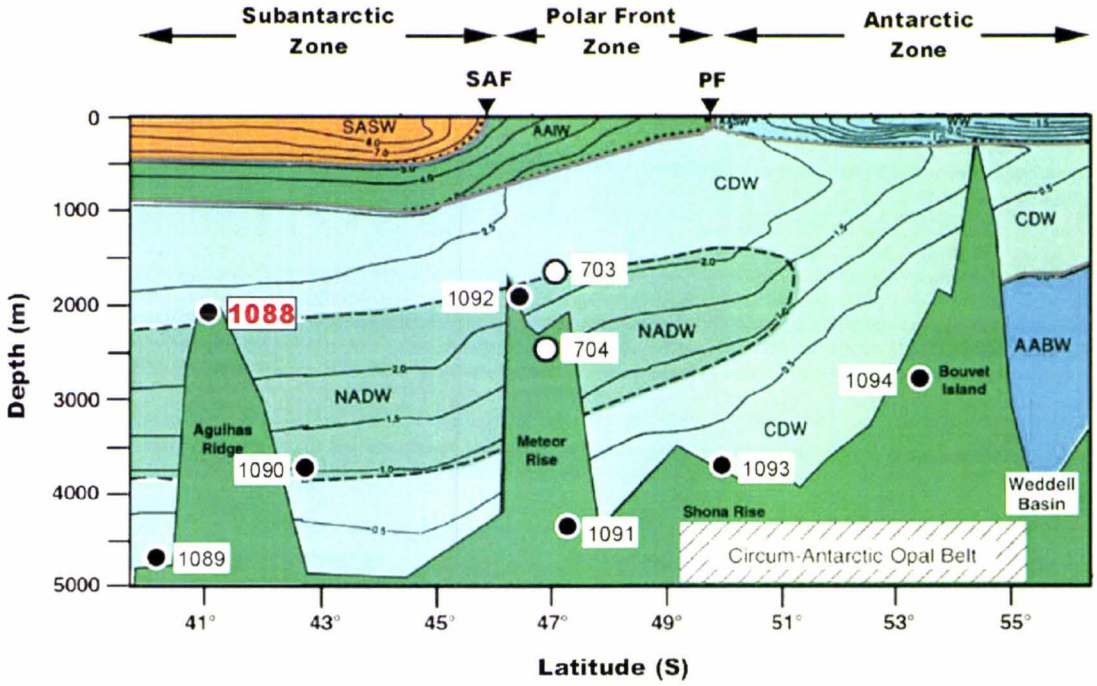

Figure 1.7: A cross-section of the present day intermediate- and deep-water masses, and frontal systems in the Southern Ocean sector of the South Atlantic Ocean, Site 1088 (modified from Gersonde *et al.*, 1999) AABW = Antarctic Bottom Water; CDW = Circum-polar Deep Water; NADW = North Atlantic Deep Water; AAIW= Antarctic Intermediate Water; SASW = South Atlantic Surface Water; SAF= Subantarctic Front; PF= Antarctic Polar Front

1.3.3 Past Oceanographic Changes

The unique location of Site 1088 gives great potential to reconstruct changes in the mean deep water mass composition over time, and elucidate past fluctuations in the production rate of Northern Component Water (NCW) (high latitude northern hemisphere sourced waters, such as the NADW), the strength of the NADW conveyor, and mixing ratios between NCW and Southern Component Water (SCW) (southern sourced waters, such as CPDW). Diekmann and Kuhn (2002) recognise two distinct modes of conveyor belt circulation in the study region during the MPT. The modern interglacial warm –route conveyor mode implies a far southward injection of relatively warm and saline NADW into the ACC, compensated to a large extent by the northward flow of warm surface and intermediate waters, which enter the South Atlantic via the Agulhas Current (Gordon *et al.*, 1992). The second mode of circulation occurred during glacial periods, when the cold-route conveyor mode is implied. This mode was characterised by prevailing cold southern-source water masses with a diminished NADW influx, in combination with only sporadic influence of the Agulhas Current leakage (Diekmann and Kuhn, 2002). These studies by Diekmann and Kuhn (2002) at nearby ODP Site 1090 revealed that glacial-interglacial contrasts in the regional

conveyor circulation strengthened across the MPT, roughly in accordance with global ice-volume fluctuations. Diekmann and Kuhn (2002) also inferred changes in deepwater circulation over the MPT using variations in sediment composition and clay mineralogy. Clay mineralogical studies revealed that Circumpolar Deep Water (CDW) expanded farther north during glacials after 1.2 Ma, further supporting the isotopic data of Venz and Hodell (2002)

1.3.4 Sediment Regime

Three holes were drilled representing a spliced record of 223.4 m, with the sediment investigated in this study, sampled between 5.39 and 14.38 mcd, being predominantly foraminifer-bearing nannofossil ooze (Gersonde *et al.*, 1999). Rock fragments interpreted as ice-rafted debris (IRD) occur at various frequencies down core. Site 1088 is situated northward of the Antarctic Polar Front (a zone centred at ~45°S with a latitudinal span of approximately ± 2.5° (Lutjeharms and Meeuwis, 1987)), such that glacial-interglacial migrations of this ecological and physical water mass boundary are unlikely to have had great influence on the biogenic sediment constituents at the site. Other than a slight shift in the area of dominant diatom deposition towards Site 1088, calcareous oozes, composed of calcareous phytoplankton (mainly coccoliths), calcareous zooplankton (mainly planktic foraminifera), form the biogenic component during both glacial and interglacial intervals (Diekmann *et al.*, 2003). Glacial-interglacial carbonate variations at Site 1088 are likely to be a result of dilution effects of biogenic and lithogenic sediment components, by changes in the mode of biological productivity and/or enhancement of terrestrial erosion and fluvial sediment supply during cold climate stages. During these stages, low stands of sea level facilitated glacigenic and fluvial sediment supply beyond the shelf and sediment gravity transport towards the deep sea. The water depth of < 3500 m places Site 1088 well above the regional lysocline, and thus the settling of calcareous particles is relatively unaffected by dissolution processes initiated by the glacial incursion of the corrosive CPDW. Furthermore, it has been inferred that improved carbonate preservation was likely at Site 1088 during the MPT, as slightly increased sedimentation rates (from 7 m/myr in the Pliocene, to 10 m/myr in the Pleistocene; Gersonde *et al.*, 1999) may promote survivability of calcareous particles.

Inorganic terrestrial sediment is sourced from the arid continental regions of South Africa and around the southern African margin, being supplied by the south-eastern trade winds, and to a lesser extent, through fluvial input and ocean currents. The latest findings from ODP Site 1090, which is situated to the west of Site 1088, have shown that fluctuations in illite chemistry (representing the major clay mineral from South Africa) are consistent with climatic oscillations in southern Africa (Diekmann and Kuhn, 2002). These studies reveal that abundant iron-bearing illite is indicative of arid conditions with prevailing physical weathering, typical of glacial intervals, whereas chemical weathering under humid interglacial conditions attacks and depletes iron-bearing illites and favours more stable Al-illites. Other significant studies, such as fluctuations in the ratio of kaolinite to chlorite, can be used to demonstrate changing source region of river particulates and latitudinal shifts in watermass boundaries. For example high kaolinite/chlorite ratios demonstrate Site 1088 was within the reaches of the Agulhas Current retroflection (Diekmann *et al.*, 2003).

A study of ice-rafted debris (IRD) delivery to the South Atlantic was undertaken by Kanfoush *et al.* (2000), in order to reconstruct the distribution of IRD across the PFZ. In the South Atlantic, IRD peaks reflect instability of ice shelves in the Weddell Sea region, and are associated with interstadial warm periods, and increased NADW production in the North Atlantic (Gersonde *et al.*, 1999) Kanfoush *et al.* (2000) revealed that the first identifiable IRD above background levels occurred at southerly ODP Site 1092 (~47°S) (Fig. 1.6) in the late Pliocene (~3.18 Ma), yet across the MPT there was no change in the amplitude or pacing of IRD delivered to the site. IRD has not been previously studied at Site 1088.

1.4 Previous Paleoceanographic Studies

1.4.1 Southeastern Atlantic Site 1082

The upwelling system associated with the Benguela Current is one of the most productive areas of the modern ocean, and as a consequence has been the focus of several studies into the evolution of upwelling and changes in productivity over geological time. Sediments from Deep Sea Drilling Project (DSDP) Sites 362 and 532 (1325 m and 1331 m water depth, respectively) (Fig. 1.1), which are close to Walvis Ridge ODP Sites 1081 and 1082, have provided a preliminary record of the evolution of upwelling and changes in biological productivity of the upwelling system.

Site 362 was rotary drilled during DSDP Leg 40 in 1975, resulting in all of the cores taken above a sub-bottom depth of 200 m being badly disturbed. Despite this, Siesser (1980) was able to conclude from changes in organic carbon and diatom abundances from Site 362 that upwelling-enhanced productivity had gradually increased since the onset of the Benguela upwelling system ~10 Ma (Miocene).

Hydraulic piston coring of Site 532 was undertaken in 1980, and yielded a more complete record of upwelling history (Hay and Brock, 1992). Peaks in concentrations of organic carbon and diatoms indicated that productivity also peaked at the Walvis Ridge location in the late Pliocene to early Pleistocene (Dean *et al.*, 1984). Further, Site 532 also revealed light-dark alternations in sediment colour, corresponding to changes in the concentrations of organic carbon, calcium carbonate, and clay minerals. Diester-Haass *et al.* (1986, 1992) conclude these colour changes record glacial-interglacial shifts of the Benguela Current, sea-level changes, oxidation strength, and source of terrigenous clastic sediment components.

Reconstructing the glacial-interglacial shifts in upwelling intensity were of high priority in studies by Durham *et al.* (2001). Preliminary investigations at ODP Sites 1081 and 1082 generally provide evidence for increased productivity during glacial periods. There is a prominent peak in all proxy records of productivity at 1100 ka that coincides with a maximum abundance of diatoms. This diatom abundance is observed in many records from the South Atlantic (Berger and Wefer, 1996) and is followed by a decrease

in abundance. Following this there is a rapid change in the dominant microfossil, with the abundance of foraminifera beginning to increase. The timing of these changes in productivity suggests that they may be related to the MPT.

The terrigenous input signal of the Walvis Ridge sites has also been a focus of previous study (Diester-Haass *et al.*, 1988). As expected, magnetic susceptibility records of Site 532 revealed increased terrigenous input during glacial periods in association with global cooling and enhanced aridity, leading to an increase in the supply of aeolian material. In the case of the Walvis Ridge location, aeolian transport from the Namib Desert by northeasterly to easterly winds was enhanced during glacial times (Durham *et al.*, 2001). In addition, Diester-Haass *et al.* (1988) suggested that the lowering of sea-levels in response to global cooling and increased ice volume during glacial periods, left greater areas of the continental shelf and slope exposed to erosion, which forms an important component of terrestrial input to Walvis Ridge sites. Studies by Diester-Haass *et al.* (1986) and Lutjeharms and Meeuwis (1987), revealed two contrasting terrigenous signals, one evident pre-MPT (prior to ~1200 ka), and another dominating the Walvis Ridge in the last 800 ka. Clay mineralogical evidence at DSDP Site 532 revealed that over the past 800 ka, supply of terrigenous material to the ridge has been a mix of reworked material from the continental shelf and material from the Orange River to the south, transported to the ridge by the intensified strength and flow of the Benguela Current during glacial periods (Lutjeharms and Meeuwis, 1987). In contrast, an opposite signal was evident in the pre-MPT period (prior to ~1200 ka), where mineralogy suggests increased terrigenous material during interglacial periods. This suggested that the supply of terrigenous material via aeolian input may have only been significant at the Walvis Ridge in the last 800 ka, implying that prior to this period a different source of terrigenous material played a major role. Further studies by Diester-Haass *et al.* (1986) revealed that the fluctuating position of the Angola-Benguela Front (ABF) (which controls the latitude at which the Benguela Current turns west, and the southerly extent of the southward-flowing Angola Current) (Fig. 1.3) influenced the source of terrigenous materials to the ridge. Kaolinite concentrations in interglacial sediments in the 1500 to 1000 ka period show a source of terrigenous material from the Kunene River, inferring that during this time the ABF may have been far enough south to allow supply and transportation to the Walvis Ridge via the Angola Current (Fig. 1.3). The timing of this change in supply and source of terrigenous input to the Walvis

Ridge coincided with the onset of the MPT. The associated increase in aridity of the African continent during this time may also have caused a decrease in the flow of the Kunene River (Durham *et al.*, 2001).

1.4.2 Southern Ocean sector Site 1088

Previous deep-sea drilling in the Southern Ocean include DSDP Leg 71 (Sites 511-514); ODP Legs 113 (Sites 689-697), 114 (Sites 698-704), 119 (Sites 739-746), and 120 (Sites 747-751), some of which are shown in figure 1.6. Sections recovered have provided a basic understanding of the paleoceanographic and paleoclimatic evolution of the southern high latitudes during the Cenozoic, but often core sections from previous Antarctic drilling are incomplete. Furthermore, cores are easily disturbed when recovered from the hostile seas of the Southern Ocean (Gersonde *et al.*, 1999). As a result of incomplete core recovery, disturbance, the presence of hiatuses, and diminished $CaCO_3$ preservation potential at high latitudes, efforts to obtain continuous paleoclimatic records in the Southern Ocean have been few and far between. Compared with the excellent records now available from the high-latitude North Atlantic Ocean, prior to Leg 177, the South Atlantic sector of the Southern Ocean had an obvious deficiency in the distribution of ocean-drilled cores, with relatively few continuous late Neogene records recovered. Of the 32 sites drilled during legs 113, 114, 119, and 120, only Site 704 (Leg 114) (Fig. 1.6) had sufficient stratigraphic continuity in the Plio-Pleistocene interval to allow for high-resolution paleoceanographic and paleoclimatic studies (Hodell and Venz, 1992). Thus, one of the primary aims during Leg 177 was to fill a critical gap in the distribution of drilled ocean sites to decipher the role the Southern Ocean had in the Quaternary history of the Earth's climatic system.

ODP Site 704 is positioned in the eastern Subantarctic South Atlantic (46°52.8'S, 7°25.3'E) (Fig. 1.6), within the mixing zone of the North Atlantic Deep Water (NADW) and Circum Polar Deep Water (CPDW), just north of the Antarctic Polar Front Zone (PFZ). The PFZ separates cold, nutrient-rich Antarctic surface water to the south from warmer, Subantarctic surface waters of lower nutrient status, to the north. Furthermore, the PFZ represents a transition zone from pure diatom ooze to the south near the Antarctic Polar Front to a mixed siliceous-calcareous ooze to the north near the Subantarctic Front (Hodell and Venz, 1992). Values of the $\delta^{18}O$ of precipitated calcite

demonstrate the PFZ is also a region of steep temperature gradients, and as a result, even subtle changes in the position of the PFZ can be recorded by the $\delta^{18}O$ of planktic foraminifers.

Isotopic data from Site 704 provided new insights into the climatic evolution of the Southern Ocean during the Plio-Pleistocene. Global climate is generally considered to have been warmer than today during the Pliocene (prior to 3.2 Ma), and the cryosphere is believed to have been unipolar and restricted to Antarctica (Hodell and Venz, 1992). During this time the amplitude of the planktic and benthic $\delta^{18}O$ signals was low (~0.5‰), accommodating some warming and minor deglaciation during the Pliocene. However, records are inconsistent with major warming and massive deglaciation of the Antarctic continent. Isotopic records from Site 704 suggest that the Antarctic glacier system did not fluctuate on a large scale prior to 3.2 Ma, rather, it was not until the late Gauss (2.7-2.4 Ma) (when the large Northern Hemisphere ice sheets developed), that the Southern Ocean underwent a major climatic transition. During this time faunal assemblages indicate the northwards advance of the PFZ and the accumulation of IRD in the Subantarctic sector. It is also thought that the lowering of sea level by increased ice in the northern hemisphere stimulated ice advance along the Antarctic margin. In addition, increased glacial suppression of NADW after 2.7 Ma may have decreased the heat flux to the Southern Ocean (Hodell and Venz, 1992). Carbon isotopic gradients between the North Atlantic (Site 607), the Southern Ocean (Site 704) and the Pacific (Site 677) suggest that the suppression of NADW intensified greatly during glacial periods after marine oxygen isotope (MIS) stage 52 (1.55 Ma), which in turn is attributed to an increase in the amplitude of the Earth's obliquity cycle (Hodell *et al.*, 2003).

Documentation of IRD, including Heinrich Events, in the North Atlantic has contributed greatly to our understanding of Laurentide Ice Sheet dynamics (Venz and Hodell, 2002). Kanfoush *et al.* (2000) found similar evidence for millennial-scale variability in the Antarctic Ice Sheet, through discrete episodes of IRD deposition throughout the last glaciation and over the last four climate cycles. The study of IRD delivery to the South Atlantic at Site 1094 (54°S) found that the last four glacial cycles were marked by high IRD abundance during the latter half of the interglacial period or onset of neoglaciation (composed predominantly of volcanic ash (source believed to be South Sandwich

Islands in the Scotia arc) and quartz with minor amounts of fine-grained volcanics, coarse-crystalline rock fragments, and mica); possibly reflecting the instability of the ice shelves in the Weddell Sea region (Venz and Hodell, 2002).

1.5 Mid-Pleistocene Climatic Transition

The mid-Pleistocene Climate Transition (MPT) is the name given to the period of time when the dominant periodicity of glacial-interglacial cycles changed from the 41-kyr obliquity signal to the 100-kyr eccentricity signal (Durham *et al.*, 2001). Broecker and van Donk (1970) described it as the transition observed in proxy climate records from symmetrical low-amplitude, high-frequency (41-kyr) ice volume variations to high-amplitude, low-frequency (100-kyr) asymmetrical saw-toothed ice volume variations indicating gradual ice build-up terminated by rapid deglaciation events. During the MPT, glacial-interglacial contrasts became more severe and the 100-kyr climate cycles developed their distinctive asymmetric pattern of the late Quaternary, resulting in a change in the mean state of the global climate system, including lower global temperatures, increased global ice volume, and lower sea-surface temperatures (Shackleton *et al.*, 1990).

The MPT occurred over several hundred thousand years (between c. 1200 and 600 ka) and is documented by benthic foraminiferal $\delta^{18}O$ records in marine sediments from the world's oceans. Benthic foraminiferal $\delta^{18}O$ records document a general increase in global ice volume and the onset of weak 100-kyr cycles between 1250 ka and 900 ka and the establishment of strong 100-kyr cycles since 600 ka (Ruddiman *et al.*, 1989; Imbrie *et al.*, 1993; Berger *et al.*, 1994; Chen *et al.*, 1995; Mudelsee and Schulz, 1997). Ruddiman *et al.* (1989) and Mix *et al.* (1995) report a benthic $\delta^{18}O$ increase of approximately 0.29‰ at ~920 ka, which corresponds to a sea level fall of about 30 m.

During the same time interval significant changes in carbon cycling was occurring, including changes in the mean ocean $\delta^{13}C$, probably caused by the addition of terrestrial carbon to the ocean-atmosphere reservoirs as global aridity increased (Raymo *et al.* 1997). Positive feedbacks to the CO_2 budget on earth, an increase in carbon in the marine realm (from increased primary production and transport from continental shelf to deep sea), along with many other factors, are thought to have affected deep-water physical and chemical composition in the North Atlantic (NADW) and subsequently the global thermohaline circulation of the oceans.

The timing, duration, and the cause of the MPT is yet to be adequately explained. It is, however, known that the MPT was a global event, and its occurrence has been well documented in both marine and continental records worldwide. The problem lies in identifying a mechanism that would amplify the climate system's response to relatively weak insolation forcing. The MPT demonstrates that the causal link between insolation and ice volume suggested by Milankovitch (1930) is, in fact, much more complex than it may first appear. During the Pliocene and early Pleistocene it appears that a linear relationship between orbital forcing, ice volume and climate variations existed (Imbrie *et al.* 1993). Yet, reconstructions of insolation values by Berger and Loutre (1991) suggest that there is no significant change in the pattern of insolation at the time of the MPT to account for the transition observed in climatic variations from 41- to 100-kyr cycles. The lag between ice growth at 920 ka and the establishment of strong 100-kyr world at ~650 ka, further complicates the problem, indicating decoupling between ice volume and the 100-kyr cycle.

1.6 Previous Studies on the Extinction of deep-sea Benthic Foraminifera

1.6.1 Cenozoic Turnover of Benthic Foraminifera

Three periods of increased taxonomic turnover and in faunal abundance changes in deep-sea foraminifera during the Cenozoic have been identified globally (Thomas, 1992; Miller *et al.*, 1992): the Paleocene-Eocene boundary, Eocene-Oligocene boundary, and middle Miocene. Of these, the first, resulted in the most severe extinctions of benthic foraminifera (loss of 30-50% of species; Thomas, 1992; MacLeod *et al.*, 2000) during the Paleocene-Eocene thermal maximum (PETM, ca. 55 Ma). This extinction has been attributed to an abrupt warming and change in ocean circulation due to circulation of oxygen-poor, warm, corrosive bottom waters, coupled with changes in primary productivity in the surface waters (Katz *et al.*, 1999). The second and third periods of increased taxonomic turnover the 36-30 Ma and 16-12 Ma were more gradual, correlating with a decrease in high latitude and deep-water temperatures (Shackleton and Kennett, 1975; Thomas, 1992), and a shift in $\delta^{13}C$ values (initiated by changes in surface ocean productivity), respectively.

1.6.2 Mid-Pleistocene Extinction of Benthic Foraminifera

The mid-Pleistocene extinction or "*Stilostomella* extinction event" (Weinholz and Lutze, 1989) has now been recognised as the most recent turnover in benthic foraminiferal taxa. First documented in DSDP Site 397 off north-west Africa in the Atlantic Ocean (Lutze, 1979), it marks the final phase in the progressive decline of elongate cylindrical taxa (belonging to the families Stilostomellidae, Pleurostomellidae and uniserial Nodosariidae). It includes the extinction of all elongate, cylindrical, uniserial, biserial or multiserial tests with highly specific apertural characteristics: i.e. cribrate (*Chyrsalogonium, Cribronodosaria*), slit lunate, hooded with two teeth (Pleurostomellidae), or secondarily toothed, necked (Stilostomellidae) apertures (Hayward, 2002). These fauna reached their greatest abundance (up to 70% of benthic foraminiferal faunas) in the latest Eocene (40-35 Ma), forming a significant proportion of middle bathyal to upper abyssal (c. 500-3000 m depth) benthic foraminiferal faunas (Thomas *et al.*, 2000). Since the latest Eocene this group of elongate taxa has

progressively declined in abundance and diversity, with strongest declines occurring during the late Eocene-early Oligocene cooling when the East Antarctic Ice Sheet formed (Thomas and Vincent, 1987), and the late middle Miocene cooling, related to the expansion of the West Antarctic Ice Sheet (Thomas 1987, 1992). The final demise of the Extinction Group taxa, called the "*Stilostomella* extinction", reported here, occurred between 1000 and 600 ka (Lutze, 1979; Weinholz and Lutze, 1989; Schönfeld, 1996), and has been hypothesized to be related to the intensification of Northern Hemisphere glaciation, and associated changes in the oxygenation of bottom-water masses and food supply fluctuations.

Figure 1.8 illustrates the global locations of deep-sea ODP and DSDP sites in which the "*Stilostomella* extinction" event has previously been documented. Lutze (1979) identified the decline and extinction of 10 benthic foraminiferal species from six genera (e.g. *Stilostomella, Orthomorphina, Plectofrondicularia, Ellipsoglandulina, Nodogenerina,* and *Pleurostomella*) between 1000 and 600 ka in DSDP 397 off northwest Africa in the Atlantic Ocean.

When Weinholz and Lutze (1989) undertook a detailed investigation of DSDP 658 and 659, off west Africa they initiated the term "*Stilostomella* Extinction", named after the family Stilostomellidae which disappeared at this time; which has been used since to describe this global benthic foraminiferal extinction event. Their study revealed the diachronous nature of the faunal boundary, with highest occurrence datums (HOs) of the Extinction Group taxa spanning some two hundred thousand years (810 - 640 ka), the timing differing between sites and water depth. An important discovery made by Weinholz and Lutze was that the final extinction of the taxa appeared to be c. 100 kyr earlier in the deeper water (DSDP 659, 3081 m) than shallower (DSDP 658, 2263 m).

Gupta (1993) then confirmed the decline in relative abundance and eventual demise of *Siphonodosaria lepidula* (as *Stilostomella lepidula*) in the Pliocene and Pleistocene of two DSDP sites (DSDP 214 and 219) in the Indian Ocean. Benthic census data showed a progressive decline in relative abundance of *Siphonodosaria lepidula*, from greatest abundance during the late Pliocene (3.2-1.8 Ma), comprising 10-20% of the benthic foraminiferal fauna >150 μm, to an abrupt decrease and regional disappearance at ~ 730 ka, near the Brunhes/Matuyama boundary (780 ka).

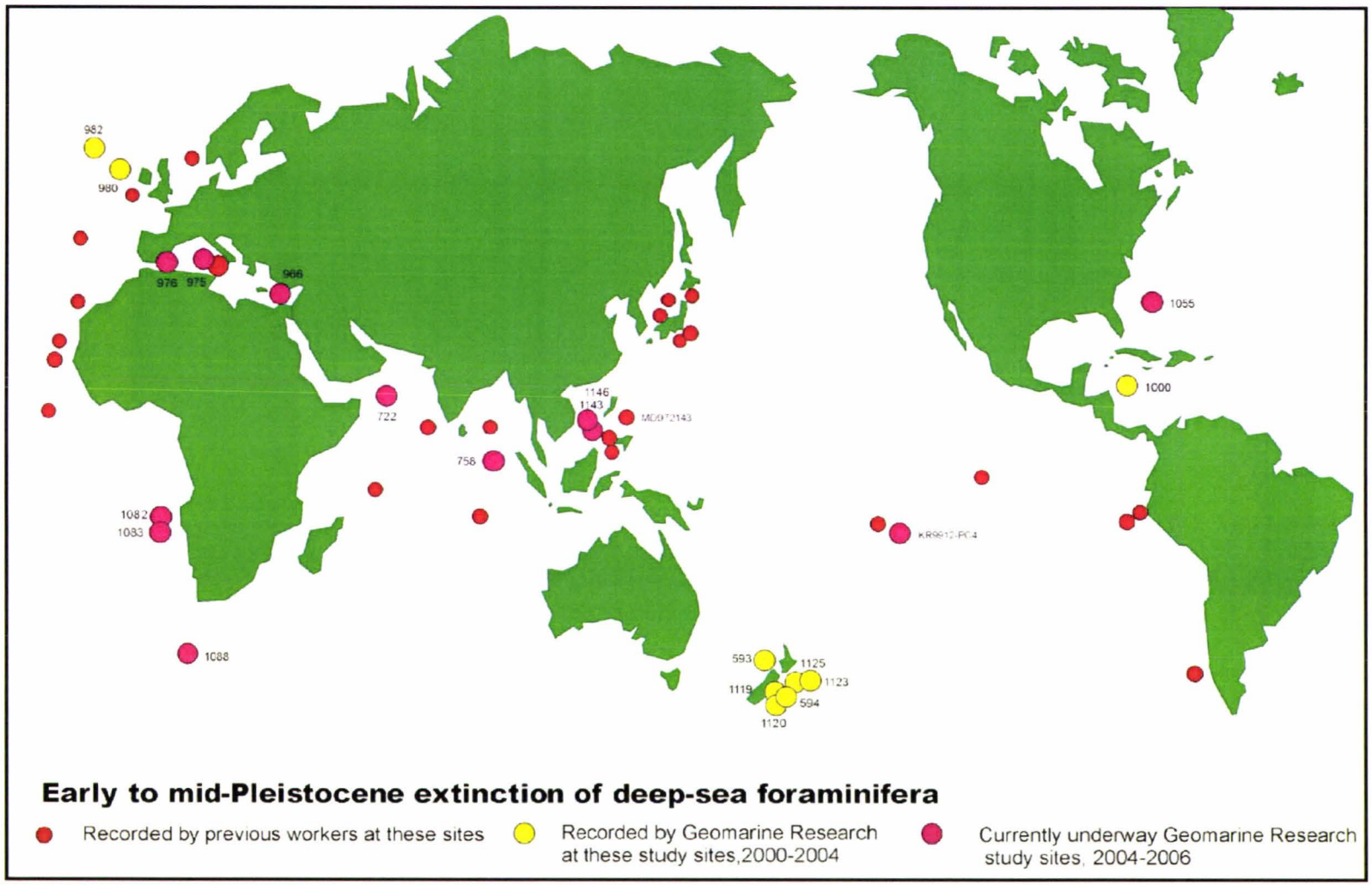

Figure 1.8: Global location of ODP and DSDP sites in which the "*Stilostomella* extinction" has previously been documented (modified after Hayward, 2002).

In the Pacific Ocean the "*Stilostomella* extinction" has been recognised in the northwest (Kaiho, 1992; Keller, 1980; Jian *et al.*, 2000), central (Schönfeld, 1995), southeast (Schönfeld and Spiegler, 1995) and southwest (Hayward, 2001, 2002).

Schönfeld (1996) reviewed all known records of the mid-Pleistocene extinction event, which confirmed the extinction (HOs) of the relevant species of elongate benthic foraminifera between 1000 and 600 ka (predominately 800 to 700 ka) with highly variable timings. He noted the diachronous nature of highest occurences in sites only a few tens or hundreds of kilometres apart, e.g. DSDP 658 and 659, or 548 and 549, in the Central and North Atlantic Ocean, with HOs of *Siphonodosaria lepidula* differing by 166,000 and 155,000 years respectively (Schönfeld, 1996). Schönfeld also concluded that regional extinctions took place earlier in water depths below 3500 m, farther offshore, and at mid- to low southern latitudes, possibly linking rapid changes in deep-water formation and ventilation with the "*Stilostomella* extinction".

Hayward (2001, 2002) undertook the first detailed "*Stilostomella* extinction" study which included the decline and extinction of the rare and small taxa (>63 μm), which had been overlooked in most previous studies. Hayward (2002) revealed that in the southwest Pacific, the total abundance of Extinction and Die-back Group specimens decline dramatically during the early and middle Pleistocene (1200-700 ka), the rate of decline is not uniform but pulsed, often with major declines coinciding with the onset of cold intervals. Further, Hayward (2002) concluded that in the southwest Pacific, the local disappearances of the Extinction Group species occurred earlier in deeper and cooler water locations (earliest site ODP 1123 and latest site ODP 1125), suggesting the pattern may be related to food supply. Contrary to Schönfeld's conclusion of highly variable youngest occurrence timings of the Extinction Group taxa (900-600 ka, Schönfeld, 1996), Hayward's southwest Pacific sites revealed a highly consistent final disappearance of the taxa, constraining the *Stilostomella* extinction datum to 650-570 ka, despite differences in depth.

Most recently, Kawagata *et al.* (in press) document the extinctions of deep-sea benthic foraminifera in the North Atlantic Gateway. ODP Sites 980 and 982, located in intermediate water depths in the northern North Atlantic, are close to the present formation area of North Atlantic Deep Water (NADW). Both cores reveal the

progressive decline and eventual regional extinction of 51 species of elongate, cylindrical benthic foraminifera, with the majority of Extinction Group taxa (~96%) having HOs between 1200 and 700 ka. The last of these species to disappear in the North Atlantic was *Pleurostomella alternans* at ~679 ka and ~694 ka in Sites 980 and 982, respectively. These North Atlantic studies are in good agreement with the previously documented final global "*Stilostomella* extinction" datum of 700-580 ka (Weinholz and Lutze, 1989; Kaiho, 1992; Gupta, 1993; Schönfeld, 1996; Hayward, 2001, 2002). They concluded that changes in chemical ventilation of the bottom water and food supply to the sea floor might have decimated the elongate, uniserial deep-sea foraminifera during the MPT.

1.7 Marine Oxygen Isotope Stages

The Milankovitch theory of climate change, linking variations in the Earth's orbital parameters to climate fluctuations, continues to gather support as the primary driver for glacial and interglacial climatic cycles. Much of the climatic cyclicity that is documented in the marine sedimentary record over the past 1 million years can be explained by linear responses of climate to the 41,000-year orbital obliquity and 23,000-year orbital precession cycles. The increasing availability of long, high quality ODP cores has made it possible to monitor spectral signals and phase relationships back beyond the Miocene. However, orbitally modulated fluctuations of solar irradiance alone cannot explain the longer-term evolution of the Earth's climate system. An important component in the long-term Cenozoic cooling trend was plate tectonics, namely its influence on mountain uplift and ocean circulation. There is now abundant evidence that the reconfiguration of oceans and continents, notably the opening and closure of oceanic gateways, and associated change in thermohaline circulation and heat transport, set the stage for northern hemisphere glaciation (Imbrie *et al.*, 1993). Thermohaline forcing through changes in deep water temperature has been proposed by Imbrie *et al.* (1993) to be one possible driver of the 100,000-year climate cycle. Further studies involving high-resolution correlations between ice core paleoclimate records and the marine $\delta^{18}O$ record support not only a dominant greenhouse forcing (Shackleton, 2000), but also reveal a lag period between ice volume (as seen in the marine record) and atmospheric CO_2 changes. Such evidence favours atmospheric CO_2 as the primary player during the long-term cycles of glacial-interglacial climatic change (Shackleton, 2000).

The marine oxygen isotope stage numbering system that is used throughout this thesis is based upon the timescale calibrated by Chen *et al.* (1995), for the 0-1.8 Ma period (Fig. 1.9). Chen *et al.* (1995) use the $\delta^{18}O$ records from the benthic foraminiferal species *Cibicides wuellerstorfi* to simulate orbitally-induced ice volume changes over the past 3.6 Ma (ODP 758). The marine isotope stages (MIS) are recognised in the glacial and interglacial periods based on the downcore variation of the $\delta^{18}O$ of foraminifera and are labelled using conventional notations of even numbers for glacial stages and odd numbers for interglacial stages.

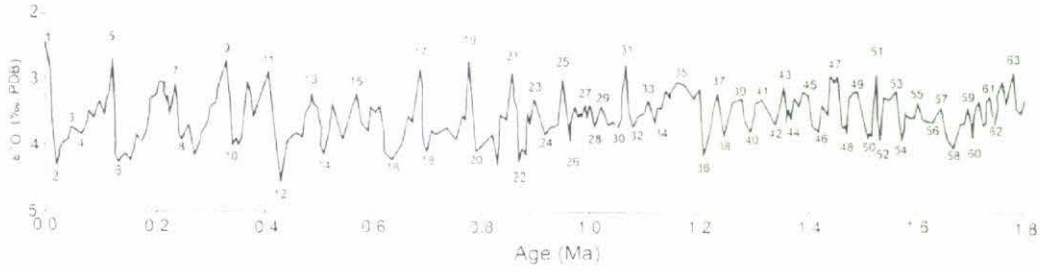

Figure 1.9: Calibrated ages for marine isotope stages (MIS) for last 1.8 Ma, using ice volume simulation (*from* Chen *et al.*, 1995).

2. ODP METHODS

2.1 ODP Drilling Operations

As with all coring operations, the recovery of complete sedimentary sections within the cored intervals was crucial to the paleoceanographic objectives of Leg 175 and 177. Two coring systems were utilised during drilling of Site 1082 and 1088: the advanced hydraulic piston corer (APC) and the extended core barrel (XCB); both were used to maximise core recovery in the specific lithology being drilled. Each cored interval was approximately 9.5 m long, which is the length of the core barrel.

Three holes were cored with the APC/XCB at Site 1082 to a maximum depth of 600.6 metres below seafloor (mbsf) (The term 'mbsf' is the depth from the seafloor to the interval being cored). Hole 1082A was cored with the APC to 128.6 mbsf and was extended with the XCB to a depth of 600.6 mbsf (Wefer *et al.*, 1998). Cores from 1082B and 1082C were taken with the APC to depths of 127.0 mbsf and 202.0 mbsf, respectively (Fig. 2.1).

Three holes were drilled at Site 1088 to a total depth of 233.7 mbsf, recovering Holocene to middle Miocene calcareous ooze. Hole 1088A was unsuccessful, because when the core was recovered it was full of disturbed sediment (Gersonde *et al.*, 1999). Hole 1088B was drilled by APC down to 129 mbsf and Hole 1088C, which was drilled without coring to 124 mbsf, was continuously cored by XCB from 124 mbsf down to 233 mbsf.

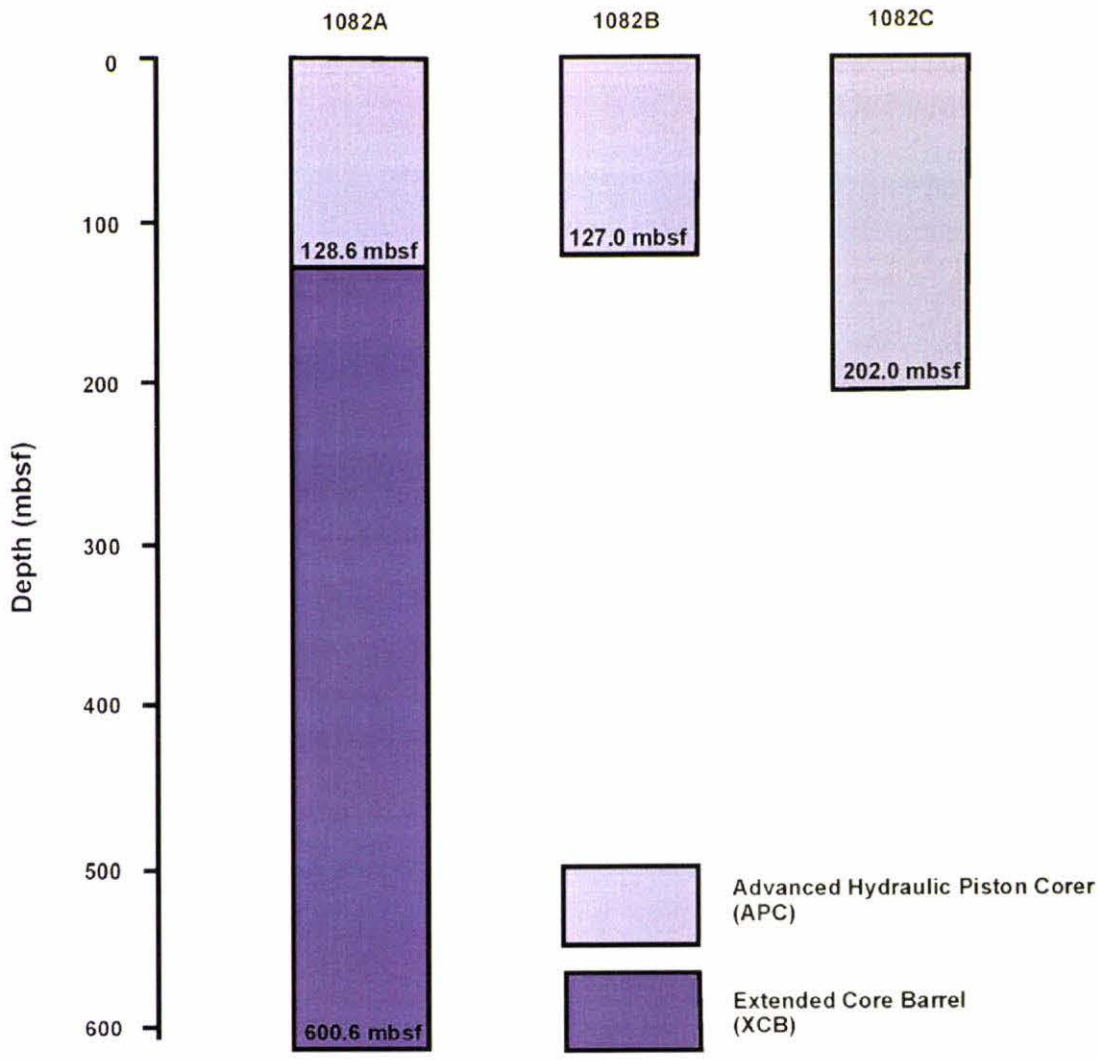

Figure 2.1: Relative core lengths and method of drilling. Example from Site 1082 (mbsf = metres below seafloor).

As with previous ODP legs, multi-hole drilling and composite depth sections were compiled at both Sites 1082 and 1088. Drilling of multiple holes ensures that intervals missing from one hole as a result of recovery gaps between cores are cored in an adjacent hole, thus ensuring the most complete record of continuous sedimentation at the site. Composite sections are constructed through various shipboard measurements that are made as soon as the core sections have equilibrated to room temperature. Before splitting, whole-round core sections were run through the multi-sensor track (MST) and thermal conductivity measurements were taken. Magnetic susceptibility, gamma-ray attenuation (GRA), wet bulk density (GRAPE), and colour reflectance parameters were all used to develop inter-hole correlations across gaps between cores,

with the integration of at least two physical properties allowing hole-to-hole correlations to be made with greater confidence. All composite section data were collected at 2-cm (MST) and 4-cm (colour reflectance and GRAPE bulk density) intervals, and data presented in composite depth scale (Fig. 2.2 - 1082 (MST and colour reflectance) and Fig. 2.3 - 1088 (MST, colour reflectance and GRAPE bulk density)).

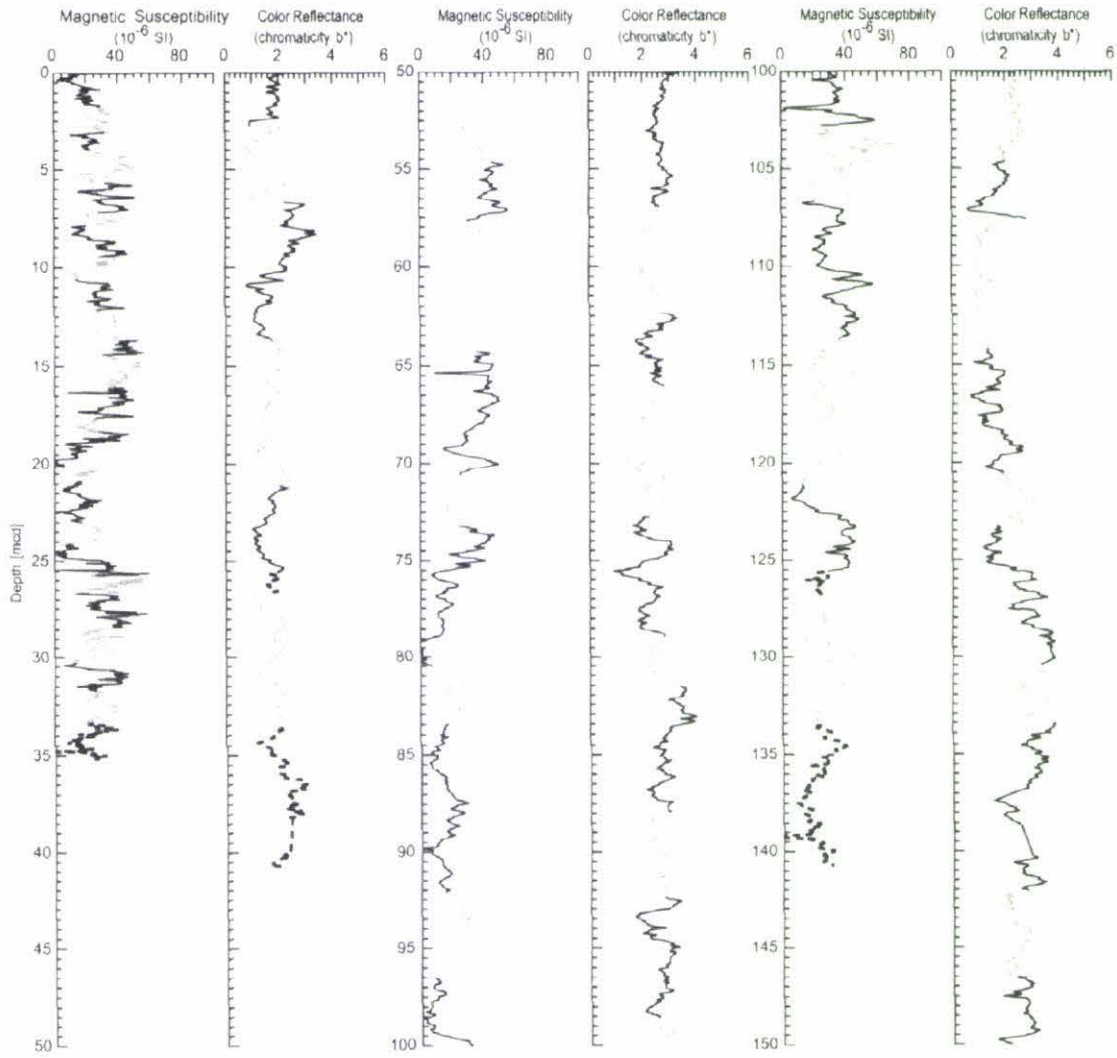

Figure 2.2: Spliced section for magnetic susceptibility and colour reflectance of Site 1082 (from Wefer *et al.*, 1998). Depth is given in mcd = metres composite depth.

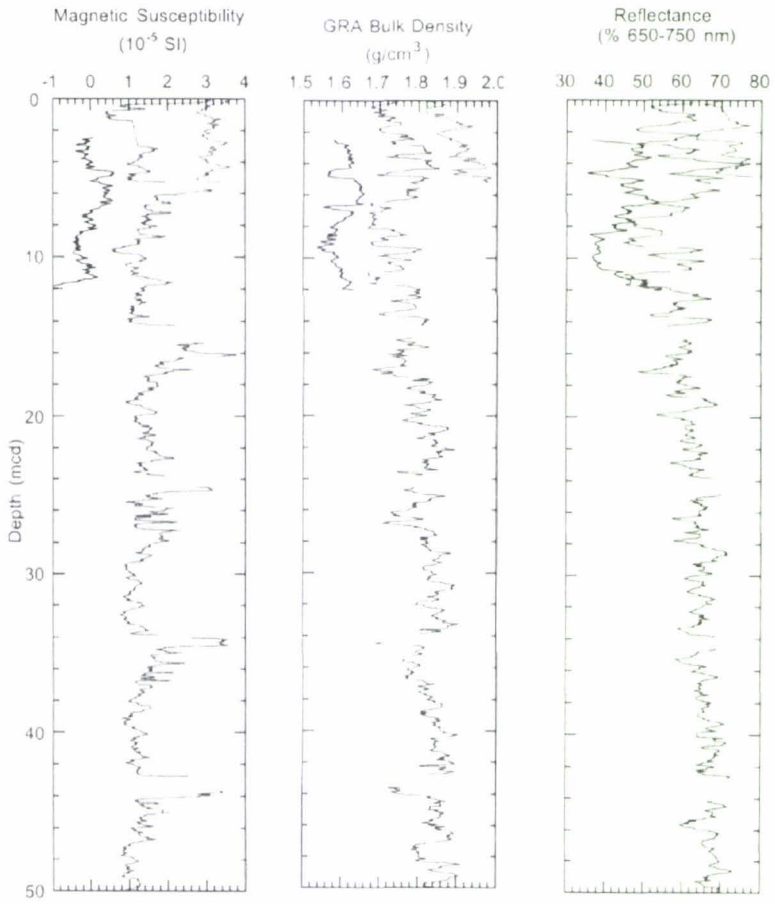

Figure 2.3: Composite section for magnetic susceptibility, bulk density and colour reflectance of Site 1088 (*from* Gersonde *et al.* 1999). Holes 1088A (left curve), 1088B (middle curve), and 1088C (right curve) are horizontally offset from each other by: 2.0 x 10^{-5} SI units (for magnetic susceptibility); 0.15 g/cm^3 (for GRA bulk density); and 15% (for colour reflectance). Depth is given in mcd = metres composite depth.

Once data had been collected, hole-to-hole correlations were made using an interactive software programme "Splicer", and 'tie points' or identifiable intervals where distinctive features are present in multiple holes, resulting in a single spliced record for each site given in an adjusted depth scale known as 'mcd' or mean composite depth. Site 1082 yielded a complete spliced section to 141 mcd (core recovery was relatively poor below this but some MS and colour reflectance data is available), and Site 1088 yielded a total thickness of 224 mcd. An example of the use of tie points in the Site 1082 continuous "spliced" stratigraphic sequence is shown in table 2.1.

Hole, core, section, interval (cm)	Depth (mbsf)	Composite depth (mcd)	Whether tied	Hole, core, section, interval (cm)	Depth (mbsf)	Composite depth (mcd)	Offset (m)
1082A-1H-5, 90	6.90	6.90	Tie to	1082B-2H-2, 93	6.14	6.90	0.76
1082B-2H-6, 36	11.56	12.32	Tie to	1082A-2H-3, 32.5	11.13	12.32	1.19
1082A-2H-5, 120	14.80	15.99	Tie to	1082B-3H-2, 31.5	15.03	15.99	0.96
1082B-3H-6, 108	21.78	22.74	Tie to	1082A-3H-3, 26.5	20.37	22.74	2.37
1082A-3H-7, 78	26.48	28.85	Tie to	1082B-4H-3, 61	26.32	28.85	2.53
1082B-4H-5, 32	29.02	31.55	Tie to	1082A-4H-2, 70.5	28.91	31.55	2.64
1082A-4H-7, 4	35.24	37.88	Tie to	1082B-5H-2, 55.5	34.27	37.88	3.61
1082B-5H-5, 56	38.76	42.37	Tie to	1082A-5H-2, 92.5	38.63	42.37	3.74
1082A-5H-7, 8	44.78	48.52	Tie to	1082B-6H-2, 84	44.04	48.52	4.48
1082B-6H-6, 96	50.16	54.64	Tie to	1082A-6H-3, 102.5	49.63	54.64	5.01
1082A-6H-5, 120	52.60	57.61	Tie to	1082B-7H-1, 35.5	51.57	57.61	6.04
1082B-7H-5, 100	58.20	64.24	Tie to	1082A-7H-3, 2.5	58.33	64.24	5.91
1082A-7H-7, 30	64.60	70.51	Tie to	1082B-8H-2, 42.5	62.63	70.51	7.88
1082B-8H-4, 12	65.32	73.20	Tie to	1082A-8H-3, 24.5	66.76	73.20	6.44
1082A-8H-8, 4	74.05	80.49	Tie to	1082B-9H-1, 52	70.72	80.49	9.77
1082B-9H-3, 48	73.68	83.45	Tie to	1082A-9H-1, 52	74.82	83.45	8.63
1082A-9H-7, 36	83.46	92.09	Tie to	1082B-10H-2, 31.5	81.53	92.09	10.56
1082B-10H-5, 24	85.94	96.50	Tie to	1082A-10H-3, 114.5	86.89	96.50	9.61
1082A-10H-8, 12	93.16	102.77	Tie to	1082B-11H-1, 90.5	90.11	102.77	12.66
1082B-11H-4, 28	93.98	106.64	Tie to	1082A-11H-1, 118.5	94.49	106.64	12.15
1082A-11H-6, 92	101.57	113.72	Tie to	1082B-12H-1, 22.5	98.93	113.72	14.79
1082B-12H-6, 4	106.24	121.03	Tie to	1082A-12H-4, 72	106.56	121.03	14.47
1082A-12H-7, 92	111.11	125.58	Tie to	1082C-13H-4, 92	108.42	125.58	17.16
1082C-13H-5, 60	109.60	126.76	Tie to	1082B-13H-2, 94.5	110.65	126.76	16.11
1082B-13H-7, 28	117.48	133.59	Tie to	1082C-14H-2, 120	115.20	133.59	18.39
1082C-14H-7, 84	122.34	140.73					

Table 2.1: Example of splice tie points used to create the continuous "spliced" stratigraphic sequence for Site 1082 (*from* Wefer *et al.*, 1998). mbsf = metres below seafloor; mcd = metres composite depth.

Once the cores were split into working and archival halves, the working half of each core was sampled for both shipboard analysis, such as physical properties (for formation of a spliced section as mentioned above), carbonate, colour reflectance, bulk X-ray diffraction (XRD) mineralogy, and shore-based studies. The archive-half sections were passed through the cryogenic magnetometer, then black-and-white and colour photographed, and described visually and by means of smear slides (Gersonde *et al.*, 1999). Once shipboard analysis was complete both halves of the core were placed into labelled plastic tubes, sealed and stored in cold-storage space on the drilling vessel. At the end of Leg 175 and 177, the cores were transferred to the ODP core repository in Bremen, Germany (Wefer *et al.*, 1998), from where the samples for this study were obtained.

2.2 *Standard ODP Sample Labelling*

General core handling procedures described in previous *Initial Reports* volumes and the Shipboard Scientist's Handbook, are summarised here. For all ODP drill sites, a letter suffix distinguishes each hole drilled at the same site. Using ODP Site 1082 as an example, the first hole drilled was assigned the site number modified by the suffix "-A", e.g. 1082A; the second hole takes the site number and suffix "-B", e.g. 1082B, and so forth. The cored interval is measured in metres below seafloor (mbsf). The depth interval assigned to individual cores begins with the depth below seafloor that the coring operation began, extending to the depth at which coring ceased. Cores taken from a hole are numbered serially from the top of the hole downward. At the base of each cored section is the core catcher sample (CC), a device at the bottom of the core barrel which catches sediment when the barrel is being retrieved from the hole. Once the cores arrive on deck core-catcher samples are the first to be analysed in terms of biostratigraphic significance. Once the recovered core is on deck in its liner it is cut into 1.5-m sections for ease of handling. When a complete core is recovered these sections are numbered from the top, 1 through 7, with the last section usually being slightly shorter than the rest.

When a sample is taken from a core for analysis, the sample is given a unique label that is based on distance (measured in centimetres) from the top of the core section to the top and bottom of each sampled interval. A full curatorial label for a sample contains the following information: leg, site, hole, hole-suffix, core number, core type, section number, and the interval measured in centimetres from the top of the core section. For example, a sample from Site 1082 can be identified as follows: "175-1082A-2H-6, 50-52 cm", representing a sample taken from the interval between 50 and 52 cm below the top of Section 6, Core 2H (H meaning that this core was taken with the APC system) of Hole 1082A cored during Leg 175 (Fig. 2.4).

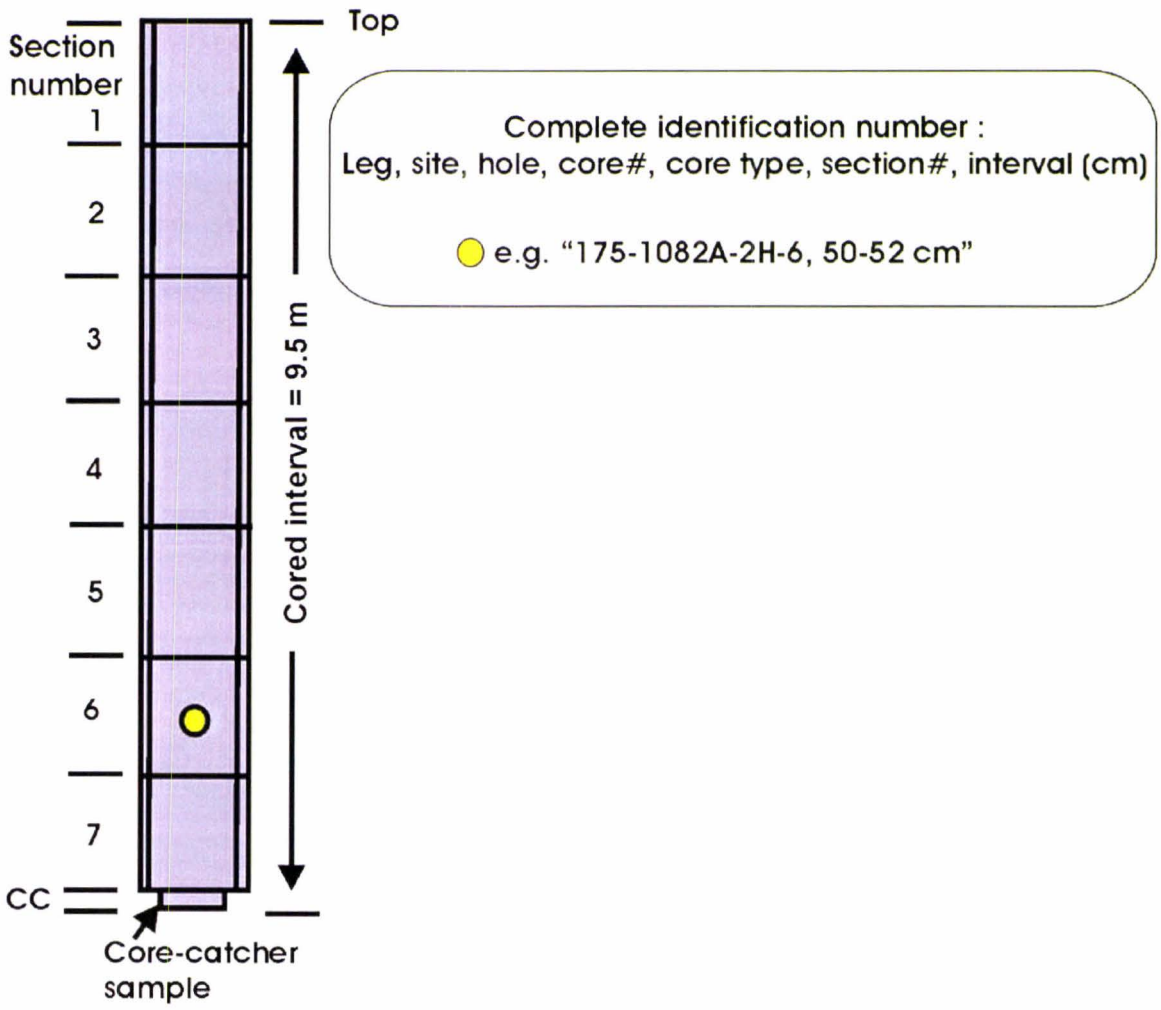

Figure 2.4: Example of ODP core numbering and sample labelling methods.

2.3 *Age Models*

It is currently proposed for the Pleistocene to be formally split into three intervals: early Pleistocene (1.8-0.78 Ma, B/M paleomagnetic boundary), middle Pleistocene (0.78-0.13 Ma, B/M - MIS 6) and late Pleistocene (0.13-0 Ma, MIS 5-1) (Gradstein *et al.*, 2004). This study deals with samples of the early and middle Pleistocene, a time period over which there has been a combination of different dating methods of different levels of accuracy.

The age models for Site 1082 and 1088 have been produced using several absolute age dates and biostratigraphic datums, coupled with variations in environmental proxy data and correlations with the marine oxygen isotope curve.

2.3.1 Biostratigraphic Datums

Basic biostratigraphy is concerned with the recognition of fossils, and relies on the physical zonation of biota, both in time and space, in order to establish the relative stratigraphic position of sedimentary units between different geographic localities. Shipboard micropaleontological studies were carried out initially on core-catcher samples from both Sites 1082 and 1088. Additional samples from within the cores were examined to improve biostratigraphic resolution. Both calcareous and siliceous microfossil groups were investigated, although through sheer abundance, good preservation, and resistance to diagenetic processes, calcareous nannofossils were found to be critical in the construction of a detailed biostratigraphy and a well-constrained age model for both sites. Besides biostratigraphical information, calcareous nannofossils can be used as tracers of upwelling dynamics and studies into trophic domains, as documented in a study by Giraudeau (1993). Ages for calcareous nannofossil, planktic foraminiferal, diatom, and radiolarian events and epoch boundaries are based mainly on the geomagnetic-polarity time scale of Berggren *et al.* (1995), and calcareous nannofossil biohorizons in accordance with Okada and Burkry's (1980) zonal markers.

2.3.2 Paleomagnetic Datums

Paleomagnetism is the term given to the study of the changing intensity and direction of the Earth's magnetic field in the geologic past through the remnant magnetism in rocks or sediment. Reversals in the Earth's magnetic field are recorded in sediments as iron-bearing minerals settle through ocean water and magnetically align themselves to the prevailing magnetic field. The use of magnetic polarity reversals as a stratigraphic tool is based on identifying characteristic patterns of reversals. The absolute age of each reversal has been established and a quantitative time scale for reversals has been set up. The geomagnetic polarity time scale has evolved since the 1960s, with various new data points being added and age estimates refined. The polarity time scale is subdivided into polarity "chrons", such as the Brunhes Normal Polarity Chron, and shorter "subchrons", such as the Jaramillo Polarity Subchron. Measurements of natural remnant magnetism (NRM) were made on all archive-half core sections from both Sites 1082 and 1088. A paleointensity curve was formed and magnetostratigraphic datums identified through studying the variations in the remnant intensity (paleointensity) in the past geomagnetic field strength.

2.3.3 Environmental Proxy Correlation

Fluctuations in several environmental proxies can be used to correlate between sites, to delineate warm and cool periods and to predict the position of marine oxygen isotope stages. The most useful properties for establishing a record of glacial-interglacial cyclicity are colour reflectance, GRA, $\delta^{18}O$ and $\delta^{13}C$.

2.3.3.1 Colour Reflectance

Reflectance of visible light from cores (using a Minolta spectrophotometer CM-2002) was used to establish semiquantitative relationships between lithologies down-hole, as an attempt to recognise climatic signals in the Pleistocene-aged sediments. Previous studies of sediment cores have shown that the ratio of reflectance values of red and blue wavelengths is closely related to the diagenetic redox conditions in the sediment, reflecting the presence of iron oxyhydroxides or sulphides (Mix *et al.*, 1995). Reflectance data can therefore be a suitable proxy for reconstructing high-resolution changes in carbonate sedimentation, which is known to vary, sometimes dramatically, during interglacial and glacial stages.

Studies by Berger (1970), Berger *et al.* (1982), and Emerson and Bender (1982), suggest that carbonate dissolution on continental margins and in water depths above the oceanic lysocline or CCD can only be attributed to decomposition of organic matter and resultant production of pore water CO_2. This dissolution is controlled by two processes: (a) surface water productivity (Berger, 1970) and (b) lateral supply of organic matter from the shelf and/or upper continental slope (Diester-Haass *et al.*, 1986). Productivity on continental margins has generally increased during glacial times, compared with interglacial periods (Wefer *et al.*, 2001). These two processes – an increase in surface water productivity, and an increase in the lateral supply of organic matter from continental shelf/upper slope areas (as a result of increased aridity and therefore increased aeolian transport of terrigenous material), results in an increase in net organic matter accumulation, and thus enhanced carbonate dissolution during glacial periods (Diester-Haass *et al.*, 1992).

Colour data was measured in 2-cm intervals in both Sites 1082 and 1088. The colour cycles reflect sharp changes in the concentrations of calcium carbonate, organic carbon and total sulphur. It is recognised that the general trend is such that dark layers have higher organic carbon concentrations, higher sulphur and lower concentrations of calcium carbonate and biogenic opal, and in the study area represent sediments deposited during glacial periods. Conversely, lighter layers represent periods of higher calcium carbonate accumulation, higher total reflectivity, and in the study area represent interglacial intervals (Gersonde *et al.*, 1999).

2.3.3.2 Natural Gamma Radiation

The natural gamma record serves as a proxy for bulk density or clay content, and like other physical property data sets, changes in gamma-ray attenuation (GRA) values down-core (reflecting sediment composition) reveal clear and pronounced glacial-interglacial cycles. High bulk-density values are consistent with interglacial intervals of high carbonate contents. Studies show a positive correlation between high reflectivity and high density, and low reflectivity and low density sediments, suggesting that colour and density variations are largely driven by variations in the carbonate content of sediments (Gersonde *et al.*, 1999).

2.3.3.3 $\delta^{18}O$ - Oxygen Isotope Record

Oxygen isotope stratigraphy from planktic and benthic foraminifera is now a routinely used stratigraphic correlation tool for deep-sea sediments, providing a time series record of globally synchronous events with a resolution of a few thousand years. Stable isotope analyses for both Sites 1082 and 1088 reveal pronounced glacial-interglacial variations in the ratio of $\delta^{18}O$ to $\delta^{16}O$; reflecting temperature-dependant fractionation and relative enrichment of the heavier isotope $\delta^{18}O$ during glacial periods and $\delta^{18}O$ depletion during interglacial periods.

2.3.3.4 $\delta^{13}C$ – Carbon Isotope Record

The $\delta^{13}C$ record reveals variations in the partitioning of carbon between different carbon reservoirs (biosphere, atmosphere, and hydrosphere), variations in ocean ventilation, and the changing ocean chemistry or nutrient content, over time. The initial studies of Shackleton (1975) and Kroopnick (1980), showed that foraminiferal carbon isotope records can be used to monitor variations in deep-water formation and deep-ocean ventilation through geologic time (e.g Duplessy, 1982; Duplessy and Shackleton, 1984). Deviations from the "global mean" record are common as there can be both species-specific deviations from carbon isotopic equilibrium (vital effects) and also local or regional overprints in areas where deep-sea circulation changes are large, such as upwelling areas (Jansen, 1989). Thus, the utilisation of carbon isotopes for correlation and dating purposes should be used only to provide additional age control, and not as the primary tool (Jansen, 1989).

2.3.4 Age Model for Site 1082

An astronomically-tuned age model at Site 1082 for the last 1.5 Ma was established by Jahn *et al.* (2003), and is based on the stable oxygen isotope records of benthic and planktic foraminifera, with the help of several nannofossil datums and magnetostratigraphic data from Wefer *et al.* (1998) (Fig. 2.5). Stable oxygen isotope data was obtained from the planktic foraminifera *Globorotalia inflata*, at down-core intervals of ~ 20 cm. For each sample, 15-20 specimens were hand-picked in the >150 μm size fraction, and $\delta^{18}O$ values were measured on a Finnigan MAT 251 micromass spectrometer, calibrated to the PDB (PeeDee Belemnite) standard scale (Jahn *et al.*, 2003). *Globorotalia inflata* is commonly used in isotope stratigraphy, and therefore was chosen to allow for comparisons of the $\delta^{18}O$ record across sites.

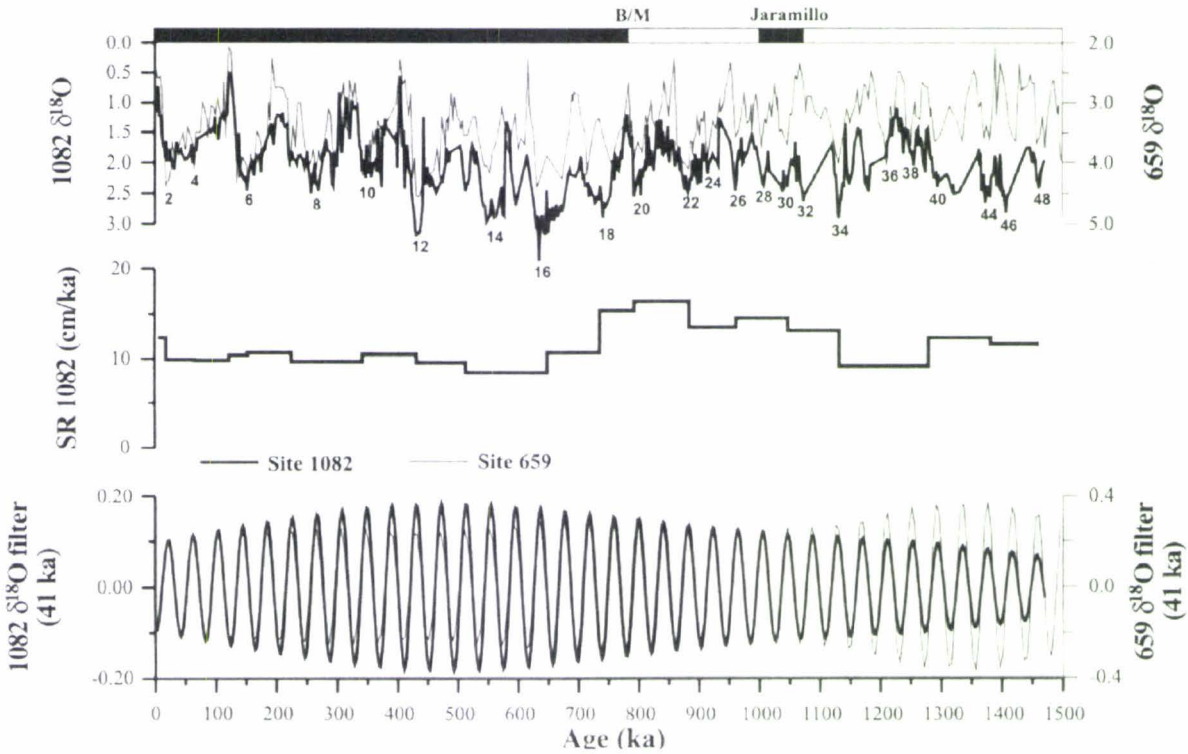

Figure 2.5: Age model for Site 1082. Isotopic data from the benthic $\delta^{18}O$ record of ODP Site 659 (thin line, upper graph) (Tiedemann *et al.* 1994) has been compared with the planktic *Globorotalia inflata* $\delta^{18}O$ record of ODP Site 1082 (thick line, upper graph) (Jahn *et al.* 2003). Sedimentation rate, band-pass-filtered 41-kyr components (lower graph), and marine oxygen isotope stages (MIS) are also given.

However, this species does not occur continuously throughout the investigated sediment sequence at Site 1082, and is absent in MIS 47, 43, 33, and 25. To overcome this, the $\delta^{18}O$ record of Site 1082 was visually aligned to the benthic $\delta^{18}O$ record of ODP Site 659 from the Cape Verde Plateau off northwest Africa, to show a good correspondence for glacial-interglacial cyclicity. The $\delta^{18}O$ record of *G. inflata* shows a much less pronounced glacial-interglacial amplitude than that of Site 659 (particularly from MIS 21 to 17), so magnetochrons (such as the well-dated boundary of Brunhes/Matuyama- 0.78 Ma (~74 mbsf), and the top and bottom of the Jaramillo – 0.99 (~97 mbsf) and 1.06 Ma (~105 mbsf)), were used to reinforce the age model. Datum events used in the reconstruction of the age model are summarised in table 2.2. Ages for microfossil data and magnetic reversals are based mainly on the geomagnetic polarity timescale of Berggren *et al.* (1995). Sedimentation rates were estimated by linear interpolation between age control points. Jahn *et al.* (2003) indicated that sedimentation rates (SR) over the past 1.5 Ma have been in the order of 10 cm/kyr, and further, that the time

interval encompassing the MPT, from 1.0 Ma (MIS 34) to about 0.75 Ma (MIS 18), is characterised by slighter higher SRs of about 15 cm/kyr (Fig. 2.5).

POLARITY CHRON/EVENT	AGE (MA)	DEPTH (MBSF)	COMMENTS
C1n	0.00 – 0.78	0-74	Brunhes epoch
C1r.1r	0.78 – 0.99	74-97	Matuyama epoch
C1r.1n	0.99 – 1.07	97-105	Jaramillo epoch
C1r.2r-1n	1.20-1.21	118	Cobb Mountain epoch
LO *Bachmannocena quadrangula*	0.80	56-65	Silicoflagellate
LO *Reticulofenestra asanoi*	0.83	65-69	Calcareous nannofossil
LO *Nitzschia fossilis*	0.92	56-65	Diatom
LO *Rhizosolenia matuyama*	1.10	94-103	Diatom
LO *Helicosphaera sellii*	1.25	115-119	Calcareous nannofossil

Table 2.2: Age datums identified in Site 1082. Biostratigraphic and magnetostratigraphic data from Wefer *et al.* (1998).Paleomagnetic timescale used is that of Berggren *et al.* (1995). LO = last occurrence; FO = first occurrence; mbsf = metres below seafloor.

2.3.5 Age Model for Site 1088

The chronostratigraphy adopted for Site 1088 (covering the past 1.2 Ma) was based on the identification and counting of isotope stages in the spliced composite $CaCO_3$ curve, $\delta^{18}O$ record for planktic and benthic foraminifera, and several nannofossil datums (Hodell *et al.*, 2003) (Fig. 2.6). Throughout the entire core, 25 age-depth biostratigraphic control points were identified, three of which help to constrain the study interval. Age datums are summarised in table 2.3.

BIOSTRATIGRAPHIC DATUM	AGE (MA)	DEPTH (MBSF)	COMMENTS
LO *R. asanoi*	0.88	11-12	Calcareous nannofossil
RE *Gephyrocapsa* medium	0.96	11-12	Calcareous nannofossil
FO *R. asanoi*	1.08	14-16	Calcareous nannofossil

Table 2.3: Age datums identified in Site 1088. Biostratigraphic data from Gersonde *et al.* (1999). LO = last occurrence; FO = first occurrence; RE = re-entrance; mbsf = metres below seafloor. Note: no useful magnetostratigraphic data was obtainable.

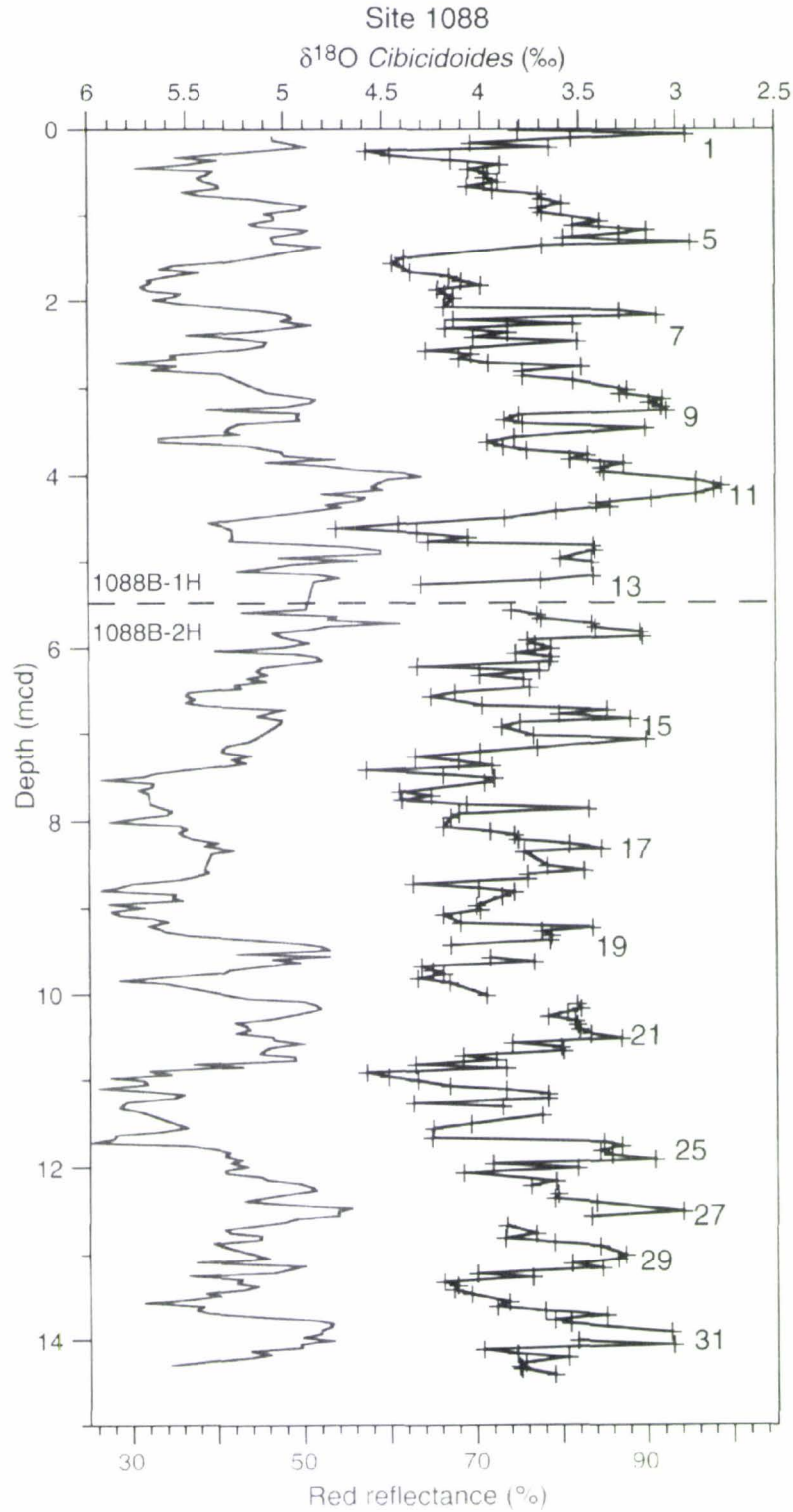

Figure 2.6: Age model for Site 1088. The benthic foraminifer *Cibicidoides* $\delta^{18}O$ record (dark black line) relative to percent red reflectance (650-750 nm; grey line) are shown (data from Hodell *et al.* 2003). Marine oxygen isotope stages (MIS) are also given.

Stable oxygen isotopes were measured on the benthic foraminifera *Cibicidoides wuellerstorfi* and the planktic foraminifera *Globigerina bulloides* in down-core intervals of ~ 5 cm. For each sample, specimens were hand-picked in the >150 μm size fraction and $\delta^{18}O$ values were measured on a Finnigan MAT 252 micromass spectrometer, calibrated to the PDB (PeeDee Belemnite) standard scale (Hodell *et al.*, 2003). Attempts to identify the Brunhes/Matuyama boundary were unsuccessful, and as a result of core-barrel-induced magnetisation problems, no useful magnetostratigraphy was obtained to constrain the age of the different intervals. Diffuse spectral reflectance measurements, obtained by OSU-SCAT and Minolta CM-2002 spectrophotometers, provided a high-resolution proxy for lithostratigraphic records over time. Interglacial (lighter, carbonate-rich) and glacial (darker and diatom-rich) cycles were easily identified, and in conjunction with biostratigraphic datums, were primarily used to estimate marine isotope stage positions down the core. Sedimentation rates at Site 1088 are low, averaging at ~ 1 cm/kyr (Hodell *et al.*, 2003). Despite this very low SR, all Pleistocene to Recent marine oxygen isotope stages (between MIS 1 and 31) are identifiable in the record.

3. METHODS

3.1 Sample Processing

Core samples of approximately 20 cc volume from the early-middle Pleistocene interval of ODP Sites 1082 and 1088 in the South Atlantic Ocean were processed. Sediment samples were taken at various depths down the cores, with each sample spanning approximately 2 cm of core thickness. From Sites 1082 and 1088, 61 samples were analysed to determine the stratigraphic ranges of specific benthic foraminifera: 23 samples from ODP Leg-175-1082A-6H to –14H, 7 core-catcher samples from ODP Leg-175-1082B-8H to –14H and 31 samples from ODP Leg-177-1088B-1H to –2H (Appendix 1). Most of these samples were selected from glacial and interglacial peaks based on oxygen isotope curves and colour reflectance. These provide an average intersample interval of 19-23 kyrs in the mid-Pleistocene transition (MPT).

All but ~2 cc of each sample was carefully disaggregated in water and washed through a 63 um sieve, the remaining sample was resealed in its original bag to be archived (at the Institute of Geological and Nuclear Sciences (IGNS), Lower Hutt, New Zealand) for possible future use. Between sieving samples the sieve was washed with water and a brush, and later soaked in a methyl blue solution to stain any remnant specimens and avoid cross contamination. Foraminifera were concentrated by washing out the mud fraction and dried in a 40°C oven overnight. The dried sample was then weighed and the weight recorded as 'g sand'. The dried sample residue >63 μm was sieved into three size fractions (63-150, 150-300, and >300 μm), weighed, labelled and stored in separate glass vials for micropaleontological studies. Between each sample all sieves were brushed and cleaned with compressed air.

Initial microscopic studies involved picking and identification of all specimens of elongate and uniserial benthic foraminiferal taxa, later to be known as the Extinction Group (EG) (Table 3.1) and the Survivor Group (SG) (Table 3.2). Certain biserial and triserial taxa were identified to species/and or genus level only and counted (known as the Low-Oxygen Tolerant Group - LOTG) (Table 3.3), as abundance changes in these

taxa may be used as a proxy to infer changes in food supply and/or oceanographic parameters, such as bottom current strength and bottom oxygen concentrations, through time.

Specimens were picked and or/counted from a small picking tray using a fine tipped paintbrush. All targeted taxa (EG and SG) were picked and mounted on a gridded slide, and LOTG benthic foraminifera abundances recorded. 100% of the >300 μm size fraction of each sample was searched for EG, SG and LOTG benthic foraminifera. Of the 150-300 μm fractions, samples were repeatedly split using a Carpco micro-splitter to give approximately 300 benthic foraminifera (EG, SG and LOTG), as part of a total census count of the benthic assemblage. In several samples it was not possible to pick 300 benthic forms due to extremely low abundances. Again the Target Group (EG and SG) specimens were picked, mounted on faunal slides, identified and counted. Each Target Group species was mounted into a separate box on the faunal slide; the layout of specimens remained the same for all samples. IRD (ice-rafted debris), gypsum rhombs, glauconized foraminifera tests, radiolarian, diatom and ostracod specimens, and any other miscellaneous objects were also counted and recorded as part of the census, however, no attempt was made to identify radiolarian, diatom or ostracod specimens as this is beyond the scope of this study.

3.2 *Extinction, Survivor and Count Groups*

For comparative purposes benthic foraminifera have been classified into three groups, based on their stratigraphic range and their presence or absence from Recent seafloor sediment in the region:

a) Extinction Group (EG)
b) Survivor Group (SG)
c) Low-Oxygen Tolerant Count Group (LOTG)

3.2.1 Target Benthic Foraminifera (Extinction and Survivor Groups)

Target Group species are commonly elongate and/or uniserial, calcareous benthic foraminifera. The Extinction Group (EG) (Table 3.1) includes all elongate cylindrical species that became extinct in the South Atlantic (this study), northern North Atlantic (Kawagata *et al.*, in press), and/or Southwest Pacific sites (Hayward, 2002), during the early and middle Pleistocene. The Survivor Group (SG) comprises elongate cylindrical species, which either died back dramatically, but survived in low numbers; or survived through to the Recent in these regions, without major evidence of die-back (Table 3.2). Both groups of target benthic foraminifera (EG and SG) were picked from the >300 μm and 150-300 μm size fractions of each sample, identified and counted.

South Atlantic Extinction Group	
Awhea tosta	*Orthomorphina trincherasensis*
Chrysalogonium calomorphum	*Parafrondicularia antonina*
Chrysalogonium crassitestum	*Parafrondicularia laevigata*
Chrysalogonium deceptorium	*Pleurostomella acuminata*
Chrysalogonium gomphiformis	*Pleurostomella alternans*
Chrysalogonium interteniatum	*Pleurostomella brevis*
Chrysalogonium stimuleum	*Pleurostomella sapperi*
Cribronodosaria sp. A	*Proxifrons maequalis*
Ellipsoglandulina labiata	*Siphonodosaria bradyi*
Myllostomella advena	*Siphonodosaria hispidula*
Myllostomella costai	*Siphonodosaria recta*
Myllostomella japonica	*Siphonodosaria sagrinensis*
Myllostomella matanzana	*Siphonodosaria spinea*
Orthomorphina ambigua	*Siphonodosaria pomuligera*
Orthomorphina glandigena	*Stilostomella fistuca*
Orthomorphina laevis	*Stilostomella holoserica*
Orthomorphina perversa	

Table 3.1: South Atlantic Extinction Group benthic foraminifera.

South Atlantic Survivor Group	
Acostina sp.A	*Laevidentalina* sp.A
Astacolus insolitus	*Laevidentalina* sp.B
Astacolus sp.A	*Laevidentalina* sp.C
Dentalina mutablis	*Marginulina obesa*
Dentalina sp. B	*Martinottiella communis*
Glandulina ovula	*Martinottiella variablis*
Glandulina sp.A	*Nodosaria inflexa*
Grigelis orectus	*Nodosaria longiscata*
Grigelis sp.A	*Nodosaria* sp.A
Grigelis sp.B	*Parafrondicularia javana*
Laevidentalina advena	*Pseudonodosaria brevis*
Laevidentalina ariena	*Vaginulina inflata*
Laevidentalina frobisherensis	*Vaginulina spinigera*
Laevidentalina guttifera	*Vaginulina sp.Elongate*
Laevidentalina sidebottomi	*Vaginulinopsis albatrossi*
Laevidentalina subsoluta	*Vaginulinopsis* sp.A
Laevidentalina vagina	

Table 3.2: South Atlantic Survivor Group benthic foraminifera.

3.2.2 Count Group Benthic Foraminifera (Low-Oxygen Tolerant Group)

Count Group benthic foraminifera are those that have previously been regarded as infaunal, low-oxygen tolerant species (Kaiho, 1991, 1994, 1999; Kaiho and Hasegawa, 1994; Harloff and Mackensen, 1997; Gooday and Rathburn, 1999). These faunas are not included in the Target Group but their abundance is thought to reflect both dissolved oxygen concentrations in the sediment porewater, and the flux of organic matter (food pulses) to the benthic environment. These 'proxy' taxa are characterised by a number of different morphotypes, including elongate agglutinated and elongate uniserial, biserial or multiserial calcareous deep-sea benthic foraminifera. Most data on seasonal fluctuations of deep-sea foraminiferal population densities have been conducted from bathyal continental margins (such as the Californian margin - Bernhard and Reimers, 1991; Corliss and Silva, 1993; Rathburn, 1996, 1998), commonly areas of high organic matter flux, such as upwelling regions, where fluctuations are most dramatic. In these areas regional differences in the intensity of organic matter supply arise from temporal variability in upwelling and terrigenous input, and are best recorded by the changes in the relative abundance of Low-Oxygen Tolerant Count Group (LOTG) benthic foraminifera (Table 3.3).

South Atlantic Low-Oxygen Tolerant Group	
Bolivina pussilla	*Fursenkoina complanata*
Bolivina subspinscens	*Globobulimina affinis*
Bolivina sp.A	*Karreriella bradyi*
Bulimina aculeata	*Praeglobobulimina spinscens*
Bulimina exilis	*Rutherfordoides mexicana*
Bulimina marginata	*Trifarina anglosa*
Bulimina mexicana	*Uvigerina peregrina*
Bulimina truncana	*Uvigerina proboscidea*
Cassidella bradyi	*Uvigerina hispida*
Eggerella bradyi	*Uvigerina hollocki*
Evolvocassidulina sp.	

Table 3.3: South Atlantic Low-Oxygen Tolerant Group benthic foraminifera.

3.3 Quantitative Studies

All benthic foraminiferal census data and grain size data (such as %sand) was entered into a standard excel spreadsheet. From this data, the total number of specimens of target species (EG and SG) and count species (LOTG) in each sample was estimated by multiplying the number of target and count specimens found (>150 μm size fraction) by number of splits in that sample. Total number of benthic species and total number of benthic specimens per g of sediment and per g of sand could then be calculated. The accumulation rate (AR) or flux of EG, SG and LOTG taxa (no/cm^2/kyr) could be calculated using linear sedimentation rates based on the age models of Jahn *et al.* (2003) for Site 1082 (Fig. 2.5), and Hodell *et al.* (2003) for Site 1088 (Fig. 2.6).

3.3.1 Planktic Foraminifera and Fragmentation Index

To evaluate carbonate dissolution effects on the samples and to compare between sites, the percentage planktic foraminifera of the total (% PF) and the ratio of fragmented to whole planktic foraminiferal tests (Fragmentation Index – FI) was calculated. The percentage of planktic foraminifera was calculated by counting the number of planktic versus benthic foraminifera from 1 picking tray volume in a random count pattern. It has long been recognised that benthic foraminifera (like radiolaria) are approximately three times more resistant to dissolution than planktic foraminifera (Berger, 1975), and are therefore likely to increase in relative abundance as the parameters that favour carbonate dissolution increase (Volbers and Heinrich, 2002). The Fragmentation Index, proposed by Le and Shackleton (1992), is an index used to quantify and compare downcore variations in carbonate dissolution through time, where:

FI = 100 * (number fragments/8) / [(number fragments/8) + (number whole)].

Le and Shackleton's formula is based on the assumption that one whole planktic foraminifera will break into 8 fragments. Fragmentation was estimated by counting the number of planktic foraminiferal fragments (3 or fewer chambers) to whole planktic foraminifera in a split of sand (>150 μm).

3.3.2 Ice-Rafted Debris (IRD)

Ice-rafted debris (IRD) is an important component of the marine sediment in the Southern Ocean equatorwards of the Antarctic Continent and in the area of Site 1088. IRD pulses represent episodic cooling events and their intensity relates to the past magnitude of discharges of icebergs (during deglaciations) from the Antarctic Ice Sheet.

Lithic fragments (mica, quartz, mineral grains) in the >150 μm fraction, interpreted as IRD, were counted. IRD components were calculated as the number of lithic sand grains (>150μm) per g of sediment, and an accumulation rate (AR) of IRD was calculated as number of lithic grains per/cm^2/kyr.

3.4 Data Analysis

The primary statistical analysis performed on the census data used Pearson's correlation coefficients.

3.4.1 Pearson's Correlation Coefficient

Correlation coefficients were calculated from the full census data from both Sites 1082 and 1088. Two data sets were calculated for each site, one which included data from the entire study interval, and another on the interval older than ~800 ka to show 'normal' background fluctuations in proxy records. Correlation is a technique for investigating the relationship between two quantitative, continuous variables. Pearson's correlation coefficient (r) is a "*measure of the strength of the association or relationship*" between the two variables. Pearson's r-values for continuous/linear data range from –1 to +1, values approaching +1 indicate positive correlations, while values approaching –1 indicate negative correlations; 0 giving no correlation. Positive correlation ($r > 0$) indicates that both variables increase or decrease together, whereas negative correlation ($r < 0$) indicates that as one variable increases, so the other decreases, and vice versa. It is always important to note that correlation does not imply causation.

4. *Stilostomella* Extinction Taxonomy

Taxonomic features, synonymies, and geographic and stratigraphic notes on species in the South Atlantic *Stilostomella* Extinction Group are listed below. 33 species of benthic foraminifera were recognised in samples > 150 μm from ODP Sites 1082 and 1088 as belonging to the Extinction Group (EG) (Table 3.1). Of these EG species approximately 42% (14 species) were common to Sites 1082 and 1088. 33 species of benthic foraminifera were identified in the Survivor Group (SG) (Table 3.2). Of these SG species approximately 48% (16 species) were common to both sites. Within this group, several *Laevidentalina, Grigelis,* and *Nodosaria* specimens were unable to be identified to species level, and have been given sp.A, sp.B or sp.C attachments. A census count of 21 species of previously recognised Low-Oxygen Tolerant infaunal benthic foraminifera (LOTG) was also undertaken in this South Atlantic study (Table 3.3). Previous studies show that population density fluctuations reflect changes in water mass ventilation and food supply in benthic environments (e.g. Boersma, 1986; Kaiho, 1994; Kawagata *et al.*, in press). A list of the LOTG is thereby given. The following account outlines the main diagnostic criteria for EG and SG genera, the morphological characteristics that were used to distinguish between EG species, and the stratigraphic distribution of EG benthic foraminifera within ODP Site 1082 and 1088.

4.1 Features of the Extinction Group and Survivor Group Genera

Key features of uniserial genera with apertural tooth:

Myllostomella: Chambers spherical to ovate; smooth to weakly pustulose; necked aperture with one flange (phialine lip) in the adult with one large internal tooth and long internal denticles. Eocene-Pleistocene.

Siphonodosaria: Chambers spherical to pyriform; sutures constricted; necked aperture, single crenulate phialine lip with distinct tooth on one margin. Eocene-Pleistocene.

Stilostomella: Chambers subglobular to ovate; finely pustular, hispid or smooth; necked or lipped, cribrate aperture, septal foramina with a infolded simple tooth on one margin. Oligocene-Pleistocene.

Key features of uniserial genera:

Awhea: Elongate, rectilinear, narrow; sutures flush and horizontal; 6-8 slightly twisted, longitudinal ribs; elongate radiate aperture. Late Miocene-mid Pleistocene.

Chrysalogonium: Elongate, rectilinear; sutures horizontal; surface smooth; aperture terminal cribrate. Late Cretaceous-Pleistocene.

Dentalina: Elongate, arcuate; apiculate proloculus; horizontal or oblique sutures; smooth surface or longitudinal costate; protruded terminal radial aperture. Cretaceous-Recent.

Glandulina: Elongate, ovate tapering at each end, circular cross-section; rectilinear, mostly uniserial; rapidly increasing in size; sutures flush; radiate aperture with short entosolenian tube. Paleocene -Recent.

Grigelis: Chambers elongate ovate separated by long narrow necks; radiate aperture on long neck. Eocene-Recent.

Laevidentalina: Elongate, arcuate; horizontal to slightly oblique sutures; unornamented; aperture of radial slits closed at apex; Cretaceous-Recent.

Marginulina: Slightly curved to rectilinear; chambers circular in section, costate; terminal radiate aperture at dorsal angle, may be necked. Jurassic-Recent.

Nodosaria: Rectilinear; globular-ovate chambers; unornamented; necked aperture radiate or rounded with radial grooves. Jurassic-Recent.

Orthomorphina: Rectilinear; globular chambers trending ovoid; inornate, striated or rugose; sutures depressed; necked, rimed or unrimed, round aperture. Eocene-Pleistocene.

Pseudonodosaria: Rectilinear, early chambers strongly overlapping, increasing rapidly in diameter; sutures horizontal, flush; aperture terminal radiate. Cretaceous-Recent.

Vaginulina: Rectilinear to arcuate; ovate to lenticular in section; dorsal margin often straight; sutures often thickened and elevated; aperture at dorsal angle. Jurassic-Recent.

Vaginulinopsis: Early planispiral, involute; later uncoiled, rectilinear; chambers ovate to lenticular in section; terminal radiate aperture at dorsal angle. Triassic-Recent.

Key features of biserial genera:

***Ellipsoglandulina*:** Uniserial, ovate to subglobular, strongly overlapping chambers; smooth; semilunate slit aperture; succesive apertures joined by an internal tube. L. Cretaceous-Pleistocene.

Parafrondicularia: Elongate, lanceolate; flattened with an ovate section; initially biserial, later uniserial arched-chevron-shaped chambers; longitudinally costate. Eocene-Pleistocene, ?Recent.

Pleurostomella: Biserial, some time cuneate and alternating in position; smooth; aperture with projecting hood and two teeth or bifid tooth or no tooth. L. Cretaceous-Pleistocene.

Proxifrons: Strongly compressed, palmate; short biserial followed by uniserial chevron-shaped chambers; surface smooth or with several short costae. Eocene-Pleistocene.

4.2 *Stilostomella Extinction Group*

Taxonomic features, synonymies, and geographic and stratigraphic notes on species in the South Atlantic *Stilostomella* Extinction Group.

Picked faunas and illustrated specimens of this study are to be held in the micropaleontological collections of the Institute of Geological and Nuclear Sciences, Lower Hutt, New Zealand. A reference to the original identification of each species is given, followed by references to published SEM images that were used in this study to identify specimens. In most cases, unpublished SEM and digital images (from Kawagata *et al.* of Geomarine Research , Auckland , New Zealand) were also used to confirm EG identities.

Stilostomella Extinction Group

Family Nodosariidae

Genus *Awhea* Vella, 1963

***Awhea tosta* (Schwager, 1866)**
Nodosaria tosta Schwager, 1866, p.219, pl.5, fig.42.
Awhea tosta (Schwager). Hayward, 2002, p.296, pl.2, figs.7-8.

Descriptive notes: Narrow, elongate, rectilinear test; symmetric cross-section; sutures flush and horizontal; 4-8 slightly twisted, longitudinal ribs; elongate radiate aperture.
South Atlantic distribution: *1082:* Present in 37% of samples; forms <1% of the total Extinction Group (EG); common between 144.2 and 93.6 mcd (1280-865 ka), with highest abundance between 144.2 and 134.2 mcd (1280-1173 ka); highest occurrence

(HO) ~ 93.6 mcd (~ 865 ka). *1088:* Present in 26% of samples; forms ~1% of the total EG; rare between 14.4 and 10.8 mcd (1101-867 ka), with highest abundance at 11.6 mcd (~928 ka); highest occurrence ~ 10.8 mcd (~867 ka). Rare at middle bathyal depths (1088) and common at lower depths (1082) in offshore southern Africa sections.
World distribution: Indo-Pacific - Andaman Sea, Taiwan, Japan, Indonesia, New Zealand, California, SE Pacific, South Atlantic, North Atlantic; Late Miocene-middle Pleistocene. Member of the South Atlantic Extinction Group.

Genus *Chrysalogonium* Schubert, 1911
Type species: *Nodosaria polystoma* Schwager, 1866

***Chrysalogonium calomorphum* (Reuss, 1866)**
Nodosaria calomorpha Reuss, 1866, p.129, pl.1, figs.15-19.
Chrysalogonium calomorphum (Reuss). Hayward, 2002, p.297, pl.2, figs.9-10.

Descriptive notes: Elongate, large uniserial test; large spherical proloculus with short spine, followed by 3 (or 4) smooth, ovate chambers with deeply incised sutures; truncate cribrate aperture, surrounded by low rim (lip).
South Atlantic distribution: *1082:* Present in 3% of samples; forms 0.02% of the total EG; only 2 specimens occur and HO at 144.2 mcd (~ 1280 ka). *1088:* Absent.
World distribution: Cosmopolitan; Oligocene-middle Pleistocene. Member of the South Atlantic Extinction Group.

***Chrysalogonium crassitestum* (Schwager, 1866)**
Nodosaria crassitesta Schwager, 1866, p.224, pl.5, fig.55.
Chrysalogonium crassitestum (Schwager). Hayward, 2002, p.297, pl.2, figs.11-12.

Descriptive notes: Elongate, robust, uniserial test, tapers towards both ends (with greatest diameter near two thirds the length); slightly pointed cribrate aperture without surrounding rim; c.20 strong longitudinal costae.

South Atlantic distribution: *1082:* Present in 10% of samples; forms 0.07% of the total EG; rare between 144.2 and 105.0 mcd (1280-940 ka), highest abundance and HO at 105.0 mcd (~940 ka). *1088:* Absent.

World distribution: Probably cosmopolitan; Indo-Pacific - Japan, Philippines, Mallorca, Andaman Sea, New Zealand, South Atlantic, North Atlantic; Miocene-early Pleistocene. Member of the South Atlantic Extinction Group.

***Chrysalogonium deceptorium* (Schwager, 1866)**

Nodosaria deceptoria Schwager, 1866, p.212, pl.5, fig.30.

Dentalina deceptoria (Schwager). Hayward, 2002, p.298, pl. 2, Figs.28-29.

Descriptive notes: Elongate, large, parallel-sided, uniserial test; ovate chambers with short, twisted, prolocular spine; numerous (18-24), straight, narrow costae; slightly pointed cribrate aperture without surrounding rim.

South Atlantic distribution: *1082:* Absent. *1088:* Present in 3% of samples; forms 0.08% of the total EG population; occurrence limited to 2 specimens at 13.95 mcd (~1068 ka).

World distribution: Cosmopolitan; Late Cretaceous-Pleistocene, Pliocene-Recent (tropical Pacific Ocean). Member of the South Atlantic Extinction Group.

***Chrysalogonium gomphiformis* (Schwager, 1866)**

Nodosaria gomphiformis Schwager, 1866, p.220, pl.5, fig.48.

Chrysalogonium gomphiformis (Schwager). Srinivasan and Sharma, 1980, p.29, pl.4, fig.15.

Chrysalogonium aff. *gomphiformis* (Schwager). Hayward, 2002, p.297, pl. 2, figs.15-16.

Descriptive notes: Elongate, large, uniserial test; distinguished by up to 20 strong longitudinal costae, which do not tend to extend over the last few chambers (last 1-3 chambers smooth). Sutures become increasingly depressed towards adult end, where chambers are more inflated and spherical. Specimens show a diverse range of forms, with differing numbers of smooth, costae-free adult end chambers in each population.

South Atlantic distribution: *1082:* Present in 47% of samples; forms ~9% of total EG; common from 144.2 to 105 mcd (1280-940 ka) with 2 large *blooms* at 115.5 and 123 mcd (1019 and 1076 ka); HO at 105 mcd (~940 ka). *1088:* Absent.

World distribution: Probably cosmopolitan; West Indies (Miocene), Andaman Sea, New Zealand, South Atlantic, North Atlantic; early Miocene-early Pleistocene. Member of the South Atlantic Extinction Group.

***Chrysalogonium intertenuatum* (Schwager, 1866)**

Nodosaria intertenuata Schwager, 1866, p.226, pl.6, fig.58.

Chrysalogonium intertenuatum (Schwager). Hayward, 2002, p. 297, pl.2, figs.17-20.

Descriptive notes: Elongate, moderate-sized, uniserial test; ovate chambers, with moderately incised sutures; smooth; last chamber tapers to a neck, bearing a radially truncate cribrate aperture.

South Atlantic distribution: *1082:* Present in 20% of samples; forms 0.3% of the total EG population; rare in samples between 144.2 to 89.7 mcd (1280-843 ka); highest abundance between 144.2 and 139.4 mcd (1280-1228 ka); HO at ~89.7 mcd (~843 ka). *1088:* Present in 6% of samples; forms 0.3% of the total EG population; found only in two samples (4 specimens in each) at 12.55 and 5.36 mcd (1000 and 508 ka); *C.intertenuatum* may have survived through the MPT at the middle bathyal Site 1088, or these specimens may be present as a result of bioturbation.

World distribution: Probably cosmopolitan; Indo-Pacific - Andaman Sea, Japan, New Zealand, South Atlantic, North Atlantic; Miocene-middle Pleistocene. Member of the South Atlantic Extinction Group.

***Chrysalogonium stimuleum* (Schwager, 1866)**

Nodosaria stimulea Schwager, 1866, p.226, pl.6, fig.57; Cushman, 1934, p.114, pl.12, fig.7.

Dentalina stimulea (Schwager). Srinivasan and Sharma, 1980, p.33, pl.5, fig.1; Hayward, 2002, p.298, pl.2, figs.34-35.

Descriptive notes: Elongate, uniserial, parallel-sided test that slightly tapers towards both ends; elongate, ovate chambers, including a proloculus with apical spines; weakly incised, horizontal sutures; unornamented, pointed cribrate aperture without surrounding rim.

South Atlantic distribution: *1082:* Present in 10% of samples; forms 0.1% of total EG; rare between 144.2 to 105 mcd (1280-940 ka), with highest abundances at 143 mcd (~1266 ka); HO at 105 mcd (~ 940 ka). *1088:* Present in 19% of samples; forms 3% of the total EG; common between 14.38 and 11.76 mcd (1101-943 ka), with highest abundances at 12.81 and 12.10 mcd (1015 and 967 ka); HO at ~ 11.76 mcd (~943 ka).

World distribution: Probably cosmopolitan; Trinidad, Mallorca, Andaman Sea, Guam, Philippines, Fiji, New Zealand, South Atlantic, North Atlantic; Oligocene-middle Pleistocene. Member of the South Atlantic Extinction Group.

Genus *Cribronodosaria* Le Calvez, de Klasz, and Brun, 1974

Type species: *Cribronodosaria africana* Le Calvez, de Klasz and Brun, 1974

***Cribronodosaria* sp. A**

Cribronodosaria sp. A. Hayward, 2002, p.297, pl.2, figs.25-27.

Descriptive notes: Elongate, uniserial test; distinguished by its campanulate chamber shape; short neck with terminal aperture consisting of pores forming a reticular mesh in a domelike hemispherical trematophore. This specimen is distinguished by its campanulate chamber shape; short neck with hemispherical trematophore; and short,

weak, backwards-pointing spines on the lower part of each chamber. Late Cretaceous-late Pliocene.

South Atlantic distribution: *1082:* Present in 3% of samples; forms 0.02% of the total EG; two specimens found at 144.2 mcd (1280 ka). *1088:* Absent.

World distribution: Only recorded from New Zealand and the South Atlantic so far. A single species was seen in the SW Pacific extinction study, occurring in late Pliocene sediment (2.9 Ma) at lower bathyal depths east of New Zealand. Member of the South Atlantic Extinction Group.

Genus *Orthomorphina* Stainforth, 1952

Type species: *Nodogenerina havanensis* Cushman and Bermudez, 1937

***Orthomorphina ambigua* (Neugeboren, 1856)**

Nodosaria ambigua Neugeboren, 1856, p.71, pl.1, figs.13-16.

Orthomorphina ambigua (Neugeboren). Stainforth, 1952; Barker 1960, p.130, pl.62, fig.3; Hayward, 2002, p.299, pl.2, figs.44-45.

Descriptive notes: Test rectilinear, uniserial; initial chambers squashed spherical and similar size throughout; smooth to weakly pustular; small, rounded terminal aperture lacking a collar or neck. Eocene-middle Pleistocene.

Srinivasan and Sharma (1980) note that untapered forms (e.g., tornata type) are the megalospheric generation and tapered forms (e.g., koina type) are the microspheric generation within a single species.

South Atlantic distribution: *1082* Present in 23% of samples; forms 0.2% of the total EG; rare between 144.2 and 100.0 mcd (1280 to 912 ka), with highest abundances at 136 mcd (1186 ka); HO at ~100.0 mcd (~912 ka). *1088:* Absent. Present only at lower bathyal depths (1082).

World distribution: Cosmopolitan; ?Eocene-, Miocene-middle Pleistocene, ?Recent. Member of the South Atlantic Extinction Group.

***Orthomorphina glandigena* (Schwager, 1866)**

Nodosaria glandigena Schwager, 1866, p.219, pl.5, fig.46.

Orthomorphina glandigena (Schwager). Stainforth, 1952; Boltovskoy, 1978, pl.5, fig.19; Srinivasan & Sharma 1980, p.36, pl.5, figs.20, 21.

Descriptive notes: Test rectilinear, uniserial; *O. glandigena* is distinguished from *O ambigua* by having chambers, which increase size and become elongate rapidly; test smooth to weakly pustular; small rounded aperture lacking a collar or neck.

South Atlantic distribution: *1082:* Present in 3% of samples; forms 0.02% of total EG; only 2 specimens found at 100.0 mcd (912 ka). *1088:* Absent. Rare at lower bathyal depths (1082).

World distribution: West Indies, North Atlantic, South Atlantic; Oligocene-Pleistocene. Member of the South Atlantic Extinction Group.

***Orthomorphina laevis* (Cushman and Bermudez, 1937)**

Nodogenerina laevis Cushman and Bermudez, 1937, p.15, pl.2, fig.2.

(?) *Orthomorphina laevis* (Cushman and Bermudez). Stainforth, 1952.

Descriptive notes: Uniserial, test small, elongate, fusiform, inornate, constricted at sutures, chamber overlapped; aperture terminal small, rounded simple opening at the end of narrow long neck without lip.

South Atlantic distribution: *1082:* Present in 3% of samples; forms 0.05% of total EG; 4 specimens found at 139.4 mcd (1229 ka). *1088:* Present in 10% of samples; forms 0.6% of total EG; rare between 13.95 and 12.1 mcd (1068-967 ka), with highest abundances at 13.95 mcd (1068 ka); HO at ~12.1 mcd (~967 ka).

World distribution: Cuba (Eocene); North Atlantic (Pleistocene), South Atlantic; Eocene-Pleistocene. Member of South Atlantic Extinction Group.

***Orthomorphina perversa* (Schwager, 1866),** Pl. 1, Figs.50-52

Nodosaria perversa Schwager, 1866, p.212, pl.5, fig.29; Brady, 1884, pl.64, figs.25-27; Cushman, 1934, p.114, pl.12, fig.14.

Orthomorphina perversa (Schwager). Stainforth, 1952; Hayward, 2002, p.288, pl.2, figs.50-51.

Descriptive notes: Uniserial, spherical chambers of markedly different diameters, often ultimate chamber smaller than penultimate; test with distinct longitudinal costae over entire test or so; aperture rounded simple opening at the end of the test with various length of neck with thick, phialine lip.

South Atlantic distribution: *1082:* Present in 23% of samples; forms 0.4% of total EG; common between 144.2 and 121.1 mcd (1280-1061 ka), with highest abundances between 144.2 and 134.2 mcd (1280-1173 ka); HO at ~121.1 mcd (~1061 ka). *1088:* Present in 32% of samples; forms 2.3% of total EG; common between 14.38 and 10.11 mcd (1101-814 ka), with highest abundances between 14.38 and 11.76 mcd (1101-943 ka); HO at ~10.11 mcd (~814 ka).

World distribution: Cosmopolitan; Oligocene-middle Pleistocene. Member of South Atlantic Extinction Group.

***Orthomorphina trincherasensis* (Bermudez, 1949),** Pl. 1, Figs.53-54

Nodogenerina trincherasensis Bermudez, 1949, p.179, pl.11, fig.60.

Orthomorphina trincherasensis (Bermudez). Hayward, 2002, p.288, pl.2, figs. 53-54.

Descriptive notes: Uniserial; test with rounded, nodular costae early, later coarsely pustular; aperture terminal small, rounded simple opening at end without lip.

South Atlantic distribution: *1082:* Present in 3% of samples; forms 0.05% of total EG; 4 specimens found only in one sample at 144.2 mcd (1280 ka). *1088:* Present in 3% of samples; forms 0.08% of total EG; 2 specimens found only in one sample at 13.95 mcd (1068 ka).

World distribution: Cosmopolitan; Caribbean, Ki Islands, New Zealand, North Atlantic, South Atlantic; rare; Eocene-middle Pleistocene. Member of the South Atlantic Extinction Group.

Genus *Parafrondicularia* Asano, 1938

Type species: *Parafrondicularia japonica* Asano, 1938

***Parafrondicularia antonina* (Karrer, 1878)**

Frondicularia antonina Karrer, 1878.

Parafrondicularia pellucida (Finlay). Gibson, 1967, pl.5, fig.93; Hayward, 2002, p.288, pl.2, figs.1-2.

Descriptive notes: Elongate, lanceolate; flattened with an ovate section; initially biserial, later uniserial, arched-chevron-shaped chambers; 8-12 thin, longitudinal costae on each face.

South Atlantic distribution: *1082:* Present in 13% of samples; forms 0.2% of total EG; rare between 144.2 and 81.5 mcd (1280-793 ka), with highest abundances between 144.2 and 136.0 mcd (1280-1186 ka); HO at ~81.5 mcd (~793 ka). *1088:* Absent. Found only at lower bathyal depths (1082).

World distribution: New Zealand, Australia, South Atlantic; late Miocene-middle Pleistocene. Member of the South Atlantic Extinction Group.

***Parafrondicularia laevigata* (Karrer, 1868)**

Frondicularia laevigata Karrer, 1868.

Proxifrons inaequalis (Costa, 1855). Hayward, 2002, p.284, pl.1, fig.4 (part).

Descriptive notes: Narrow elongate test, uniserial chevron-shaped chambers; smooth surface with several short longitudinal costae over the early portion of the test; small

spherical proloculus. Differ from *P. javana* specimens that tend to be very irregular in their early chamber arrangement.

South Atlantic distribution: *1082:* Present in 83% of samples; forms 34% of total EG; moderately common between 144.2 and 74.6 mcd (1280-749 ka), with highest abundances at 81.5 mcd (793 mcd) and between 123.0 and 97.9 mcd (1070-895 ka); HO at ~74.6 mcd (~749 ka). *1088:* Present in 13% of samples; forms 0.5% of total EG; rare between 11.76 and 7.06 mcd (943-613 ka), with highest abundances at 10.95 mcd (881 ka); HO at ~7.06 mcd (~613 ka). Moderately common in lower bathyal depths (1082); rare at middle bathyal depths (1088).

World distribution: ?Cosmopolitan; Eocene-Pleistocene. Member of the South Atlantic Extinction Group.

Genus *Proxifrons* Vella, 1963

Type species: *Frondicularia advena* Cushman, 1923

***Proxifrons inaequalis* (Costa, 1855)**

Frondicularia inaequalis Costa, 1855, p.372, pl.3, fig.3.

Proxifrons inaequalis (Costa). Hayward, 2002, p.284, pl.1, figs.8-9 (in part).

Descriptive notes: Strongly compressed, palmate; broadly flaring, non-costate, and have a large ovate proloculus, almost completely surrounded by the first post-prolocular chamber (see Hayward, 2002, p.284, pl.1, figs.8-9 – macrospheric form).

South Atlantic distribution: *1082:* Present in 20% of samples; forms 0.14% of total EG; rare between 144.2 and 100.0 mcd (1280-912 ka), with highest abundances between 144.2 and 139,6 mcd (1280-1229 ka); HO at ~100.0 mcd (~912 ka). *1088:* Present in 16% of samples; forms 0.5% of total EG; rare between 11.76 and 9.85 mcd (943-794 ka), with highest abundance at 11.56 mcd (928 ka); HO at ~ 9.85 mcd (~794 ka).

World distribution: Cosmopolitan; Eocene-Pleistocene, ?Recent. This distinctive species has been recorded as rare specimens in Recent sediments in a variety of places

around the world and may have survived through to the present day in low numbers. Member of the South Atlantic Extinction Group.

Family Pleurostomellidae Reuss, 1860

Genus *Ellipsoglandulina* Silvestri, 1900

Type species: *Ellipsoglandulina laevigata* A. Silvestri, 1900

***Ellipsoglandulina labiata* (Schwager, 1866)**

Glandulina labiata Schwager, 1866, p.237, pl.6, figs.77a-b.

Ellipsoglandulina labiata (Schwager). Hayward, 2002, p.284, pl.1, figs.15-16.

Descriptive notes: Test large, uniserial throughout, circular cross-section; chambers increasing rapidly in size; final chamber enveloping up to two-thirds of test length; unornamented; semilunate, terminal aperture.

South Atlantic distribution: *1082:* Absent. *1088:* Present in 6% of samples; forms 0.12% of total EG; 3 specimens found in total, in 2 samples at 10.55 and 8.06 mcd, 850 and 673 ka, respectively; HO at ~8.06 mcd (~673 ka). Rare and only found at middle bathyal depth Site 1088.

World distribution: Cosmopolitan; Eocene-middle Pleistocene. Member of the South Atlantic Extinction Group.

Genus *Pleurostomella* Reuss, 1860

Pleurostomellina Schubert 1911

Ellipsonodosaria (*Ellipsodentalina*) Franke 1928

Pleuroskelidion Patterson 1987

Type species: *Dentalina subnodosa* Reuss, 1851

***Pleurostomella acuminata* Cushman, 1922.**

Pleurostomella acuminata Cushman, 1922, p.50, pl.19, fig.6; Loeblich and Tappan, 1994, p.133, pl.261, figs.11-12.

Pleurostomella sp. I. Hayward, 2002, p.284, pl.1, figs.20-21.

Descriptive notes: Elongate ovate chambers, biserial throughout, slender to moderately inflated, smooth test; ovate cross-section; often small; terminal aperture, with projecting hood on one side; often with initial spine.

South Atlantic distribution: *1082:* Absent. *1088:* Present in 19% of samples; forms 0.5% of total EG; common between 12.55 and 8.25 mcd (1000-684 ka), with highest abundance (13 specimens) at 12.55 mcd (1000 ka); HO at ~8.25 mcd (~684 ka). Found only at middle bathyal depths (1088).

World distribution: Cosmopolitan; ?Eocene-, Miocene-middle Pleistocene. Member of the South Atlantic Extinction Group.

***Pleurostomella alternans*, Schwager, 1866**

Pleurostomella alternans Schwager, 1866, p.238, pl.6, fig.79; Hayward, 2002, p.284, pl.1, figs.22-24.

Descriptive notes: Elongate, smooth, slender, moderately large test; chambers squat; initially regular biserial, becoming staggered; terminal aperture with projecting hood on one side.

South Atlantic distribution: *1082:* Absent. *1088:* Present in 42% of samples; forms 7% of total EG; common between 13.31 and 6.85 mcd (1035-601 ka), highest abundances between 12.10 and 11.56 mcd (967-928 ka); HO at ~6.85 mcd (~601 ka). Present only in middle bathyal depth Site 1088.

World distribution: Cosmopolitan; Oligocene-middle Pleistocene, ?Recent- Several live (stained) specimens recorded from the South Atlantic (Timm, 1992), may indicate that this species has survived in greatly reduced numbers in local refuges. Member of the South Atlantic Extinction Group.

***Pleurostomella brevis* Schwager, 1866**.

Pleurostomella brevis Schwager, 1866, p.239, pl.6, fig.81; Hayward, 2002, p.284, pl.1, figs.25-26.

Descriptive notes: Elongate, large, smooth, inflated test; chambers inflated, overlapping about half the test; terminal apertural medial slit long; prolocular end pointed or broadly rounded; apertural end broadly rounded.

South Atlantic distribution: *1082:* Absent. *1088:* Present in 3% of samples; forms 0.08% of total EG; 2 specimens in total found at 13.05 mcd (1025 ka). Rare and found only in middle bathyal depth Site 1088.

World distribution: Cosmopolitan; Late Eocene-middle Pleistocene. Member of the South Atlantic Extinction Group.

***Pleurostomella sapperi* Schubert, 1911**

Pleurostomella sapperi Schubert, 1911, p.56, figs.3a-b; Hayward, 2002, p.284, pl.1, figs.35-36.

Descriptive notes: Elongate, slender, moderately large test; chambers squat to ovate, biserial becoming staggered; costate; terminal aperture usually has a projecting hood on one side and the lower side with two small teeth projecting into it.

South Atlantic distribution: *1082:* Absent. *1088:* Present in 23% of samples; forms 1% of total EG; rare between 12.81 and 9.10 mcd (1015-752 ka), with highest abundance at 12.10 mcd (967 ka); HO at ~9.10 mcd (~752 ka). Found only at middle bathyal depth Site 1088.

World distribution: Cosmopolitan - SW Atlantic Ocean, Fiji, Cook Islands, Papua New Guinea, New Zealand, South Atlantic, North Atlantic; Pliocene-middle Pleistocene. Member of the South Atlantic Extinction Group.

Family Stilostomellidae Finlay, 1947

Genus *Myllostomella* Hayward, 2002

Type species: *Siphonodosaria fijiensis* Cushman, 1934

Remarks: This genus differs from *Stilostomella* in the possession of a flange-like, phialine lip around the aperture with internal denticles; and from *Siphonodosaria* in possessing a single, rather than double flange on the neck; long, rather than short, apertural denticles; and simple rather than strongly T-shaped apertural tooth.

***Myllostomella advena* (Cushman and Laiming, 1931)**

Nodogenerina advena Cushman and Laiming, 1931, p.106, pl.11, fig.19.

Myllostomella advena (Cushman and Laiming). Hayward, 2002, p.290, pl.3, figs.6-9.

Descriptive notes: Uniserial, elongate, gently tapering test of small-medium size; chambers squarish; sutures flush to weakly incised; smooth; rounded proloculus, spine absent; aperture at end of neck with single collar, 8-12 apertural denticles (Plate 4.1).

South Atlantic distribution: *1082:* Present in 20% of samples; forms 0.7% of total EG; common between 144.2 and 87.9 mcd (1280-833 ka), with highest abundances between 144.2 and 139.4 mcd (1280-1229 ka); HO at ~87.9 mcd (~833 ka). *1088:* Absent. Found only in lower bathyal depth Site 1082.

World distribution: Cosmopolitan – Japan, Taiwan, Gulf of Mexico, California, Indonesia, New Zealand, South Atlantic, North Atlantic; Miocene-early Pleistocene. Member of the South Atlantic Extinction Group.

***Myllostomella costai* (Schwager, 1866)**

Dentalina costai Schwager, 1866; Srinivasan and Sharma, 1980, (includes neotype).

Myllostomella fijiensis (Cushman, 1931). Hayward, 2002, p.290, pl.3, figs.10-12.

Descriptive notes: Uniserial, elongate, slightly arcuate test of medium to small size; globular prolocular "spine"; chambers becoming ovate; sutures flush to weakly incised; terminal aperture on end of neck with single collar, 4-8 long apertural denticles (Plate 4.1).

South Atlantic distribution: *1082:* Present in 30% of samples; forms 6% of total EG; common between 144.2 and 87.9 mcd (1280-833 ka), with highest abundance (400 specimens) at 134.2 mcd (1173 ka); HO at ~87.9 mcd (~833 ka). *1088:* Present in 45% of samples; forms 27% of total EG; common between 13.95 and 9.45 mcd (1068-771 ka), with highest abundance (151 specimens) at 11.95 mcd (957 ka); HO at ~9.45 mcd (~771 ka). Common in both lower and middle bathyal depths (1082 and 1088).

World distribution: Cosmopolitan; late Eocene-middle Pleistocene. Member of the South Atlantic Extinction Group.

***Myllostomella* cf. *japonica* (Ishizaki, 1943)**

Ellipsonodosaria japonica Ishizaki, 1943, p.682, figs.14-15.

Descriptive notes: Uniserial, elongate, small, slender test; chambers spherical in earlier part and become fusiform, later chambers show some ornamentation with short spines; terminal aperture on end of neck with single collar.

South Atlantic distribution: *1082:* Absent. *1088:* Present in 3% of samples; forms 0.2% of total EG; 4 specimens present at 11.95 mcd (957 ka). Found only in middle bathyal depth (1088).

World distribution: Cosmopolitan - Japan, Mexico, South Atlantic, North Atlantic; early Pliocene-middle Pleistocene. Member of the South Atlantic Extinction Group.

***Myllostomella matanzana* (Palmer and Bermudez, 1936)**

Ellipsonodosaria matanzana Palmer and Bermudez, 1936, p. 298, pl. 18, fig. 12.

Siphonodosaria lepidula f. *hyugaensis* (Ishizaki). Hayward, 2002, p.290, pl.3, figs.23-24 (non *Ellipsonodosaria hyugaensis* Ishizaki, 1943).

Descriptive notes: Uniserial, elongate, small test; chambers spherical in earlier part and fusiform, some specimens with small pustules on the lower part of adult chambers; some specimens showing a globular proloculus; terminal aperture on end of short neck with a single collar (Plate 4.1).

South Atlantic distribution: *1082:* Present in 77% of samples; forms 5% of total EG; common between 144.2 and 69.2 mcd (1280-704 ka), with highest abundances between 124.0 and 113.6 mcd (1076-1008 ka); HO at ~69.2 mcd (704.5 ka). *1088:* Present in 52% of samples; forms 20% of total EG; common between 14.38 and 6.85 mcd (1101-601 ka), with highest abundances between 12.10 and 11.56 mcd (967-928 ka); HO at ~6.85 mcd (~601 ka). Common at both lower and middle bathyal depths (1082 and 1088).

World distribution: Cosmopolitan - Malaysia, Japan, Aleutians, California, Mexico, Cuba, Caribbean, North Atlantic, South Atlantic, New Zealand; Oligocene-middle Pleistocene. Member of the South Atlantic Extinction Group.

Genus *Siphonodosaria* Silvestri, 1924

Nodogenerina Cushman, 1927

Sagrinodosaria Jedlitschka, 1931

Type species: *Nodosaria abyssorum* Brady, 1881

***Siphonodosaria sagrinensis* (Bagg, 1912)**

Nodosaria sagrinensis Bagg, 1912, p.58, pl.16, fig.4.

Siphonodosaria lepidula f. *lepidula* (Schwager), Hayward, 2002, p.290, pl.3, figs.25-32.

Siphonodosaria lepidula f. *spinata* (Cushman). Hayward, 2002, p.290, pl.3, figs.33-36.

Siphonodosaria hispidula (Cushman) Hayward, 2002, p.290, pl.3, figs.19-20 (in part).

Descriptive notes: *Siphonodosaria sagrinensis* (=*antillea*=*"lepidula"* s.l. of Hayward, 2002). Uniserial, elongate test of various size; chambers spherical, occasionally slightly campanulate, with some specimens with pustules or short spines on the lower part of each chamber; specimens can be highly variable, forming a continuum; rounded aperture, with one large T-shape dentate projection inside, and numerous, short internal denticles. Apertural opening at the terminal end of a long neck with double flanges (phialine lips).

South Atlantic distribution: *1082:* Present in 50% of samples; forms 5.4% of total EG; common between 144.2 and 69.2 mcd (1280-704 ka), with highest abundances between 136.0 and 124.0 mcd (1186-1076 ka); HO at ~69.2 mcd (~704.5 ka). *1088:* Present in

52% of samples; forms 32% of total EG; common between 14.38 and 9.85 mcd (1101-794 ka), with highest abundances between 12.10 and 11.19 mcd (967-899 ka); HO at ~9.85 mcd (~794 ka). Common fauna of the South Atlantic lower and middle bathyal depths (1082 and 1088).

World distribution: Cosmopolitan; early Miocene-middle Pleistocene. Member of the South Atlantic Extinction Group.

Siphonodosaria bradyi *Cushman, 1927*

Nodogenerina bradyi Cushman, 1927, p.79; Loeblich and Tappan, 1987, pl.585, figs.13-15.

Stilostomella sp. Weinholz and Lutze, 1989, p.117, fig.3A.

Descriptive notes: Uniserial, elongate, small to medium test; chambers distinctively bell-shaped (with continous keel around angled part of each chamber), with small spines at the edge of chambers; rounded aperture, with one large T-shaped dentate projection inside, and numerous, short internal denticles. Apertural opening at the terminal end of a long neck with double flanges (phialine lips).

South Atlantic distribution: *1082:* Present in 57% of samples; forms 36% of total EG; common between 144.2 and 87.9 mcd (1280-833 ka), with highest abundances between 144.2 and 112.0 mcd (1280-997 ka), with a large 'bloom' at 124.0 mcd (1076 ka) of 1240 specimens in one sample; HO at ~87.9 mcd (~832.5 ka). *1088:* Absent. *S. bradyi* is a dominant component (36% of the EG census population) of lower bathyal depth Site 1082, but is absent from middle bathyal depths of the South Atlantic study area.

World distribution: Cosmopolitan; Cuba (Oligocene), North Atlantic, South Atlantic (early-middle Pleistocene), New Zealand (Pliocene); Oligocene-middle Pleistocene. Member of the South Atlantic Extinction Group.

Siphonodosaria hispidula **(Cushman, 1917)**

Nodosaria lepidula var. *hispidula* Cushman, 1917, p.654; Cushman, 1921, pl.36, fig.7.

Siphonodosaria hispidula (Cushman), Hayward, 2002, p.290, pl.3, fig.18 (in part).

Descriptive notes: Uniserial, elongate, medium-large sized test; globular chambers, sutures weakly incised; dense, strongly developed ornamentation of short downward-pointing costae and spines; rounded aperture, with one large T-shaped dentate projection inside, and numerous, short internal denticles. Apertural opening at the terminal end of a long neck, with double flanges (phialine lips); prolocular spine may be present. Specimens are highly variable in their development of costate and spinose ornament.

South Atlantic distribution: *1082:* Present in 10% of samples; forms 0.3% of the total EG; rare between 144.2 and 123.0 mcd (1280-1070 ka), with highest abundance at ~144.2 mcd (1280 ka); HO at ~123.0 mcd (~1070 ka). *1088:* Present in 23% of samples; forms 1.5% of the total EG; rare between 13.31 and 10.11 mcd (1035-814 ka), with highest abundance (22 specimens) at 10.76 mcd (867 ka); HO at ~10.11 mcd (~814 ka). *S. hispidula* was rare but present at both lower and middle bathyal depths in the South Atlantic study area.

World distribution: Cosmopolitan – South Atlantic, North Atlantic, Japan, Philippines, New Zealand; Eocene-middle Pleistocene. Member of the South Atlantic Extinction Group.

***Siphonodosaria pomuligera* (Stache, 1864)**

Dentalina pomuligera Stache, 1864, p.204, pl.22, fig.31; Cushman, 1933, pl.3, fig.7.

Siphonodosaria pomuligera (Stache), Hayward, 2002, p.290, pl.3, figs.37-40.

Descriptive notes: Uniserial, elongate, medium to large sized test; robust, spherical chambers, with sutures becoming deeply incised; unornamented; rounded aperture, with one large T-shaped dentate projection inside, and 14-18 apertural denticles. Apertural

opening at the terminal end of a long neck, with double flanges (phialine lips); one/or several long prolocular spine/s.

South Atlantic distribution: *1082:* Absent. *1088:* Present in 3% of samples; forms 0.3% of the total EG; only 8 specimens found at 11.95 mcd (957 ka). Although rare, *S. pomuligera* was present in middle bathyal depths (1088) in the South Atlantic study area.

World distribution: Cosmopolitan; Eocene-middle Pleistocene. Member of the South Atlantic Extinction Group.

***Siphonodosaria recta* Palmer and Bermudez, 1936**

Ellipsonodosaria recta Palmer and Bermudez, 1936, p.297, pl.18, figs.6-7.

Siphonodosaria ketienziensis (Ishizaki), Hayward, 2002, p.290, pl.3, figs.21-22.

Descriptive notes: Uniserial, elongate, medium to large sized test; robust, globular chambers throughout, with wide limbate sutures throughout, becoming constricted, thick and opaque; may have weak, pustular spines on lower half of chambers; rounded aperture, with one large T-shaped dentate projection inside, and numerous apertural denticles. Apertural opening at the terminal end of a long neck, with double flanges (phialine lips); strong , off-centre, prolocular spine/or spines.

South Atlantic distribution: *1082:* Present in 7% of samples; forms 0.04% of the total EG; 3 specimens found in 2 samples, 143.0 and 134.2 mcd (1266 and 1173 ka, respectively); HO at ~134.2 mcd (~1173 ka). *1088:* Present in 10% of samples; forms 0.7% of total EG; rare between 11.95 and 10.95 mcd (957-881 ka), with highest abundance at 11.95 mcd (957 ka); HO at ~10.95 mcd (~881 ka). Rare but present in both lower and bathyal depths in the study area.

World distribution: Cosmopolitan- Japan, Cuba, New Jersey, New Zealand, South Atlantic, North Atlantic; Eocene-middle Pleistocene. Member of the South Atlantic Extinction Group.

***Siphonodosaria spinea* (Cushman, 1934)**

Ellipsonodosaria curvatura var. *spinea* Cushman, 1939, p.71, pl.12, fig.11.

Ellipsonodosaria sp. Cushman and Jarvis, 1934, pl.10, figs.4,5.

Siphonodosaria hispidula (Cushman). Hayward, 2002, p.290, pl.3, fig.15 (in part).

Descriptive notes: Uniserial, elongate, medium-large sized test; globular chambers, sutures weakly incised; dense, strongly developed ornamentation of short downward-pointing costae and spines. Differs from *S.hispidula* in the development of much heavier spinose ornament; rounded aperture, with one large T-shaped dentate projection inside, and numerous, short internal denticles. Apertural opening at the terminal end of a long neck, with double flanges (phialine lips); prolocular spine may be present (Plate 4.1).

South Atlantic distribution: *1082:* Absent. *1088:* Present in 10% of samples; forms 0.8% of the total EG; rare between 11.95 and 8.76 mcd (957-724 ka), with highest abundances at 11.95 and 11.19 mcd (957 and 899 ka); HO at ~8.76 mcd (~724 ka). Rare in middle bathyal depths in the South Atlantic study area (1088), absent in lower bathyal depths (1082).

World distribution: ?Cosmopolitan; Eocene-middle Pleistocene. Member of the South Atlantic Extinction Group.

Genus *Stilostomella* Guppy, 1894

Type species: *Stilostomella rugosa* Guppy, 1894, OD.

***Stilostomella fistuca* (Schwager, 1866)**

Nodosaria fistuca Schwager, 1866, p.216, pl.5, figs.36-37.

Stilostomella fistuca (Schwager). Hayward, 2002, p.290, pl.3, figs.41-45.

Descriptive notes: Uniserial, elongate, large test; ovate chambers, becoming elongate-ovate in adult specimens, seperated by incised sutures; dense, short, pustulose ornament

over the entire test, including short neck; aperture on end of stout neck, lacking a phialine lip or flange, however bearing one or several (4 or more) infolded triangular teeth (Hayward, 2002, p.290, pl.3, fig.45). In some specimens internal apertural teeth may development into a loose mesh network (Hayward, 2002, p.290, pl.3, fig.43) (Plate 4.1).

South Atlantic distribution: *1082:* Present in 30% of samples; forms 0.2% of the total EG; rare between 144.2 and 89.7 mcd (1280-843 ka), with highest abundances between 144.2 and 136.0 mcd (1280-1186 ka); HO at ~89.7 mcd (~843 ka). *1088:* Present in 23% of samples; forms 0.8% of the total EG; rare between 14.38 and 11.56 mcd (1101-928 ka), with highest abundances at 12.55 and 11.95 mcd (1000 and 957 ka, respectively); HO at ~11.56 mcd (~928 ka). Rare at both lower and middle bathyal depths in the South Atlantic study area.

World distribution: Cosmopolitan; middle Eocene-middle Pleistocene. Member of the South Atlantic Extinction Group.

***Stilostomella holoserica* (Schwager, 1866)**

Nodosaria holoserica Schwager, 1866, p.221, pl.5, fig.49.

Stilostomella holoserica (Schwager, 1866). Hayward, 2002, p.290, pl.3, figs.46-48.

Descriptive notes: Uniserial, elongate, variable-sized test; spherical chambers, tending ovate in adult specimens, seperated by narrow necks (after the first two chambers); finely spinose over the entire test; stout apertural neck lacking a phialine lip or flange, rather a wavy-rimmed aperture with loose infolded, triangulat teeth, commonly connected by a partially developed mesh network (Hayward, 2002, p.290, pl.3, fig.47) (Plate 4.1).

South Atlantic distribution: *1082:* Present in 13% of samples; forms 0.09% of total EG; rare between 144.2 and 89.7 mcd (1280-843 ka), with highest abundance at 144.2 mcd (1280 ka); HO at ~89.7 mcd (~843 ka). *1088:* Absent. *S. holoserica* is found only in lower bathyal depth site 1082.

World distribution: Cosmopolitan; early Eocene-middle Pleistocene. Member of the South Atlantic Extinction Group.

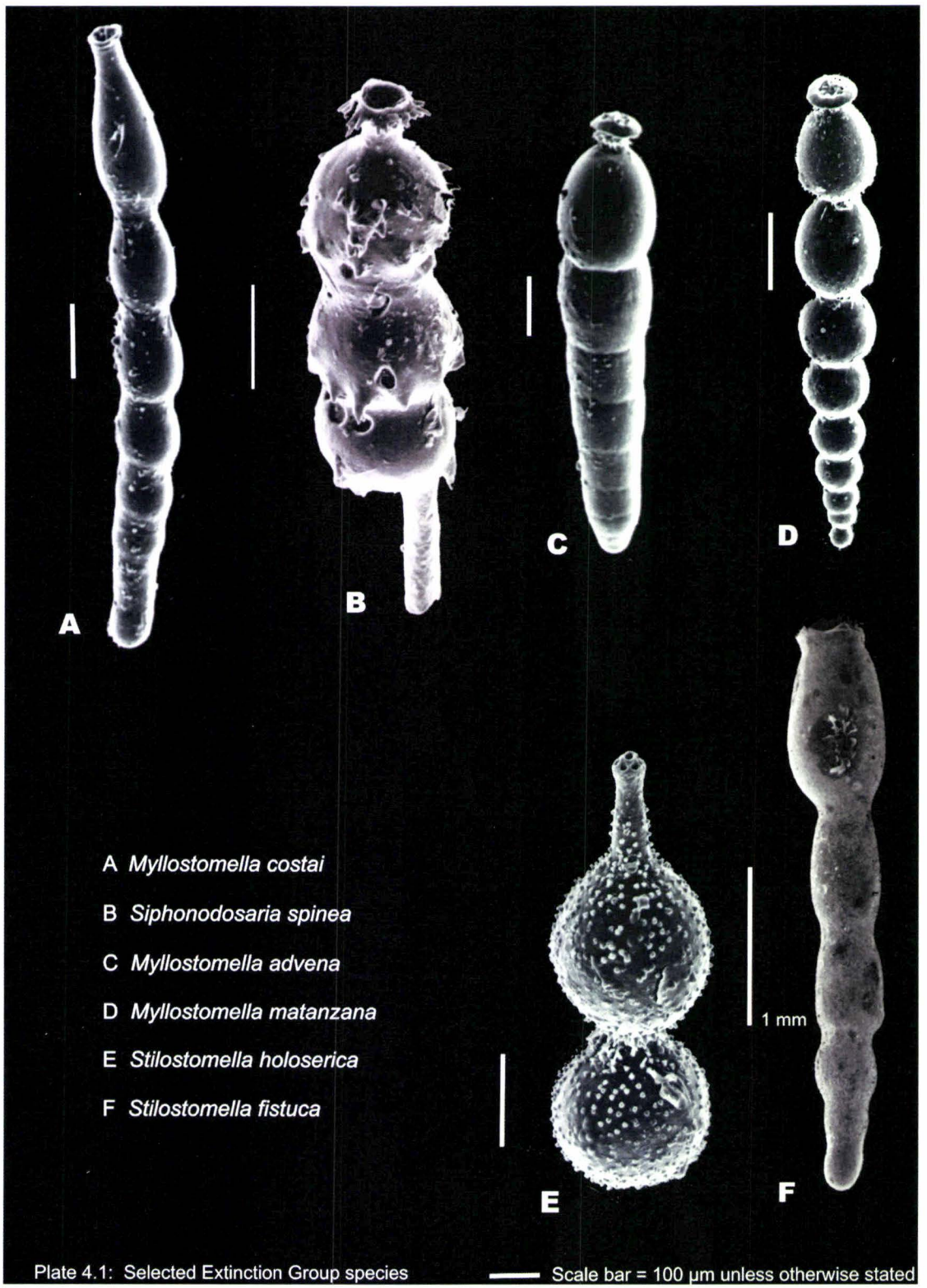

Plate 4.1: Selected Extinction Group species — Scale bar = 100 µm unless otherwise stated

4.3 *South Atlantic Survivor Group*

Reference list of calcareous, elongate, uniserial Survivor Group species of benthic foraminifera present in late Pliocene and Pleistocene sections of ODP Sites 1082 and 1088 and surviving through the MPT in the South Atlantic study region. SG species were identified from original descriptions, sketches and published SEM images. In some cases unpublished SEM and digital images (from Kawagata and others of Geomarine Research, Auckland, New Zealand) were also used to confirm SG identities. Some SG specimens were unable to be identified to species level, and have been given sp.A, sp.B or sp.C attachments.

South Atlantic Survivor Group

Acostina sp.A	
Astacolus insolitus	(Schwager). Jones, 1994, pl.67, fig.17.
Astacolus sp.A	
Dentalina mutablis	(Costa). Cushman, 1923, pl. 1, figs. 30-32; Jones, 1994, pl.64, figs.20-22.
Dentalina sp. B	
Glandulina ovula	(d'Orbigny). Jones, 1994, pl. 61, figs. 17-22.
Glandulina sp.A.	
Grigelis orectus	Loeblich and Tappan. Hayward *et al.*, 1999, pl.6, fig.14.
Grigelis sp.A.	
Grigelis. sp.B.	
Laevidentalina advena	(Cushman). Jones, 1994, pl.63, fig.1.
Laevidentalina ariena	Patterson and Pettis 1986. Jones, 1994, pl.62, figs.27-31.
Laevidentalina frobisherensis	Loeblich and Tappan, 1953, pl. 10, figs.1-9.
Laevidentalina guttifera	Reuss, 1851, pl. 3, figs. 4a-b.
Laevidentalina sidebottomi	(Cushman, 1933). Loeblich and Tappan, 1994, pl.113, figs.13-19.

Laevidentalina subsoluta	(Cushman, 1923). Jones, 1994, pl.62, figs.13-16.
Laevidentalina vagina	(Stache, 1864). Hornibrook, 1971, pl.7, figs.119-124; Jones, 1994, pl.62, figs.25-26 (as *Dentalina subemaciata*).
Laevidentalina sp.A	
Laevidentalina sp.B	
Laevidentalina sp.C	
Marginulina obesa	(Cushman). Jones, 1994, pl.65, figs.5-6.
Martinottiella communis	(d'Orbigny, 1826). Loeblich and Tappan, 1964, C280,pl.188, figs.10-11.
Martinottiella variablis	(Schwager). Hayward, 2002, p.288, pl.2, fig.4.
Nodosaria inflexa	(Silvestri, 1872). Jones, 1994, pl.62, fig.9.
Nodosaria longiscata	d'Orbigny, 1846, pl. 1, fig. 43.
Nodosaria sp.A	
**Parafrondicularia javana*	(Boomgaart). Hayward, 2002, p.284, pl.1, figs.5-7 (in part-as *Proxifrons inaequalis*-see note below).
Pseudonodosaria brevis	(Reuss). Loeblich and Tappan, 1994, pl. 117, figs. 1-6.
Vaginulina inflata	Parr, 1950, pl.11, figs.21,22.
Vaginulina spinigera	Brady. Jones, 1994, pl.67, figs.13-14.
Vaginulina sp.Elongate	
Vaginulinopsis albatrossi	(Cushman). Jones, 1994, pl.66, figs.24-25.
Vaginulinopsis sp.A	

***Parafrondicularia javana* (Boomgaart, 1949)**

Proxifrons javana (Boomgaart). Loeblich and Tappan, 1994, pl. 118, figs.8-10.

Frondicularia inaequalis Costa. Brady, 1884, pl.66, figs. 8-10.

Proxifrons inaequalis (Costa). Hayward, 2002, p.300, pl.1, figs.5-7 (in part).

Descriptive notes: Narrow elongate test, especially in the initial part; early irregular chamber arrangement, later uniserial chevron-shaped chambers; maybe one or two weak

early costae. Once 'lumped' together with *Proxyifrons inaequalis,* forms are somewhat irregular and narrowly flaring (Hayward, 2002, Pl. 2, Figs.5-7), and are thought to die-back to rare specimens during the mid Pleistocene and possibly persist into the Recent.

South Atlantic distribution: *1082:* 2 specimens present at 57.69 mcd (582.5 ka). This species is thought to have persisted through the mid-Pleistocene extinction interval in the South Atlantic study area. No specimens were found in ODP 1088.

World distribution: New Zealand, North Atlantic, South Atlantic; mid Pleistocene-Recent.

4.4 *South Atlantic Low-Oxygen Tolerant Group*

Population density changes in infaunal, low-oxygen tolerant species (e.g. *Bolivina* spp., *Bulimina* spp., *Trifarina* spp., *Uvigerina* spp., etc.), are thought to reflect changes in water mass ventilation (dissolved oxygen concentrations) and food supply (organic carbon flux) in benthic environments (e.g Boersma, 1986; Kaiho, 1994; Kawagata *et al.*, in press). These survivor taxa are elongate agglutinated and elongate, biserial or multiserial calcareous deep-sea benthic foraminifera. Several species termed the Low-Oxygen Tolerant Group were counted during this study and absolute abundance and accumulation rate calculated for use as a proxy for changes in the parameters mentioned above. LOTG species were identified from original descriptions, sketches and published SEM images. In some cases unpublished SEM and digital images (from Kawagata and others of Geomarine Research, Auckland, New Zealand) were also used to confirm LOTG identities.

South Atlantic Low-Oxygen Tolerant Group

Bolivina pussilla	(Schwager, 1866).
Bolivina subspinscens	(Cushman, 1922). Jones, 1994, pl.52, figs.24-25.
Bolivina sp.A	
Bulimina aculeata	d'Orbigny, 1826, p.7; Hayward *et al.*, 2002, pl.1, figs.5-6.
Bulimina exilis	Brady, 1884, pl.3, figs.1-2.
Bulimina marginata	d'Orbigny, 1826, p.269, no.4, pl.XII, figs.10-12; Hayward *et al.*, 1999, pl.9, figs.13-15.
Bulimina mexicana	d'Orbigny, 1826. Jones, 1994, pl.51, figs.10-13.
Bulimina truncana	Gumbel, 1868; Hayward *et al.*, 2002, pl.1, figs.9-10.
Cassidella bradyi	(Cushman, 1922). Jones, 1994, pl.52, fig.9.
Eggerella bradyi	(Cushman, 1911). Loeblich and Tappan, 1964, C276, pl.186, fig.1; Jones, 1994, pl.47, figs.4-6.
Evolvocassidulina spp.	

Fursenkoina complanata	(Egger, 1893). Jones, 1994, pl.52, figs.1-3.
Globobulimina affinis	(Cushman, 1927). Jones, 1994, pl.50, figs.7-8.
Karreriella bradyi	(Cushman, 1911). Jones, 1994, pl.46, figs.1-4; Hayward, 2002, p.288, pl.2, fig.1.
Praeglobobulimina spinscens	(Brady, 1884). Jones, 1994, pl.50, figs.11-12.
Rutherfordoides rotundata	(Parr, 1950). Jones, 1994, pl.52, figs.10-11.
Trifarina anglosa	(Williamson, 1858). Jones, 1994, pl.74, figs.15-16; Hayward *et al.*, 2002, pl.1, figs.16-17.
Uvigerina peregrina	(Cushman). Hayward *et al.*, 2002, pl.1, figs.20-21.
Uvigerina proboscidea	Schwager, 1866, p.250, pl.7, fig.96.
Uvigerina hispida	Schwager, 1866, p.249, pl.7, fig.95; Boersma, 1984, p.74, figs.1-4.
Uvigerina hollocki	(Thalmann, 1950). Jones, 1994, pl.74, figs.6-7.

5. RESULTS

A census was undertaken on each sample at both Sites 1082 and 1088 (Appendix 1). The census included measuring and recording several sedimentological properties (proxies), miscellaneous microfossil abundance data, and changes in the abundance and accumulation rate of individual Extinction Group, Survivor Group and Low-Oxygen Tolerant Group species. Statistical analyses using Pearson's correlation coefficient were employed to measure the strength of the relationship between any two variables. Each group of data is summarised below.

5.1 Environmental Proxies

Changes in the $\%CaCO_3$, Sedimentation Rate (SR), Fragmentation Index (FI), Accumulation Rate (AR) of Ice-Rafted Debris (IRD) (Site 1088), %Planktic Foraminifera (%PF), and the Number of Gypsum Rhombs (Site 1082), were investigated and are recorded in appendix 1. Energy Dispersive Spectrometry (EDS) results for gypsum rhombs are given in appendix 2.

5.1.1 Site 1082

Proxy environmental data for Site 1082 are shown in figure 5.1. The colour reflectance data of Wefer *et al.* 1999 showed clear cyclic variations in chromaticity b values, suggesting fluctuations in $\%CaCO_3$ over glacial-interglacial cycles. $CaCO_3$ values range between 10 and 70% over the MPT, reflecting fluctuations in the delivery of organic matter across the study interval. Sedimentation rates (SR) ranged between 16.4 and 8.5 cm/kyr (Fig. 5.1), with the highest rate of sediment deposition occurring during the late MPT, between 865 and 720 ka (94 and 71 mcd); SR steadily declined to 8.5 cm/kyr in the youngest sample at 580 ka (58 mcd). No IRD was found in Site 1082. The FI values ranged from 100 to 1, with a period of complete dissolution of planktic foraminifera at 1075 ka (124 mcd) (FI = 100) (Fig. 5.1). This high dissolution interval coincides with a peak in gypsum rhomb accumulation, and also, a %PF value of zero (complete dissolution of planktic foraminifera). %PF in Site 1082 ranged from 91% to 0%. Low troughs in %PF correlate with peaks in FI (especially at 1075 ka (124 mcd), 930 ka (103 mcd) and 750 ka (75 mcd)). The number of gypsum rhombs/g sediment for

each sample was recorded, ranging from 0 to 46. There is a clear peak in gypsum rhomb accumulation (46/g sed) coinciding with a period of elevated dissolution at 1075 ka (124 mcd, FI = 100, %PF = 0). However, although some peaks in the number of gypsum rhombs/g sed correspond with peaks in dissolution proxy, this relationship was not consistent down the core. For example, the peak at 1075 ka (124 mcd) where gypsum rhombs = 46/g sed, the FI = 100, whereas at 1010 ka (114 mcd) the gypsum rhombs = 30/g sed, and the FI = 1.7; at 940 ka (105 mcd) the gypsum rhombs = 33/g sed, and the FI = 2.1; and at 650 ka (64 mcd) the gypsum rhombs = 42/g sed, and the FI = 3.0 (Fig. 5.1).

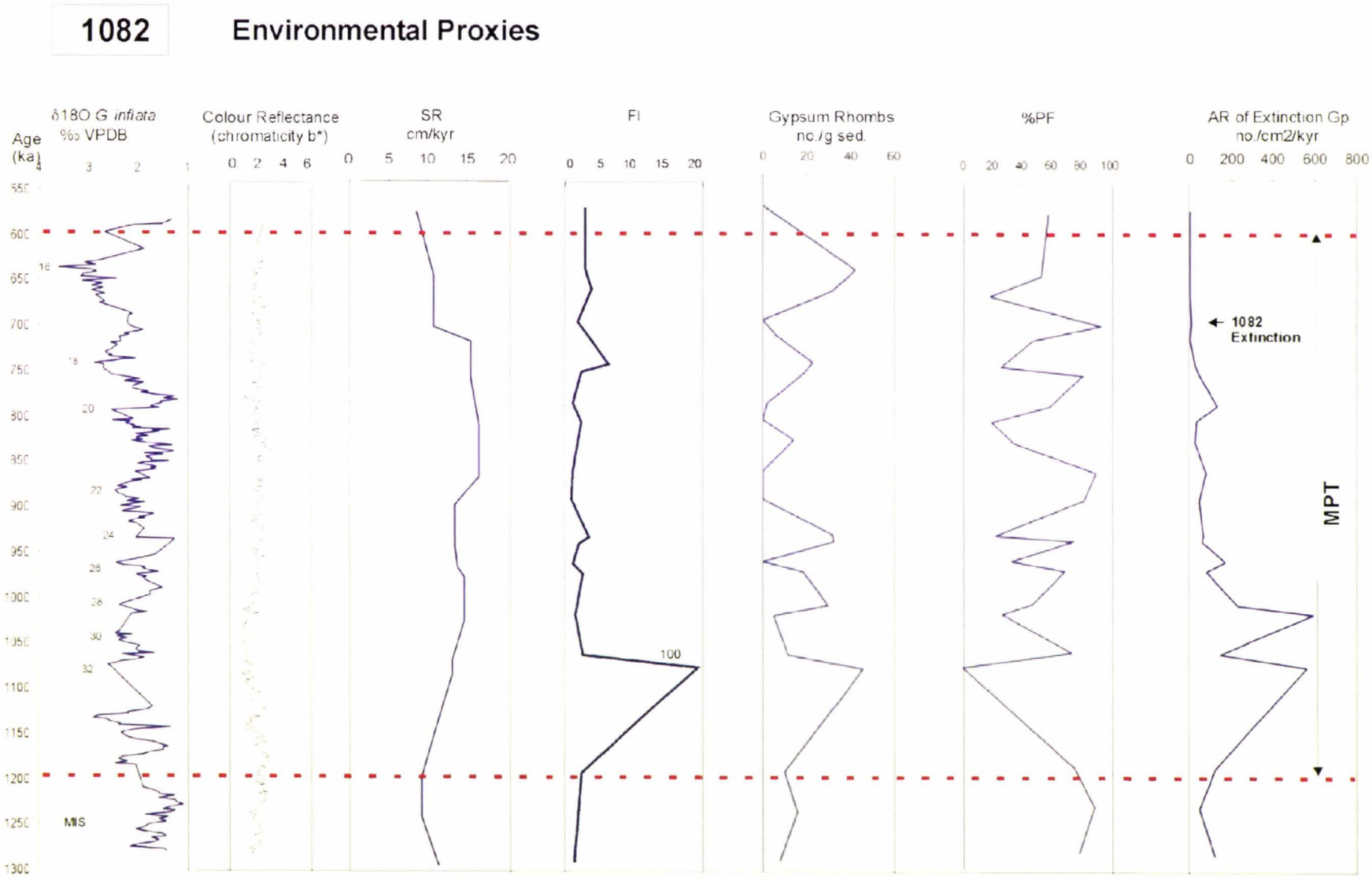

FIGURE 5.1: Environmental Proxy records for Site 1082. Planktic foraminiferal oxygen isotope data from Jahn *et al.* 2003; spliced composite colour reflectance curve is from Wefer *et al.* 1998. Selected glacial marine oxygen isotope stages (MIS) are labelled.

5.1.2 Site 1088

Proxy environmental data for Site 1088 is shown in figure 5.2. Calcium carbonate data of Hodell *et al.* (2003) showed clear cyclic glacial-interglacial fluctuations, with values fluctuating between 83 and 90%. Lowest values occurred at 1015 ka (12.8 mcd), 750 ka (9.1 mcd) and 685 ka (8.3 mcd) (all 83%), with a clear increase in the amplitude of $\%CaCO_3$ fluctuation during the MPT. $CaCO_3$ variations return to near 90% values post~650 ka (~ 7.8 mcd), with only minor fluctuations after this point. The SRs varied from 1 to 2.6 cm/kyr, with a fairly constant rate during the MPT. SR declined from 1.7 to 1 between 700 ka (8.5 mcd) and the youngest sample at 508 ka (5.4 mcd). Cyclic fluctuations in IRD accumulation were present at Site 1088. The accumulation rate of IRD ranged from 69 to 1 per cm^2/kyr, with major peaks in AR at 930 (11.6 mcd) and 760 ka (6.7 mcd). The FI values at Site 1088 ranged from 2.4 to 0.9. There were two slight peaks in FI at 945 (11.8 mcd) and 590 ka (6.7 mcd), with FI values of 2.3 and 2.4 respectively. These peaks coincide with %PF values of 98 and 95% respectively. Between these two points, the MPT is characterised by only minor fluctuations in FI, with the period between 900 and 600 ka having an average FI of ~ 1.5. The %PF values in Site 1088 ranged from 99% to 95%. The lowest value occurred at 590 ka (6.7 mcd), with a %PF value of 95. Gypsum rhombs were not found in any Site 1088 samples.

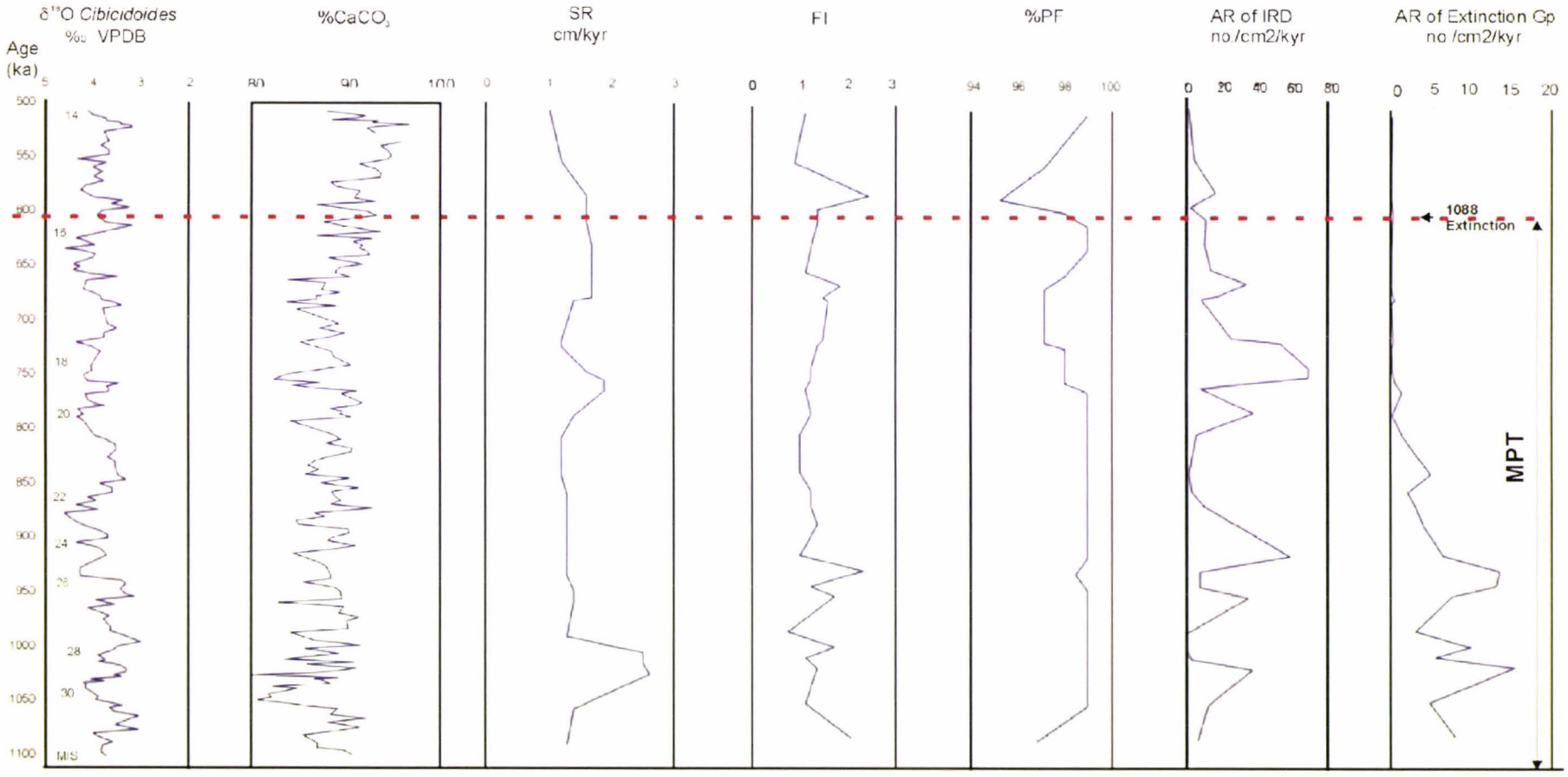

FIGURE 5.2: Environmental Proxy records of Site 1088. Benthic foraminiferal oxygen isotope data and $CaCO_3$ data from Hodell *et al.* 2003. Selected glacial marine oxygen isotope stages (MIS) are labelled.

5.2 *Miscellaneous Microfossil Data*

The numbers of radiolaria and ostracods encountered were recorded and are shown in figures 5.3 and 5.4. There was no attempt made to identify radiolarian and ostracod specimens to genus or species level, as this was beyond the scope of this study. However, changes in the abundance of these microfossils as a whole were recorded as fluctuations may coincide with the decline and extinction of the EG taxa.

5.2.1 Site 1082

In the study interval of Site 1082 there were two prominent peaks in the abundance of radiolaria (Fig. 5.3). These peaks occurred at 1075 ka (124 mcd) and 845 ka (90 mcd), with values of 23 and 14/g sed., respectively. Throughout the interval, radiolarian abundance ranged from 0 to 23/g sed. The AR of radiolaria in Site 1082 was highly variable, with values ranging from 308 radiolaria/cm^2/kyr at 1075 ka (124 mcd) to as low as 8 radiolaria/cm^2/kyr at 1020 ka (116 mcd). The AR of radiolaria declined after a sharp drop at ~ 1060 ka (121 mcd), with relatively low abundances occurring throughout the MPT. Ostracods occurred less frequently than radiolaria, with abundances ranging between 0 and 2/g sediment (Fig. 5.3). Peaks of 2/ g sed. occurred at 865 ka (94 mcd) and 705 ka (69 mcd) at Site 1082. The AR of ostracods ranged between 31 to 0/cm^2/kyr. There were two distinct peaks in the AR of ostracods, one at 895 ka (94 mcd) and another at 705 ka (69 mcd), with values of 31 /cm^2/kyr and 25/cm^2/kyr, respectively (Fig. 5.3). Between these prominent peaks there was a sharp drop in AR at 865 ka (94 mcd), where values remained between 0 – 2/cm^2/kyr.

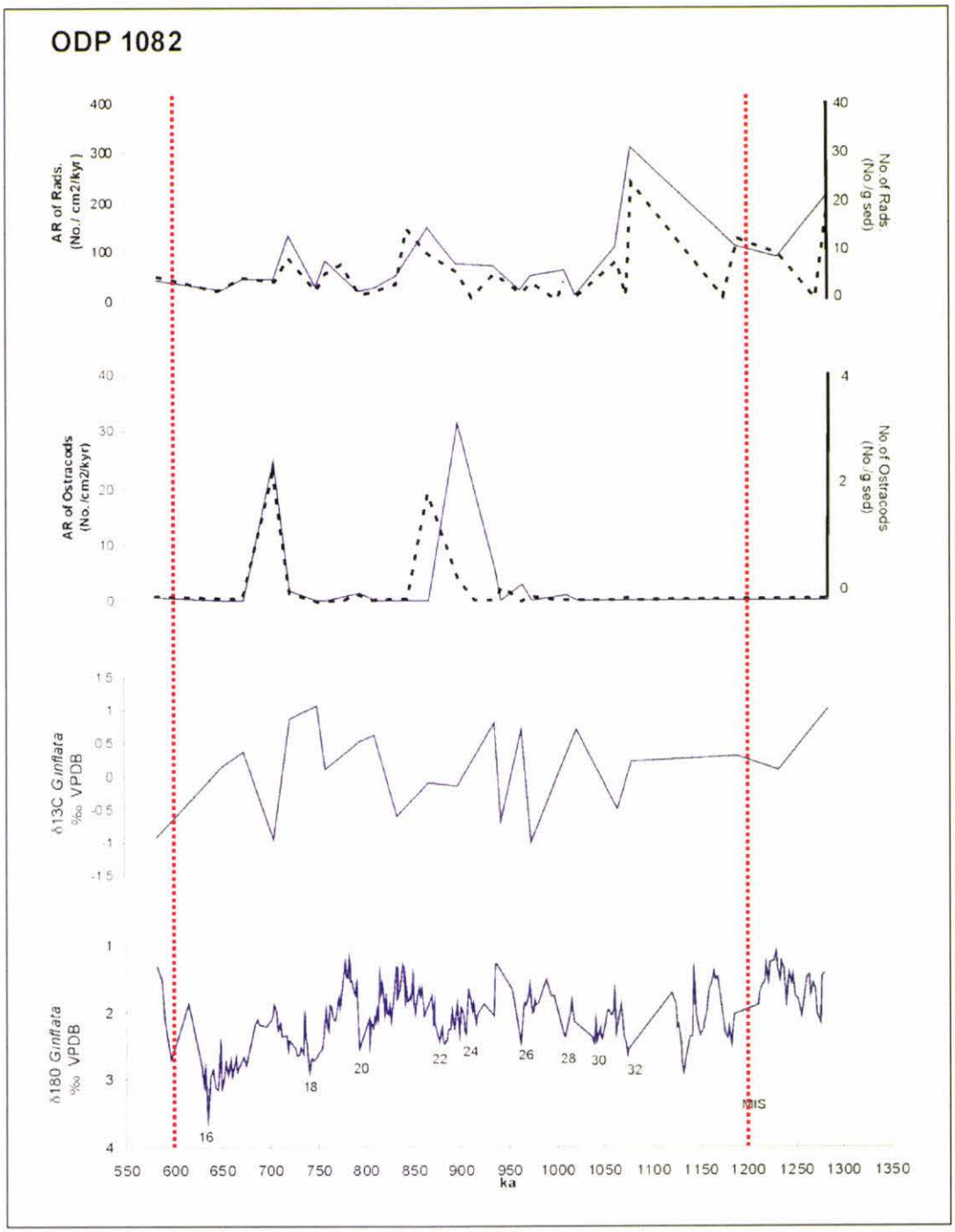

FIGURE 5.3. Absolute abundance (specimens/g sediment) (-----) and accumulation rate (——) of radiolaria and ostracods in Site 1082. Isotopic oxygen and carbon records are from Jahn *et al.* (2003).

5.2.2 Site 1088

In Site 1088 abundances of radiolaria ranged from 0.4 to 24/ g sed., with peaks at 945 ka (11.8 mcd), 795 ka (9.9 mcd), 750 ka (9.1 mcd), and 560 ka (6.3 mcd) (Fig. 5.4). These peaks have values of 24, 14, 12 and 13/g sed., respectively. There is also a visible decline in abundance between 750 and 600 ka (9.1 and 6.9 mcd). The AR of radiolaria at Site 1088 was highly variable across the study interval, with values ranging from 31 radiolaria/cm^2/kyr at 945 ka (11.8 mcd) to 1 radiolaria/cm^2/kyr at 615 ka (7.1 mcd).

As in Site 1082 ostracods occurred less frequently than radiolaria, abundances ranging between 0 and 5/g sed. (Fig. 5.4). Peaks of 4 and 5/g sed. occurred at 1000 ka (12.6 mcd) and 850 ka (10.6 mcd). Again, as with radiolaria, there was a clear decline in abundance in Site 1088 between 750 and 600 ka (9.1 and 6.9 mcd), to zero at 588 ka (6.7 mcd). The AR of ostracods at Site 1088 was again highly variable across the MPT and ranged from 6 ostracods/cm^2/kyr at 1000 ka (12.6 mcd) to 0 ostracods/cm^2/kyr at 590 ka (6.7 mcd).

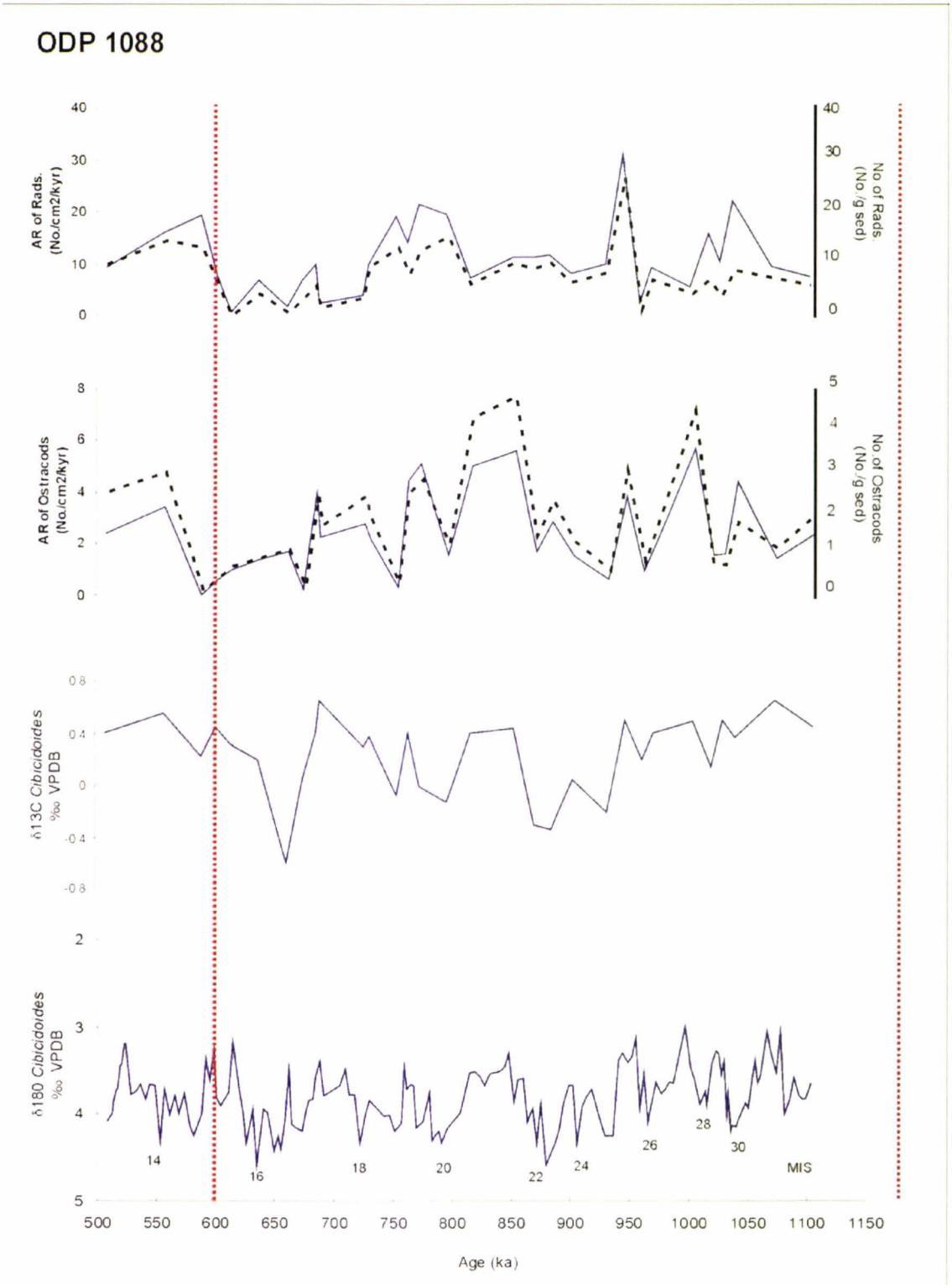

FIGURE 5.4. Absolute abundance (specimens/g sediment)(-----) and accumulation rate (——) of radiolaria and ostracods at Site 1088. MPT (-----). Isotopic oxygen and carbon records are from Hodell *et al.* (2003).

5.3 The Stilostomella Extinction Group (EG)

5.3.1 Taxonomic Composition

In these two South Atlantic deep sea sites 33 species from 11 genera of elongate and/or uniserial benthic foraminifera (Table 3.1, Appendix 1) became extinct, at least regionally, in the MPT (1200 – 600 ka).

At the shallower Site 1082, the EG comprises 24 species from 9 genera: *Awhea, Chrysalogonium, Cribronodosaria, Myllostomella, Orthomorphina, Parafrondicularia, Proxifrons, Siphonodosaria,* and *Stilostomella* (Fig. 5.5). The deeper Site 1088 has 22 species from 10 genera in the EG: *Awhea, Chrysalogonium, Ellipsoglandulina, Myllostomella, Orthomorphina, Parafrondicularia, Pleurostomella, Proxifrons, Siphonodosaria,* and *Stilostomella* (Fig. 5.6).

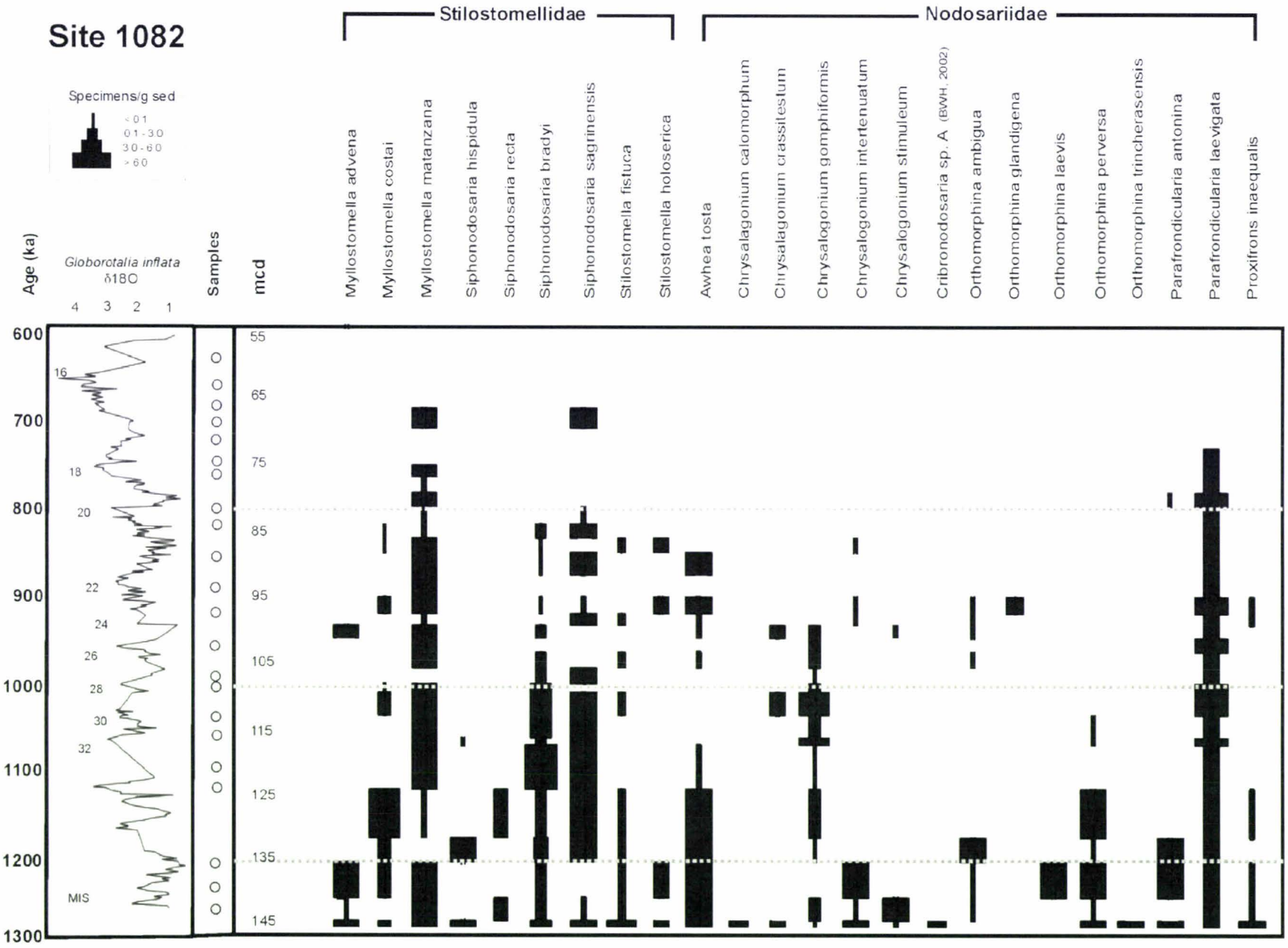

FIGURE 5.5. Stratigraphic records and highest occurrence (HO) of Extinction Group taxa (absolute abundance - specimens/g sediment) versus age (of Jahn *et al.*, 2003) from Site 1082. Marine oxygen isotope stages (MIS) are given.

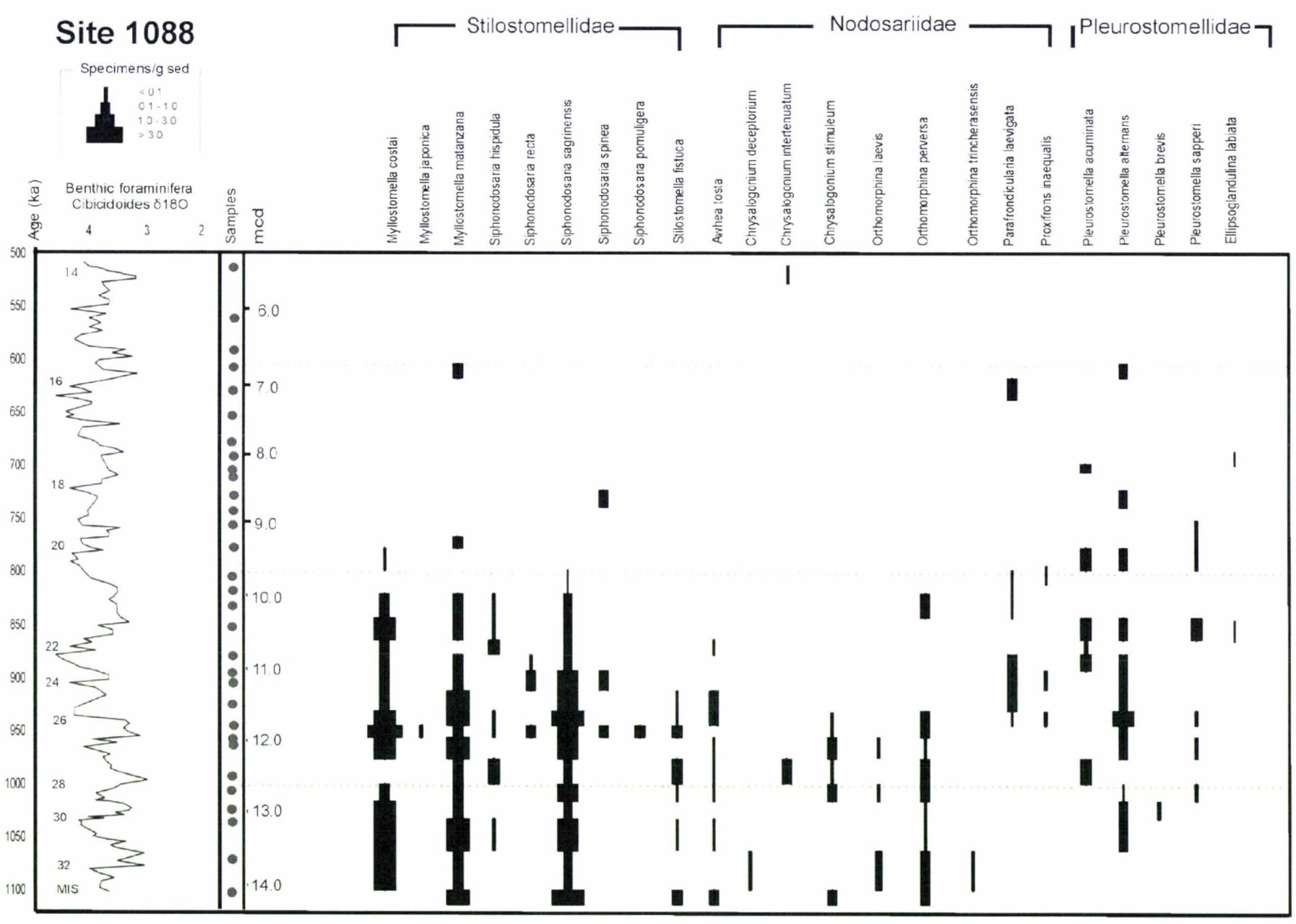

FIGURE 5.6. Stratigraphic records and highest occurrence (HO) of Extinction Group taxa (absolute abundance - specimens/g sediment) versus age (of Hodell *et al.*, 2003) from Site 1088. Marine oxygen isotope stages (MIS) are given. Note: *Chrysalogonium intertenuatum* survived through the MPT at Site 1088.

In the Pleistocene, 10 EG species (*Chrysalogonium calomorphum, C. crassitestum, C. gomphiformis, Cribronodosaria* sp.A, *Myllostomella advena, Orthomorphina ambigua, O. glandigena, Parafrondicularia antonina, Siphonodosaria bradyi,* and *Stilostomella holoserica*) were restricted in their occurrence to the shallower Site 1082 (1280 m depth); whereas 9 EG species (*Chrysalogonium deceptorium, Ellipsoglandulina labiata, Myllostomella japonica, Pleurostomella acuminata, P. alternans, P. brevis, P. sapperi, Siphonodosaria pomuligera,* and *S. spinea*) were found only in the deep Site 1088 (2082 m depth). Approximately 40% (13 species) of all recovered EG species are common to both sites. These species were *Awhea tosta, Chrysalogonium stimuleum, Myllostomella costai, Myllostomella matanzana, Orthomorphina laevis, Orthomorphina perversa, Orthomorphina trincherasensis, Parafrondicularia laevigata, Proxifrons inaequalis, Siphonodosaria hispidula, Siphonodosaria recta, Siphonodosaria sagrinensis,* and *Stilostomella fistuca*. Of the most recently recorded total number of mid-Pleistocene '*Stilostomella*' Extinction Group taxa, this study shows 33 of 67 (Hayward, 2002; Kawagata *et al.*, in press) species were recognised to become extinct in the South Atlantic Ocean, representing approximately 50% of the total known EG taxa. *Chrysalogonium intertenuatum*, a member of the EG taxa in previous studies (North Atlantic and SW Pacific), occurs in both cores in the study area, however, becomes locally extinct at Site 1082 only, seemingly surviving in low numbers at Site 1088.

5.3.2 Pattern of MPT Declines in Absolute Abundances and Diversity

The abundance and diversity of the EG was greatest at middle bathyal depth Site 1082, beneath AAIW (at 1280 m, 24 species, up to 42.5 specimens per g/sed.), and slightly lower at lower bathyal Site 1088 (at 2082 m, 22 species, up to 10.4 specimens per g/sed.), bathed in waters of the uCPW/NADW interface. The absolute abundances (specimens/g sediment) and accumulation rate (specimens/cm^2/kyr) of the EG had higher values prior to ~1000 ka, and declined progressively throughout the MPT. The EG was dominant within the targeted species (EG and SG) in both sites pre ~1000 ka, with several low troughs in the relative abundance of the EG during this time (Figs. 5.1 and 5.2). Figure 5.7 and 5.9 show the overall decline at both sites, typically, with substantial reductions in abundance and diversity going into and during glacial periods, with partial, although generally decreasing recovery during the mid- to end of the intervening warm interglacial period.

5.3.2.1 Site 1082

The pulsed decline and eventual local extinction of the EG taxa at Site 1082 is shown in figure 5.7. Oxygen isotope records obtained for the planktic foraminifera *Globorotalia inflata* (of Jahn *et al.*, 2003) and fluctuations in the number of EG specimens encountered per gram of sediment and AR show a clear trend of declining abundance and AR going into and during glacial cool periods throughout the MPT, and partial recoveries in the EG taxa during the intervening warm interglacial periods. Abundance and AR of EG taxa peaked at 124 mcd (1075 ka, ~MIS 31), with an abundance of 42 EG taxa/g sed. and AR of 556 specimens/cm^2/kyr. Abundance and AR dropped dramatically going into glacial period MIS 30, with numbers dropping to 11 specimens/g sed. and 142 specimens/cm^2/kyr, at 121 mcd (1060 ka). Complete recovery of abundance of the EG was obtained in the next intervening warm interglacial MIS 29, 116 mcd (1020 ka), with abundance and AR reaching 41 specimens/g sed. and 595 specimens/cm^2/kyr, respectively. After ~1000 ka, the abundance and AR of EG taxa declined abruptly, with comparatively smaller amplitude pulses (decline and partial recovery) in abundance and AR towards the final extinction datum for the *Stilostomella* EG taxa at Site 1082. Entering into glacial period MIS 28, numbers dropped to 5 specimen/g sed., and AR of 76 specimens/cm^2/kyr, at 112 mcd (1000 ka), after which recovery to pre ~ 1000 ka levels were never achieved. Declines in EG taxa occurred at MIS 24 (105 mcd (940 ka); with an abundance of 5 specimens/g sed.; AR: 62 specimens/cm^2/kyr), MIS 22 (98 mcd (895 ka); with an abundance of 3 specimens/g sed.; AR: 44 specimens/cm^2/kyr), MIS 20 (88 mcd (835 ka); with an abundance of 2 specimens/g sed.; AR: 26 specimens/cm^2/kyr), entering into MIS 18 (79 mcd (775 ka); with an abundance of 1 specimen/g sed.; AR: 18 specimens/cm^2/kyr), and to zero entering into MIS 16 (71 mcd (720 ka)). Declining partial recoveries of EG taxa occurred during intervening warm periods and are shown in figure 5.7. Also shown in this figure is a very slight increase in abundance and AR following MIS 16, at 69 mcd (705 ka), and represented the identification of 4 *Myllostomella matanzana* specimens and 16 *Siphonodosaria sagrinensis* specimens in this sample. No EG taxa were encountered in any samples after this point (post ~700 ka); the highest occurrence of these two species is thought to represent the *Stilostomella* Extinction Datum at Site 1082 (Figs. 5.5 and 5.7).

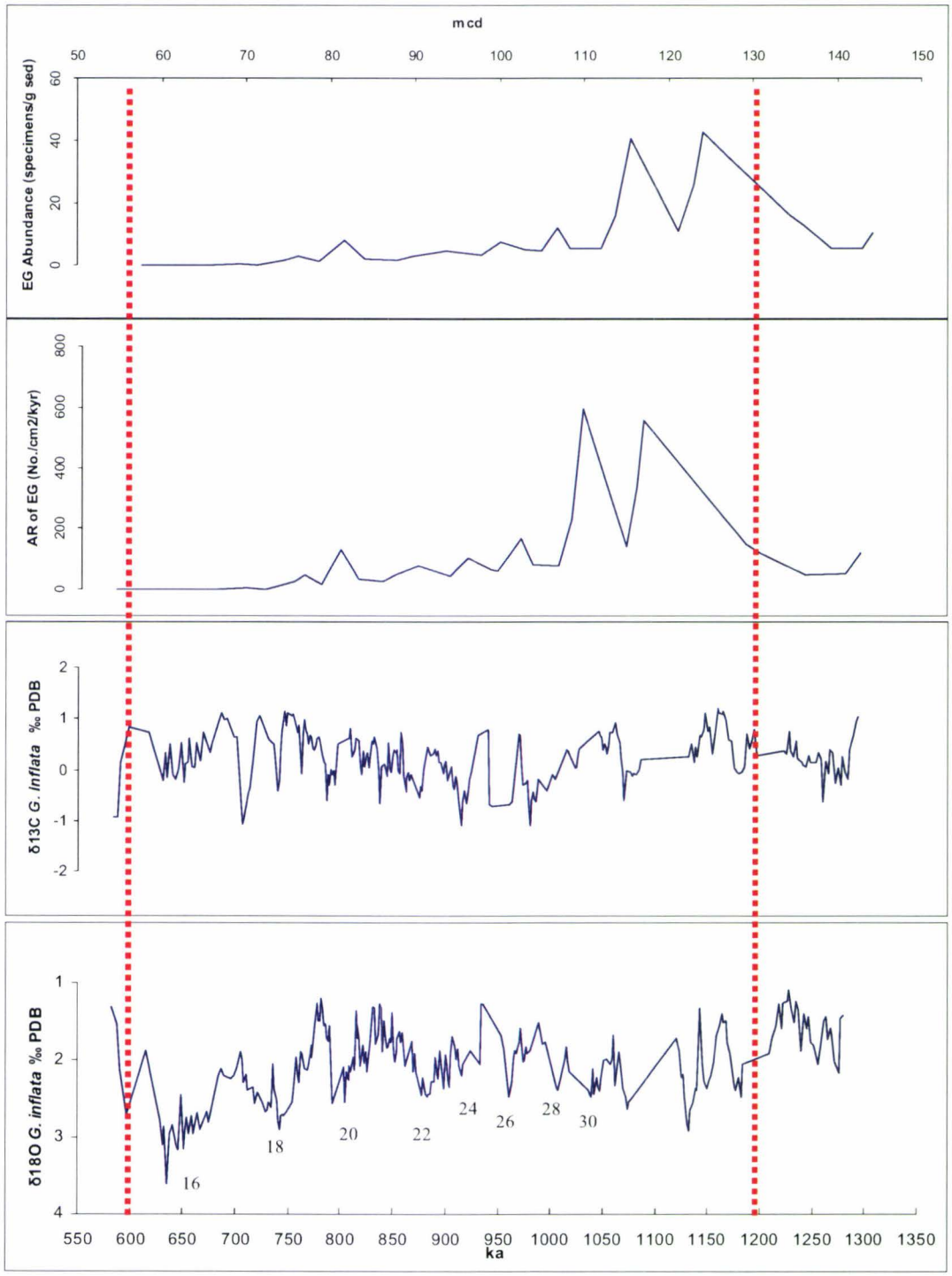

Figure 5.7. Declines in absolute abundance (specimens/g sed.) and accumulation rate (no./cm^2/kyr) of Extinction Group taxa at Site 1082. Isotopic $\delta^{13}C$ and $\delta^{18}O$ records are from Jahn *et al.* (2003). MPT

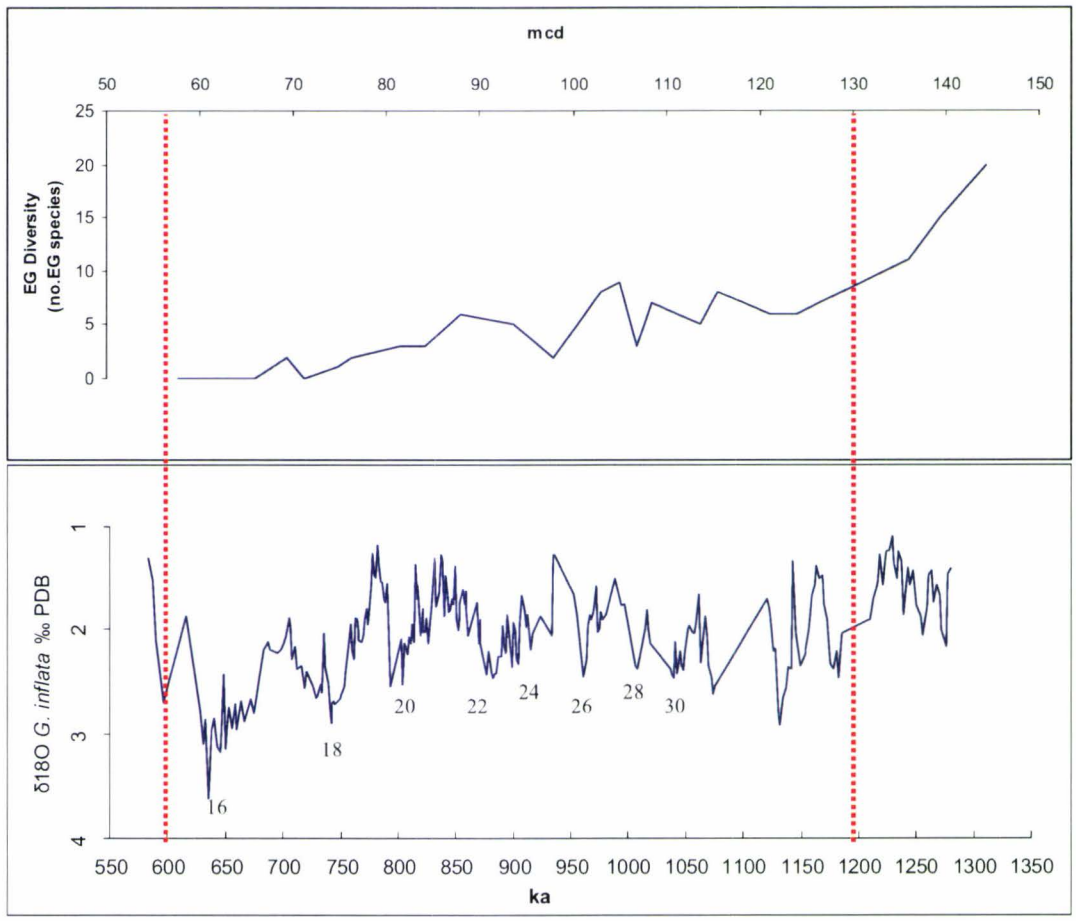

Figure 5.8. Extinction Group diversity across the MPT at Site 1082. Isotopic data sourced from Jahn *et al.* (2003). MPT ·····

At Site 1082 declines in EG taxa were generally contemporaneous with lowest (more negative) $\delta^{13}C$ values. Declines in EG taxa at 121, 112, 105, 88, 79 and 69 mcd (1060, 1000, 940, 835, 775 and 705 ka), all coincided with periods of lowest $\delta^{13}C$ value (Fig. 5.7).

Figure 5.8 shows the fluctuation of EG species diversity across the MPT. Of the 24 EG species encountered at Site 1082, never at one time were all EG species identified in the one sample. Diversity peaked at 144 mcd (1280 ka) with 20 EG species identified within the sample. These included *Awhea tosta*, *Chrysalagonium calomorphum*, *C. crassitestum*, *C. gomphiformis*, *C. intertenuatum*, *Cribronodosaria* sp. A, *Laevidentalina stimulea*, *Myllostomella advena*, *M. costai*, *M. matanzana Orthomorphina perversa*, *O. trincherasensis*, *Parafrondicularia antonina*, *P. laevigata*, *Proxifrons inaequalis*, *Siphonodosaria bradyi*, *S. hispidula*, *S. sagrinensis*, *Stilostomella*

fistuca, and *Stilostomella holoserica*. Diversity gradually decreased to 6 EG species (*C. gomphiformis*, *M. matanzana*, *O. perversa*, *P. laevigata*, *S. bradyi* and *S. sagrinensis*) at 121 mcd (1060 ka, MIS 30), with a slight recovery to 8 EG species (*C. crassitestum*, *C. gomphiformis*, *M. costai*, *M. matanzana*, *P. laevigata*, *S. bradyi*, *S. sagrinensis*, and *S. fistuca*) at 116 mcd (1020 ka, MIS 29). Small fluctuations in species diversity followed after ~ 1000 ka, with EG species varying between 9 and 0 per sample. Most declines in diversity coincided or directly followed glacial intervals (for example, MIS 30 (121 mcd (1060 ka); diversity: 6 (see above), MIS 22 (98 mcd (895 ka); diversity: 2 (*M. matanzana*, *P. laevigata*)), MIS 20 (84 mcd (810 ka); diversity: 3 (*M. matanzana*, *P. laevigata*, and *S. sagrinensis*)), MIS 18 (75 mcd (750 ka); diversity: 1 (*P. laevigata*)), MIS 16 (69 mcd (705 ka); diversity: 2 (*M. matanzana*, *S. sagrinensis*) and MIS 16 (71 and 66 mcd (720 and 675 ka); diversity: 0), where no EG taxa were found (Fig. 5.8).

5.3.2.2 Site 1088

Figure 5.9 shows the pulsed decline and local extinction of EG taxa at Site 1088. Oxygen isotope records were obtained from benthic foraminifera *Cibicidoides* sp. (of Hodell *et al.*, 2003), and as in Site 1082, there was a clear relationship between the enrichment of $\delta^{18}O$ in the benthic foraminifera *Cibicidoides* (during and approaching cool glacial periods) and the pulsed decline and eventual extinction of EG taxa. The record of EG taxa abundance and AR in Site 1088 begins at 14.4 mcd (1100 ka), during warm interglacial period MIS 31. Abundance and AR dropped from 6 specimens/g sed. and 8 specimens/cm^2/kyr at 14.4 mcd to 3 specimens/g sed. and 5 specimens/cm^2/kyr as the EG was subjected to the glacial conditions of MIS 30 at 14.0 mcd (1070 ka). Complete recovery of EG abundance was obtained in the next intervening warm interglacial period MIS 29, 13.3 mcd (1035 ka), with abundance and AR reaching 6 specimens/ g sed. and 15 specimens/cm^2/kyr, respectively. This peak in relative abundance and AR was once again followed by a decline in EG taxa upon entering glacial period MIS 28 at 12.8 mcd (1025 ka), with a partial recovery (12.8 mcd, 1015 ka; MIS 27) and followed by another decline at MIS 26, 12.6 mcd (1000 ka) to a pre~ 1000 ka low of 2 specimens/g sed. and AR of 3 specimens/cm^2/kyr. During interglacial period MIS 25, between 12.2 and 11.8 mcd (965 to 945 ka), complete recovery of EG taxa occurred, with abundance and AR reaching a peak of 10 specimens/g sed. and 14 specimens/cm^2/kyr at 11.8 mcd (945 ka). After ~ 950 ka, the abundance and AR of EG taxa began a progressive and gradual decline, interrupted by small amplitude slight

recoveries signalling warmer interglacial periods (Fig. 5.9). Abundance of EG taxa never recovered to pre ~950 ka levels, with declines going into MIS 22 (11.0 mcd (880 ka); with an abundance of 2 specimens/g sed.; AR: 3 specimens/cm^2/kyr), MIS 20 (10.1 mcd (815 ka); with an abundance of 1 specimen/g sed.; AR:1 specimen/cm^2/kyr), MIS 19 (9.9 mcd (795 ka)),to zero at MIS 18 (8.8 mcd (730 ka), MIS 16 (8.3 mcd (685 ka) and 7.9 mcd (660 ka)), and MIS 14 (7.1 mcd (615 ka)). Declining partial recoveries of EG taxa occurred during intervening warm periods and are shown in figure 5.9. This figure also shows a decrease in abundance and AR at MIS 19 (9.9 mcd (795 ka)), MIS 17 (9.1 mcd (750 ka)), and a slight recovery of EG taxa following MIS 14, at 6.9 mcd (600 ka), which represents the identification of 4 specimens of *Myllostomella matanzana* and 4 specimens of *Pleurostomella alternans*. The highest occurrence of these two species is thought to represent the *Stilostomella* Extinction Datum at Site 1088 (Fig. 5.6).

Carbon isotope data for Site 1088 were obtained from the epifaunal benthic foraminifera *Cibicidoides* sp. (from Hodell *et al.*, 2003). Fluctuations in the record of relative enrichment and depletion of $\delta^{13}C$ in the test of this foraminifer were studied across the MPT with respect to the decline and eventual local extinction of EG taxa. There was no consistent relationship between more negative or more positive $\delta^{13}C$ values and the declining EG taxa, with the major declines of MIS 30 and 28 (14.0 and 13.1 mcd (1070 and 1025 ka) coinciding with highest $\delta^{13}C$ values, whilst declines into MIS 22, 11.0 mcd (880 ka) and MIS 16, 7.9 mcd (660 ka) coincided with the lowest $\delta^{13}C$ values (Fig. 5.9).

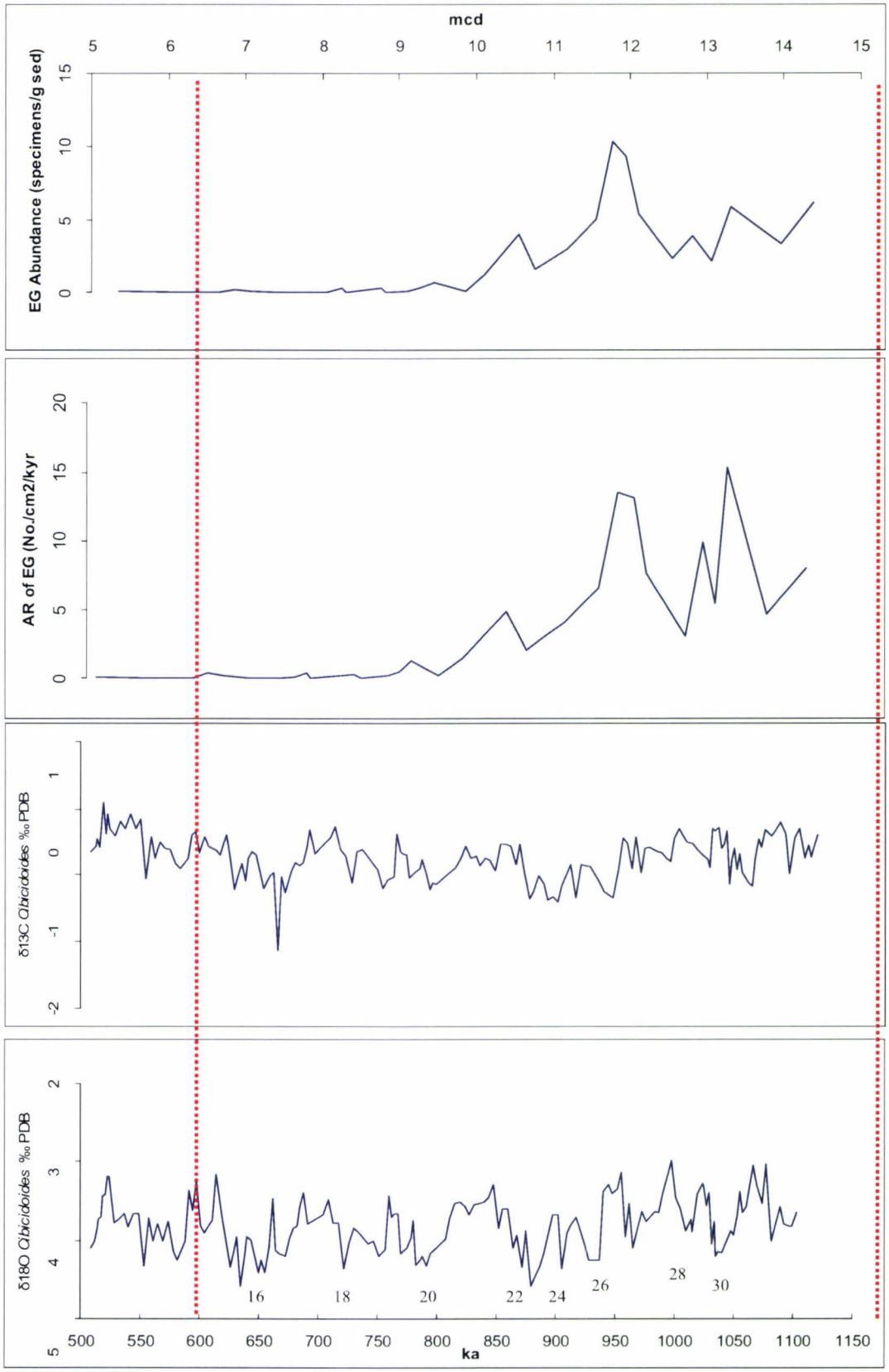

Figure 5.9. Declines in absolute abundance (specimens/g sed.) and accumulation rate (no./cm^2/kyr) of Extinction Group taxa at Site 1088. Isotopic $\delta^{13}C$ and $\delta^{18}O$ records are from Hodell *et al.*(2003).
MPT ·····

Figure 5.10 shows the variability of EG species diversity across the MPT at Site 1088. Of the 22 EG species identified at Site 1088, the highest number of EG species encountered in one sample was 12, at 12.0 to 11.8 mcd (955 to 945 ka (MIS 25)). The following EG taxa were identified at 12.0 mcd (955 ka): *Laevidentalina stimulea*, *Myllostomella costai*, *M. matanzana*, *M. japonica*, *Orthomorphina perversa*, *Pleurostomella alternans*, *Siphonodosaria hispidula*, *S. pomuligera*, *S. recta*, *S. sagrinensis*, *S. spinea* and *Stilostomella fistuca*. At 11.8 mcd (945 ka) the following 12 EG species were encountered: *Awhea tosta, L. stimulea*, *M. costai*, *M. matanzana*, *O. perversa*, *Parafrondicularia laevigata*, *P. alternans*, *Pleurostomella sapperi*, *Proxifrons inaequalis*, *S. hispidula*, *S. sagrinensis* and *S. fistuca*. Prior to this peak in species diversity, the number of EG species fluctuated between 10 and 6 EG species per sample, with lowest values coinciding with cool glacial periods. For example, at 13.1 mcd (1025 ka, MIS 28), EG diversity was 6 (*M. costai*, *M. matanzana*, *O. perversa*, *P. alternans*, *P. brevis* and *S. sagrinensis*); at 12.6 mcd (1000 ka, MIS 26), diversity was 9 (*A. tosta*, *C. intertenuatum*, *L. stimulea*, *M. matanzana*, *O. perversa*, *P. acuminata*, *S. hispidula*, *S. sagrinensis* and *S. fistuca*). Following the peak in EG diversity between 12.0 and 11.8 mcd (955 to 945 ka), diversity gradually declined throughout the MPT. Lowest diversity values often coincided with full glacial or cooling intervals (e.g. at 11.2 mcd (900 ka, MIS 22); diversity: 7 (*M. costai*, *M. matanzana*, *P. alternans*, *P. inaequalis*, *S. recta*, *S. sagrinensis*, and *S. spinea*); at 10.8 mcd (865 ka, MIS 20); diversity: 5 (*A. tosta*, *M. costai*, *P. acuminata*, *S. hispidula* and *S. sagrinensis*); at 8.8 mcd (730 ka, MIS 18); diversity: 0; and at 8.3 and 7.9 mcd (685 and 660 ka, MIS 16); diversity: 0). However, there were also occasions when low diversity coincided with interglacial periods, for instance at 9.9 mcd (795 ka, MIS 19); diversity: 2 (*P. inaequalis* and *S. sagrinensis*); at 9.1 mcd (750 ka, MIS 17); diversity: 1 (*P. sapperi*); at 7.5 mcd (635 ka, MIS 15); diversity: 0; and at 6.7 mcd (590 ka, MIS 15); diversity: 0. Figures 5.6 and 5.9 show the occurrence of previously recognised EG species, *Chrysalogonium intertenuatum*, identified at 5.4 mcd (510 ka).

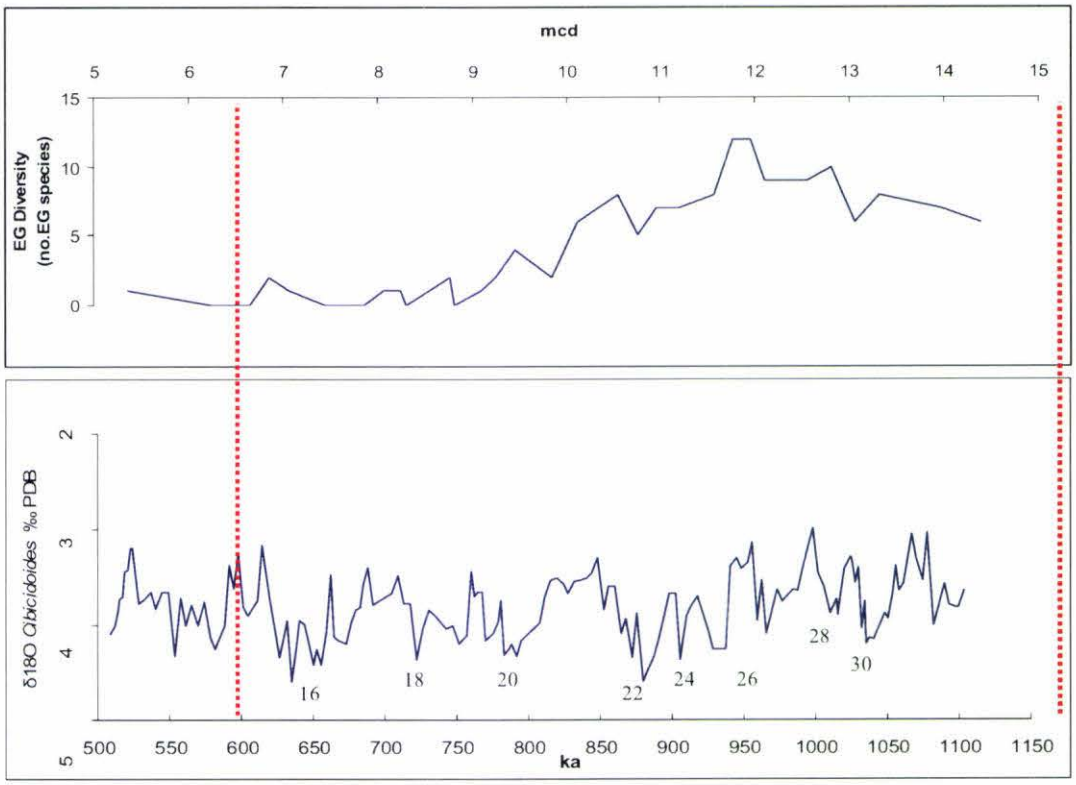

Figure 5.10. Extinction Group diversity across the MPT at Site 1088. Isotopic data sourced from Hodell *et al.* (2003). MPT .....

5.3.3 Stratigraphic Ranges of EG Taxa

The stratigraphic ranges and highest occurrences (HOs) of EG taxa from Site 1082 and 1088 are summarised in table 5.1. It is important to mention that the reliability of the HOs of rarer species with disjointed ranges is uncertain.

South Atlantic EG	Stratigraphic Range in Site 1082 and 1088	HO Site 1082	HO Site 1088	HO South Atlantic
Awhea tosta	1082: 144 - 94 mcd (1280-865 ka); 1088: 14.4 - 10.8 mcd (1100-865 ka)	~865 ka	~865 ka	~865 ka
Chrysalogonium calomorphum	1082: 2 specimens at 144 mcd (1280 ka); 1088: Absent	~1280 ka	-	~1280 ka
Chrysalogonium crassitestum	1082: 144 - 105 mcd (1280-940 ka); 1088: Absent	~940 ka	-	~940 ka
Chrysalogonium deceptorium	1082: Absent; 1088: 2 specimens at 14.0 mcd (1070 ka)	-	~1070 ka	~1070 ka
Chrysalogonium gomphiformis	1082: 144 - 105 mcd (1280-940 ka); 1088: Absent	~940 ka	-	~940 ka
Chrysalogonium intertenuatum	1082: 144 - 90 mcd (1280-845 ka); 1088: part of SG	~845 ka	SG	....
Chrysalogonium stimuleum	1082: 144 - 105 mcd (1280-940 ka); 1088: 14.4 - 11.8 mcd (1100-945 ka)	~940 ka	~945 ka	~940 ka
Cribronodosaria sp. A	1082: 2 specimens at 144 mcd (1280 ka); 1088: Absent	~1280 ka	-	~1280 ka
Ellipsoglandulina labiata	1082: Absent; 1088: 10.6 - 8.1 mcd (850-675 ka)	-	~675 ka	~675 ka
Myllostomella advena	1082: 144 - 88 mcd (1280-835 ka); 1088: Absent	~835 ka	-	~835 ka
Myllostomella costai	1082: 144 - 88 mcd (1280-835 ka); 1088: 14.0 - 9.5 mcd (1070-770 ka)	~835 ka	~770 ka	~770 ka
Myllostomella japonica	1082: Absent; 1088: 4 specimens at 12.0 mcd (955 ka)	-	~955 ka	~955 ka
Myllostomella matanzana	1082: 144 - 69 mcd (1280-705 ka); 1088: 14.4 - 6.9 mcd (1100-600 ka)	~705 ka	~600 ka	~600 ka
Orthomorphina ambigua	1082: 144 - 100 mcd (1280-910 ka); 1088: Absent	~910 ka	-	~910 ka
Orthomorphina glandigena	1082: 2 specimens at 100 mcd (910 ka); 1088: Absent	~910 ka	-	~910 ka
Orthomorphina laevis	1082: 4 specimens at 139 mcd (1230 ka); 1088: 14.0 - 12.1 mcd (1070-965 ka)	~1230 ka	~965 ka	~965 ka
Orthomorphina perversa	1082: 144 - 121 mcd (1280-1060 ka); 1088: 14.4 - 10.1 mcd (1100-815 ka)	~1060 ka	~815 ka	~815 ka
Orthomorphina trincherasensis	1082: 4 specimens at 144 mcd (1280 ka); 1088: 2 specimens at 14.0 mcd (1070 ka)	~1280 ka	~1070 ka	~1070 ka
Parafrondicularia antonina	1082: 144 - 82 mcd (1280-795 ka); 1088: Absent	~795 ka	-	~795 ka
Parafrondicularia laevigata	1082: 144 - 75 mcd (1280-750 ka); 1088: 11.8 - 7.1 mcd (945-615 ka)	~750 ka	~615 ka	~615 ka
Pleurostomella acuminata	1082: Absent; 1088: 12.6 - 8.3 mcd (1000-685 ka)	-	~685 ka	~685 ka
Pleurostomella alternans	1082: Absent; 1088: 13.3 - 6.9 mcd (1035-600 ka)	-	~600 ka	~600 ka
Pleurostomella brevis	1082: Absent; 1088: 2 specimens at 13.1 mcd (1025 ka)	-	~1025 ka	~1025 ka
Pleurostomella sapperi	1082: Absent; 1088: 12.8 - 9.1 mcd (1015-750 ka)	-	~750 ka	~750 ka
Proxifrons inaequalis	1082: 144 - 100 mcd (1280-910 ka); 1088: 11.8 - 9.9 mcd (945-795 ka)	~910 ka	~795 ka	~795 ka
Siphonodosaria bradyi	1082: 144 - 88 mcd (1280-835 ka); 1088: Absent	~835 ka	-	~835 ka
Siphonodosaria hispidula	1082: 144 - 123 mcd (1280-1070 ka); 1088: 13.3 - 10.1 mcd (1035-815 ka)	~1070 ka	~815 ka	~815 ka
Siphonodosaria recta	1082: 143 - 134 mcd (1265-1175 ka); 1088: 12.0 - 11.0 mcd (955-880 ka)	~1175 ka	~880 ka	~880 ka
Siphonodosaria sagrinensis	1082: 144 - 69 mcd (1280-705 ka); 1088: 14.4 - 9.9 mcd (1100-795 ka)	~705 ka	~795 ka	~705 ka
Siphonodosaria spinea	1082: Absent; 1088: 12.0 - 8.8 mcd (955-725 ka)	-	~725 ka	~725 ka
Siphonodosaria pomuligera	1082: Absent; 1088: 8 specimens at 12.0 mcd (955 ka)	-	~955 ka	~955 ka
Stilostomella fistuca	1082: 144 - 90 mcd (1280-845 ka); 1088: 14.4 - 11.6 mcd (1100-930 ka)	~845 ka	~930 ka	~845 ka
Stilostomella holoserica	1082: 144 - 90 mcd (1280-845 ka); 1088: Absent	~845 ka	-	~845 ka

TABLE 5.1. Stratigraphic ranges of South Atlantic Extinction Group taxa

5.3.4 Dominant EG Species and Blooms

Dominant EG species were singled out as those that form greater than 5% of the total encountered EG taxa throughout the study interval, and their ARs are shown in figures 5.11 and 5.12. There were six dominant species at Site 1082: *Chrysalogonium gomphiformis*, *Myllostomella costai*, *M. matanzana*, *Parafrondicularia laevigata*, *Siphonodosaria bradyi*, and *S. sagrinensis*. Four species were shown to dominate the EG assemblage at Site 1088: *Myllostomella costai*, *M. matanzana*, *Pleurostomella alternans*, and *Siphonodosaria sagrinensis*.

5.3.4.1 Site 1082

Six dominant EG species were identified at Site 1082, fluctuations in AR are shown in figure 5.11.

Chrysalogonium gomphiformis was present in 47% of samples at Site 1082, and forms ~9% of the total EG specimens. *C. gomphiformis* was common from 144 to 105 mcd (1280-940 ka) with 2 large "blooms" with AR of 96 specimens/cm^2/kyr and 211 specimens/cm^2/kyr at 123 and 116 mcd (1070 and 1020 ka), respectively. There was another small peak in AR at 107 mcd, where 30 specimens/cm^2/kyr were encountered. The highest occurrence (HO) of *C. gomphiformis* at Site 1082 was at ~105 mcd (~940 ka) (Fig. 5.5, Table 5.1). No specimens were found at Site 1088.

Myllostomella costai was present in 30% of samples, forming ~6% of the total EG specimens. This species was common between 144 and 88 mcd (1280-835 ka), with a highest AR of 84 specimens/cm^2/kyr at 134 mcd (~1175 ka). AR declined dramatically after 1100 ka with two peaks at 116 and 100 mcd (1020 and 910 ka) of 7 specimens/cm^2/kyr and 5 specimens/cm^2/kyr, respectively. The HO of *M. costai* at Site 1082 was at ~88 mcd (~835 ka) (Fig. 5.5, Table 5.1).

Myllostomella matanzana, present in 77% of samples, formed ~5% of the total EG specimens. The abundance and AR of *M. matanzana* was highly variable across the MPT, and was common between 144 and 69 mcd (1280-705 ka). The highest abundances and ARs of this species occurred between 136 and 114 mcd (1185 and 1010 ka), with ARs averaging 24 specimens/cm^2/kyr. The HO of *M. matanzana* in Site 1082 was at ~69 mcd (~705 ka) (Fig. 5.5, Table 5.1).

Parafrondicularia laevigata was present in 83% of samples, and formed ~34% of the total EG specimens encountered. This species was common throughout the stratigraphic range of 144 to 75 mcd (1280-750 ka), and despite AR and abundance being highly variable across the MPT, three distinct peaks in AR are observed at 123, 107, and 82 mcd (1070, 960, and 795 ka), of 160, 136, and 124 specimens/cm^2/kyr, respectively. The HO of *P. laevigata* in Site 1082 was at ~75 mcd (~750 ka) (Fig. 5.5, Table 5.1).

Siphonodosaria bradyi, present in 57% of samples, formed ~36% of the total EG specimens of Site 1082. Abundance and AR progressively declined across the MPT, with two distinct "blooms" at 124 and 116 mcd (1075 and 1020 ka), with ARs of 465 and 277 specimens/cm^2/kyr, respectively. There was a sharp drop in AR between these peaks, to 60 specimens/cm^2/kyr at ~123 mcd (~1070 ka), and again to zero specimens/cm^2/kyr at ~107 mcd (~960 ka). The HO of *S. bradyi* at Site 1082 was at ~88 mcd (~835 ka) (Fig. 5.5, Table 5.1).

Siphonodosaria sagrinensis was a dominant species at Site 1082, present in 50% of samples, and formed 5% of the total EG specimens. *S. sagrinensis* was common between 144 and 69 mcd (1280 and 705 ka), with highest abundances and ARs between 136 and 124 mcd (1185 and 1075 ka), of 30 and 48 specimens/cm^2/kyr, respectively. Occurrence declined dramatically after 124 mcd (~1075 ka), with ARs between 17 and zero specimens/cm^2/kyr for the reminder of the MPT. The HO of *S. sagrinensis* at Site 1082 was at ~69 mcd (~705 ka) (Fig. 5.5, Table 5.1).

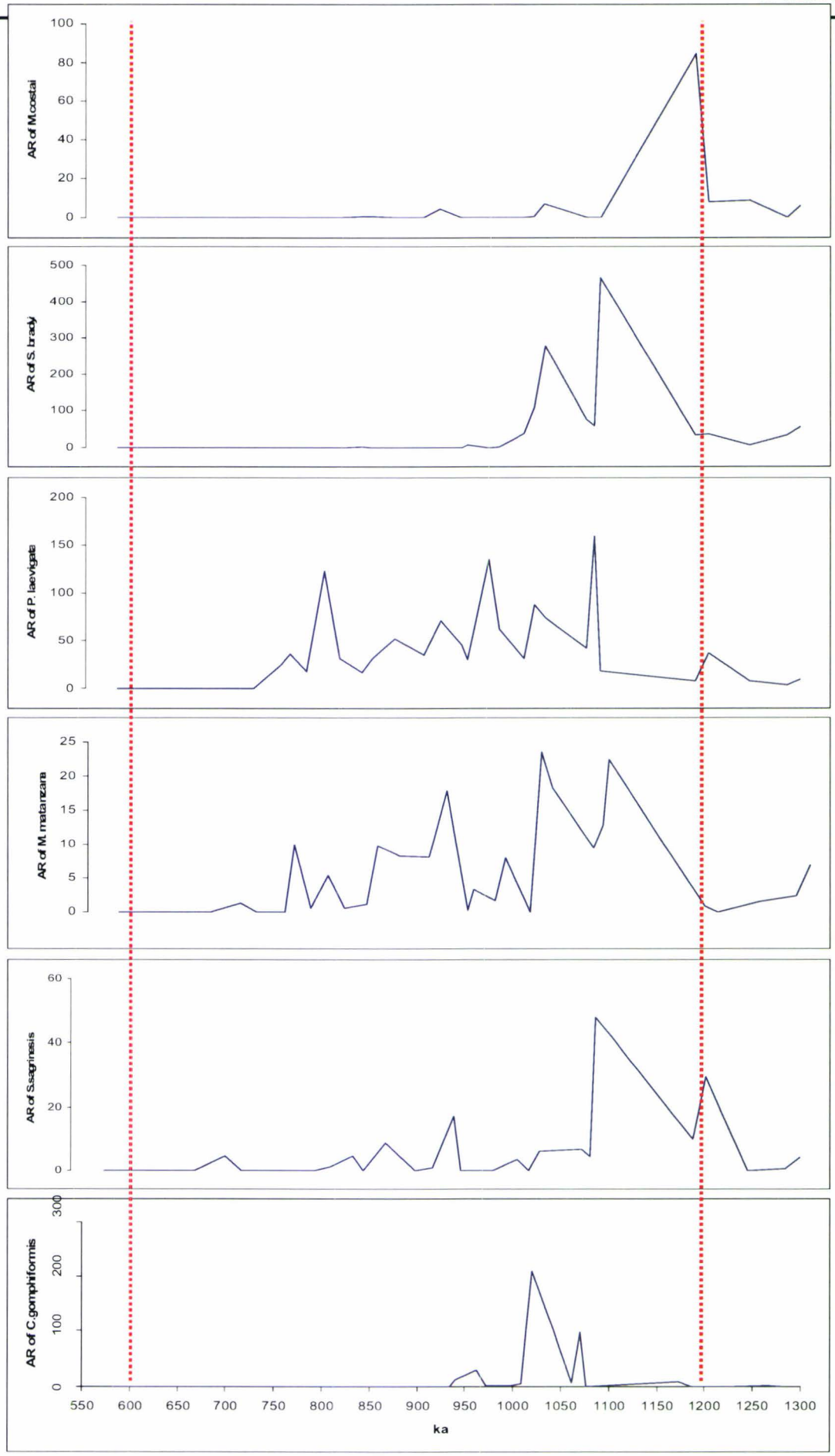

Figure 5.11: Dominant EG species of Site 1082. MPT

5.3.4.2 Site 1088

Four dominant EG species were identified at Site 1088 (Fig. 5.12), three of which have also been included in the dominant EG species at Site 1082. ARs and abundances of these EG taxa were much lower than at Site 1082, with no obvious "blooms" in any species identified.

Myllostomella costai was present in 45% of samples at Site 1088, and formed ~27% of the total EG specimens. This species was common between 14 and 9.5 mcd (1070-770 ka), with the highest AR of 7 specimens/cm^2/kyr at 12 mcd (960 ka). There was a gradual decline in AR of *M. costai* throughout the MPT, with three distinct peaks in AR observed, at 13.3, 12, and 10.6 mcd (1035, 960, and 850 ka), 7, 5, and 3 specimens/cm^2/kyr, respectively. The HO of *M. costai* occurred at ~9.5 mcd (~770 ka) (Fig. 5.6, Table 5.1).

Myllostomella matanzana was present in 52% of samples, and formed ~20% of the total EG specimens encountered at Site 1088. *M. matanzana* was common between 14.4 and 6.9 mcd (1100-600 ka), and again, a progressive decline in AR was evident across the MPT. Highest ARs occurred between 13.3 and 11.6 mcd (1035-960 ka), 4 and 3 specimens/cm^2/kyr, respectively. The HO of *M. matanzana* at Site 1088 occurred at ~6.9 mcd (~600 ka) (Fig. 5.6, Table 5.1).

Pleurostomella alternans was present in 42% of samples, forming ~7% of the total EG specimens. *P. alternans* commonly occurred between 13.3 and 6.9 mcd (1035-600 ka), with highest ARs of ~1.3 specimens/cm^2/kyr occurring between 12.1 and 11.6 mcd (970-930 ka). AR was highly variable across the MPT, with several instances when no specimens were found, at 12.5 and 10.7 mcd, and between 10.1 and 9.9, 9.3 and 8.8, and 8.3 and 7.1 mcd (1000 and 865 ka, and between 815-795, 760-730, and 685-615 ka, respectively). The HO of *P. alternans* at Site 1088 was at ~6.9 mcd (~600 ka) (Fig. 5.6, Table 5.1). This species was not found at Site 1082.

Siphonodosaria sagrinensis was identified as a dominant EG species at Site 1088. *S. sagrinensis* was present in 52% of samples, forming ~32% of the total EG specimens encountered. This species was common between 14.4 and 9.9 mcd (1100-795 ka), with peaks in AR at 12.8 and 11.8 mcd (1015 and 945 ka), of 4 and 7 specimens/cm^2/kyr,

respectively. After a sharp decline in accumulation at ~11.7 mcd (940 ka), the AR of *S. sagrinensis* drops steadily to zero specimens/cm^2/kyr at ~9.9 mcd (HO = ~795 ka) (Fig. 5.6, Table 5.1).

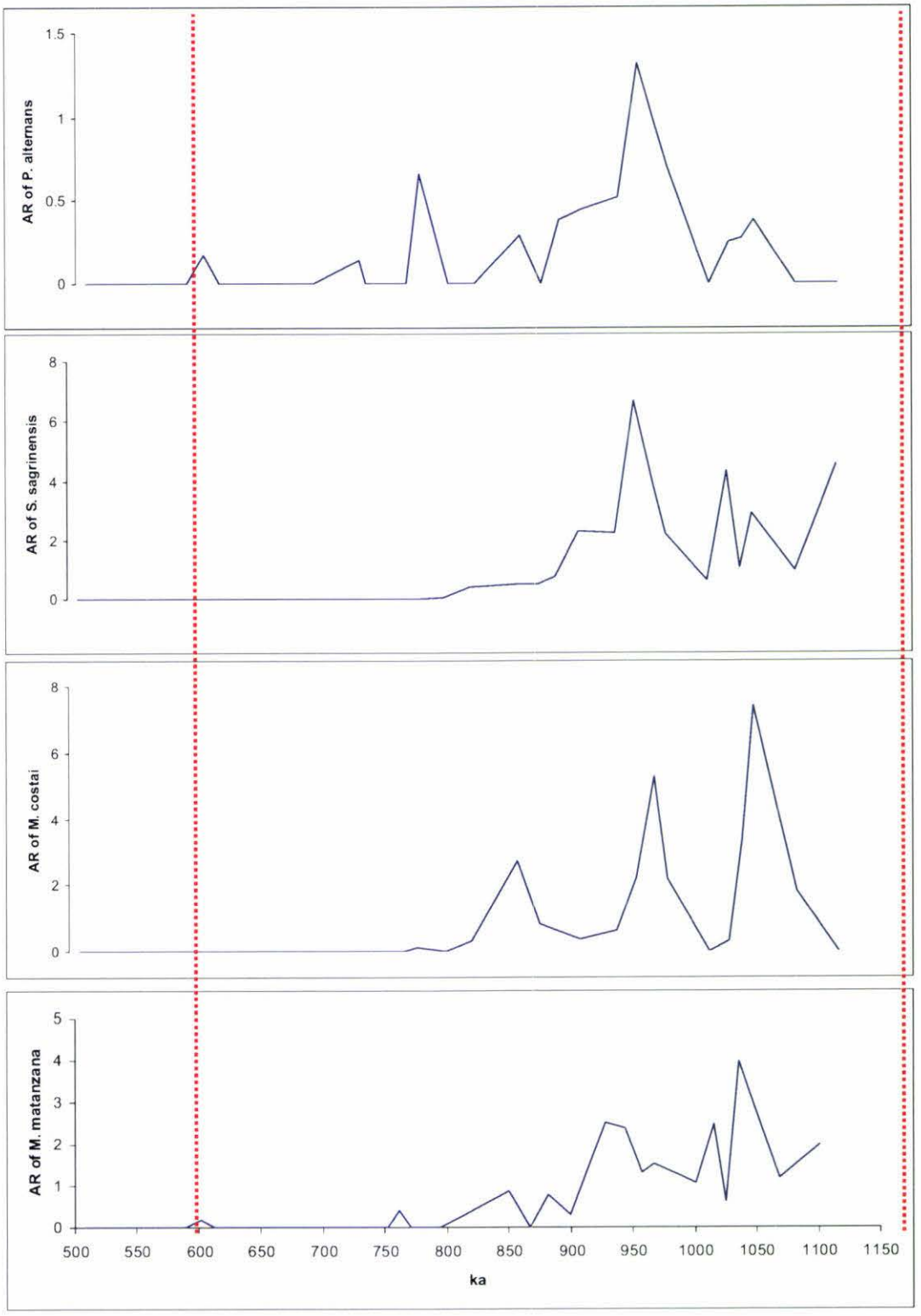

Figure 5.12. Dominant EG species of Site 1088. MPT ·····

5.3.5 Timing of Local Disappearances (HOs)

The highest occurrences (HOs) of each EG species in each site are shown in figures 5.5 and 5.6. Most species show diachronous HOs, but the disappearance of two species was synchronous between sites (eg. *Awhea tosta* (~ 860 ka) and *Chrysalogonium stimuleum* (~ 940 ka)). The uncommon species in the EG (e.g. *Chrysalogonium calomorphum, C. crassitestum, C. deceptorium, Cribronodosaria* sp. A, *Ellipsoglandulina labiata, Myllostomella japonica, Orthomorphina glandigena, Pleurostomella brevis, Siphonodosaria pomuligera, S. recta, Stilostomella holoserica*) occurred so infrequently that studying the relative timing of local disappearances is of little value. The diachronous nature of HOs between sites is clearly shown in the more common species (e.g. *Myllostomella costai, M. matanzana, Orthomorphina laevis, O. perversa, Parafrondicularia laevigata, Proxifrons inaequalis, Siphonodosaria hispidula, S. sagrinensis, Stilostomella fistuca*), but the time lag of inter-sites HOs are different between these species. In this study there was clearly a steady increase in the rate of HOs through the MPT (prior to 1000 ka = 2-4HOs/100 kyr; after 1000 ka = 4-7HOs/100 kyr). The maximum number of HOs occurred between 1000 and 700 ka at both sites, with a peak (7HOs/100 kyr) between 900 and 800 ka for Site 1082 and 5HOs/100 kyr between 800 and 600 ka for Site 1088 (Fig. 5.13). The highest level at which an EG species occurs in the record is known as the *Stilostomella* Extinction Datum. The *Stilostomella* Extinction Datum occurs at ~ 705 ka for *Myllostomella matanzana* and *Siphonodosaria sagrinensis* in Site 1082 (Fig. 5.5) and at ~ 600 ka for *Myllostomella matanzana* and *Pleurostomella alternans* in Site 1088 (Fig. 5.6), but see discussion elsewhere on the higher occurrence of *Chrysalogonium intertenuatum*.

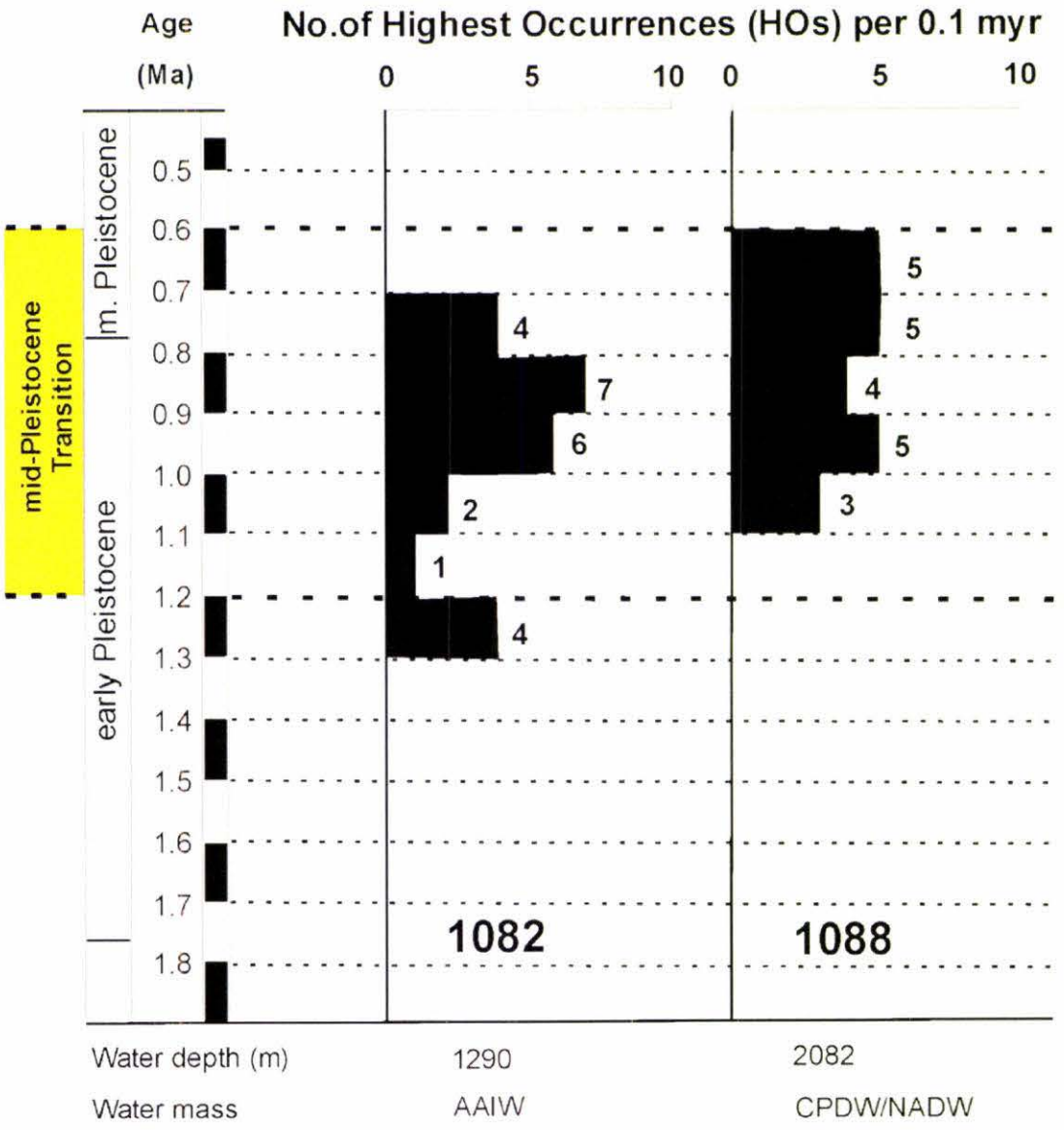

FIGURE 5.13. Number of highest occurrences of EG species per 100 kyr in South Atlantic Sites 1082 and 1088.

5.4 The Survivor Group (SG)

Thirty-three species of benthic foraminifera were identified in the Survivor Group, with abundances progressively declining in samples from both cores after 700 ka (Appendix 1, Table 3.2). Of these Survivor Group (SG) species approximately 48% (16 species) were common to both sites. Within this group, several *Laevidentalina, Grigelis,* and *Nodosaria* specimens were unable to be identified to species level, and are referred to as sp.A, sp.B or sp.C. The majority of the 33 species in this group belong to 7 genera (Appendix 1) having radiate or circular apertures: *Astacolus* (2 spp.), *Dentalina* (2 spp.), *Laevidentalina* (10 spp.), *Nodosaria* (3 spp.), *Martinottiella* (2 spp.), *Vaginulina* (3 spp.), *Vaginulinopsis* (2 spp.).

5.4.1 Abundance and Diversity Patterns

The majority of the 33 species of SG benthic foraminifera were relatively rare prior to ~1000 ka, with the relative abundance in the early Pleistocene samples (prior to the die-back and extinction period), being only a small proportion of the total uniserial Target Group (EG plus SG), 5% in Site 1082 and 4% in 1088 (figure 5.1 and 5.2). Conversely, post-700 ka samples at both Sites show the SG forming a large proportion of the total uniserial fauna, 25% in Site 1082 and 58% in Site 1088, the remaining proportion (75% in Site 1082, and 42% in Site 1088) being occupied by Low-Oxygen Tolerant Group (LOTG) species.

5.4.1.1 Site 1082

Prior to ~116 mcd (~1000 ka), the mean absolute abundance of SG specimens at Site 1082 averaged 0.7/g sed., with peaks of 2/g sed. at 134 mcd (1175 ka) and 116 mcd (1020 ka) (Fig. 5.14). The absolute abundance of SG specimens declined to a late MPT mean of 0.4/g sed. after ~69 mcd (~700 ka, MIS 16).

The AR of the SG at Site 1082 peaked to 34/cm^2/kyr at 116 mcd (1020 ka), after which the AR dropped sharply to 10/cm^2/kyr at 108 mcd (970 ka). After ~1000 ka, the MPT was characterised by low amplitude fluctuations (declines and recoveries) in SG abundance and AR, declines usually coincided with abrupt interglacial warmings, for instance at 107, 100, 84, 79, 71 and 64 mcd (960, 910, 810 and 775, 720, and 650 ka, MIS 25, 23, 19, 17 and 15, respectively), with partial recoveries in abundance and AR

during the intervening cool glacial periods. Species diversity of SG taxa fluctuated with glacial and interglacial cycles, with declines in diversity during interglacial warm periods and near complete recoveries in subsequent glacial intervals (Fig. 5.14). For instance, SG diversity reached lowest levels at 116, 107, 94, 75 and 66 mcd (1020, 960, 865, 750 and 675 ka, MIS 27, 25, 21, 19 and 15, respectively), and reached zero SG species at 84 mcd (810 ka, MIS 19).

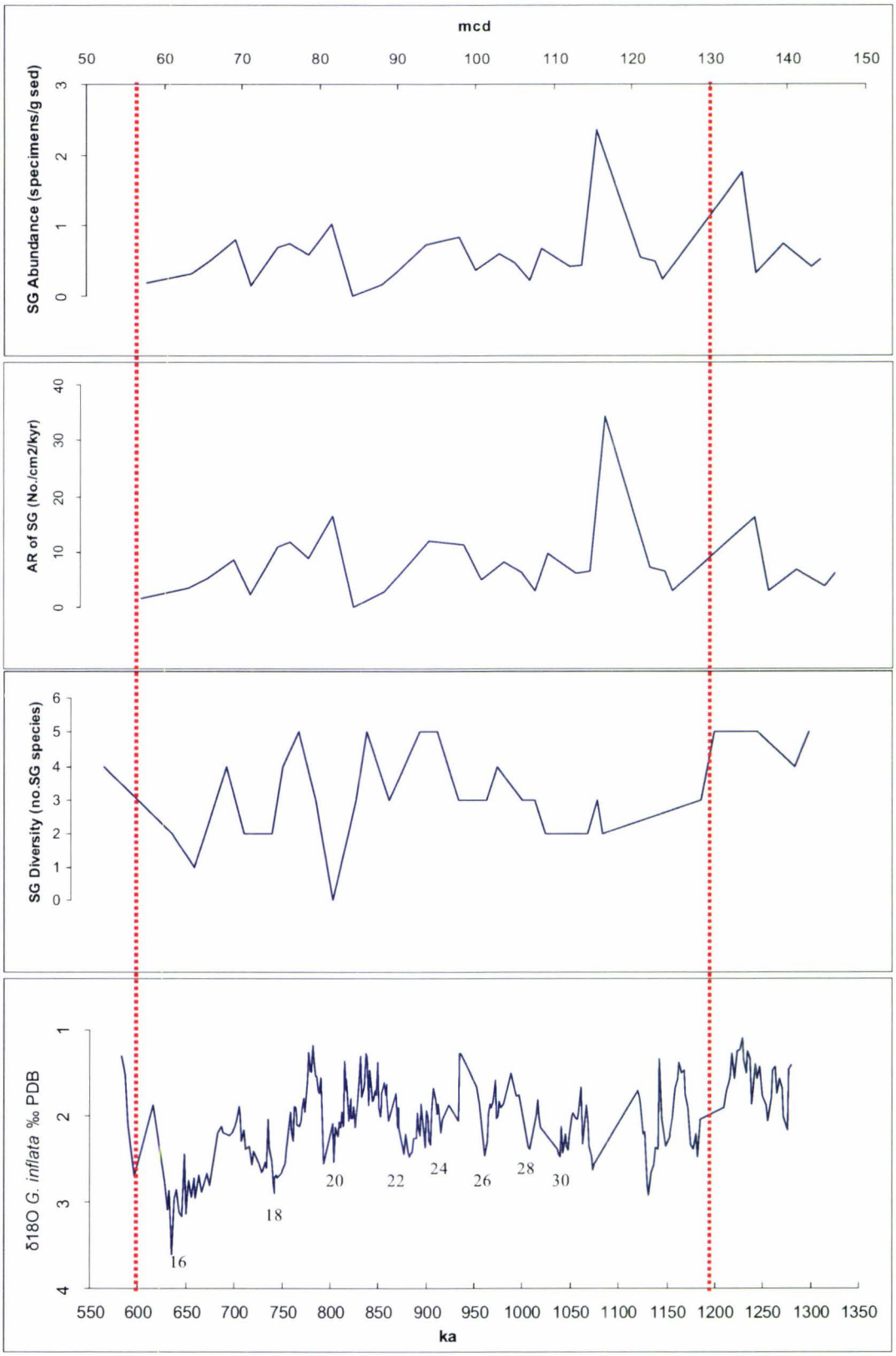

Figure 5.14. Absolute abundance (specimens/g sed.), accumulation rate (no./cm^2/kyr), and diversity of SG taxa at Site 1082. Isotopic data sourced from Jahn *et al.* (2003). MPT

5.4.1.2 Site 1088

Site 1088 followed a similar trend of pulsating abundance across the MPT (Fig. 5.15). However, unlike Site 1082, declines in SG abundance and AR did not consistently coincide with interglacial warming periods. Peaks in abundance and AR occurred at 11.8 (0.5 specimens/g sed), 11.0 (0.5 specimens/g sed), and 9.3 mcd (0.4 specimens/g sed) (945, 880 and 760 ka, MIS 24, 21, and 18, respectively). After ~1000 ka, abundance and AR of SG taxa neared zero on three occasions at 10.6, 8.3 and 7.5 mcd (850, 685 and 635 ka, MIS 20, 16 and 15), and similarly, these occurrences did not consistently correspond to either glacial or interglacial intervals. Species diversity at Site 1088 fluctuated between 5 and 0 species/sample across the MPT (Fig. 5.15). SG diversity was 1 species/sample at 8.3, 7.5 and 6.9 mcd (685, 635 and 600 ka, MIS 16, 15 and 13, respectively), and was zero at 13.1 and 11.0 mcd (1025 and 850 ka, MIS 28 and 20). SG diversity was 5 species/sample at 12.6, 10.1 and 8.8 mcd (1000, 815 and 730 ka, MIS 26, 20 and 17).

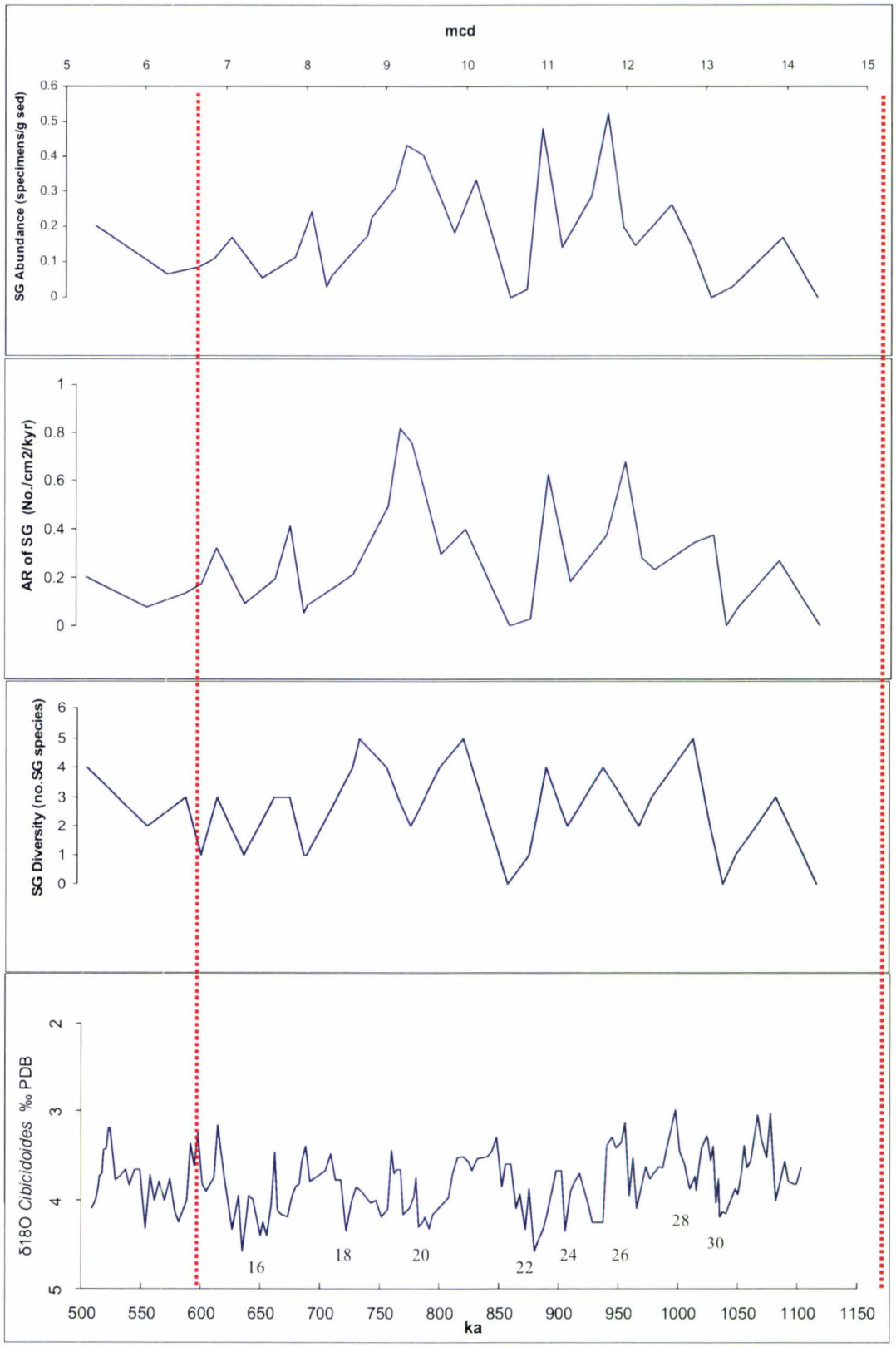

Figure 5.15. Absolute abundance (specimens/g sed.), accumulation rate (no./cm^2/kyr) and diversity of SG taxa at Site 1088. Isotopic data sourced from Hodell *et al.* (2003). MPT .....

5.5 *The Low-Oxygen Tolerant Group (LOTG)*

Twenty-one species of previously recognised Low-Oxygen Tolerant infaunal benthic foraminifera (from Mackensen *et al.*, 1995), known as the Low-Oxygen Tolerant Group (LOTG), were identified in this South Atlantic study (Appendix 1, Table 3.3). The majority of the 21 species in this group belong to 3 genera: *Bolivina* (3 spp.), *Bulimina* (5 spp.), and *Uvigerina* (4 spp.); with other species including: *Cassidella bradyi*, *Eggerella bradyi*, *Evolvocassidulina* spp., *Fursenkoina complanata*, *Globobulimina affinis*, *Karreriella bradyi*, *Praeglobobulimina spinscens*, *Rutherfordoides mexicana*, and *Trifarina anglosa*.

5.5.1 Abundance and Diversity Patterns

It is evident from the census count of LOTG specimens that absolute abundance and AR did not show a progressive decline over the MPT period (as seen with SG and EG benthic foraminifera populations), but on the contrary, sharp declines and often complete recoveries were evident (Figs. 5.16 and 5.17).

5.5.1.1 Site 1082

Site 1082 showed a general trend of pulsed decline and near-to-complete recovery across glacial and interglacial cycles of the MPT, with declines in abundance and accumulation rate generally coinciding with glacial intervals; and recovery with peak abundance and highest AR values during the intervening warm interglacial periods (particularly after ~1000 ka) (Fig. 5.16). There were six prominent peaks in LOTG abundance and AR across the study interval at Site 1082. These peaks occurred at 134 mcd (1175 ka; abundance of 95 specimens/g sed.; AR 875 specimens/cm^2/kyr), 116 mcd (1020 ka; abundance = 150; AR = 2170), 105 mcd (940 ka; abundance = 70; AR = 940), 94 mcd (865 ka; abundance = 60; AR = 1010), 81 mcd (795 ka; abundance = 85; AR = 1415), and 69 mcd (705 ka; abundance = 80; AR = 855). These peaks in LOTG abundance and AR generally coincided with warm interglacial periods, such as at 134 mcd (MIS 31), 116 mcd (MIS 27), 94 mcd (MIS 21) and 81 mcd (MIS 19), however peak values at 105 and 69 mcd corresponded with glacial periods MIS 24 and 16 respectively. Declines in LOTG taxa were therefore usually contemporaneous with full glacial periods or during the onset of glacial conditions, such as at 114 mcd (1010 ka;

MIS 26; abundance = 40; AR = 600), 103 mcd (935 ka; MIS 24; abundance = 20; AR = 250), 98 mcd (895 ka; MIS 22; abundance = 20; AR = 270), 84 mcd (810 ka; MIS 20; abundance = 12; AR = 200), 79 mcd (775 ka; MIS 18; abundance = 10; AR = 190), and 58 mcd (585 ka; MIS 14; abundance = 20; AR = 190).

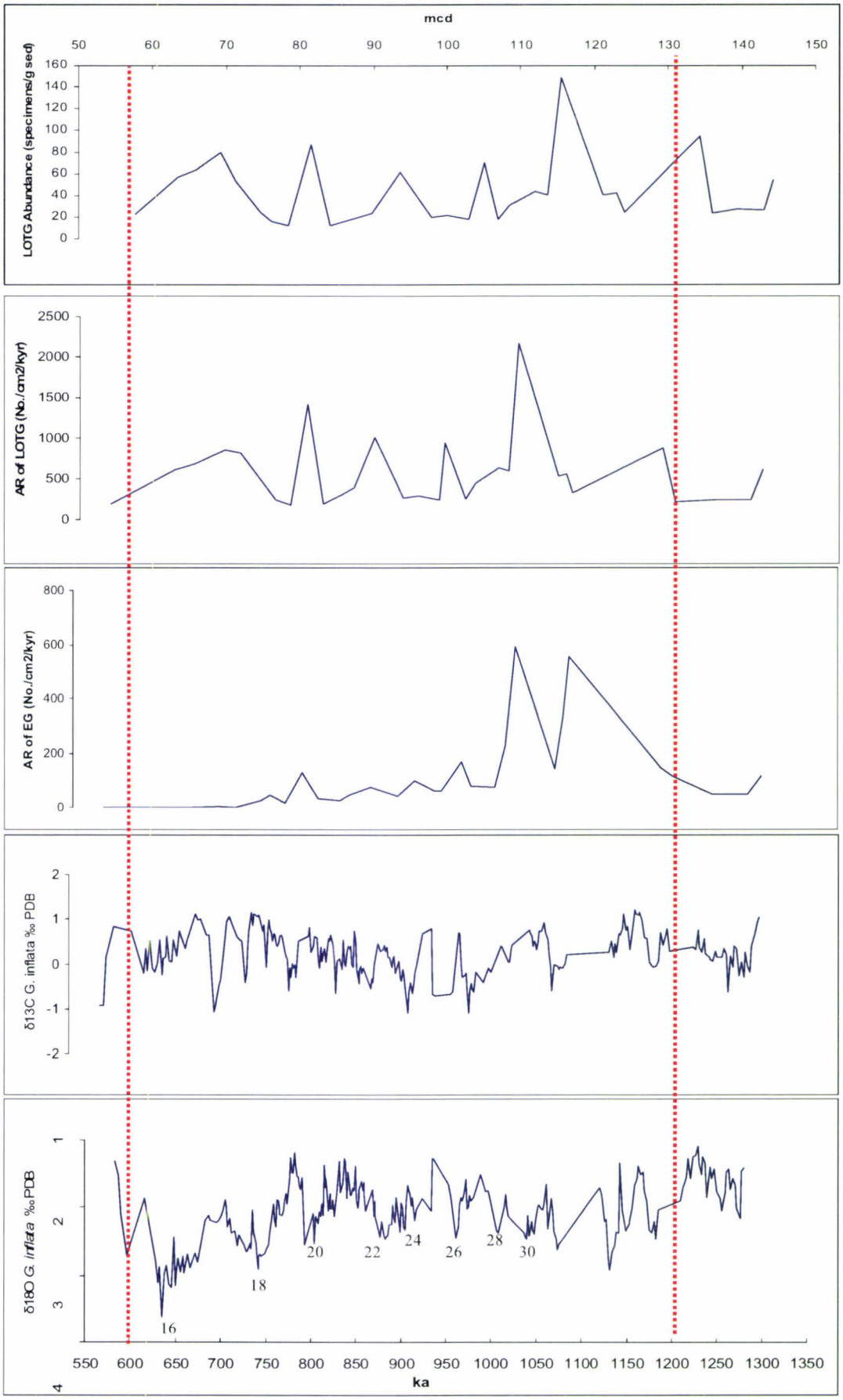

Figure 5.16. Absolute abundance (specimens/g sed.) and accumulation rate (no./cm^2/kyr) of LOTG taxa of Site 1082. Isotopic data sourced from Jahn *et al.* (2003). MPT

5.5.1.2 Site 1088

Site 1088 followed a similar trend to shallow South Atlantic Site 1082, with a pulsed decline and complete-to-near complete recovery of LOTG abundance and AR across the MPT (Fig. 5.17). Both abundance and AR of LOTG taxa were much lower throughout the entire study interval at Site 1088, compared with Site 1082, with the largest peak in abundance of 35 LOTG specimens/g sed. occurring at 11.8 mcd (945 ka) in Site 1088, in contrast to 150 LOTG specimens/g sed. at 116 mcd (1020 ka) in Site 1082. Similarly, AR of LOTG taxa reached a peak value at 13.3 mcd (1035 ka) of 70 specimens/cm^2/kyr in Site 1088, compared to a peak value at 116 mcd (1020 ka) of 2170 specimens/cm^2/kyr in Site 1082. Declines in the abundance and AR of LOTG species consistently coincided with glacial intervals, such as at 13.1 mcd (1025 ka; MIS 28; abundance = 10; AR = 45), 12.6 mcd (1000 ka; MIS 26; abundance = 10; AR = 25), 11.2 mcd (900 ka; MIS 22; abundance = 10; AR = 20), 9.5 mcd (770 ka; MIS 18; abundance = 10; AR = 30), 8.3 mcd (690 ka; MIS 16; abundance = 8; AR = 20), 7.9 mcd (660 ka; MIS 16; abundance = 6; AR = 14), 6.9 mcd (600 ka; MIS 14; abundance = 7; AR = 15), and 6.3 mcd (550 ka; MIS 12; abundance = 6; AR = 8). All peaks in abundance and AR of LOTG taxa coincided with interglacial warm periods, excluding a prominent peak in abundance and AR at 11.8 mcd (945 ka), coinciding with glacial MIS 24, and another peak at 8.2 mcd (685 ka), which coincided with glacial MIS 16.

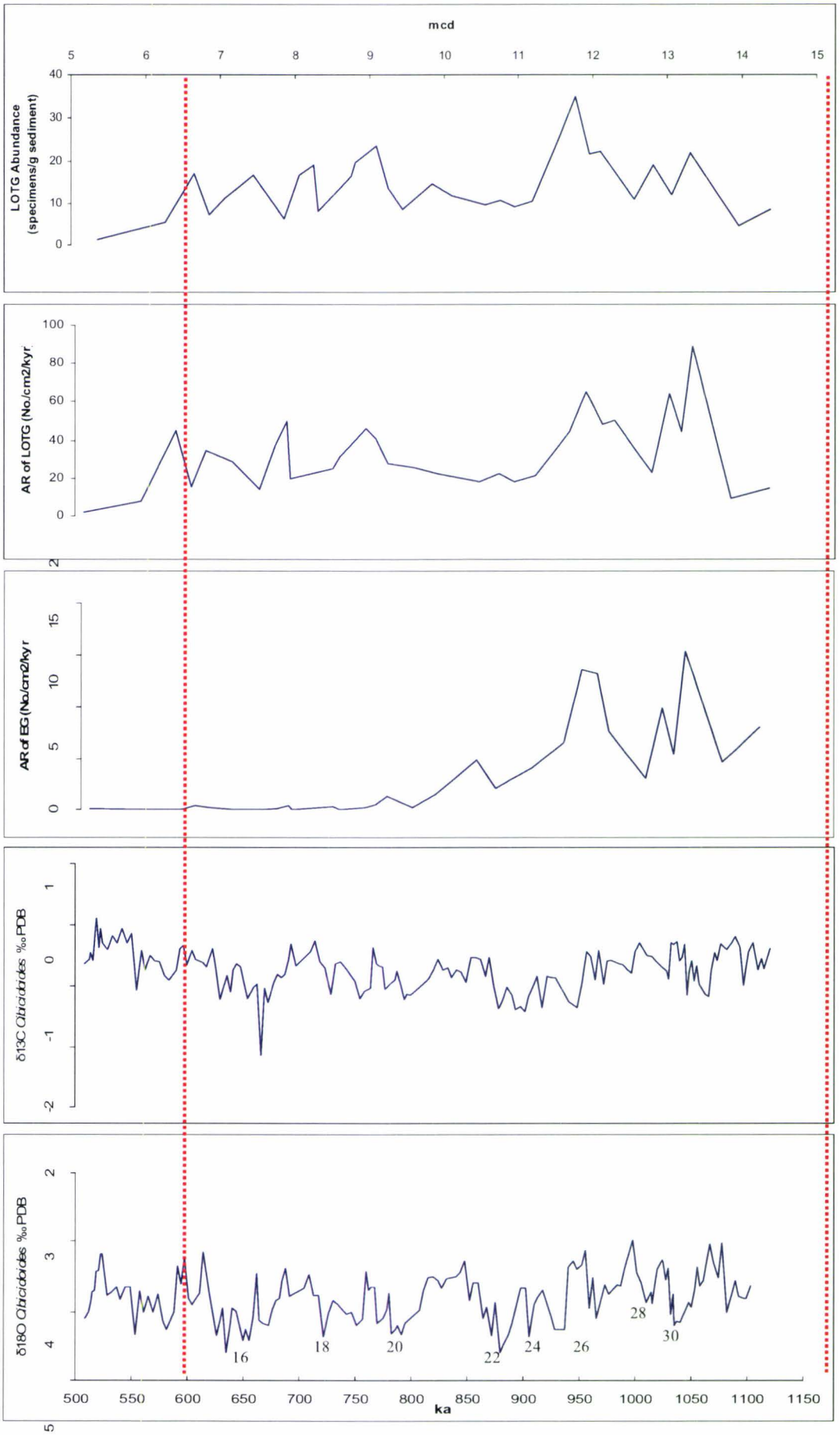

Figure 5.17. Absolute abundance (specimens/g sed.) and accumulation rate (no./cm^2/kyr) of LOTG taxa at Site 1088. Isotopic data sourced from Hodell *et al.* (2003). MPT

5.6 *Correlation Coefficients*

Correlation coefficients were calculated from the census data from both Sites 1082 and 1088. Two data sets were calculated for each site, one which included data from the entire study interval, and another on the interval older than ~800 ka to show 'normal' background fluctuations in environmental parameters prior to the major declines and extinctions of the MPT (Tables 5.2, 5.3, 5.4 and 5.5)(Full correlation coefficient data is shown in Appendix 3). Correlation coefficients between benthic foraminiferal records and measured environmental proxies were calculated to try to determine the important factors relating to the extinction (Figs. 5.1 and 5.2). Significant values of r (>0.3) are highlighted in bold, with several strong negative and positive correlations >|0.6| evident, bolded and underlined. Significant associations are outlined below:

5.6.1 Site 1082 – Pre ~800 ka (Table 5.2)

- The AR of the EG shows a significant positive correlation with the AR of the LOTG (r = +0.52), FI (r = +0.56) mcd (r = +0.49), and age (r = +0.42). %PF (r = -0.41) shows a significant negative correlation with the abundance of EG specimens.
- The AR of the LOTG is positively correlated with subsets within the EG: *Chrysalogonium* spp. (r = +0.73), *Siphonodosaria* spp. (r = +0.32), Nodosariidae (r = +0.72), and Stilostomellidae (r = +0.32).
- The abundance of gypsum rhombs is positively correlated with FI (r = +0.44), EG subfamily *Siphonodosaria* spp. (r = +0.34) and Stilostomellidae (r = +0.36), and $\delta^{18}O$ (*G. inflata*) (r = +0.34), and negatively correlated to the abundance of ostracods (r = -0.31).
- %PF is negatively correlated with $\delta^{13}C$ (*G. inflata*) (r = -0.47), $\delta^{18}O$ (*G. inflata*) (r = -0.50), abundance of gypsum rhombs (r = -0.34) and FI (r = -0.44), and positively correlated to the abundance of ostracods (r = +0.42).
- The abundance of radiolaria is positively correlated to FI (r = +0.59) and mcd (r = +0.48).
- $\delta^{13}C$ (*G. inflata*) was positively correlated to $\delta^{18}O$ (*G. inflata*) (r = +0.55), and showed a significant negative correlation to the abundance of ostracods (r = -0.36).

Site 1082 - pre~800 ka	mcd	Age	O18	C13	SR	FI	% PF	Gypsum/gsed	*Chrysalogonium*	*Orthomorphina*	*Myllostomella*	*Siphonodosaria*	Nodosariidae	Stilostomellidae	Plectofrondicularinae	EG. TOTAL NO	SG. TOTAL NO	*Bolivina*	*Bulimina*	*Uvigerina*	LOTG. TOTAL NO	RADS	OSTRACODS
mcd																							
Age	1.00																						
O18 (*G. inflata*)	-0.36	-0.36																					
C13 (*G. inflata*)	0.16	0.19	**0.55**																				
SR	-0.15	-0.32	0.21	0.23																			
FI	0.20	0.13	0.19	0.04	-0.02																		
% PF	0.15	0.09	**-0.50**	**-0.47**	-0.16	-0.44																	
Gypsum/gsed	0.05	0.15	**0.34**	0.06	-0.28	**0.44**	**-0.34**																
Chrysalogonium	0.20	0.19	0.11	0.20	0.07	-0.06	-0.27	-0.10															
Orthomorphina	0.68	0.69	**-0.50**	0.11	-0.48	-0.11	**0.39**	0.08	-0.06														
Myllostomella	0.71	0.48	-0.12	0.16	-0.25	0.12	0.05	0.27	0.19	0.40													
Siphonodosaria	0.43	0.36	0.17	0.14	-0.03	0.84	-0.45	0.34	0.40	-0.04	0.30												
Nodosariidae	0.24	0.23	0.08	0.21	0.05	-0.06	-0.24	-0.10	1.00	-0.01	0.21	0.40											
Stilostomellidae	0.46	0.41	0.15	0.15	-0.07	0.81	**-0.41**	**0.36**	0.41	0.02	0.43	0.99	0.41										
Plectofrondicularinae	0.24	0.16	0.20	0.22	0.36	-0.11	-0.11	-0.15	0.42	-0.09	0.02	0.05	0.41	0.05									
EG. TOTAL NO	**0.49**	**0.42**	0.19	0.23	0.07	**0.56**	**-0.41**	0.21	0.71	-0.01	0.39	0.88	0.71	0.89	0.44								
SG. TOTAL NO	0.11	0.10	0.11	0.14	0.18	-0.15	0.02	-0.12	0.69	-0.05	0.39	0.23	0.69	0.28	0.24	0.47							
Bolivina	0.22	0.27	-0.02	-0.03	-0.07	-0.13	-0.05	0.09	0.77	0.04	0.61	0.30	0.77	0.38	0.23	0.57	0.70						
Bulimina	0.15	0.11	0.17	0.21	0.11	0.00	-0.20	-0.13	0.67	-0.03	0.05	0.40	0.67	0.38	0.23	0.55	0.61	0.44					
Uvigerina	-0.10	-0.15	0.35	0.09	0.22	0.05	-0.02	0.00	0.33	-0.22	-0.11	0.23	0.32	0.20	0.02	0.25	0.39	0.30	0.48				
LOTG. TOTAL NO	0.01	-0.02	0.24	0.12	0.18	-0.07	-0.10	-0.10	**0.73**	-0.16	0.12	**0.32**	**0.72**	**0.32**	0.24	**0.52**	**0.75**	0.66	0.89	0.69			
RADS	**0.48**	0.15	-0.11	0.11	0.14	**0.59**	0.06	0.04	-0.23	0.13	0.02	**0.47**	-0.22	0.45	-0.25	0.21	-0.21	-0.22	-0.06	0.06	-0.14		
OSTRACODS	-0.21	-0.22	-0.07	**-0.36**	0.05	-0.08	**0.42**	**-0.31**	-0.10	-0.17	-0.11	-0.13	-0.09	-0.14	-0.09	-0.16	0.12	0.12	-0.10	0.42	0.17	0.08	

Table 5.2. Correlation coefficients between pre~800 ka records of Extinction Group foraminifera and selected environmental proxies. Correlation coefficients > 0.30 are bolded, and >0.60 are bolded and underlined. Isotopic values are interpolated based upon data from Jahn *et al.* (2003).

5.6.2 **Site 1082 – Entire study interval** (Table 5.3)

- The AR of the EG shows a significant positive correlation with $\delta^{13}C$ (*G. inflata*) (r = +0.30), LOTG (r = +0.59), FI (r = +0.59) and $\delta^{18}O$ (*G. inflata*) (r = +0.55). %PF (r = -0.54) shows a significant negative correlation with the abundance of EG specimens.
- The AR of the LOTG is positively correlated with subsets within the EG: *Chrysalogonium* spp. (r = +0.77), *Siphonodosaria* spp. (r = +0.34), Nodosariidae (r = +0.77), Stilostomellidae (r = +0.34), and Plectrofrondicularinae (r = +0.31); and with the AR of the SG (r = +0.86), and $\delta^{18}O$ (*G. inflata*) (r = +0.31).
- The abundance of gypsum rhombs is positively correlated with FI (r = +0.53), age (r = +0.33) and EG subfamilies *Myllostomella* (r = +0.36), *Siphonodosaria* (r = +0.45) and family Stilostomellidae (r = +0.48).
- %PF is negatively correlated with $\delta^{13}C$ (*G. inflata*) (r = -0.38), $\delta^{18}O$ (*G. inflata*) (r = -0.53), FI (r = -0.49), and EG subfamilies *Chrysalogonium* (r = -0.32), *Siphonodosaria* (r = - 0.54), and family Stilostomellidae (r = - 0.51). %PF is positively correlated with the EG subfamily *Orthomorphina* (r = +0.46) and abundance of ostracods (r = +0.35).
- The abundance of radiolaria is positively correlated with FI (r = +0.62), mcd (r = +0.52), and the EG family and subfamily, Stilostomellidae (r = +0.46), *Siphonodosaria* (r = +0.48); and negatively correlated with the EG family Plectofrondiculariinae (r = -0.34).
- $\delta^{13}C$ (*G. inflata*) is positively correlated with $\delta^{18}O$ (*G. inflata*) (r = +0.52).
- $\delta^{18}O$ (*G. inflata*) is positively correlated with FI (r = +0.32), the EG subfamily *Siphonodosaria* (r = +0.41), the families Stilostomellidae (r = +0.40) and Plectofrondiculariinae (r = +0.69) and negatively correlated to the EG subfamily *Orthomorphina* (r = -0.60).

Site 1082 - All data	mcd	Age	O18 (*G. inflata*)	C13 (*G. inflata*)	SR	FI	% PF	Gypsum/gsed	*Chrysalogonium*	*Orthomorphina*	*Myllostomella*	*Siphonodosaria*	Nodosariidae	Stilostomellidae	Plectofrondicularinae	EG. TOTAL NO	SG. TOTAL NO	*Bolivina*	*Bulimina*	*Uvigerina*	LOTG. TOTAL	RADS	OSTRACODS
mcd																							
Age	1.00																						
O18 (*G. inflata*)	-0.28	-0.31																					
C13 (*G. inflata*)	0.18	0.21	**0.52**																				
SR	-0.88	-0.89	0.34	-0.13																			
FI	0.19	0.11	**0.32**	0.03	-0.03																		
% PF	0.26	0.11	**-0.53**	**-0.38**	-0.21	**-0.49**																	
Gypsum/gsed	0.26	**0.33**	-0.02	-0.19	-0.38	**0.53**	-0.28																
Chrysalogonium	0.08	0.08	0.25	0.25	0.07	-0.08	**-0.32**	-0.12															
Orthomorphina	0.75	0.71	**-0.60**	0.14	-0.67	-0.15	**0.46**	0.11	-0.13														
Myllostomella	0.61	0.37	0.14	0.24	-0.41	0.10	0.02	**0.36**	0.14	0.32													
Siphonodosaria	0.35	0.25	**0.41**	0.19	-0.08	**0.85**	**-0.54**	**0.45**	0.37	-0.14	0.23												
Nodosariidae	0.12	0.12	0.22	0.26	0.03	-0.08	-0.29	-0.12	1.00	-0.08	0.15	0.37											
Stilostomellidae	0.37	0.30	**0.40**	0.19	-0.13	0.83	**-0.51**	**0.48**	0.37	-0.09	0.37	0.99	0.37										
Plectofrondicularinae	-0.36	-0.31	**0.69**	0.25	0.34	-0.17	-0.18	-0.20	0.39	-0.29	-0.17	-0.08	0.37	-0.10									
EG. TOTAL NO	0.27	0.19	**0.55**	**0.30**	0.00	**0.59**	**-0.54**	0.29	0.71	-0.18	0.29	0.88	0.70	0.88	0.30								
SG. TOTAL NO	-0.08	-0.04	0.25	0.14	0.08	-0.17	-0.02	-0.15	0.72	-0.10	0.38	0.22	0.72	0.27	0.18	**0.48**							
Bolivina	0.07	0.13	0.14	0.08	-0.07	-0.16	-0.14	0.15	0.77	-0.05	0.59	0.25	0.78	0.33	0.15	**0.54**	0.75						
Bulimina	0.10	0.05	0.28	0.31	0.21	-0.01	-0.23	-0.20	0.68	-0.08	0.01	0.39	0.68	0.38	0.24	**0.58**	0.70	0.44					
Uvigerina	0.01	-0.10	0.20	-0.08	0.31	0.07	0.04	-0.11	0.41	-0.22	-0.06	0.31	0.41	0.28	0.15	**0.39**	0.55	0.39	0.51				
LOTG. TOTAL	-0.05	-0.09	**0.31**	0.16	0.27	-0.08	-0.14	-0.15	**0.77**	-0.20	0.13	**0.34**	**0.77**	**0.34**	**0.31**	**0.59**	**0.86**	0.68	0.90	0.69			
RADS	0.52	0.11	-0.01	0.06	0.04	**0.62**	0.05	0.15	-0.26	0.11	-0.01	0.48	-0.25	0.46	-0.34	0.20	-0.24	-0.25	-0.08	0.06	-0.16		
OSTRACODS	-0.30	-0.27	0.04	-0.19	0.28	-0.08	**0.35**	-0.26	-0.10	-0.19	-0.09	-0.15	-0.09	-0.15	0.00	-0.15	0.15	0.04	-0.18	0.54	0.07	0.17	

Table 5.3. Correlation coefficients between records of Extinction Group foraminifera and selected environmental proxies. Correlation coefficients > 0.30 are bolded, and >0.60 are bolded and underlined. Isotopic values are interpolated, based upon data from Jahn *et al.* (2003).

5.6.3 Site 1088 – Pre ~800 ka (Table 5.4)

- The AR of the EG shows a significant positive correlation with the LOTG (r = +0.80), $\delta^{13}C$ (*Cibicidoides*) (r = +0.31), FI (r = +0.53) and age (r = +0.35).
- The LOTG is positively correlated with subsets within the EG: *Chrysalogonium* spp. (r = +0.30), *Myllostomella* spp. (r = +0.75), *Siphonodosaria* spp. (r = +0.49), Stilostomellidae (r = +0.78), and *Pleurostomella* spp. (r = +0.51); and the AR of IRD (r = +0.36). The LOTG is negatively correlated with $CaCO_3$ (r = -0.58).
- %PF is negatively correlated with the EG subfamilies *Siphonodosaria* (r = -0.44), *Orthomorphina* (r = -0.38) and family Nodosariidae (r = -0.33); and FI (r = -0.60).
- The abundance of radiolaria is positively correlated to FI (r = +0.56), the AR of the EG taxa (r = +0.53) and mcd (r = +0.52), and is negatively correlated with $CaCO_3$ (r = -0.63).
- $\delta^{13}C$ (*Cibicidoides*) is positively correlated with $CaCO_3$ (r = +0.33), the EG subfamilies *Myllostomella* (r = +0.31), *Orthomorphina* (r = +0.47), the EG family Stilostomellidae (r = +0.30), and the abundance of ostracods (r = +0.36).
- $\delta^{18}O$ (*Cibicidoides*) is negatively correlated with $\delta^{13}C$ (*Cibicidoides*) (r = -0.78), $CaCO_3$ (r = -0.46), and the EG subfamily member *Orthomorphina* (r = -0.42).
- The AR of IRD is significantly positively correlated to $\delta^{18}O$ (r = +0.37) and significantly negatively correlated to CaCO3 (r = -0.49).
- $CaCO_3$ is significantly negatively correlated with FI (r = -0.39), the AR of the EG taxa (r = -0.48), the EG subfamilies *Siphonodosaria* (r = -0.43), *Chrysalogonium* (r = -0.44), *Pleurostomella* (r = -0.43), and the EG families Nodosariidae (r = -0.49), Stilostomellidae (r = -0.41), Pleurostomellidae (r = -0.43); and the AR of the SG (r = -0.40).

Site 1088 - Pre~800 ka	Age	O18 (*Cibicidoides* sp.)	C13 (*Cibicidoides* sp.)	CaCO3	SR	FI	% PF	IRD AR	EG. TOTAL NO	*Myllostomella*	*Siphonodosaria*	*Chrysalogonium*	*Orthomorphina*	*Pleurostomella*	Nodosariidae	Stilostomellidae	Pleurostomellidae	SG. TOTAL NO	*Bolivina spp*	*Bulimina spp*	*Uvigerina spp*	LOTG. TOTAL NO	RADS	OSTRACODS
O18 (*Cibicidoides* sp.)	**-0.43**																							
C13 (*Cibicidoides* sp.)	**0.62**	**-0.78**																						
CaCO3	0.22	**-0.46**	**0.33**																					
SR	0.45	-0.01	0.18	**-0.36**																				
FI	0.26	-0.03	0.18	**-0.39**	0.04																			
% PF	-0.48	0.10	-0.24	-0.14	0.19	**-0.60**																		
IRD AR	-0.06	**0.47**	-0.25	-0.11	-0.01	-0.06	0.17																	
EG. TOTAL NO	**0.35**	-0.04	**0.31**	**-0.48**	0.43	**0.53**	-0.15	0.18																
Myllostomella	0.28	0.06	**0.31**	-0.28	0.54	0.10	0.13	0.29	0.83															
Siphonodosaria	0.25	-0.14	0.16	**-0.43**	0.07	**0.79**	**-0.44**	0.00	0.78	0.32														
Chrysalogonium	0.34	0.03	0.10	**-0.44**	0.35	**0.41**	-0.13	-0.18	0.20	-0.11	0.32													
Orthomorphina	0.73	**-0.42**	**0.47**	-0.14	0.25	**0.46**	**-0.38**	**-0.29**	0.32	0.05	0.43	0.65												
Pleurostomella	-0.35	-0.03	0.07	**-0.43**	-0.12	**0.34**	0.24	0.05	0.49	0.26	0.52	0.03	-0.18											
Nodosariidae	0.50	-0.07	0.19	**-0.49**	0.30	**0.57**	**-0.33**	-0.08	0.36	-0.04	0.52	0.91	0.82	0.03										
Stilostomellidae	0.33	-0.03	0.30	**-0.41**	0.43	**0.46**	-0.13	0.21	0.99	0.88	0.73	0.08	0.25	0.44	0.23									
Pleurostomellidae	-0.35	-0.03	0.07	**-0.43**	-0.12	**0.34**	0.24	0.05	0.49	0.26	0.52	0.03	-0.18	1.00	0.03	0.44								
SG. TOTAL NO	-0.18	0.10	-0.21	**-0.46**	-0.23	0.23	0.19	0.05	0.16	-0.12	0.33	0.11	0.12	0.61	0.25	0.07	0.61							
Bolivina	0.14	-0.08	0.11	-0.16	0.68	0.12	0.23	-0.20	**0.31**	0.35	0.12	0.33	0.03	0.15	0.11	0.31	0.15	**-0.34**						
Bulimina	0.39	0.20	0.32	0.03	0.30	0.26	-0.10	0.48	0.54	0.66	0.18	0.10	0.09	0.02	0.10	0.57	0.02	-0.23	0.18					
Uvigerina	0.07	0.20	0.10	-0.53	0.43	0.25	0.23	0.42	0.82	0.82	0.47	0.03	-0.05	0.56	0.11	0.83	0.56	0.29	0.24	0.60				
LOTG. TOTAL NO	0.16	0.16	0.08	**-0.58**	0.65	0.28	0.26	**0.36**	**0.80**	**0.75**	**0.49**	**0.30**	0.06	**0.51**	0.29	**0.78**	**0.51**	0.15	0.58	0.51	0.89			
RADS	-0.02	0.00	0.13	**-0.63**	0.30	**0.56**	0.00	0.05	**0.53**	0.40	0.45	0.03	0.13	0.43	0.22	0.50	0.43	**0.38**	0.08	0.17	0.62	**0.51**		
OSTRACODS	-0.12	-0.06	**0.36**	-0.08	0.04	-0.07	0.14	-0.04	0.26	0.45	-0.06	-0.25	-0.18	0.19	-0.23	0.30	0.19	-0.05	-0.16	0.39	0.50	0.19	**0.46**	

Table 5.4. Correlation coefficients between pre~800 ka records of Extinction Group foraminifera and selected environmental proxies. Correlation coefficients > 0.30 are bolded, and >0.60 are bolded and underlined. Isotopic values are interpolated based upon data from Hodell *et al.* (2003).

5.6.4 Site 1088 – Entire study interval (Table 5.5)

- The AR of the EG shows a significant positive correlation with the LOTG (r = +0.66), %PF (r = +0.34), radiolaria (r = +0.32), ostracods (r = +0.31), and age (r = +0.76).
- The LOTG is positively correlated with subsets within the EG: *Chrysalogonium* spp. (r = +0.33), *Myllostomella* spp. (r = +0.66), *Siphonodosaria* spp. (r = +0.51), Stilostomellidae (r = +0.65), Nodosariidae (r = +0.38) and *Pleurostomella* spp. (r = +0.47); and FI (r = +0.37). The LOTG is negatively correlated with $CaCO_3$ (r = -0.36).
- %PF is positively correlated with the EG subfamilies *Myllostomella* ssp. (r = +0.36), *Pleurostomella* spp. (r = +0.38), Stilostomellidae (r = +0.33), and ostracods (r = +0.33); and negatively correlated with FI (r = -0.57).
- The abundance of radiolaria is positively correlated with FI (r = +0.30), the AR of the EG taxa (r = +0.32), the AR of the LOTG (r = +0.33), and mcd (r = +0.52), and negatively correlated with $CaCO_3$ (r = -0.37).
- $\delta^{13}C$ (*Cibicidoides*) is positively correlated with EG subfamily *Orthomorphina* (r = +0.31).
- $\delta^{18}O$ (*Cibicidoides*) is negatively correlated with $\delta^{13}C$ (*Cibicidoides*) (r = -0.56) and the EG subfamily member *Orthomorphina* (r = -0.37).
- The AR of IRD is significantly positively correlated with $\delta^{18}O$ (r = +0.37), and the AR of SG (r = +0.35); and significantly negatively correlated with $CaCO_3$ (r = -0.49).
- $CaCO_3$ is significantly negatively correlated to the AR of the LOTG (r = -0.36), the AR of the SG (r = -0.40), the abundance of radiolaria (r = -0.37) and the AR of IRD (r = -0.49).

Site 1088 - All data	Age	O18 (*Cibicidoides* sp.)	C13 (*Cibicidoides* sp.)	CaCO3	SR	FI	% PF	IRD AR	EG. TOTAL NO	*Myllostomella*	*Siphonodosaria*	*Chrysalogonium*	*Orthomorphina*	*Pleurostomella*	Nodosariidae	Stilostomellidae	Pleurostomellidae	SG. TOTAL NO	*Bolivina*	*Bulimina*	*Uvigerina*	LOTG. TOTAL NO	RADS	OSTRACODS
Age																								
O18 (*Cibicidoides* sp.)	-0.20																							
C13 (*Cibicidoides* sp.)	0.08	**-0.56**																						
CaCO3	-0.02	-0.29	0.18																					
SR	0.24	-0.03	-0.03	-0.20																				
FI	0.03	0.03	0.12	-0.18	0.10																			
% PF	0.42	-0.04	-0.16	0.02	0.09	**-0.57**																		
IRD AR	-0.02	**0.37**	-0.22	**-0.49**	0.07	0.01	-0.09																	
EG. TOTAL NO	**0.76**	-0.15	0.15	-0.09	0.31	0.24	**0.34**	-0.09																
Myllostomella	0.66	-0.09	0.17	-0.04	0.41	0.06	**0.36**	-0.01	**0.91**															
Siphonodosaria	0.68	-0.19	0.09	-0.09	0.10	0.42	0.21	-0.14	**0.90**	0.65														
Chrysalogonium	0.41	-0.03	0.07	-0.20	0.30	0.28	0.13	-0.18	**0.40**	0.18	0.47													
Orthomorphina	0.65	**-0.37**	**0.31**	0.00	0.18	0.24	0.16	-0.28	**0.56**	0.37	0.61	0.68												
Pleurostomella	0.44	-0.04	-0.02	-0.13	0.11	0.11	**0.38**	-0.14	**0.62**	0.47	0.60	0.20	0.14											
Nodosariidae	0.63	-0.15	0.12	-0.18	0.24	0.33	0.20	-0.17	**0.62**	0.37	0.70	0.89	0.86	0.28										
Stilostomellidae	0.74	-0.14	0.15	-0.07	0.31	0.22	**0.33**	-0.07	**0.99**	0.94	0.87	0.33	0.52	0.57	0.55									
Pleurostomellidae	0.44	-0.04	-0.02	-0.13	0.11	0.11	**0.38**	-0.14	**0.62**	0.47	0.60	0.20	0.14	1.00	0.28	0.57								
SG. TOTAL NO	0.03	0.12	-0.22	-0.40	0.03	0.01	0.21	**0.35**	0.01	-0.11	0.08	0.02	0.04	0.39	0.09	-0.04	0.39							
Bolivina	0.48	-0.25	0.12	-0.17	0.61	0.06	0.29	-0.10	0.52	0.52	0.40	0.41	0.24	0.39	0.32	0.51	0.39	-0.09						
Bulimina	-0.02	0.08	0.15	0.10	0.27	0.11	-0.01	0.19	0.16	0.25	0.01	0.02	-0.04	0.13	-0.01	0.17	0.13	0.06	0.03					
Uvigerina	0.23	-0.04	0.09	-0.37	0.40	0.42	-0.07	0.26	0.53	0.58	0.38	0.08	0.08	0.40	0.18	0.54	0.40	0.21	0.36	0.24				
LOTG. TOTAL NO	0.39	0.00	0.03	**-0.36**	0.64	**0.37**	0.12	0.23	**0.66**	**0.66**	**0.51**	**0.33**	0.20	**0.47**	**0.38**	**0.65**	**0.47**	0.16	**0.65**	0.25	0.85			
RADS	0.16	0.23	0.00	**-0.37**	0.25	**0.30**	0.00	0.19	**0.32**	0.28	0.29	0.06	0.10	0.42	0.17	0.31	0.42	0.37	0.09	0.13	0.42	**0.33**		
OSTRACODS	0.35	-0.10	0.19	-0.09	0.00	-0.19	**0.33**	-0.09	**0.31**	0.39	0.15	-0.08	0.16	0.30	0.05	0.32	0.30	0.15	0.05	-0.02	0.32	0.17	0.21	

Table 5.5. Correlation coefficients between records of Extinction Group foraminifera and selected environmental proxies. Correlation coefficients > 0.30 are bolded, and >0.60 are bolded and underlined. Isotopic values are interpolated based upon data from Hodell *et al.* (2003).

6 DISCUSSION

6.1 South Atlantic Declines and Extinctions

6.1.1 Taxa Comprising the *Stilostomella* Extinction

This study identifies 33 species of elongate benthic foraminifera that appear to have become extinct during the late-early and middle Pleistocene (Table 3.1). Table 6.1 shows the occurrence and biogeographic affinity of the South Atlantic EG species from *Stilostomella* Extinction studies by previous workers. Twenty six of these species have a known cosmopolitan distribution (from Hayward, 2002) and include, *Awhea tosta, Chrysalagonium calomorphum, C. crassitestum, C. gomphiformis, C. intertenuatum, C. stimuleum, Ellipsoglandulina labiata, Myllostomella advena, M. costai, M. matanzana, Orthomorphina ambigua, O. perversa, O. trincherasensis, Parafrondicularia laevigata, Pleurostomella acuminata, P. alternans, P. brevis, P. sapperi, Proxifrons inaequalis, Siphonodosaria hispidula, S. recta, S. sagrinensis, S. spinea, S. pomuligera, Stilostomella fistuca,* and *S. holoserica.* Of the remaining 7 EG species, 5 were limited to the Atlantic Ocean (from Kawagata *et al.*, in press; and this study), and include *Chrysalagonium deceptorium, Myllostomella japonica, Orthomorphina glandigena, O. laevis,* and *Siphonodosaria bradyi.* Two species, *Cribronodosaria* sp. A and *Parafrondicularia antonina*, were found only in Southern Hemisphere sites (from Hayward, 2002). All EG taxa identified in the South Atlantic have been previously recorded in studies around the world's oceans (e.g. Weinholz and Lutze, 1989; Schönfeld, 1995, 1996; Hayward, 2002; Kawagata *et al.*, in press), however, *Chrysalogonium intertenuatum* appears to have survived through the MPT in low numbers in isolated refuges in the Southern Ocean sector of the South Atlantic Ocean (Site 1088). *Chrysalogonium intertenuatum* was identified very infrequently in Site 1088 (8 specimens found over the entire study interval, with 4 identified in the youngest sample at 5.36 mcd (~508 ka)). A possible explanation for this youngest isolated record (Figs. 5.6 and 5.10) may be upwards displacement of specimens by bioturbation or reworking (although bioturbation does not discriminate between species), or it may be possible that this species is not part of the *Stilostomella* Extinction Group in the region of Site 1088 in the South Atlantic.

Extinction Group - South Atlantic	Biogeog. affinity	ODP 1082	ODP 1088
Awhea tosta	cos	y	y
Chrysalagonium calomorphum	cos	y	n
Chrysalagonium crassitestum	cos	y	n
Chrysalagonium deceptorium	sa, na	n	y
Chrysalogonium gomphiformis	cos	y	n
Chrysalogonium intertenuatum	cos	y	y^
Chrysalogonium stimuleum	cos	y	y
Cribronodosaria sp. A	swp, sa	y	n
Ellipsoglandulina labiata	cos	n	y
Myllostomella advena	cos	y	n
Myllostomella costai	cos	y	y
Myllostomella japonica	sa, na	n	y
Myllostomella matanzana	cos	y	y
Orthomorphina ambigua	cos	y	n
Orthomorphina glandigena	sa, na	y	n
Orthomorphina laevis	sa, na	y	y
Orthomorphina perversa	cos	y	y
Orthomorphina trincherasensis	cos	y	y
Parafrondicularia antonina	swp, sa	y	n
Parafrondicularia laevigata	cos	y	y
Pleurostomella acuminata	cos	n	y
Pleurostomella alternans	cos	n	y
Pleurostomella brevis	cos	n	y
Pleurostomella sapperi	cos	n	y
Proxifrons inaequalis	cos	y	y
Siphonodosaria bradyi	sa, na	y	n
Siphonodosaria hispidula	cos	y	y
Siphonodosaria recta	cos	y	y
Siphonodosaria sagrinensis	cos	y	y
Siphonodosaria spinea	cos	n	y
Siphonodosaria pomuligera	cos	n	y
Stilostomella fistuca	cos	y	y
Stilostomella holoserica	cos	y	n
Total number of species	33	24	22

* cos = cosmopolitan, swp = SW Pacific, na = North Atlantic, sa = South Atlantic.
^ *C. intertenuatum* extends through the MPT in ODP 1088 (not part of EG)

TABLE 6.1. South Atlantic occurrence of Extinction Group taxa and global biogeographic affinity during the MPT.

6.1.2 Preferential Extinction of Specific Morphologies

In contrast to earlier periods of deep-sea faunal turnover, the middle Pleistocene *Stilostomella* extinctions are almost entirely limited to elongate shell morphologies with highly specific apertural characteristics, and will be discussed in turn (see Appendix 1; Table 6.2; Plate 6.1).

MORPHOLOGY	EG	SG	LOTG
Cribrate aperture	*Chrysalogonium* spp. *Cribronodosaria* sp.A		
Necked or lipped cribrate aperture loose meshed network	*Stilostomella* spp.		
Semilunate slit aperture	*Ellipsoglandulina labiata*		
Uniserial test, rounded aperture with secondary tooth	*Myllostomella* spp. *Siphonodosaria* spp.		
Uniserial test, terminal round aperture with/without neck or phialine lip	*Orthomorphina* spp.		
Hooded aperture with teeth	*Pleurostomella* spp.		
Slender test, narrow loop aperture toothplate may be present			*Bulimina exilis* *Cassidella bradyi* *Fursenkoina complanata* *Bulimina* spp.
Uniserial test, narrow		*Nodosaria longiscata*	
Multiserial to uniserial test, narrow spout aperture		*Martinottiella variabilis* *Martinottiella communis*	*Karreriella bradyi* *Trifarina anglosa* *Uvigerina* spp.
Multiserial to uniserial, flabellate to spathulate test	*Parafrondicularia antonina* *Proxifrons inaequalis*	*Parafrondicularia javana*	
Radiate aperture	*Awhea tosta*	*Glandulina ovula* *Laevidentalina* spp. *Grigelis* spp. *Dentalina* spp. *Vaginulina* spp. *Vaginulinopsis* spp. *Marginulina* spp. *Nodosaria simplex* *Pseudonodosaria brevis*	

Table 6.2: Apertural characteristics of South Atlantic EG, SG and LOTG benthic foraminifera (Modified from Hayward, 2002).

6.1.2.1 Test Morphology and Ecology

Many researchers have documented the complex relationship between food supply (organic carbon flux), oxygen availability, and the morphotypic characteristics (test size, wall thickness, degree of ornamentation, and test morphology) of benthic foraminifera (Lutze and Coulbourn, 1984; Corliss and Chen, 1988; Kaiho, 1991, 1994, 1999; Kaiho and Hasegawa, 1994; and Schönfeld, 2001). Kaiho and Hasegawa (1994) investigated ocean dysoxic events in the northwestern Pacific Ocean, and concluded that dissolved oxygen level and organic carbon flux were the main abiotic factors controlling the abundance and distribution of many benthic foraminiferal morphotypes. They further speculated that increases in flux of organic debris commonly leads to decreases in dissolved oxygen in bottom water, such that variations in the abundance of oxygen sensitive morphogroups may reflect paleoceanographic changes over time. To estimate paleodissolved oxygen, Kaiho (1994) subdivided calcareous benthic foraminifera into *dysoxic* (0.1-0.3 mL/L), *suboxic* (0.3-1.5 mL/L), and *oxic* (>1.5 mL/L) indicators, based on the relationship between morphotypes and oxygen levels suggested in recent reports (Bernhard, 1986; Berger and Wefer, 1988; Corliss and Chen, 1988).

6.1.2.2 Extinction Group Morphology and Ecology

Kaiho (1991,1994) interpreted the *Stilostomella* Extinction Group species to be dominated by dysoxic species based on a series of known morphologic characteristics and previous studies. These commonly elongate, flattened, tapered and cylindrical morphologies, are generally considered to live as infaunal dwellers inhabiting the near-surface (between 4 to 15 cm depth) sediment beneath well-oxygenated waters, or can live as both epifauna or infauna in low-oxygen conditions with or without high organic carbon flux (Gupta, 1993; Boersma, 1990; Kaiho, 1994). The most important morphologic characteristic of dysoxic species is a thin wall, which is thought to be related to the difficulty of calcium carbonate secretion in low oxygen environments (Rhoads and Morse, 1971). In addition, most dysoxic species are small, flat or elongate-tapered morphotypes, with high porosity tests. The small test size, high porosity, and high surface-area to volume ratios of such morphotypes are thought to provide improved mitochondrial oxygen uptake (Kaiho, 1994). The mid-Pleistocene elongate EG foraminifera were dominated by unornamented, thin-walled *Stilostomella, Myllostomella, Siphonodosaria,* and *Pleurostomella* species, which are common in lower Eocene, upper Oligocene and organic- and glauconite-rich Pliocene deep-sea

sediments in all oceans; periods of time recognised for lower oxygen levels in the geological record (Kaiho, 1992).

6.1.2.3 Apertural Shape

As mentioned, the majority of the *Stilostomella* Extinction species belong to two families, Stilostomellidae, and Pleurostomellidae, with some Nodosariidae also affected. These families were initially discriminated primarily on shell morphology, including apertural shape. In the South Atlantic the *Stilostomella* Extinction resulted in the decline and extinction of elongate species with cribrate (*Chrysalogonium* spp., *Cribronodosaria* spp.), slit lunate (*Ellipsoglandulina* spp), hooded with two teeth (*Pleurostomella* spp.), and secondary toothed (*Myllostomella* spp., *Siphonodosaria* spp., *Stilostomella* spp.) apertures (Hayward, 2002; Kawagata *et al.*, in press). Some exceptions to the rule exist with some uniserial EG taxa having a simple round aperture (*Orthomorphina* spp.), and flabellate tests with simple round or terminal radiate apertures (*Parafrondicularia* spp., *Proxifrons inaequalis*). The apertural characteristics of the South Atlantic EG and SG species are summarised in table 6.2, and the apertures of selected EG members are illustrated in plate 6.1.

The aperture has long been known to be the principal orifice by which the protoplasm flows in and out of the shell (Boltovskoy and Wright, 1976). As mentioned, the apertures of the EG species contain distinctive supplementary structures such as teeth, sieve plates, phialine lips, and thick rims, yet the exact functional role of apertual modifications characteristic of the EG is poorly understood. It is possible that some may serve as devices to channel or retain the protoplasm or to prevent the entry of parasites or predators; as a device to subdivide incoming food mass, or orientate particles that are to be ingested; as a holdfast mechanism; or it is possible they may serve as devices to mechanically strengthen the apertural margin (Boltovskoy and Wright, 1976). Further research into this aspect of the biology/ecology of benthic foraminifera would be helpful to understand the nature of the *Stilostomella* Extinction, and whether these structures did indeed make their possessor more susceptible to extinction and unable to adapt to the fluctuating environmental conditions of the MPT.

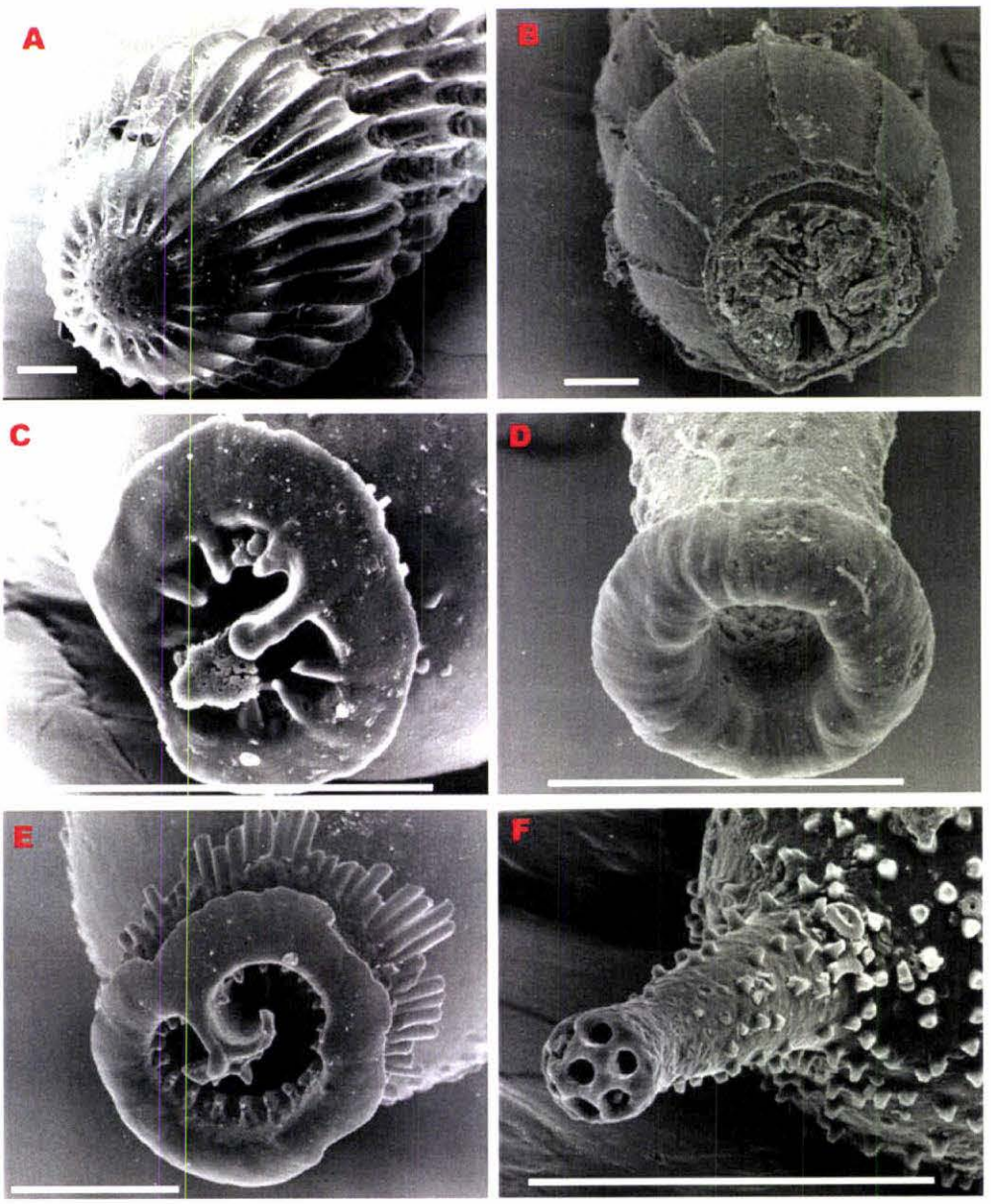

Plate 6.1: Scanning electron micrographs of examples of the apertural characteristics of the selected Extinction Group species. A = *Chrysalogonium crassitestum*; B = *Chrysalogonium gomphiformis*; C = *Myllostomella advena*; D = *Orthomorphina perversa*; E = *Siphonodosaria* sp. F = *Stilostomella holoserica*. Scale bars represent 100 µm.

6.1.3 Decline in Extinction Group

Detailed census studies at South Atlantic Sites 1082 and 1088 record a pattern of progressive change in abundance and diversity over the late early and middle Pleistocene (1200 – 500 ka). The time period prior to the MPT was characterised by a constantly high abundance, diversity, and AR of EG benthic foraminifera until ~ 1000 ka. After this time the group declined until the final *Stilostomella* Extinction datum at ~700 ka for *Myllostomella matanzana* and *Siphonodosaria sagrinesis,* in Site 1082, and

~600 ka for *Myllostomella matanzana* and *Pleurostomella alternans*, in Site 1088. The decline towards the MPT is pulsed (timings often diachronous between sites), with major declines in abundance and AR associated with the onset of cold glacial periods (Figs. 5.7 and 5.9). Both sites exhibit two notable sharp declines in AR of EG specimens, the shallower Site 1082 having a sharp drop from 560 to 140 specimens/cm^2/kyr between 1075 and 1060 ka, and a second sharp decline from 600 to 75 specimens/cm^2/kyr between 1020 and 1000 ka. Deeper Site 1088 shows a similar 2-pulsed decline, from a peak AR of EG of 15 specimens/cm^2/ka at 1035 ka to 3 specimens/cm^2/kyr at 1000 ka, and another more gradual decline between 940 and 870 ka, from 14 to 2 specimens/cm^2/kyr. Throughout the overall decline, partial recoveries of EG species are visible at both sites, generally occurring in the intervening warm interglacial period, such as MIS 29,23,21 and 19 at Site 1082 (Fig. 5.7) and at MIS 29, 25, 21 and 19 at Site 1088 (Fig. 5.9). Given that the EG favour living in lower oxygen environments (predominantly dysoxic indicators), sharp declines were observed during the cool, high oxygen, and vigorous circulation glacial periods of the middle Pleistocene. A similar pattern of decline is found in the record of the uniserial SG at both Sites 1082 and 1088, although these taxa are infrequent and exhibit only a slight decline in absolute abundance over the same time interval (Figs. 5.14 and 5.15).

Correlation coefficients between benthic foraminiferal records and various environmental proxies were calculated to determine the important factors influencing the decline and extinction of EG species (Tables 5.2 – 5.5). In accordance with a recent North Atlantic study by Kawagata *et al.* (in press), there is a strong positive correlation ($r = +0.60, +0.66$, Site 1082 and 1088, respectively) between the abundance and AR of the EG and the LOTG, in the South Atlantic study area. This verifies that it is likely that the EG favoured living in lower oxygen benthic environments. Furthermore, LOTG species are not only tolerant of low oxygen, but they are also indicators of high food supply (particularly at Site 1082 where AR and absolute abundance of LOTG is very high). At Site 1082 prominent peaks in the AR of several dominant EG species: *Chrysalogonium gomphiformis*, *Myllostomella matanzana*, and *Parafrondicularia laevigata*, coincided with peaks in AR of the LOTG, particularly between 1070 and 1020 ka and 960 to 940 ka (Figs. 5.11 and 5.16). Correlation coefficients showed strongly significant and significant relationships between these dominant EG species and the LOTG (*C. gomphiformis*/AR of the LOTG: $r = +0.77$; *M. matanzana*/AR of the

LOTG: r = +0.36; and *P. laevigata*/AR of LOTG: r = +0.31) (Table 5.3, Appendix 3), further reinforcing that several key EG species may have occupied the same niche as the LOTG. Similar trends are shown between peaks in AR of dominant Site 1088 species, such as *M. costai, M. matanzana*, *P.alternans* and *S. sagrinensis*, and the AR of the LOTG (*M. costai*/AR of the LOTG: r = +0.58; *M. matanzana*/AR of the LOTG: r = +0.64; *P. alternans*/AR of the LOTG: r = +0.50; and *S. sagrinensis*/AR of the LOTG: r = +0.52) (Table 5.5, Appendix 3) Unlike the EG species the LOTG did not show a progressive decline and extinction over the MPT, and on the contrary, sharp declines and often complete recoveries were evident in both Sites 1082 and 1088 (Figs. 5.16 and 5.17). This may indicate that the LOTG were able to adapt more readily to the strong seasonality in surface productivity associated with the establishment of 100 kyr glacial/interglacial cycles. In contrast the *Stilostomella* Extinction Group may have been unable to tolerate the competition associated with highly variable changes in productivity (as suggested by Hess and Kuhnt, 2005). It is likely that the changes in food supply and physical characteristics of the bottom waters impacted on the eating habits and metabolic rates of EG species, possibly opening a niche-gap for more suitable, readily adaptable LOTG species or possibly suboxic/oxic benthic foraminifera.

At Site 1082, declines in EG taxa were generally contemporaneous with lowest (more negative) $\delta^{13}C$ values (Fig. 5.7). Declines in the AR of EG species at 121, 112, 105, 88, 79 and 69 mcd (1060, 1000, 940, 835, 775 and 705 ka), all coincided with periods of lowest $\delta^{13}C$ value. However, the significance of this observation is questionable because Site 1082 $\delta^{13}C$ values were obtained from the planktic foraminifera *Globorotalia inflata*, and are not representative of bottom water changes, rather, giving an indication of water character fluctuations in the water column shallower than Site 1082.

There was a less consistent relationship between $\delta^{13}C$ values and the declining EG taxa at lower productivity Site 1088. This inconsistency may by caused by the $\delta^{13}C$ values being obtained from the epifaunal benthic foraminifera *Cibicidoides* sp., and may not be representative of the dwelling environment of the infaunal EG species (EG/$\delta^{13}C$ (*Cibicidoides*) r = +0.15) (Table 5.5). Most major declines in AR of EG species at Site 1088 coincided with highest $\delta^{13}C$ values (such as during MIS 30 and 28 (14.0 and 13.1 mcd; 1070 and 1025 ka), however some declines coincided with the low $\delta^{13}C$ values (MIS 22 and 16 (11.0 and 7.9 mcd; 880 and 660 ka))(Fig. 5.9).

6.1.4 Highest Occurrences and the Final *Stilostomella* Extinction Datum in the South Atlantic

This research confirms the general patterns of previous *Stilostomella* Extinction studies, placing the final *Stilostomella* Extinction Datum between 900 and 600 ka. The youngest extinction is dated at ~700 ka for *Myllostomella matanzana* and *Siphonodosaria sagrinensis* in Site 1082 and at ~600 ka for *Myllostomella matanzana* and *Pleurostomella alternans* in Site 1088 (Figs. 5.5 and 5.6). Figure 6.1 summarises the timings of HOs in the South Atlantic. The majority of the HOs of the EG taxa were diachronous between Site 1082 and 1088, although two species, *Awhea tosta* (~ 860 ka), and *Chrysalogonium stimuleum* (~ 940 ka), were synchronous between sites (Fig. 6.1). There was clearly a steady increase in the rate of South Atlantic HOs through the MPT (early MPT (1200 - 1000 ka) = 2-3HOs/100 kyr; late MPT (post ~1000 ka) = 4-7HOs/100 kyr) (Fig. 5.13). The maximum number of HOs occurred between 1000 and 700 ka at both sites, with a peak (7HOs/100 kyr) between 900 and 800 ka for Site 1082 and 5HOs/100 kyr between 1000 and 900 ka, and 800 and 700 ka for Site 1088 (Fig. 5.13). Site 1082 peaks in the number of HOs per 100 kyr approximately 100 kyr earlier than Site 1088. Diachroneity of HOs between sites may be related to differences in bottom water circulation at intermediate and deep water depths and the relative productivity of the sites. This pattern of the final extinction datum for the study area occurring earlier in the shallower Site 1082 does not fit the pattern of Schönfeld's (1996) summation of (then) known records, or Hayward's (2002) SW Pacific study, in which local disappearances commonly begin earliest in deeper waters (and shallow ODP 1119). This difference is likely to be attributed to the proximity of Site 1082 to the Benguela Current Upwelling System. In the case of Site 1082, located on the margin of the Namibian upwelling cell, variations in upwelling strength in glacial versus interglacial periods, and consequently, high seasonality of food supply may be the over-riding factor in the timing of highest occurrences.

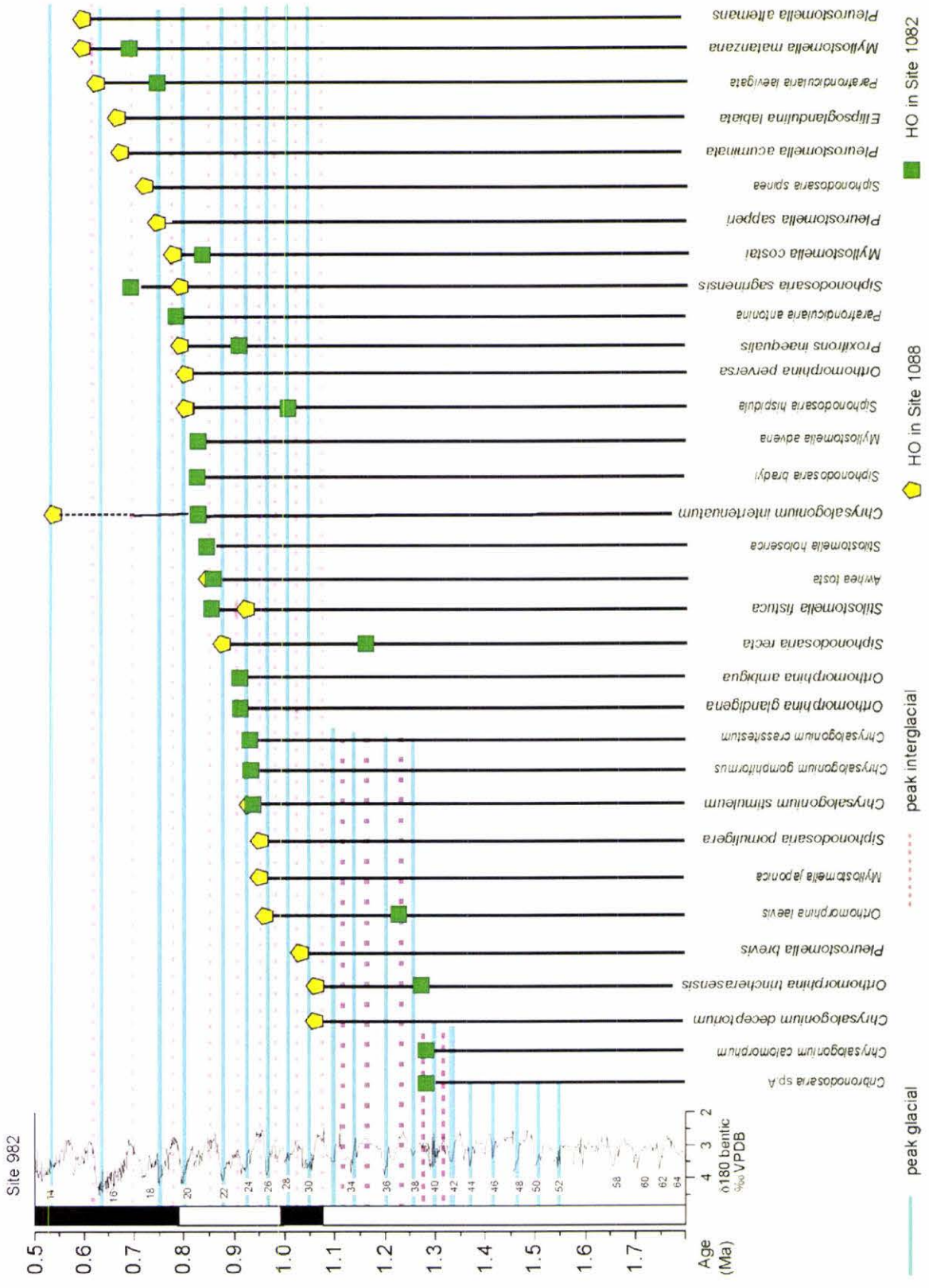

Figure 6.1: Comparison of the timing of the highest occurrences (HOs) of Extinction Group species in South Atlantic Sites 1082 and 1088. Oxygen isotope records are based on ODP Site 982 (Venz and Hodell, 1999). Marine oxygen isotope stages (MIS) are shown. Solid and dashed lines represent peak glacial and interglacial stages, respectively. Note: *Chrysalogonium interfenuatum* survived through the MPT at Site 1088.

6.1.5 Paleoceanographic Change and Possible Explanations

The South Atlantic Ocean plays an important role in global thermohaline circulation. Historically, the switching on and off of the Atlantic heat conveyor with glacial-interglacial cyclicity, has greatly modified conditions in the deep ocean and the benthic communities living there. Schmiedl *et al.* (1997) have identified food supply and corresponding dissolved oxygen contents in the pore and bottom waters as the most important factors controlling the distribution pattern of Recent benthic foraminifera in the eastern South Atlantic. The major implications of glacial-interglacial changes to thermohaline circulation, and the possible impacts on the Extinction Group benthic foraminifera is now discussed.

Today circulation in the intermediate and deep South Atlantic is dominated by the interactions between North Atlantic Deep Water (NADW-high $\delta^{13}C$, oxygen-rich, nutrient-depleted) flowing toward the south (between ~1500 and 4000 m water depth), and Circum Polar Deep Water (CPDW) flowing to the north (below ~4000 m water depth) (Bickert and Mackensen, 2003). The density characteristics of these water masses are such that at about 45°S the NADW divides the southern water mass into an upper (upper-CPDW-^{13}C-depleted, low-oxygenated, nutrient-rich) and a lower (lower-CPDW- ^{13}C-depleted, low-oxygenated, nutrient-rich) branch (Bickert and Mackensen, 2003). Thus, above the NADW (at ~1500 m water depth) is the upper-CPDW mass, which in places mixes with the overlying Antarctic Intermediate Water (AAIW), which is characterised by relatively low salinity values (Figs. 1.2 and 1.7).

The carbon isotopic gradients ($\delta^{13}C$) between benthic foraminifera from different locations have been used to infer past changes in deep water circulation, particularly, fluctuations in deep water production, and the changing influence and mixing ratios of Northern Component Water (NCW, such as NADW) and Southern Component Water (SCW, such as CPDW) over glacial-interglacial cycles (Hodell and Venz, 2002). This method is likely to be best suited to areas of lower primary productivity. Previous studies at higher productivity sites exposed to seasonally high fluxes of organic carbon have shown substantially lower $\delta^{13}C$ values compared with surrounding lower productivity cores (Bickert and Mackensen, 2003). For example, in the core IOW226920 from the central Namibia upwelling zone (isotopes by Mollenhauer *et al.* 2002), epibenthic $\delta^{13}C$ values were shown to deviate from the local intermediate- to–

deep $\delta^{13}C$ gradient (DIC) values by up to 0.4 ‰ (Bickert and Wefer, 1999; Mackensen *et al.*, 2001). This apparent deviation associated with high-productivity areas in glacial times can be explained by the phytodetritus-effect (for a summary see Mackensen and Bickert, 1999), and to overcome this problem a constant value of 0.4 ‰ is added to $\delta^{13}C$ values derived from epibenthic foraminifera (such as *Cibicidoides* sp.) in upwelling areas (Bickert and Mackensen, 2003).

Significant changes to the intermediate- and deep-water South Atlantic and Southern Ocean thermohaline circulation are assumed to have accompanied the enhanced severity of glacial and interglacial cycles associated with the MPT (Venz and Hodell, 2002; Bickert and Mackensen, 2003; Hodell *et al.*, 2003). Last Glacial Maximum (LGM) reconstructions of Atlantic circulation by Bickert and Mackensen (2003) show that most cores in the South Atlantic had a typical glacial-to interglacial $\delta^{13}C$ shift of 1.4 to 2.1‰, a large part of which is related to ice volume changes, with the additional effect of deep water temperature and salinity changes (Bickert and Mackensen, 2003). Reductions in NCW formation and thinning (decreased vertical extension), the presence of well-ventilated Glacial North Atlantic Intermediate Water (GNAIW), as well as increased northerly extent and advection of SCW during glacial periods and the possible impacts on the Extinction Group benthic foraminifera at each site are now discussed below.

6.1.5.1 Site 1082

Below the coastal upwelling areas high organic matter fluxes favour the occurrence of high productivity faunas along the continental margin that are adapted to low oxygen conditions in the ambient bottom water mass (LOTG faunas). Modern day inhabitants of such areas are characteristically highly adaptive, opportunistic species, forming low diversity communities with extraordinary high standing stocks, reflecting the complex relationship between organic matter flux rates and dissolved oxygen concentrations in the bottom and pore waters (Schmiedl *et al.*, 1997). Modern day upwelling off the Namibian coast is such that small seasonal fluctuations in upwelling intensity and subsequently food supply are commonplace, and Recent highly adapted assemblages in this high productivity site are able to flourish amidst seasonal changes in food supply. These Recent benthic communities prefer a shallow to deep infaunal lifestyle, but, certain *Nonionella* and *Bolivina* species are able to live epi- or infaunally and change their microhabitat in response to organic matter fluxes and oxygen concentrations in the

bottom and pore waters (Jorissen *et al.*, 1992). Furthermore, these highly adaptive Recent faunas comprising the genera *Bolivina, Bulimina,* and *Globobulimina,* as examples, have advantageous morphological adaptations, such as thin walled tests and numerous pores to facilitate gas exchange, making them better suited for the environmental stresses of high productivity environments.

At Site 1082 declines in EG taxa are contemporaneous with the lower peak values of planktic foraminiferal (*G. inflata*) $\delta^{13}C$ (correlation coefficient of +0.30) and higher peak values of $\delta^{18}O$ (r = +0.55) (Figs. 5.7 and Table 5.3), particularly during glacial MIS 30, 26, 24, and MIS 20. However, the significance of this observation is questionable as Site 1082 $\delta^{13}C$ and $\delta^{18}O$ values were obtained from the planktic foraminifera *Globorotalia inflata*, and are not representative of bottom water changes, rather, giving an indication of water character fluctuations in the water column shallower than Site 1082. Without appropriate benthic $\delta^{13}C$ data it is difficult to determine changes in thermohaline circulation to the region of Site 1082, however studies by Hay and Brock (1992) and Hodell *et al.* (2003) infer GNAIW influence during cold periods. They suggest that during glacials, when the production of NADW is reduced, as too is the production of AAIW, and nutrient-poor, well ventilated GNAIW extends into the Southern Ocean (as later indicated at Site 1088) to become the dominant water mass in the South Atlantic (Hay and Brock, 1992; Hodell *et al.* 2003).

However, in high productivity areas, such as the Benguela Upwelling System and Site 1082 (with modern day primary productivity rates of more than 125-180 g $C/m^2/yr$) (Schmiedl *et al.*, 1997), changes in the organic carbon flux are also likely to have had a major effect on the structure of benthic communities (Mackensen *et al.*, 1985; Corliss and Chen, 1988; Loubere, 1991), particularly infaunally-dwelling EG species. Durham *et al.* (2002) studied changes in productivity over glacial-interglacial cycles at nearby Site 1081. Through the use of paleoproductivity proxies (chlorin mass accumulation rates (MAR) and Total organic carbon (TOC) MAR records) the authors found evidence for increased productivity during MPT glacial periods as the Benguela Current intensified with subsequent upwelling. They attributed the increased productivity between 800 to 500 ka to global cooling, increased aridity on the African continent (with increased terrigenous inputs by strengthened SE trade winds, possible iron fertilisation), and rapid sea-level drop, bringing nutrient-enriched bottom waters to the

surface. Enhanced upwelling and subsequently increased carbon flux caused increased FI and a corresponding decrease in %PF; both indicate increased dissolution of planktic foraminifera at Site 1082 during MPT glacial intervals (correlation coefficient r values: $\delta^{18}O$/FI = +0.32; $\delta^{18}O$/%PF = -0.53, Table 5.3). Durham *et al.* (2002) also concluded that the resultant productivity peak, associated with enhanced upwelling and increased carbon flux during glacial periods, was only short-lived, because enhanced productivity removed nutrients faster than they could be replaced, hence productivity subsequently declined at c.500 ka. In an overview on the use of benthic foraminifers as paleoenvironmental proxies, Van der Zwaan *et al.* (1999) commented that in all cases there is a direct proportional increase in abundance and biomass in response to increased supply of organic matter. However, in high productivity upwelling environments it has been suggested that reproduction potential (the efficiency with which offspring are generated) is the underlying control of species diversity, because competition for seasonally fluctuating food and space resources is likely to be high. It can therefore be inferred that "blooms" and the occurrences of dominant species in Site 1082 (and also Site 1088) may be due to reproductive superiority over competing EG, SG and LOTG species. Accumulation rate comparisons between individual EG species at Site 1082 indicate that some EG and LOTG species (such as *Chrysalogonium gomphiformis*, *Myllostomella matanzana*, and *Parafrondicularia laevigata*) clearly profit from an organic matter pulse (Fig. 5.11), with AR reaching a high peak, before rates of accumulation decline again as nutrients are removed faster than they are replaced, or increasing oxygen demand leads to lower oxygen contents (Van der Zwaan *et al.*, 1999). Such dominant species possess the ability to reproduce rapidly and even immaturely, so that they can reach high numbers in a short period of time (the so-called opportunistic model), making best use of the short-lived fluctuations in food supply associated with high productivity sites during the MPT.

It is my interpretation that the glacial declines and eventual extinction of EG benthic foraminifera at high productivity Site 1082 were primarily driven by highly fluctuating food supply associated with increased productivity with intensified upwelling during MPT glacial periods. Second to this, the glacial replacement of nutrient-rich AAIW with nutrient-poor, $\delta^{13}C$-enriched, GNAIW may also have been a major influencing factor; the phytodetritus-effect masking the high-$\delta^{13}C$ signal of the GNAIW watermass. It is likely that this highly fluctuating food supply, competition for food resources with

highly adept LOTG species, and changes in ventilation, created a high level of environmental stress and was detrimental to the survival of the EG benthic foraminifera, who were unable to adapt to the rapidly changing environmental conditions of the MPT.

6.1.5.2 Site 1088

The $\delta^{18}O$ benthic (*Cibicidoides* sp.) record from Site 1088 (from Hodell *et al.*, 2003) captures the full glacial-interglacial signal of the MPT. During the MPT the $\delta^{13}C$ benthic (*Cibicidoides* sp.) signal is consistent with other mid-depth South Atlantic $\delta^{13}C$ records, although it is of a smaller magnitude, compared with deeper sites (such as nearby Site 1090 (Hodell *et al.*,2003)). As a means of recreating changes in South Atlantic thermohaline circulation over the MPT, Hodell *et al.* (2003) reconstructed the vertical $\delta^{13}C$ gradient between middle-depth Site 1088 (2082 m) and deep Site 1090 (3702 m) waters by subtracting $\delta^{13}C$ (*Cibicidoides* sp.) values at Site 1088 from those at Site 1090. They revealed that the benthic carbon isotope gradient between deep and intermediate sites (DIC) approached zero during most interglacial stages and increased to -1 to -1.5 ‰ during glacial stages of the last ~1100 ka (Fig. 6.2).

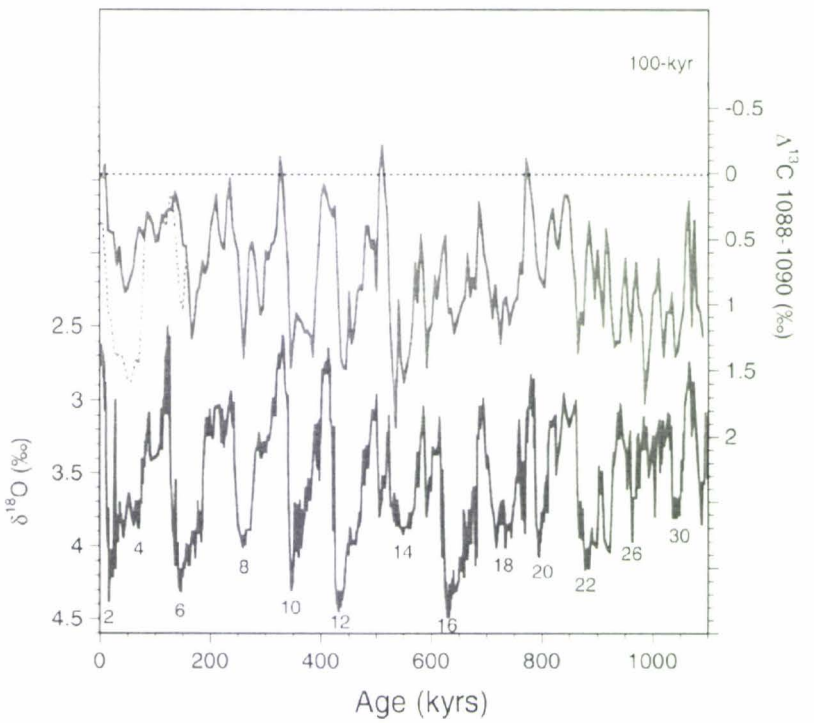

Figure 6.2: Vertical fractionation of intermediate (Site 1088) and deep (Site 1090) watermasses within the Southern Ocean during the last 1000 ka. Benthic oxygen isotope stratigraphy at Site 1090 (bottom line with glacial MIS stages given), and benthic carbon isotope gradient data based on *Cibicidoides wuellerstorfi* (from Hodell *et al.*, 2003).

Figure 6.2 shows that the largest amplitudes of change in both benthic $\delta^{13}C$ and $\delta^{18}O$ occurred during the MPT, particularly between 900 and 700 ka (MIS 22-18), a time of the greatest number of HOs of EG taxa per 100 kyr (4-5 HOs/kyr)(Fig. 5.13). These variations in benthic $\delta^{13}C$ can be caused by changes in nutrient distribution, air-sea exchange, or possibly the "phytodetritus effect". However, given that these two sites are separated by less than 2° latitude, it is unlikely that they experienced dramatically different changes in productivity or organic rain rates (Hodell *et al.*, 2003), and so, this observed increase in DIC over the MPT supports a change in the vertical fractionation of watermasses and is suggestive of the mid-depth waters (< 2100 m, Site 1088) evolving differently from the deep-depth waters (> 2700 m, Site 1090) over this time. This $\delta^{13}C$ gradient indicates the presence of a pronounced chemocline between 2100 and 2700 m, signalling the mixing zone between GNAIW and CPDW.

Hodell *et al.* (2003) further suggested that although the production of NADW was reduced during glacials, GNAIW was enhanced (Oppo and Lehman, 1993), and this well-ventilated water extended the depth of the South Atlantic Ocean to at least 2100 m, encompassing Site 1088. Furthermore, during MPT glacial periods, GNAIW was locally thinned in the water column, as a result of the enhanced advection of low-oxygenated and nutrient enriched CPDW. Its decreased vertical extension, led to the well-oxygenated and nutrient depleted water mass sitting higher in the water column compared to today and MPT interglacial times (Hodell *et al.*, 2003). A reconstruction of the glacial-interglacial reorganisation of the South Atlantic thermohaline circulation across the MPT is shown in figure 6.3

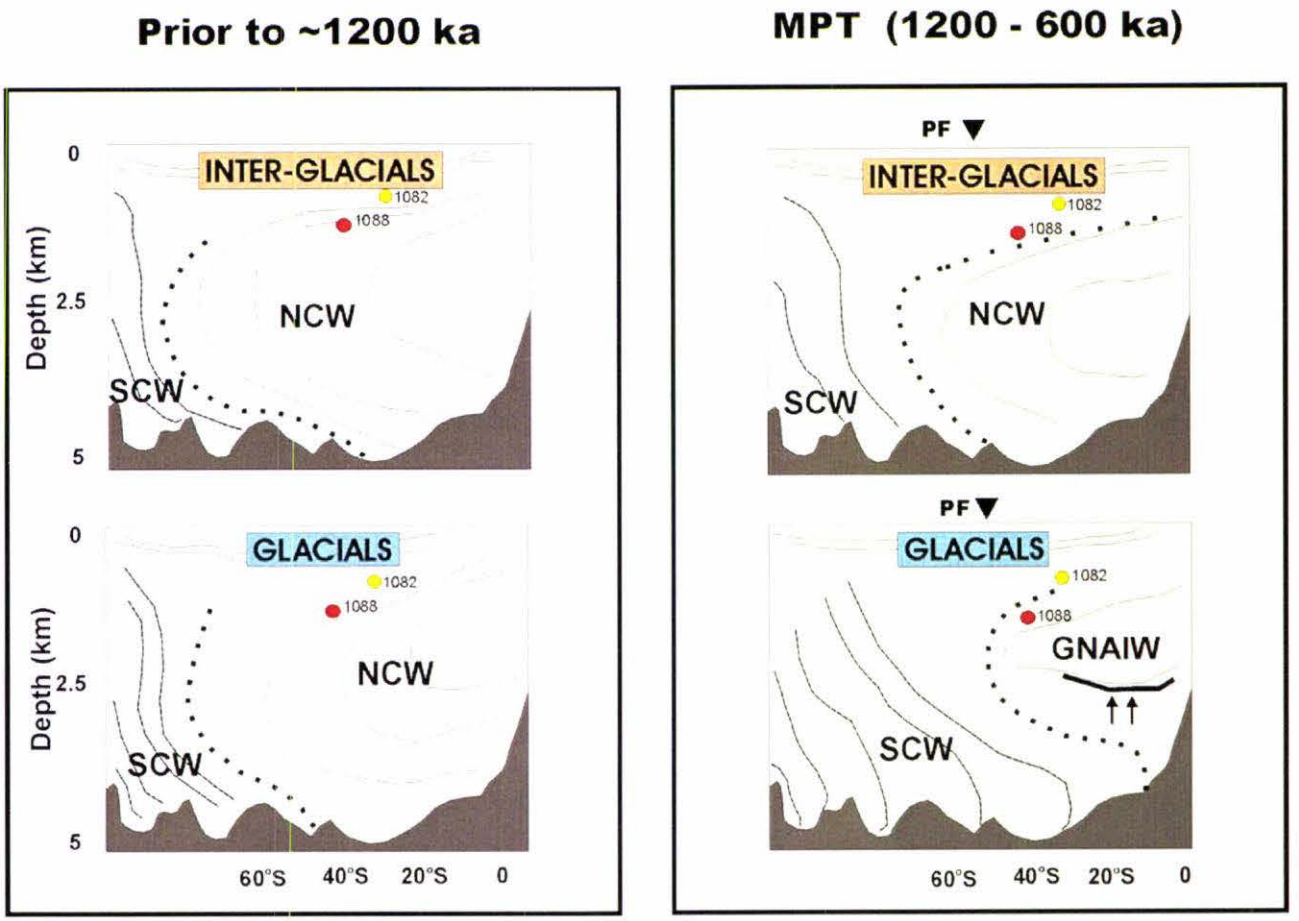

Figure 6.3: Schematic representation of glacial-to-interglacial changes in thermohaline circulation in the South Atlantic prior to the MPT and during the MPT. Positions of water masses are inferred from benthic $\delta^{13}C$ records and intermediate to deep water ^{13}C gradients from Sites 982, 607, 925,929, and 1090 *from* Venz and Hodell (2002). NCW = Northern Component Water; SCW = Southern Component Water; GNAIW = Glacial Northern Atlantic Intermediate Water; PF = Antarctic Polar Front (which shifted north during MPT glacial periods). ▪ ▪ ▪ ▪ ▪ ▪ ▪ ▪ ▪ Mixing zone between NCW and SCW

MPT declines in the AR and abundance of EG species at Site 1088 were contemporaneous with highest values of $\delta^{18}O$ and more-often-than-not with highest $\delta^{13}C$ values, particularly at MIS 30, 28, 26, 20, 18, and MIS 14 (Fig. 5.9). However, there is conflicting evidence that some EG declines at Site 1088 may have occurred during periods of encroachment by colder, lower dissolved oxygen (DO), higher nutrient (lower $\delta^{13}C$) waters (such as during glacial MIS 24, 22 and 16) (Fig. 5.9). Lower DO and lower $\delta^{13}C$ values may indicate mixing of glacial expanded lower-CPDW with GNAIW in the region of Site 1088 during some (but not all) mid-Pleistocene glacial periods.

It is therefore likely that during most glacial periods of the MPT, Site 1088, currently positioned at the interface of the NADW and upper CPDW (Fig. 1.7), was rapidly encroached on by cool, high-dissolved oxygen (well-ventilated), nutrient-depleted GNAIW. There may have also been instances, particularly during colder glacial MIS 22 and 16, when lower DO (compared with GNAIW), lower-CPDW expanded into the intermediate depths towards Site 1088 and mixed with the overlying GNAIW. During both of these instances Site 1088 was bathed in higher dissolved oxygen waters which may have been highly detrimental to the survival of the EG species.

Exactly how these infaunal EG species reacted to the invading well-ventilated watermass is unknown, although a change in microhabitat position can be speculated, as illustrated in figure 6.4.

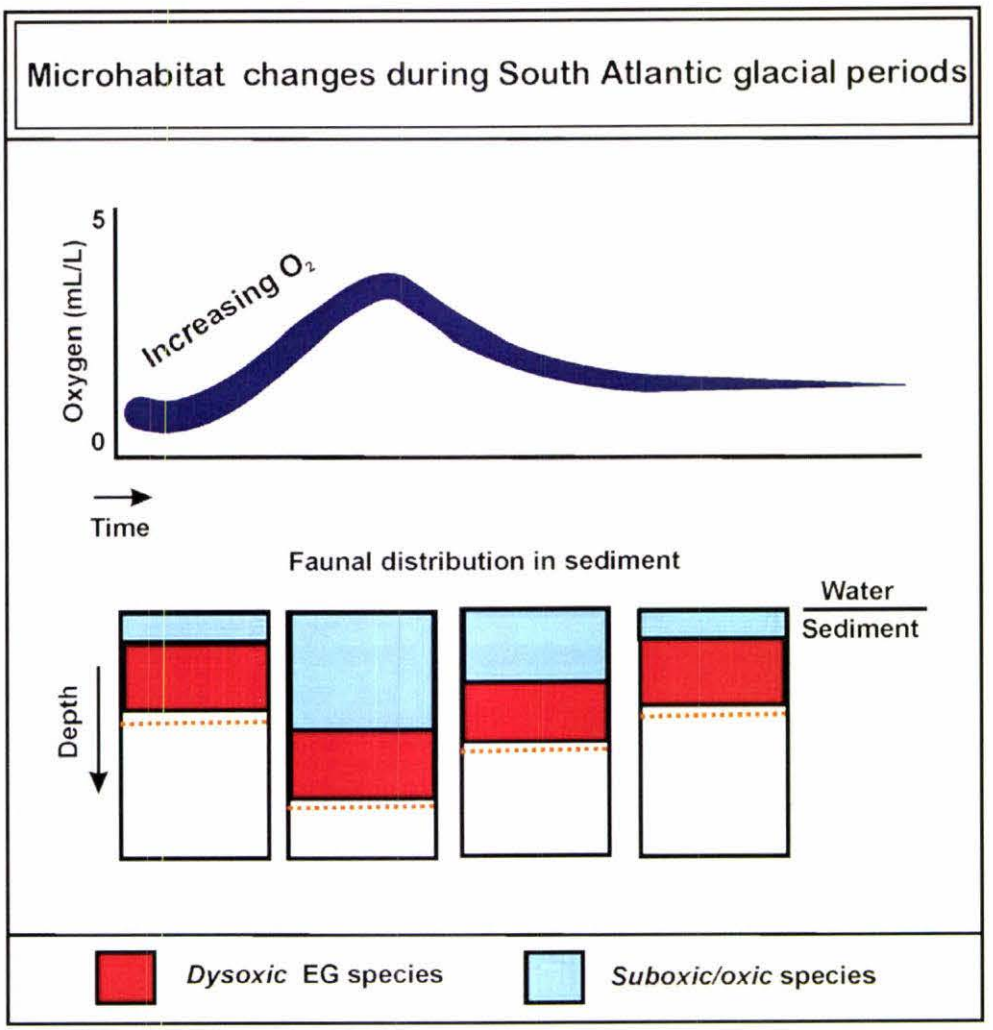

Figure 6.4: Inferred change in microhabitat by *dysoxic* Extinction Group species during well-ventilated MPT glacial periods. ····· Sulphide producing front.

Figure 6.4 shows that with increasing environmental stress associated with increasing dissolved oxygen concentrations in the bottom and pore waters, infaunally dwelling EG species may have migrated with the moving redox front, further from the water/sediment interface (deeper into the sediment). However, associated with this change in microhabitat position may have been a decrease in readily available food supply or more specifically, their favoured source, possibly governed by their specific apertural modifications, which may have eventually proven critical for the survival of the group.

In contrast to the coastal upwelling region of high productivity, the oceanic region of Site 1088 is an area characterised by comparatively low and short-lived small seasonal fluctuations in biological productivity, with modern day primary productivity rates of approximately 30-70 g $C/m^2/yr$ (Schmiedl *et al.*, 1997). Diekmann and Kuhn (2002) found evidence of slightly increased productivity (MAR of organic carbon) during MPT glacial intervals (particularly after ~900 ka) at nearby Site 1090. Organic carbon records at Site 1090 fluctuated between 0.8 and 0.05 wt.%, with 6-10 fold increases during some glacial intervals. It is assumed that changes in biological productivity were mostly triggered by frontal movements, such as northward advances of the Antarctic Polar Front during extremely cold phases of glacial stages; however, Site 1088 is well northward of the influence of the glacially migrating Antarctic Polar Front (Venz and Hodell, 1992).

Winnowing of fine particles by strong glacial bottom currents may have impacted on the food supply of the infaunally living EG species. During glacial intervals sediments on the crest of the Agulhas Ridge are likely to have been removed by strong currents (Diekmann and Kuhn, 2002) and may have prevented the accumulation of a phytodetritus layer, thus reducing food supply. In low productivity areas, such as Site 1088, strong glacial currents may have amplified an already adverse environment, with benthic communities struggling to adapt to the rapidly changing watermass ventilation.

It is my interpretation that the glacial declines and eventual extinction of EG benthic foraminifera at low productivity Site 1088 were primarily driven by the MPT reorganisation of the glacial-interglacial modes of NADW production in the North Atlantic, and subsequent glacial encroachment of the well-ventilated, high-dissolved

oxygen, nutrient depleted GNAIW, or an admixture of glacial, expanded lower-CPDW and GNAIW. Fluctuations in food supply, caused by the winnowing effect of strong bottom currents during glacial periods may have also contributed to the overall decline.

6.2 *The Stilostomella Extinction*

Cenozoic bottom water temperature fluctuations are mainly driven by climatic changes in the high latitudes. Deep-sea benthic foraminiferal oxygen isotope ratios thus reflect not only these deep water temperature changes, but also changes in high latitude climates, and their Pleistocene ice sheet growth and decline.

Earlier and more severe extinctions of deep-sea benthic foraminifera occurred during the late Paleocene thermal maximum (LPTM: ~55 Ma), resulting from the influence of oxygen-poor, warm, corrosive bottom water. In contrast the youngest episode of benthic foraminiferal extinctions has been attributed to global cooling during the Pleistocene ice ages (Hayward, 2002). It is thought that during the middle Pleistocene, high latitude oxygen-rich cold waters drove global deep water circulation. Although decreases in foraminiferal abundance and diversity began at the onset of the Northern Hemisphere glaciations in the late Pliocene, the major extinctions coincided with the MPT. This was a time in which increases in the amplitude, severity and longevity of climatic fluctuations (based on $\delta^{13}C$ and $\delta^{18}O$ values), coupled with changes in the chemical and physical properties of intermediate and deep watermasses, and a highly seasonal food influx, appear to have been detrimental to Extinction Group taxa.

6.2.1 Local Extinction Patterns

This South Atlantic study reveals that the extinction of particular elongate deep-sea foraminifera belonging to the families Stilostomellidae, Pleurostomellidae, and part of Nodosariidae, shows a pulsed pattern of decline during the mid-Pleistocene Climatic Transition (MPT, ~1200 – 600 ka), and final extinction at ~ 705 ka at Site 1082, and ~ 600 ka at Site 1088 (Fig.6.1). This progressive pulsed decline, together with the final extinction ages confirms the general patterns observed by previous *Stilostomella* Extinction workers, placing the final *Stilostomella* Extinction Datum between 900 and 600 ka (e.g. Schönfeld, 1996; Hayward, 2001, 2002; Kawagata *et al.* in press).

A major decrease in accumulation rates (AR) of the EG occurs between ~1070 and 1000 ka at both core sites (Figs. 5.7 and 5.9). The AR of the EG never recovered after ~1000 ka at Site 1082, whereas the EG shows a last peak centred at ~ 950 ka at Site 1088.

This variation was probably caused by a difference in paleoceanographic changes between the two South Atlantic sites.

Globally, the timing of declines in EG taxa and their respective HOs is highly variable and more often than not diachronous even over very short geographic distances. Weinholz and Lutze (1989) were first to recognise this diachroneity in HOs over short spatial distances during their study, DSDP Sites 658 and 659 off northwest Africa. It was at this time that the extinction of the genus *Siphonodosaria* (= their *Stilostomella*) in deeper water Site 659 was thought to have a lead time of ~166 kyr over shallower water Site 658. Schönfeld (1996) confirmed this discovery, with a 155 kyr difference for the local extinction datum of *Siphonodosaria sagrinensis* in DSDP Sites 548 and 549 in the North Atlantic. Following this observation, Schönfeld proposed that declines and extinctions of the "*Stilostomella*" Extinction Group took place earlier in deeper water (particularly > 3000 m), at farther distances from shore, and at mid- to low southern latitudes (Schönfeld, 1996). A SW Pacific study by Hayward (2002) confirmed the inferences of early workers, with the earliest HO of *Siphonodosaria sagrinensis* occurring in CPDW-bathed, upper abyssal site ODP Site 1123 (3290 m depth) at ~ 1050 ka, and latest local disappearance in shallow, AAIW-bathed, lower bathyal ODP Site 1125 (1365 m depth) at ~570 ka. Hayward (2002) inferred that EG taxa had progressively withdrawn from abyssal and upper bathyal (ODP Site 1119) depths to survive longest at AAIW (lower bathyal) depths. Furthermore, the highest number of HOs per 100 kyr at Site 1123 occurred some 150 kyr prior to Site 1125 (Fig. 6.5). Both sites are in close proximity, north of the STF, and would be expected to have similar histories of phytoplankton food production (Hayward, 2002), thus indicating vertical fractionation and differing chemical evolution of watermasses was the driving force over glacial-interglacial intervals.

However, this relationship between depth and timing of the disappearance of EG taxa is not as simple as first thought. This South Atlantic study shows a ~ 100 kyr difference in the peak number of HOs in the shallower Site 1082 (7HOs/100 kyr, between 900 and 800 ka) than in the deeper (and further offshore) Site 1088 (5HOs/100 kyr, between 800 and 700 ka) (Fig. 5.13). This is concordant with the result reported from a similar North Atlantic study of Site 980 (2168 m depth, lower-NADW) and Site 982 (1145 m depth, upper-NADW) (Kawagata *et al.*, in press), which also differs from Schönfeld's

'normal' relationship between water depth and peak number of HOs (Schönfeld, 1996). A similar relationship exists when comparing final *Stilostomella* extinction datums between sites. For example, the youngest extinction species in the North Atlantic study is *Pleurostomella alternans*, with a HO datum of ~695 ka in shallower Site 982, and ~680 ka in deeper Site 980 (Kawagata *et al.*, in press). Similarly, in the South Atlantic the youngest extinction is dated at ~705 ka for *Myllostomella matanzana* in shallower Site 1082 and at ~ 600 ka in deeper Site 1088 (Fig. 6.1).

Reasons for this observed deviation from the 'deep leading the shallow' when comparing intrabasin South Atlantic Sites 1082 and 1088, and North Atlantic Sites 980 and 982 are likely to be related to both progressive (sequential) changes in the character of different deepwater masses – impacting shallowest and deepest watermasses first and intermediate watermass last (Hayward, 2002); and local differences in primary productivity. Low productivity sites, such as a central gyre, should not be directly compared with high productivity sites, such as an upwelling region, as the timings of HOs in these contrasting benthic environments are much more complex than depth and distance from the continental landmass alone. In such cases, paleoproductivity, carbon flux (i.e. potential for rapidly fluctuating food supply and subsequent oxygen content in sediment), proximity to frontal systems (migrating with glacial-interglacial cyclicity), topographical location (i.e. potential for winnowing by vigorous glacial bottom currents), as well as parameters such as depth and distance from shore (suggestive of watermass chemical and physical properties), should be carefully examined before conclusions are made.

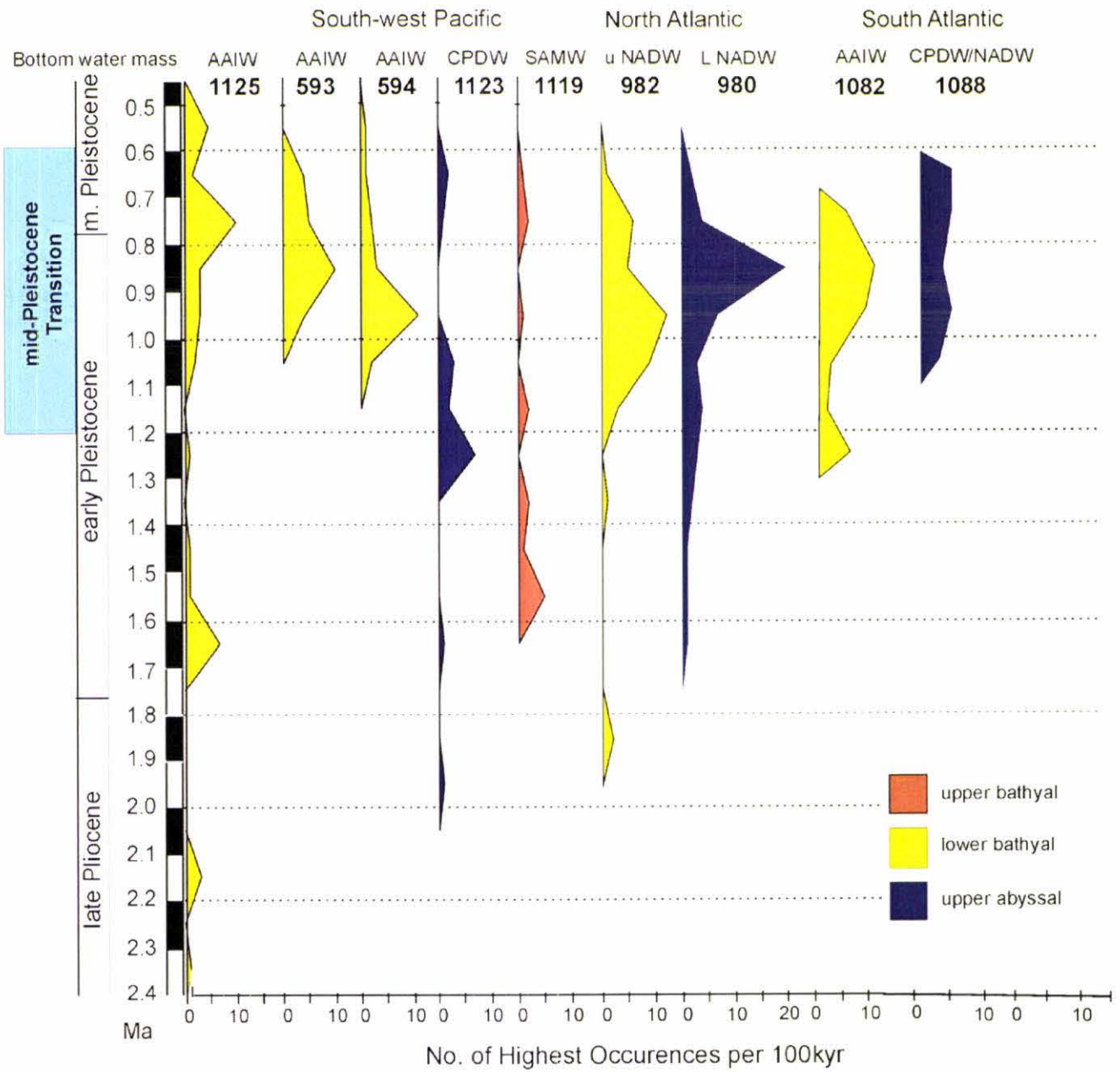

Figure 6.5: Global comparisons of the number of highest occurrences (H0s) of Extinction Group taxa per 100 kyr. AAIW = Antarctic Intermediate Water; CPDW = Circum-Polar Deep Water; SAMW = Subantarctic Mode Water; u-NADW = upper-North Atlantic Deep Water; L-NADW = lower-North Atlantic Deep Water; NADW = North Atlantic Deep Water. SW Pacific data from Hayward (2002); North Atlantic data from Kawagata *et al.* (in press).

6.2.2 Global Extinction Patterns

Globally, the timing of declines and HOs of EG taxa reflect the complex nature of the thermohaline circulation system. Simplistically, Broecker's (1989) thermohaline 'conveyor belt' is composed of northward transports of warm surface- and intermediate-layer waters, southward transport of NCW (such as NADW), and at the bottom, northward flowing SCW (such as CPDW). Accompanying the increased amplitude and severity of glacial-interglacial climate cycles in the MPT, were changes in global thermohaline circulation. These were mainly the relative contributions (mixing ratios) of SCW and NCW to a region (governed by thinning, advection, and reductions in formation) and the chemical parameters of these watermasses.

The middle Pleistocene *Stilostomella* Extinction event has now been recorded globally (Schönfeld, 1996; Hayward, 2002; Kawagata *et al.*, in press); this study documents the first records from the South Atlantic. Table 6.3 summarises the global biogeographic affinity of the South Atlantic EG during the MPT (data from North Atlantic studies by Kawagata *et al.* (in press) (ODP Sites 980 and 982) with SW Pacific studies by Hayward (2002) (ODP Sites 1119, 1120, 1123 and 1125, and DSDP Sites 593 and 594). The location, water depth, bottom water, number of EG species and the approximate age of the youngest extinction at each of these sites is summarised in table 6.4.

Extinction Group - South Atlantic	Biogeog. affinity	ODP 1082 1280 m	ODP 1088 2082 m	ODP 980 2168 m	ODP 982 1145 m	DSDP 593 1050 m	DSDP 594 1204 m	ODP 1119 395 m	ODP 1120 545 m	ODP 1123 3290 m	ODP 1125 1365 m
Awhea tosta	cos	y	y	y	y	y	y	y	y	y	y
Chrysalagonium calomorphum	cos	y	n	y	n	y	y	y	n	n	y
Chrysalagonium crassitestum	cos	y	n	y	n	n	n	n	n	n	y
Chrysalagonium deceptorium	sa, na	n	y	y	y	n	n	n	n	n	n
Chrysalogonium gomphiformis	cos	y	n	y	n	n	n	n	n	n	y
Chrysalogonium intertenuatum	cos	y	y	n	y	y	y	y	y	n	y
Chrysalogonium stimuleum	cos	y	y	y	y	y	n	y	n	y	y
Cribronodosaria sp. A	swp, sa	y	n	n	n	n	n	n	n	n	y
Ellipsoglandulina labiata	cos	n	y	y	y	y	y	n	y	y	y
Myllostomella advena	cos	y	n	n	y	n	n	n	n	n	y
Myllostomella costai	cos	y	y	y	y	y	y	y	y	y	y
Myllostomella japonica	sa, na	n	y	y	y	n	n	n	n	n	n
Myllostomella matanzana	cos	y	y	y	y	y	y	n	y	y	y
Orthomorphina ambigua	cos	y	n	y	y	y	n	n	n	n	y
Orthomorphina glandigena	sa, na	y	n	y	y	n	n	n	n	n	n
Orthomorphina laevis	sa, na	y	y	y	y	n	n	n	n	n	n
Orthomorphina perversa	cos	y	y	y	y	y	y	n	y	y	y
Orthomorphina trincherasensis	cos	y	y	y	y	y	n	n	n	n	y
Parafrondiculana antonina	swp, sa	y	n	n	n	n	n	n	y	n	y
Parafrondiculana laevigata	cos	y	y	y	n	y	y	y	y	n	y
Pleurostomella acuminata	cos	n	y	n	n	y	y	y	y	y	y
Pleurostomella alternans	cos	n	y	y	y	y	y	y	y	y	y
Pleurostomella brevis	cos	n	y	y	y	n	n	n	n	y	y
Pleurostomella sapperi	cos	n	y	y	y	y	n	n	n	n	y
Proxifrons inaequalis	cos	y	y	y	n	y	y	y	y	n	y
Siphonodosaria bradyi	sa, na	y	n	n	y	n	n	n	n	n	n
Siphonodosaria hispidula	cos	y	y	y	n	n	n	n	n	n	y
Siphonodosaria recta	cos	y	y	y	y	y	y	n	y	n	y
Siphonodosaria segrinensis	cos	y	y	y	y	y	y	n	y	y	y
Siphonodosaria spinea	cos	n	y	n	n	n	n	n	n	n	n
Siphonodosaria pomuligera	cos	n	y	y	y	y	y	y	y	y	y
Stilostomella fistuca	cos	y	y	y	y	y	y	n	n	y	y
Stilostomella holoserica	cos	y	n	y	n	y	n	n	n	n	y
Total number of species		24	23	26	22	20	15	10	16	12	27

* cos = cosmopolitan, swp = SW Pacific, na = North Atlantic, sa = South Atlantic.

Table 6.3: Global biogeographic affinity of the South Atlantic Extinction Group during the MPT.

Site	Region	Latitude	Longitude	Water depth	Bottom water	EG	Youngest extinction
ODP 1082	South Atlantic	21 05.64'S	11 49.24'E	1290 m	AAIW	24	700 ka
ODP 1088	South Atlantic	41 08. 02'S	13 33. 08'E	2082 m	uCPDW/NADW	22	600 ka
ODP 980	North Atlantic	55 29.10'N	14 42.10'W	2168 m	lNADW	49	680 ka
ODP 982	North Atlantic	57 31.00'N	15 52.00'W	1145 m	uNADW	43	690 ka
DSDP 593	SW Pacific	40 30.47'S	167 40.47'E	1050 m	AAIW	23	650 ka
DSDP 594	SW Pacific	45 31.41'S	174 56.88'E	1204 m	AAIW	21	580 ka
ODP 1119	SW Pacific	44 45.33'S	172 23.60'E	395 m	SASW	13	650 ka
ODP 1123	SW Pacific	41 47.17'S	171 29.94'W	3290 m	CPDW	17	650 ka
ODP 1125	SW Pacific	42 32.98'S	178 09.99'W	1365 m	AAIW	47	570 ka

Table 6.4: Global comparison core site data, with number of Extinction Group species and time of youngest extinction.
AAIW = Antarctic Intermediate Water; uCPDW = upper-Circum Polar Deep Water; NADW = North Atlantic Deep Water; lNADW = lower-North Atlantic Deep Water; SASW = Subantarctic Surface Water; CPDW = Circum Polar Deep Water.

Recent research has shown that the major declines in abundance and diversity of EG taxa occurred during cold periods in the MPT (e.g. Hayward, 2001, 2002; Kawagata *et al.*, in press). These coincided with highest values of $\delta^{13}C$ in North Atlantic intermediate depths, which is thought to indicate the encroachment of high dissolved-oxygen, nutrient-depleted Glacial North Atlantic Intermediate Water (GNAIW) (Kawagata *et al.*, in press). Colder, higher oxygenated (better ventilated) watermasses might have been transported to intermediate and deep-water depths in the glacial North Atlantic, and similar well-ventilated glacial equivalents in other oceans, such as the glacial Antarctic Intermediate Water (AAIW) or Circum Polar Deep Water (CPDW) in the SW Pacific (Hayward, 2002). Such glacial-interglacial replacement of intermediate and deep water can be caused by variations in the strength of the global thermohaline 'conveyor belt'.

Early in the MPT (between ~1200 and 900 ka), deep water circulation changes were centred in the North Atlantic (Venz and Hodell, 2002), however, it is inferred that the eastern South Atlantic and Southern Ocean sector did not experience significant change in surface and deep water isotopic changes until ~ 900 ka (Venz and Hodell, 2002; Hodell *et al.*, 2003). Given that basin-to-basin travel for these deep water masses is in the order of hundreds of years, an intrabasin and interbasin lag period between regional declines and HOs in ocean basins farthest from the source of deep water formation is expected. However, this does not explain diachronous HOs in the order of 10's or 100's of kyr. Figure 6.6 summarises the global timings of HOs of the studied South Atlantic EG taxa. This figure illustrates that earliest HOs commonly occurred in the North Atlantic, followed by the South Atlantic, and latest HOs commonly occurred in the SW Pacific; diachroneity (particularly between North and South Atlantic sites) may reflect the distance from source the well-ventilated GNAIW (or other well-ventilated glacial equivalent, such as the glacial-AAIW in the SW Pacific) had to travel around the world's ocean basins. One such example is the HO datum of *Myllostomella matanazana*, whose earliest regional HO took place at ~ 725 ka in the North Atlantic (ODP Site 980) (Kawagata *et al.*, in press), followed by ~ 600 ka in the South Atlantic (ODP Site 1088) (this study). This diachroneity possibly reflects the distance well-ventilated GNAIW had to travel to impact the sites. Another example is *Siphonodosaria sagrinensis* (=*lepidula*), whose earliest regional HO again occurred in the northern North Atlantic (ODP Sites 980/982) at ~ 780 ka (Kawagata *et al.*, in press),

followed by ~ 700 ka at Site 1082 in the South Atlantic (this study), ~ 730 ka in the Indian Ocean (Gupta, 1993), and at ~ 570 ka (Site 1125) in the SW Pacific (Hayward, 2002). It should be noted that researchers have not suggested that GNAIW penetrated into the SW Pacific during MPT glacial times, so in this case, latest HOs occurring in this region cannot be linked to GNAIW basin-to-basin travel times. Rather, the influence of the glacial-AAIW is likely to have contributed to the timings of HOs in the SW Pacific Ocean.

A similar pattern can be interpreted between the peak number of HOs per 100 kyr and distance from source of deep water formation (Fig. 6.5). By comparing similar depth sites: North Atlantic Site 982 (1145 m, upper-NADW), South Atlantic Site 1082 (1290 m, AAIW), and SW Pacific Site 593 (1050 m, AAIW), the earliest peak number of HOs occurred in the North Atlantic (between 1000 and 900 ka), followed by the South Atlantic (900 – 800 ka), and SW Pacific (900 – 800 ka).

It seems that the distance and time taken for well-ventilated glacial waters to travel from source areas is likely to be an important factor in the timing of HOs in global ocean basins. In terms of the GNAIW, North Atlantic sites are impacted first, with earliest HOs occurring at Sites 980 and 982, followed by a lag of approximately 80 – 100 kyr before which HOs occur at South Atlantic Sites 1082 and 1088 (Fig. 6.6). This lag is possibly the result of deep waters progressively losing oxygen as they travel (i.e. oxygen is consumed), and consequently it may have taken hundreds of kyr for high dissolved oxygen waters to reach levels that could be carried all the way to distant places and influence EG taxa (Hayward, pers. com.).

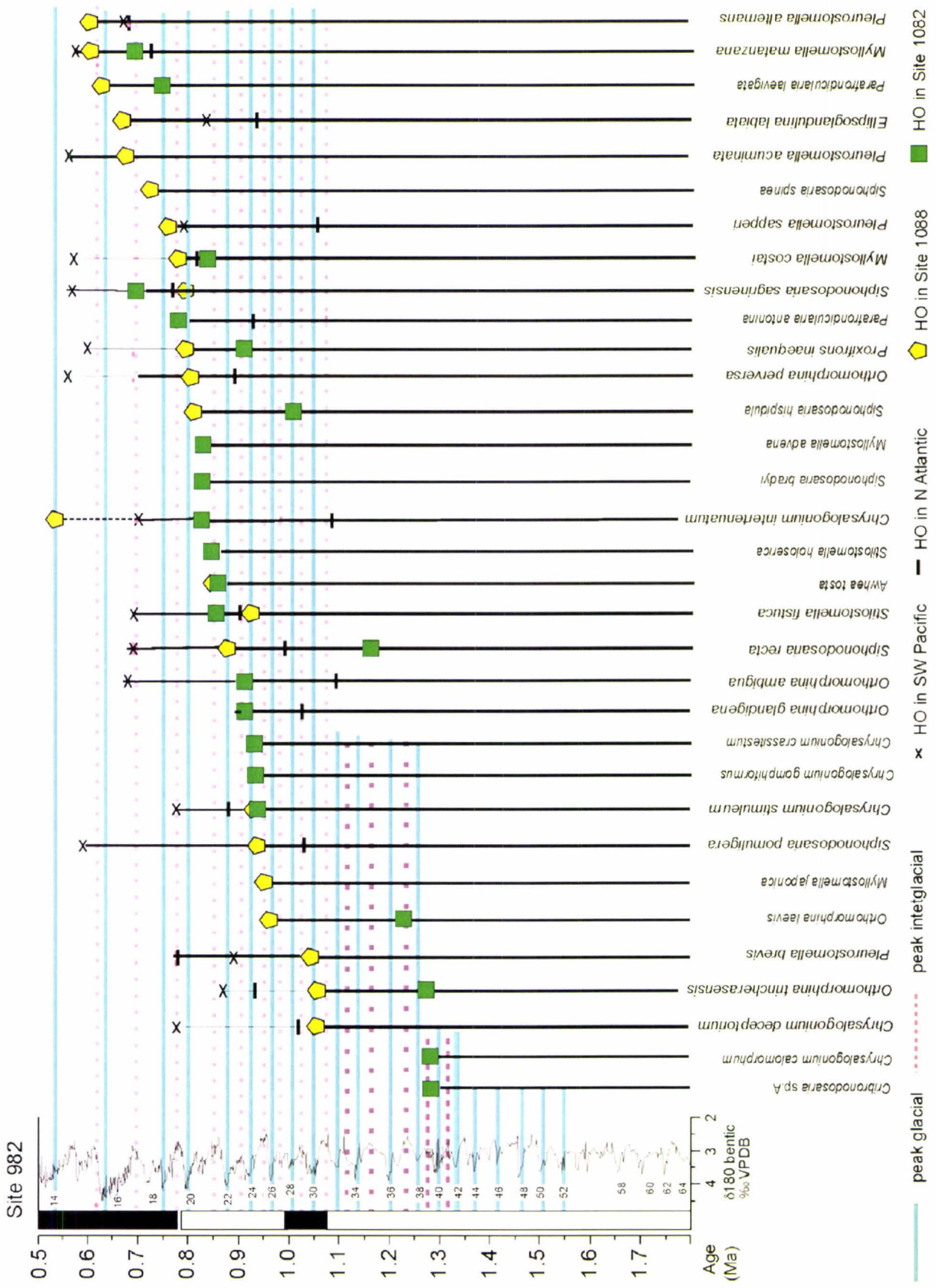

Figure 6.6: Global timing of highest occurrences (HOs) of the studied South Atlantic Extinction Group species. Oxygen isotope records are based on ODP Site 982 (Venz and Hodell, 1999). Marine oxygen isotope stages (MIS) are shown. Solid and dashed lines represent peak glacial and interglacial stages, respectively. SW Pacific data is from Hayward (2002); North Atlantic data is from Kawagata *et al.* (in press).

6.2.3 Extinction Orderings and EG Morphology

With our current limited understanding of the complex ecological and biological nature of Recent benthic foraminifera (let alone the extinct genera belonging to the EG), the question of whether specific morphologic characteristics common to the *Stilostomella* Extinction Group, such as highly specialised apertural structures, predisposed the EG taxa to decline and eventual extinction remains a difficult question to answer. As yet, no factual information as to the precise functional role of the apertural modifications characteristic of the EG is available. It has been observed that the pseudopodial network protruding from the aperture is likely to facilitate motion (in response to moving redox fronts and food resources). However, the exact role of cribrate, hooded-toothed, or secondary toothed apertural structures in these feeding and automotive processes is unclear.

Local South Atlantic and global HO studies reveal that despite the final demise of the EG species, not all species were impacted equally. Rather certain genera, possibly due to their associated apertural structures, were more resilient than others to the rapidly fluctuating environmental conditions. Figure 6.6 shows that both locally (South Atlantic Sites 1082 and 1088) and globally there is a common ordering of HOs. The earliest HOs are commonly represented by species from the *Chrysalogonium* and *Cribronodosaria* genera (cribrate aperture), followed by the genus *Orthomorphina* (terminal round aperture), and the youngest global HOs are commonly represented by the *Myllostomella*, *Siphonodosaria*, and *Pleurostomella* genera (round, secondary toothed, and hooded, secondary toothed apertures, respectively) (Table 6.2, Plate 6.1). This ordering of HOs is similar within the world's oceans and may be indicative of the most tolerant genera and species remaining present for the longest time as EG diversity decreases with the increasing environmental stress associated with the MPT. The question remains as to why 'round, secondary toothed and hooded, secondary toothed' aperture *Myllostomella*, *Siphonodosaria* and *Pleurostomella* were able to resist the deteriorating MPT conditions for longer than 'cribrate' aperture *Chrysalogonium* and *Cribronodosaria* EG genera.

This observation of a set extinction ordering with a possible link to the specific apertural characteristics of the foraminifera, further highlights the need for future

research on the functional role of these apertural structures, and how they may have contributed to the targeted extinction of their possessor.

7. CONCLUSIONS

This South Atlantic study reveals that the extinctions of 33 species of elongate benthic foraminifera belonging to the families Stilostomellidae, Pleurostomellidae, and part of Nodosariidae, show a pulsed pattern of decline during the mid-Pleistocene Climatic Transition (MPT, ~1200 – 600 ka), to become finally extinct at ~705 ka at Site 1082, and ~600 ka at Site 1088.

- The foraminiferal abundances during the MPT and the accumulation rate (AR) of Extinction Group (EG) taxa were pulsed, with major declines associated with the onset of cold glacial periods, and partial recoveries during intervening warm periods.
- The abundance and AR of EG taxa began to decline between ~1070 and 1000 ka at both core sites; the AR of the EG never recovered after ~1000 ka at Site 1082, whereas at Site 1088 the EG shows a last peak centred at ~950 ka before a progressive decline to extinction.
- The timing of highest occurrences (HOs) of each species is diachronous between Sites 1082 and 1088, excluding the HO of the two species, *Awhea tosta* and *Chrysalogonium stimuleum*, which are synchronous.
- The maximum number of HOs of EG species occurred between 1000 and 700 ka at both sites. However, the number of HOs per 100 kyr peaks in the shallower Site 1082 approximately 100 kyr earlier than deeper Site 1088.
- The final *Stilostomella* extinction datum in the South Atlantic is marked by the uppermost occurrence of *Myllostomella matanzana* and *Siphonodosaria sagrinensis* at ~705 ka in Site 1082, and *Myllostomella matanzana* and *Pleurostomella alternans* at ~600 ka in Site 1088. This corresponds with the global *Stilostomella* extinction datum being between 700 and 570 ka (Schönfeld, 1996; Hayward, 2002; Kawagata *et al.* in press).
- All EG taxa that were identified in the South Atlantic have been previously recorded in studies around the world's oceans. An anomaly is *Chrysalogonium intertenuatum*, which is not part of the EG in Site 1088 and appears to have survived through the MPT in the Southern Ocean sector of the South Atlantic Ocean.

- The AR of EG species at both sites show a strong positive correlation with the AR of low-oxygen tolerant (LOTG) benthic species (Site 1082: r = +0.60, Site 1088: r = +0.66), verifying that the EG favoured living in lower oxygen conditions. These conditions may have been caused by high organic carbon flux to sediments in high productivity upwelling regions such as Site 1082, or by the ventilation characteristics of the surrounding watermass causing stagnation of the bottom water such as at Site 1088.
- Declines and extinctions at high productivity Site 1082 were primarily driven by highly fluctuating food supply associated with increased productivity caused by intensified upwelling during MPT glacial periods. Consequent competition for food resources with prolific high productivity faunas (such as the LOTG) is likely. Subsidiary to this, changes in the chemical ventilation of the South Atlantic intermediate waters as a result of encroachment by Glacial North Atlantic Intermediate Water (GNAIW) (high dissolved oxygen) may have also been a factor in the final demise of the EG benthic foraminifera.
- Away from the influence of the Benguela Upwelling System, extinctions at Site 1088 were primarily driven by the MPT reorganisation of the glacial-interglacial modes of the global deep-water 'conveyor belt' (Broecker and Denton, 1989). $\delta^{13}C$ gradients reveal nutrient-depleted, high dissolved oxygen GNAIW or an admixture of expanded lower-Circum Polar Deep Water (CPDW) and GNAIW during some cool periods.
- Sites 1082 and 1088 are located on topographical highs on the seafloor. As a consequence, fluctuations in food supply, caused by the winnowing effect of strong bottom currents during glacial periods may have also contributed to the overall declines.
- Detailed comparisons with North Atlantic and Southwest Pacific studies reveal the highly diachronous nature of HOs of EG species. The distance and time required for well-ventilated glacial waters to reach the study site is likely to be important in the timing of HOs in global ocean basins. During glacial times North Atlantic sites were impacted first by GNAIW, with earliest HOs occurring at Sites 980 and 982, followed by a lag period of ~ 80 – 100 kyr before HOs occurred at South Atlantic Sites 1082 and 1088.

- EG taxa were not impacted equally by the environmental stresses associated with the MPT. A common ordering of HOs exists both locally and globally, with earliest HOs represented by species from the *Chrysalogonium* and *Cribronodosaria* genera (cribrate aperture), followed by the genus *Orthomorphina* (terminal round aperture), with youngest global HOs represented by the *Myllostomella, Siphonodosaria,* and *Pleurostomella* genera (round secondary toothed, and hooded secondary toothed, apertures, respectively). This observation of a set extinction ordering with a possible link to the specific apertural characteristics of the foraminifera, further highlights the need for future research on the functional role of these apertural structures, and how they may have contributed to the targeted extinction of their possessor.

It is evident that foraminiferal population declines are not necessarily a simple response to change in a single parameter. Rather, numerous factors seem to have interacted to influence the decline, partial recovery, and eventual extinction of the EG taxa. Furthermore, it is likely that certain apertural characteristics and morphology predisposed the EG taxa to decline and extinction, yet currently no factual information exists as to the exact functional role of these apertural structures. Such studies are a reminder of the gaps in our current understanding of the biology and ecology of foraminifera. The results of this study demonstrate the complexity of the Earth's interacting atmosphere, hydrosphere, biosphere and lithosphere. It emphasises the fine tuning benthic communities are required to make in response to critical environmental thresholds being breached, to ensure their survival in rapidly changing oceanographic conditions.

8. REFERENCES

Asano, K., 1938. Japanese fossil Nodosariidae, with notes on the Frondiculariidae. Sci. Rep. Tohoku University. Series 2, 19:179-220.

Bagg, R.M., 1912. Pliocene and Pleistocene foraminifera from Southern California. US Geological Survey Bulletin 513:5-153.

Bang, N.D., 1971. The southern Benguela Current region in February 1966: Part II: Bathythermography and air-sea interactions. Deep Sea Research, 18: 209-224.

Barker, R.W., 1960. Taxonomic note on the species figured by H.B. Brady in his report on the foraminifera dredged by H.M.S. Challenger during the year 1873-1876. Society of Economic Paleontologists and Mineralogists, Special Publication (9): 238pp.

Berger, A., Loutre, M., 1991. Insolation values for the climate of the last 10 million years. Quaternary Science Reviews, 10: 297-317.

Berger, W.H. and Wefer, G., 1988. Benthic deep-sea foraminifera: Possible consequences of infaunal habitat for paleoceanographic interpretation. Journal of Foraminiferal Research, 18(2): 147-150.

Berger, W.H., 1970. Planktonic foraminifera: selective solution and the lysocline. Marine Geology, 8: 111-138.

Berger, W.H., 1975. Deep-sea carbonates: dissolution profiles from foraminiferal preservation. In: W.V. Sliter, Be, A. W. H., Berger, W. H (Editor), Dissolution of Deep-sea Carbonate. Cushman Foundation Spec. Publ. Cushman Foundation Spec. Publ., p 82-86.

Berger, W.H., Bonneau, M. C., Parker, F. L., 1982. Foraminifera on the deep-sea floor: lysocline and dissolution rate. Oceanologica Acta, 5: 249-258.

Berger, W.H., Wefer, G., 1996. Expeditions into the past: paleocenographic studies in the South Atlantic. In: G. Wefer, Beger, W. H., and Richter, C. (Editor), The South Atlantic: Present and Past Circulation. Springer-Verlag, Berlin, pp. 363-410.

Berggren, W.A., Kent, D.V., Swisher, C.C., and Aubrey, M.-P., 1995. A revised Cenozoic geochronology and chronostratigraphy. In: W.A. Berggren and others (Editors), Geochronology, time scales and global stratigraphic correlation. SEPM Special Publication, pp. 129-212.

Bermúdez, P.J., 1937 Nuevas especies de foraminíferos del Eoceno de las cercanías de Guanajay, Provincia Pinar del Rio, Cuba. Memorias de la Sociedad Cubana de Historia Natural "Felipe Poey", 11: 237-247.

Bermúdez, P.J., 1949. Tertiary smaller foraminifera of the Dominican Republic. Cushman Laboratory for Foraminiferal Research Special Publication, 25: 1-322.

Bernhard, J.M. and Reimers, C.E., 1991. Benthic foraminiferal population fluctuations related to anoxia - Santa Barbara Basin. Biogeochemistry, 15(2): 127-149.

Bernhard, J.M., 1986. Characteristic assemblages and morphologies of benthic foraminifera from anoxic, organic-rich deposits: Jurassic through Holocene. Journal of foraminiferal research, 16: 207-215.

Bickert, T., Mackensen, A., 2003. Last Glacial to Holocene changes in South Atlantic deep water circulation. In: G. Wefer, Mulitza, S., Ratmeyer, V. (Editor), The South Atlantic in the Late Quaternary: reconstruction of material budgets and current systems. Springer-Verlag, pp. 671-695.

Bickert, T., Wefer, G., 1999. South Atlantic and benthic foraminifer delta C-13 deviations: implications for reconstructing the Late Quaternary deep-water circulation. Deep-Sea Research Part Ii-Topical Studies In Oceanography, 46(1-2): 437-452.

Boersma, A., 1984. Handbook of common Tertiary *Uvigerina*: Microclimates Press, Stony Point, New York.

Boersma, A., 1986. Biostratigraphy and biogeography of Tertiary bathyal benthic foraminifers: Tasman Sea, Coral Sea and on the Chatham Rise (Deep Sea Drilling Project, Leg 90). Initial Reports of the Deep Sea Drilling Project, 90: 961-1035.

Boersma, A., 1990. Late Oligocene to late Pliocene benthic foraminifers from depth traverses in the Central Indian Ocean. Proceeedings of the Ocean Drilling Programme, Scientific Results 115: 315-379.

Bolli, H.M., Ryan, W. B. F, 1978. Initial Reports of the Deep Sea Drilling Project Leg 40. 40.

Boltovskoy, E. and Wright, R., 1976. Recent Foraminifera. Dr W. Junk, The Hague, 515 pp.

Boltovskoy, E., 1978. Late Cenozoic benthonic foraminifera of the Ninetyeast Ridge (Indian Ocean). Marine Geology, 26: 139-175.

Bonatti, E., 1978. Vertical tectonism in oceanic fracture zones. Earth and Planetary Science Letters, 37: 369-379.

Boomgaart, L., 1949. Smaller foraminifera from Bodjonegoro (Java). Utrecht Doct dissertation, 1-175.

Boyd, W., Law, C., Wong. C., *et al.*, 2004. The decline and fate of an iron-induced subarctic phytoplankton bloom. Nature, 428: 549-553.

Brady, H.B., 1881. Notes on some of the reticularian Rhizopoda of the "Challenger" Expedition. Part III. 1. Classification. 2. Further notes on new species. 3. Note on *Biloculina* Mud. Quarterly journal of microscopical science, n.s, 21: 31-71.

Brady, H.B., 1884. Report on the foraminifera dredged by the H.M.S Challenger, during the years 1873-1876. Rep. Scientific Results Explor. Voyage H.M.S. Challenger, Zoology, 9: 1-814.

Broecker, W., and van Donk, J., 1970. Insolation changes, ice volumes, and the 18O record in deep-sea cores. Rev. Geophys. Space Phys., 8: 169-198.

Broecker, W.S. and Denton, G.H., 1989. The role of ocean-atmosphere reorganizations in glacial cycles. Geochimica et Cosmochimica Acta, 53: 2465-2501.

Chen, J., Farrell, J.W., Murray, D.W. and Prell, W.L., 1995. Timescale and paleoceanographic implications of a 3.6 m.y. oxygen isotope record from the northeast Indian Ocean (Ocean Drilling Program site 758). Paleoceanography, 10: 21-47.

Corliss, B. and Silva, K.A., 1993. Rapid growth of deep sea benthic foraminifera. Geology, 21(11): 991-994.

Corliss, B.H. and Chen, C., 1988. Morphotype patterns of Norwegian Sea deep sea benthic foraminifera and ecological implications. Geology, 16: 716-719.

Costa, O.G., 1855. Foraminiferi fossili delle marine Terziarie di Messina. Reale Accademia Scienza Napoli, Mem., 2: 28-147, 367-373.

Cushman, J.A., 1911. A monograph of the foraminifera of the North Pacific Ocean, part 2, Textulariidae: United States National Museum Bulletin 72, 108 pp.

Cushman, J.A., 1917. A monograph of the foraminifera of the North Pacific Ocean, part 1, Astrorhizidae and Lituolidae: United States National Museum Bulletin 71, 134 pp.

Cushman, J.A., 1921. Foraminifera of the Philippine and adjacent seas - contributions to the biology of the Philippine Archipelago and adjacent regions: United States National Museum Bulletin 100, 608 pp.

Cushman, J.A., 1922. Foraminifera of the Atlantic Ocean, Part 3. Textulariidae: United States National Museum Bulletin 104, (3) 143 pp.

Cushman, J.A., 1923. The foraminifera of the Atlantic Ocean. Pt. 4. Lagenidae. United States National Museum Bulletin 104: 1-228.

Cushman, J.A., 1927. An outline of a re-classification of the foraminifera: Contributions from the Cushman Laboratory for Foraminiferal Research, 3: 1-105.

Cushman, J.A., 1931. New late Tertiary foraminifera from Viti Levu, Fiji: Contributions from the Cushman Laboratory for Foraminiferal Research, 7: 23-32.

Cushman, J.A., 1933. The foraminifera of the tropical Pacific collections of the "Albatross", 1899-1900: United States National Museum Bulletin 161, 79 pp.

Cushman, J.A., 1934. Smaller foraminifera from Vitilev, Fiji. Bernice P. Bishop Museum Bulletin, 119: 102-142.

Cushman, J.A., 1939. Eocene foraminifera from submarine cores off the eastern coast of North America: Contribution from the Cushman Laboratory for foraminiferal Research 15: 49-76.

Cushman, J.A., Bermudez, P.J., 1934. Some interesting new uniserial foraminifera from Trinidad: Contributions from the Cushman Foundation for Foraminiferal Research 10: 71-75.

Cushman, J.A., Bermudez, P.J., 1937. Further new species of foraminifera from the Eocene of Cuba: Contributions from the Cushman Laboratory for Foraminiferal Research 13: 1-29.

Cushman, J.A., Harris, R.W., 1927. Notes on the genus *Pleurostomella.* Cushman Laboratory for Foraminiferal Research Contribution, 3: 128-135.

Cushman, J.A., Jarvis, P.W., 1934. Some interesting new uniserial foraminifera from Trinidad. Contribution from Cushman Laboratory for Foraminiferal Research, 10.

Cushman, J.A., Laiming, B., 1931. Miocene foraminifera from Los Sauces Creek, Ventura County, California: Contributions from the Cushman Laboratory for Foraminiferal Research 5: 79-120.

D'Orbigny, A., 1826. Tableau méthodique de la classe des Cephalopodes. Annales des Sciences Naturelles 1(7): 96-169, 245-314.

D'Orbigny, A., 1846. Foraminifères fossiles du Bassin Tertiare de Vienne (Austriche): Gide et comp, Paris, 312 pp.

Dean, W.E., Gardner, J., 1985. Cyclic variations in calcium carbonate and organic carbon in Miocene to Holocene sediments, Walvis Ridge, South Atlantic Ocean. In: K.J. Hsu, Weissert, H. J (Editor), South Atlantic Paleoceanography. Cambridge University Press, Cambridge, pp. 61-78.

Dean, W.E., Parduhn, N. L., 1984. Inorganic geochemistry of sediments and rocks recovered from the southern Angola Basin and adjacent Walvis Ridge, Sites 530 and 532, Deep Sea Drilling Project Leg 75, Initial Reports, Deep Sea Drilling Project 75, pp. 923-958.

Diekmann, B. and Kuhn, G., 2002. Sedimentary record of the mid-Pleistocene climate transition in the southeastern South Atlantic (ODP Site 1090). Palaeogeography, Palaeoclimatology, Palaeoecology, 182: 241-258.

Diekmann, B., Falker, M. and Kuhn, G., 2003. Environmental history of the south-eastern South Atlantic since the Middle Miocene: evidence from the

sedimentological records of ODP Sites 1088 and 1092. Sedimentology 50: 511-529.

Diester-Haass, L., 1985. Late Quaternary upwelling history off southwest Africa (DSDP Leg 75, HPC 532). In: K.J. Hsu, Weissert, H. J (Editor), South Atlantic Paleoceanography. Cambridge University Press, Cambridge.

Diester-Haass, L., Heine, K., Rothe, P., Schrader, H., 1988. Late Quaternary history of continental climate and the Benguela Current off South West Africa. Pal Pal Pal, 65: 81-91.

Diester-Haass, L., Meyers, P. A., Rothe, P., 1986. Light-dark cycles in opal-rich sediments near the Plio-Pleistocene boundary, DSDP Site 532, Walvis Ridge Continental Terrace. Marine Geology, 73: 1-23.

Diester-Haass, L., Meyers, P. A., Rothe, P., 1992. The Benguela Current and associated upwelling on the southwest African Margin: a synthesis of the Neogene-Quaternary sedimentary record at DSDP sites 362 and 532. In: C.P. Summerhayes, Prell, W. L., Emeis, K. C. (Editor), Upwelling Systems: Evolution Since the Early Miocene. Geological Society Special Publication, pp. 331-342.

Dowsett, H.J., Willard, D., 1996. Southeast Atlantic marine and terrestrial response to middle Pliocene climate change. Marine Micropaleontology, 27: 181-193.

Duplessy, J.C., 1982. Glacial to interglacial contrasts in the northern Indian Ocean. Nature 295: 494-498.

Duplessy, J.C., Shackleton, N.J., 1984. Carbon-13 in the World Ocean during the Last Interglaciation and the Penultimate Glacial Maximum. Reevaluation of the possible biosphere response to the Earth's climatic changes. Progress in Biometeorology 3: 48-54.

Durham, E.L., Maslin, M. A., Platzman, E., Rosell-Mele, A., Marlow, J. R., Leng, M., Lowry, D., Burns, S. J., and the ODP Leg 175 Shipboard Scientific Party, 2001. Reconstructing the climatic history of the western coast of Africa over the past 1.5 m.y.: A comparison of proxy records from the Congo Basin and the Walvis Ridge and the search for evidence of the Mid-Pleistocene Revolution. In: G. Wefer, Beger, W. H., and Richter, C. (Editor), Proceedings of the Ocean Drilling Program, Scientific Results Volume 175. Ocean Drilling Program, College Station, TX, pp. 1-45.

Eade, J.V., 1967. New Zealand Recent Foraminifera of the families Islandiellidae and Cassidulinidae. New Zealand Journal of Marine and Freshwater Research 1(4): 421-454.

Egger, J.G., 1893. Foraminiferen aus Meeresgrundproben, gelothet von 1874 bus 1876 von S.M. Sch. "Gazelle". Abhandlungen der Mathematisch-Physikalischen Classe der Königlich Bayerischen Akademie der Wissenschaften (2) 18(2): 193-458.

Emerson, S. and Bender, M., 1982. Carbon fluxes at the sediment-water interface of the deep sea: Calcium carbonate preservation. Journal of Marine Research, 39: 139-162.

Finlay, H.J., 1947. New Zealand Foraminifera: Key Species in Stratigraphy 5. New Zealand Journal of Science and Technology, 5: 259-292.

Franke, A., 1925-1928. Die Foraminiferen der pommerschen Kreide. Abhandlungen aus dem geologisch-paläontologischen Institut der Universität Greifswald, 6: 1-96.

Gersonde, R., Hodell, D.A., Blum, P., et al.,, 1999. Proceedings of the Ocean Drilling Program, Initial Reports, Volume 177.

Gibson, G.W., 1967. Foraminifera and stratigraphy of the Tongaporutuan Stage in the Taranaki coastal and six other sections. Part I. - Systematics and distribution: Transactions of the Royal Society of New Zealand, Geology 5: 1-70.

Gibson, G.W., Grenfell, H.R., Reid, C.M., and Hayward, K.A., 1999. Recent New Zealand benthic foraminifera: taxonomy, ecologic distribution, biogeography, and use in paleoenvironmental assessment: New Zealand Geological Survey Paleontological Bulletin 75: 258 p.

Giraudeau, J., 1993. Planktonic foraminiferal assemblages in surface sediments from the Southwest African continental margin. Marine Geology, 110(1-2): 47-62.

Gooday, A.J. and Rathburn, A.E., 1999. Temporal variability in living deep-sea benthic foraminifera: a review. Earth Science Reviews, 46(1-4): 187-212.

Gordon, A.L., Weiss, R. F., Smethie, W. M., Warner, M. J., 1992. Thermohaline and intermediate water communication between the South Atlantic and Indian Oceans. Journal of Geophysical Research, 97(C5): 7223-7240.

Gradstein, F.M., Ogg, J.G., Smith, A.G., 2004. A new Geological Time Scale, with special reference to Precambrian and Neogene. Episodes, 27(2).

Gumbel, C.W., 1868. Beitrage zur Foraminiferen fauna der Nordalpinen Eocangebilde. Munchen,. Quarto, pp. 152, 4 plates

Guppy, R.J.L., 1894. On some foraminifera from the Microzoic deposits of Trinidad, West Indies. Prceeedings of the Zoological Society of London 1894: 647-652.

Gupta, A.K., 1993. Biostratigraphic vs. paleoceanographic importance of *Stilostomella lepidula* (Schwager) in the Indian Ocean. Micropaleontology, 39: 47-51.

Harloff, J. and Mackensen, A., 1997. Recent benthic foraminiferal associations and ecology of the Scotia sea and Argentine basin. Marine Micropaleontology, 31(1-2.): 1-29.

Hartnady, C.a.l.R., A., 1985. Southern ocean hotspot tracks and the Cenozoic absolute motion of the African, Antarctic, and South American plates. Earth and Planetary Science Letters, 75: 245-257.

Hay, W.W., Brock, J. C., 1992. Temporal variation in intensity of upwelling off southwest Africa. In: C.P. Summerhayes, Prell, W. L., Emeis, K. C. (Editor), Upwelling Systems: Evolution since the Early Miocene. Geological Society Special Publication.

Hayward, B.W., 2001. Global deep-sea extinctions during the Pleistocene ice ages. Geology, 29(7): 599-602.

Hayward, B.W., 2002. Late Pliocene to middle Pleistocene extinctions of deep-sea benthic foraminifera ("*Stilostomella* extinction") in the South-west Pacific. Journal of Foraminiferal Research, 32: 274-306.

Hodell, D.A. and Venz, K., 1992. Toward a high-resolution stable isotopic record of the Southern Ocean during the Pliocene-Pleistocene (4.8 to 0.8 Ma). The Antarctic Paleoenvironment: a perspective on global change antarctic research series, 56: 265-310.

Hodell, D.A., Venz, K.A., Charles, C.D. and Ninnemann, U.S., 2003. Pleistocene vertical carbon isotope and carbonate gradients in the South Atlantic sector of the Southern Ocean. Geochemistry, Geophysics, Geosystems, 4(1): 19.

Hornibrook, N.deB., 1971. Revision of the Oligocene and Miocene foraminifera from New Zealand, described by Karrer and Stache in the reports of the "Novara" Expedition (1864). New Zealand Geological Survey paleontological bulletin 43, 85 pp.

Imbrie, J., Berger, A., Boyle, E., et al., 1993. On the structure and origin of major glaciation cycles, 2: the 100,000-year cycle. Paleoceanography, 8(699-735.).
Interglaciation and the Penultimate Glacial Maximum. Reevaluation of the possible biosphere response to the Earth's climatic changes. Progress in Biometeorology 3: 48-54.

Ishizaki, K., 1943. On the species of *Ellipsonodosaria* from Japan: Transactions of the Natural History Society of Taiwan 33: 678-689.

Jahn, B. et al., 2003. Pleistocene variations in dust input and marine productivity in the northern Benguela Current: Evidence of evolution of global glacial-interglacial cycles. Palaeogeography, Palaeoclimatology, Palaeoecology, 193: 515-533.

Jansen, E., Spiegler, D., 1989. Planktonic foraminifer biostratigraphy of Norwegian Sea sediments: ODP Leg 104. Journal of Quaternary Science 4: 61-66.

Jedlitshka, H., 1931. Neue Beobachtungen *Dentalina verneuilli* und *Nodosaria abyssorum* (Brady). Firgenwald, Reichenberg (Liberec) Czech., Tschchoslowakei, Jahrg 4: 121-127.

Jian, Z. et al., 2000. Foraminiferal response to major Pleistocene paleoceanographic changes in the southern China Sea. Paleoceanography, 15: 229-243.

Jones, R.W., 1994. "The Challenger Foraminifera." Oxford science publications, 149 pp.

Jorissen, F.J., Barmaidjaja, D.M., Puskaric, S. and Van der Zwaan, G.J., 1992. Vertical distribution of benthic foraminifera in the northern Adriatic Sea: The relation with the organic flux. Marine Micropaleontology, 19: 131-146.

Kaiho, K. and Hasegawa, T., 1994. End-Cenomanian benthic foraminiferal extinctions and oceanic dysoxic events in the Northwestern Pacific. Palaeogeography, Palaeoclimatology, Palaeoecology, 111(1-2): 29-43.

Kaiho, K., 1991. Global changes of Paleogene aerobic anaerobic benthic foraminifera and deep sea circulation. Palaeogeography Palaeoclimatology Palaeoecology, 83(1-3): 65-85.

Kaiho, K., 1992. Eocene to Quaternary benthic foraminifers and paleobathymetry of the Izu-Bonin Arc, Legs 125 and 126. In: B. Taylor, K. Fujioka and others (Editors), Proceedings of the Ocean Drilling Program, Scientific Results, College Station, Texas, pp. 285-310.

Kaiho, K., 1994. Benthic foraminiferal dissolved-oxygen index and dissolved-oxygen levels in the modern ocean. Geology, 22: 719-722.

Kaiho, K., 1994. Planktonic and benthic foraminiferal extinction events during the last 100 m.y. Palaeogeography, Palaeoclimatology, Palaeoecology, 111(1-2): 45-71.

Kaiho, K., 1999. Effect of organic carbon flux and dissolved oxygen on the benthic foraminiferal oxygen index (BFOI). Marine Micropaleontology, 37: 67-76.

Kanfoush, S.L., Hodell, D. A., Charles, C. D., Guilderson, T. P., Mortyn, P. G., Ninnemann, U. S., 2000. Millenial-scale instability of the Antarctic ice sheet during the last glaciation. Science, 288: 1815-1818.

Karrer, F.W., 1878. Die Foraminiferen der Tertiaren Thone von Luzon, in von, Dracshe, R., Fragmente zu einer Geologie der Insel Luzon (Philippinen), p. 75-99.

Kastens, K., 1987. A compendium of causes and effects of processes at transform faults and fracture zones. Rev. Geophys.,, 25: 1554-1562.

Katz, M.E., Pak, D.M., Dickens, G.R. and Miller, K.G., 1999. The source and fate of massive carbon input during the latest Paleocene thermal maximum. Science, 286: 1531-1533.

Kawagata, S., Hayward, B. W., Grenfell, H. R., Sabaa, A., (in press). Mid-Pleistocene extinction of deep-sea foraminifera in the North Atlantic Gateway (ODP Sites 980 and 982). Palaeogeography Palaeoclimatology Palaeoecology.

Keller, G., 1980. Benthic foraminifers and paleobathymetry of the Japan Trench area, Leg 57, Deep Sea Drilling Project. In: R. von Huene, N. Nasu and others (Editors), Initial Reports of the Deep Sea Drilling Project. US Govt. Printing Office, Washington DC, pp. 835-865.

Kroopnick, P., 1980. The distribution of ^{13}C in the Atlantic Ocean. Earth and Planetary Science Letters 49: 469-484.

Le Calvez, De Klasz, and Brun, L., 1974. Nouvelle contribution a la connaissance des microfaunes du Gabon. Revista Espanola Micropaleontologia 6: 381-400.

Le, J. and Shackleton, N.J., 1992. Carbonate dissolution fluctuations in the western equatorial Pacific during the late Quaternary. Paleoceanography, 7: 21-42.

Little, M.G. et al., 1997. Rapid Palaeoceanographic Changes In The Benguela Upwelling System For The Last 160,000 Years As Indicated By Abundances Of Planktonic Foraminifera. Palaeogeography Palaeoclimatology Palaeoecology, 130(1-4): 135-161.

Loeblich, A.R., Tappan, H., 1994. Foraminifera of the Sahul Shelf and Timor Sea: Cushman Foundation for Foraminiferal Research, Special Publication 31: 661 p.

Loeblich, A.R.; Tappan, H., 1964. Treatise on the Invertebrate Paleontology, Part C, Protista 2., 2 vols., Geological Society of America & Kansas University Press, 900 pp.

Loeblich, A.R.; Tappan, H., 1987. "Foraminiferal genera and their classification". 2 vols., Van Nostrand Reinhold, New York, 1182 pp.

Loubere, P., 1991. Deep-sea benthic foraminiferal assemblage response to a surface ocean productivity gradient: a test. Paleoceanography, 6: 193-204.

Lutjeharms, J.R.E., Meeuwis, J. M, 1987. The extent and variability of South-east Atlantic upwelling. South African Journal of Marine Science, 5: 51-62.

Lutze, G.F. and Coulbourn, W.T., 1984. Recent benthic foraminifera from the continental margin of Northwest Africa: community structure and distribution. Marine Micropaleontology, 8: 361-401.

Lutze, G.F., 1979. Benthic foraminifers at Site 397: fluctuations and ranges in the Quaternary. In: U. Von Rad, W.B.F. Ryan and others (Editors), Initial Reports of the Deep Sea Drilling Project, v. 47. US Government Printing Office, Washington DC, pp. 419-431.

Mackensen, A., Bickert, T., 1999. Stable carbon isotopes in benthic foraminifera. In: G. Fischer, Wefer, G. (Editor), Use of Proxies in Paleoceanography: Examples from the South Atlantic. Springer, Berlin, pp. 229-254.

Mackensen, A., Rudolph, M., Kuhn, G., 2001. Late Pleistocene deep-water circulation in the subantarctic eastern Atlantic. Global and Planetary Change, 30: 197-229.

Mackensen, A., Schmiedl, G., Harloff, J. and Giese, M., 1995. Deep-sea foraminifera in the South Atlantic Ocean: ecology and assemblage generation. Micropaleontology, 41: 342-358.

Macleod, N. et al., 2000. Phenotypic resonse of foraminifera to episodes of global environmental change. In: S.J. Culver and P.F. Rawson (Editors), Biotic Response to Global Change - The Last 145 Million Years. Cambridge University Press, Cambridge, United Kingdom, pp. 51-78.

Milankovitch, M., 1930. Mathematische Klimalehre und Astronomische Theorie der Klimaschwankungen. Gebruder Borntaeger, Berlin.

Miller, K.G., Katz, M.E. and Berggren, W.A., 1992. Cenozoic deep-sea benthic foraminifera: A tale of three turnovers. In: Y. Takayanagi and T. Saito (Editors), Studies in Benthic Foraminifera. Tokai University Press, pp. 67-76.

Mix, A., Pisias, N. G., Rugh, W., et al., 1995. Proceedings of Ocean Drilling Program, Scientific Results, Volume 138.

Mollenhauer, G., Schneider, R. R., Muller, P. J., SpieB, V, and Wefer, G., 2002. Glacial/interglacial variability in the Benguela Upwelling System: spatial distribution and budgets of organic carbon accumulation. Global Biogeochemical Cycles, 81: 1-15.

Moroshkin, K., Bubnov, V., Bulatov, R, 1970. Water circulation in the eastern South Atlantic Ocean. Oceanology, 10: 27-37.

Motoyama, I., 2001. Late Cenozoic radiolarians from South Atlantic Hole 1082A, Leg 175. *In* Wefer, G., Berger, W.H., and Richter, C. (Eds.), Proc. ODP, Sci. Results, Leg 175.

Mudelsee, M. and Schulz, M., 1997. The Mid-Pleistocene climate transition: onset of 100 ka cycle lags ice volume build-up by 280 ka. Earth and Planetary Science Letters, 151: 117-123.

Nelson, G., Hutchings, L., 1983. The Benguela upwelling area. Prog. Oceanogr., 12: 333-356.

Neugeboren, J.L., 1856. Die Foraminiferen aus der Ordnung der Stichostegier von Ober-Lapugy in Siebenbürgen.. Denkschriften der Kaiserlichen Akademie der Wissenschaften, Mathematische-Naturwissenschaftliche Classe 12: 65-108.

Oberhansli, H., 1991. Upwelling signals at the northeastern Walvis Ridge during the last 500,000 years. Paleoceanography, 6: 53-71.

Okada, H., Bukry, D., 1980. Supplementary modification and introduction of code numbers to the low-latitude coccolith biostratigraphic zonation (Bukry, 1973, 1975). Marine Micropaleontology 5(3): 321-325.

Oppo, D.W., Lehman, S.J., 1993. Mid-depth circulation of the subpolar North Atlantic during the last glacial maximum. Science, 259: 1148-1152.

Palmer, D.K, Bermúdez, P.J., 1936. An Oligocene foraminiferal fauna from Cuba. Memorias de la Sociedad Cubana de Historia Natural "Felipe Poey" 10: 227-271.

Parr, W.J., 1950. Foraminifera: Reports of the British, Australian and New Zealand Antarctic research expedition 1929-1931, series B (zoology and botany) 5: 233-392.

Patterson, R.T., 1987. Four new foraminiferal (Protozoa) genera from the Rio Grande Rise, south-west Atlantic Ocean: Transactions of the American Microscopical Society 106: 139-148.

Patterson, R.T., Pettis, R.H., 1986. *Galwayella*, a new foraminiferal genus and new names for two foraminiferal homonyms. Journal of Foraminiferal Research 16. Planetary Science Letters 49:469-484.

Rathburn, A.E., 1996. Inter-annual variations in living (stained) deep-sea benthic foraminiferal assemblages from the Southern Californian Margin, Transactions American Geophysical Union 77.

Rathburn, A.E., 1998. Living (stained) deep-sea benthic foraminifera from the Southern Californian margin: relationship to productivity. Transactions American Geophysical Union 79.

Raymo, M.E., Oppo, D. W., and Curry, W., 1997. The mid-Pleistocene climate transition: A deep sea carbon isotope perspective. Paleoceanography, 12: 546-559.

Reid, J.L., 1994. On the total geostrophic circulation of the North Atlantic Ocean: flow patterns, tracers and transports. Prog. Oceanogr., 33: 1-92.

Reuss, A.E. von, 1851. Uber die fossilen Foraminiferen und Entomostraceen der Septarienthone der Umgegend von Berlin: Zeitschrift de Deutschen Geologischen Gesellschaft 3: 49-91.

Reuss, A.E. von, 1866. Die foraminiferen, Anthozoen und Bryozoen des deutschen Septarienthones: Kaiserlichen Akademie der Wissenschaften in Wien, Mathematisch-Naturwissenschaftliche 25: 117-214.

Rhoads, D.C., Morse, J. W., 1971. Evolutionary and ecologic significance of oxygen-deficient marine basins. LETHAIA(4): 413-428.

Ruddiman, W.F., Raymo, M. E., Martinson, D. G., et al., 1989. Pleistocene evolution: Northern hemisphere ice sheets and North Atlantic Ocean. Paleoceanography, 4: 353-412.

Schmiedl, G., Mackensen, A., 1997. Late Quaternary paleoproductivity and deep water circulation in the eastern South Atlantic Ocean: Evidence from benthic foraminifera. Paleogeography, Paleoclimatology, Paleoecology, 130: 43-80.

Schönfeld, J., 1995. Biostratigraphy and assemblage composition of benthic foraminifera from the Manihiki Plateau, southwestern tropical Pacific. Journal of Micropalaeontology, 14(2): 165-175.

Schönfeld, J., 1996. The 'Stilostomella Extinction'; structure and dynamics of the last turn-over in deep-sea benthic foraminiferal assemblages. In: E.A. Moguielvsky and R. Whatley (Editors), Microfossils and Oceanic Environments. Aberystwyth Press, Wales, pp. 27-37.

Schönfeld, J., 2001. Benthic foraminifera and pore-water oxygen profiles: a re-assessment of species boundary conditions at the western Iberian margin. Journal of Foraminferal Research, 31(2): 86-107.

Schönfeld, J., Spiegler, D. and Erlenkeuser, H., 1995. Late Quaternary stable isotope record of planktonic and benthic foraminifera: Site 861, Chile Triple Junction, southeastern Pacific. Proceedings of the Ocean Drilling Program, Scientific Results, 141(Sept): 235-240.

Schubert, R.J., 1900. Sur genere *Ellipsoglandulina*: Atti e Rendiconti R. Accademnia di Scienze, Lettere ed Arte degli Zelanti, Acireale, Cl. Sci. Mem 10: 1-9.

Schubert, R.J., 1911. Die fossilen foraminiferen des Bismarckarchipels und einiger angrenzender Inseln: Abhandlungen der geologischen Reischsanstalt 20: 1-130.

Schwager, C., 1866. Fossile Foraminiferen von Kar Nicobar. Novara Expedition, 2: 187-268.

Shackleton, N.J., 2000. The 100,000-Year Ice-Age Cycle Identified and Found to Lag Temperature, Carbon Dioxide, and Orbital Eccentricity. Science 289: 1897-1902.

Shackleton, N.J., Berger, A. and Peltier, W.R., 1990. An alternative astronomical calibration of the lower Pleistocene timescale based on ODP site 677. Transactions of the Royal Society Of Edinburgh: Earth Sciences, 81: 251-261.

Shackleton, N.J., Kennett, J.P., 1975. Paleotemperature history of the cenozoic and the initiation of Antarctic glaciation: oxygen and carbon isotope analysis in DSDP sites 277, 279 and 281. In: J.P. Kennett and R.E. Houtz (Editors), Initial Reports of DSDP. U.S. Government Printing Office, Washington, pp. 743-755.

Shannon, L.V., 1985a. The Benguela ecosystem, Part I. Evolution of the Benguela, physical features and processes. Annual Review of Oceanography Marine Biology., 23: 105-182.

Shannon, L.V., 1985b. South African ocean colour and upwelling experiment. Sea Fisheries Research Institute, Cape Town.

Shannon, L.V., Nelson, G., 1996. The Benguela: large scale features and processes and system variability. In: G. Wefer, Beger, W. H., and Siedler, G., Webb, D. J. (Editor), The South Atlantic: Present and past circulation. Springer-Verlag, Berlin, pp. 163-210.

Siesser, W.G., 1980. Late Miocene origin of the Benguela upwelling system off northern Namibia. Science, 208: 283-285.

Silvestri, O., 1872. Saggio di studyj sulla fauna micropica fossile appartenente al terreno subapennino italiano; Mrmoria I – monografia delle Nodosarie. Atti della Accademia gioenia di scienze naturali in Catania, Catania, Italia, 3(7).

Srinivasan, M.S., Sharma, V., 1980. Schwager's Car Nicobar Foraminifera in the reports of the Novara Expedition - A revision. Today & Tomorrow's Printers and Publishers, New Delhi, 83 p.

Stache, G., 1864. Die foraminiferen der Tertiären Mergel des Whaingaroa - Hafens (Prov. Auckland): Novara Expedition, Wien, Geologische Theil 2: 159-304.

Stainforth, R.M., 1952. Classification of uniserial calcareous foraminifera. Contributions from Cushman Foundatrion for Foraminiferal Research, 3 (1), 6-14.

Summerhayes, C.P., Kroon, D., Rosell-Mele, A., Jordan, R. W., Schrader, H. J., Hearn, R., Villanueva, J., Grimalt, J. O., Eglinton, G., 1995. Variability in the Benguela Current upwelling system over the past 70,000 years. Prog. Oceanogr., 35: 207-251.

Talley, L.D., 1996. Antarctic Intermediate Water circulation in the South Atlantic. The South Atlantic: present and past circulation. Springer-Verlag, Berlin-Heidelberg, 219-238 pp.

Thalmann, H. E., 1950. Bibliography and index to new genera, species, and varieties of Foraminifera for the year 1949. Journal of Paleontology, 24 (6) 699-745.

Thomas, E. and Vincent, E., 1987. Major changes in benthic foraminifera in the equatorial Pacific before the middle Miocene polar cooling. Geology, 15: 1035-1039.

Thomas, E., 1987. Late Oligocene to Recent deep-sea benthic foraminifers from the central equatorial Pacific Ocean. In: W.F. Ruddiman, R.B. Kidd and others (Editors), Initial Reports of the Deep Sea Drilling Project, v. 94. US Government Printing Office, Washington, D.C, pp. 997-1032.

Thomas, E., 1992. Cenozoic deep-sea circulation: evidence from deep-sea benthic foraminifera. In: J.P. Kennett and D. Warnke (Editors), The Antarctic

Paleoenvironment: A perspective on global change. Antarctic Research Series. American Geophysical Union, pp. 141-165.

Thomas, E., Zachos, J.C. and Bralower, T.J., 2000. Deep-sea environments on a warm earth: latest Paleocene - early Eocene. In: B. Huber, K. Macleod and S. Wing (Editors), Warm climates in earth history. Cambridge University Press, pp. 132-160.

Tiedemann, R., Sarnthein, M., and Shackleton, N.J., 1994. Astronomic timescale for the Pliocene Atlantic d18O and dust flux records of ODP Site 659, Paleoceanography 9 (4), 619-638.

Tyson, P.D., 1986. Climatic change and variability in Southern Africa. Oxford University Press, 220 pp.

Van der Zwaan, GJ., Duijnstee, I.A.P., Den Dulk, M., Ernst, S.R., Jannink, N.T., Kouwenhoven, T.J., 1999. Benthic foraminifers: proxies or problems? a review of paleocological concepts Earth Science Reviews 46 (1-4), 213-236.

Vella, P.P., 1963. Some foraminifera from the Upper Miocene and Pliocene of Wairarapa, New Zealand. Transactions of the Royal Society of New Zealand, Geology v.2 (1): 1-14.

Venz, K., Hodell, D. A., 2002. New evidence for changes in Plio-Pleistocene deep water circulation from Southern Ocean ODP Leg 177 Site 1090. Paleogeography, Paleoclimatology, Paleoecology, 182: 197-220.

Volbers, A.N.A., Henrich, R, 2002. Late Quaternary variations in calcium carbonate preservation of deep-sea sediments in the northern Cape Basin: results from a multiproxy approach. Marine Geology, 180: 203-20.

Wefer, G., Beger, W. H., and Richter, C., 2001. Proceedings of the Ocean Drilling Program, Scientific Results.

Wefer, G., W. H. Berger., C. Richter *et al.*, 1998. Proc. ODP, Initial Reports 175, Ocean Drilling Program, College Station, TX.

Weinholz, P. and Lutze, G.F., 1989. The Stilostomella extinction. In: W.F. Ruddiman, M. Sarnthein and others (Editors), Proceedings of the Ocean Drilling Program, Scientific Results, v. 108, College Station, Texas, pp. 113-117.

Williamson, W.C. (1858). On the recent Foraminifera of Great Britain. London, The Ray Society.